Alkylation of benzene and toluene with propane over bifunctional metal-acid catalysts

Thesis submitted in accordance with the requirements of the University of Liverpool for the degree of Doctor in Philosophy by

Abdullah Abdulrahman Alotaibi

2017/2018

Abstract

Effective functionalization of light alkanes is one of the greatest challenges for catalysis science. Involving alkanes in reactions with other organic molecules, e.g., aromatic hydrocarbons, is important direction of light alkane utilization. The alkylation of benzene with ethane and propane to produce ethylbenzene (EtPh) and isopropylbenzene (iPrPh)) has attracted particular interest as these are the key intermediates in manufacturing styrene and phenol and produced commercially on a large scale by the well-established acid-catalysed alkylation of benzene by alkenes, ethene and propene. The replacement of ethene and propene by abundant and inexpensive alkanes would lead to more cost effective and environmentally benign production of these commodity chemicals.

The first aim of this study is studying the direct alkylation of benzene with propane over bifunctional metal-acid catalysts in the gas phase using Pt and Pd as the metal components and silica-supported tungsten heteropoly acids ($H_3PW_{12}O_{40}$ and $H_4SiW_{12}O_{40}$, which are the strongest Keggin HPAs) as the acid components. It was found that with these catalysts, the alkylation yields isopropylbenzene (iPrPh) with high selectivity in a fixed-bed reactor at 250-350 ^oC and 1 bar pressure. Most efficiently the reaction occurs over $Pt/H_4SiW_{12}O_{40}/SiO_2$ catalyst, giving iPrPh with 90-93% selectivity at 6-8% conversion of benzene at 300 ^oC and an inlet C_6H_6/C_3H_8 molar ratio of 1:9. This significantly exceeds the efficiency of previously reported zeolite-based catalyst Pt/HZSM-5. There is important difference in performance between $Pt/HPA/SiO_2$ and Pt/HZSM-5 catalysts. With the Pt/HZSM-5 catalyst, reaction selectivity is controlled by acid-catalysed transformations within zeolite microporous structure (product shape selectivity), leading to preferential formation of nPrPh together with cracking and transalkylation products such as MePh and EtPh rather that the desired iPrPh. In contrast, the mesoporous $Pt/HPA/SiO_2$ catalyst gives selectively iPrPh, i.e., the alkylation product favoured from the carbenium ion mechanism.

Next, the alkylation of benzene with propane was tested using Pd/HSiW and Pd/HZSM-5, similar to the corresponding platinum catalysts. The palladium catalysts were also active in this reaction under similar conditions. The mesoporous catalyst Pd/HSiW/SiO_2 was much more selective to iPrPh (up to 88%) than the microporous Pd/HZSM-5 catalyst, which gave only 11-18% iPrPh selectivity. Overall, the Pd/HSiW and Pt/HSiW catalysts performed similarly in the alkylation of benzene by propane, with the Pt catalysts predictably more active than Pd ones per metal loading. This, however, is compensated for by the lower price (by a factor of ~1.5) of Pd as compared to Pt. Addition of gold to Pd-HSiW was tested in the alkylation of benzene and found to slightly enhance the activity of Pd catalysts.

Finally, we looked at the direct alkylation of toluene with propane over the above bifunctional metal-acid catalysts in the gas phase in comparison with the corresponding catalysts based on zeolite HZSM-5. This reaction was found to occur most efficiently over silica-supported Pt/HPA/SiO_2 catalysts giving p-cymene with up to 75% selectivity at 300 ^{o}C. Pt/HZSM-5 catalysts were much less selective ($\leq$ 5.5% p-cymene selectivity), which may be explained by product shape selectivity control imposed by HZSM-5 microporous environment. The Pd-based bifunctional catalysts performed similarly to Pt catalysts, albeit with a lower activity per metal loading. Addition of gold to Pt and Pd in these catalysts was tested, but had little effect on their activity and p-cymene selectivity in toluene alkylation with propane.

List of publications

Published literature

1. Alotaibi, A.; Bayahia, H.; Kozhevnikova, E. F.; Kozhevnikov, I. V. *Selective alkylation of benzene with propane over bifunctional Pt-heteropoly acid catalyst,* ACS Catalysis, **2015,** *5*, 5512.
2. Alotaibi, A.; Hodgkiss, S.; Kozhevnikova, E. F.; Kozhevnikov, I. V. *Selective alkylation of benzene with propane over bifunctional Pd-acid catalysts,* Catalysis, **2017,** *7*, 233.
3. North, J.; Poole, O.; Alotaibi, A.; Bayahia, H.; Kozhevnikova, E. F.; Alsalme, A.; H. Siddiqui, M.R.; Kozhevnikov, I. V. *Efficient hydrodesulfurization catalysts based on Keggin polyoxometalates,* Appl. Catal. A **2015,** *508*, 16.
4. Alsalme, A.; Alzaqri, N.; Alsaleh, A.; H. Siddiqui, M.R.; Alotaibi, A.; Kozhevnikova, E. F.; Kozhevnikov, I. V. *Efficient Ni-Mo hydrodesulfurization catalyst prepared through Keggin polyoxometalate,* Appl. Catal. B **2015,** *182*, 102.

Presentations

1. Alotaibi, A.; Kozhevnikova, E. F.; Kozhevnikov, I. V. *NORSC PG Symposium, King's Manor,* York, UK **2015**.
2. Alotaibi, A.; Kozhevnikova, E. F.; Kozhevnikov, I. V. *The 8th Saudi Students Conference, Imperial College,* London, UK **2015**.
3. Alotaibi, A.; Kozhevnikova, E. F.; Kozhevnikov, I. V. *The 9th Saudi Students Conference, University of Birmingham,* Birmingham, UK **2016**.
4. Alotaibi, A.; Kozhevnikova, E. F.; Kozhevnikov, I. V. *The Royal Society of Chemistry Conference, Burlington House,* London, UK **2016**.
5. Alotaibi, A.; Kozhevnikova, E. F.; Kozhevnikov, I. V. *Poster Day, University of Liverpool,* Liverpool, UK **2016**.
6. Alotaibi, A.; Kozhevnikova, E. F.; Kozhevnikov, I. V. *The 16th International Congress on Catalysis,* Beijing, China **2016**.
7. Alotaibi, A.; Kozhevnikova, E. F.; Kozhevnikov, I. V. *The UK Catalysis Conference (UKCC2018),* Loughborough, UK **2018**.

Acknowledgements

I would like to express my sincere appreciation to my supervisor, Prof. Ivan V. Kozhevnikov, for his guidance and support during my PhD study. Due to his advice and experience, this work has been completed and I have learned many skills.

Many thanks should be given to Dr. Elena F. Kozhevnikova for her kind assistance in solving multiple technical issues in our group as well as conducting experiments.

I would also like to thank all members of the technical support team in the Chemistry Department and all members of my group at the University of Liverpool.

Let me also extend my great thanks and love to my parents, my brothers, my sisters and my wife for their support and encouragement.

Finally, thanks are due to Shaqra University for their financial support and to the Saudi Cultural Bureau in London for their financial management.

Abbreviations

HPA	Heteropoly acid
HPW	$H_3[PW_{12}O_{40}]$
HSiW	$H_4[SiW_{12}O_{40}]$
CsPW	$Cs_{2.5}H_{0.5}[PW_{12}O_{40}]$
HZSM-5	Proton form of ZSM-5 zeolite
MePh	Methylbenzene (toluene)
EtB	Ethylbenzene
iPrPh	iso-Propylbenzene (cumene)
nPrPh	n-Propylbenzene
p-cymene	Isopropyltoluene
BET	Brunauer-Emmett-Teller method
BJH	Barrett-Joyner-Halenda method
TGA	Thermogravimetric analysis
TPR	Temperature programmed reduction
XRD	X-ray diffraction
ICP	Inductively coupled plasma
FTIR	Fourier transform infrared spectroscopy
GC	Gas chromatography
FID	Flame ionization detector
TOS	Time on stream
TOF	Turnover frequency

Contents

List of Figures

List of Tables

Chapter 1: Introduction

This chapter presents definitions and some applications of heterogeneous and bifunctional catalysis as well as a brief introduction to heteropoly acids and zeolites. Additionally, the literature on alkylation of benzene and toluene with light alkenes and light alkanes is reviewed.

1.1. Heterogeneous catalysis

A catalyst is a material that can increase the rate of a chemical reaction without itself being consumed during the process [1, 2]. It acts by providing a more efficient reaction pathway which reduces the activation energy [3]. Catalysis is a very important industrial technology. Approximately 90% of industrial chemical processes use catalysts to produce fuels, building materials, food, medicines and other products in a single stage or more [2, 4]. Many large-scale industrial catalytic processes are heterogeneous, where the catalyst is in one phase (e.g., solid) and reactant is in a different phases (e.g., gas or liquid). Heterogeneous catalysis is used, for example, in the naphtha cracking process over ZSM-5 catalyst to produce ethene and propene [5, 6]. Industrially, heterogeneous catalysis has the advantages of easy catalyst treatment, recycling and easy product separation comparing to costly and difficult product separation in homogeneous catalysis, where the catalyst and reactant are in one phase [7, 8]. Historically, the early use of heterogeneous catalysis can be traced back to the early 19th Century, when Faraday studied an oxidation reaction over heterogeneous catalysis by using platinum as a catalyst [1, 9].

The reaction steps that occur over heterogeneous catalysts are represented in Figure 1.1 for the oxidation of CO to CO_2 using a metal-supported catalyst (gas-solid interface) [4]:

1- Diffusion of substrate molecules through the gas phase to the metal surface of the catalyst.
2- The molecules are adsorbed upon the metal surface.

3- The molecules can dissociate into atoms at the metal surface (depending on their bond strength).
4- The surface reaction between the dissociated molecules on the metal to form adsorbed product, which may be the rate-determining step in a catalytic reaction.
5- The adsorbed product then desorbs from the metal surface into the gas phase.

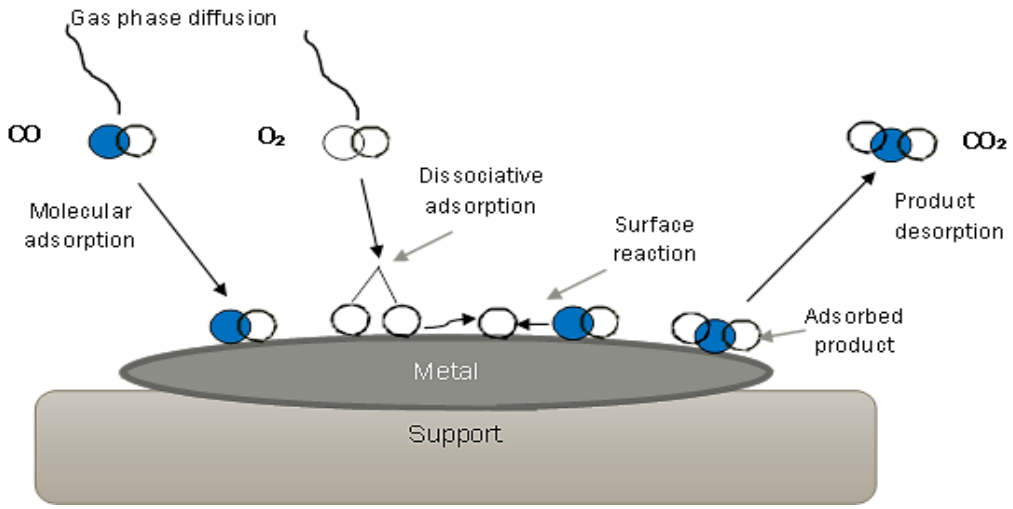

Figure 1.1. Atomic and molecular events occurring in a heterogeneous catalytic reaction over a supported metal catalyst [4].

Several factors should be considered to prepare and develop a catalyst to be used for a particular catalytic reaction [4, 10]. The first factor is the active phase of the catalyst, which is important for kinetic reaction parameters (represented as product yield per unit time). The second factor is the surface area and porosity of active phase. When producing an optimised yield, the catalyst will often have a high surface area. However, in some reactions, a moderate surface area is required to prevent undesired products to be formed (e.g. over-oxidation). The stability of catalyst during the reaction is the third important factor, as almost all catalysts decay in activity with the time of the reaction. This can be caused by 1) poisoning, which can reduce active sites density on the catalyst; 2) coke formation on the catalyst surface through side reactions of organic compounds; 3) sintering of a deposited metal, which can reduce the surface area of active phase. The fourth factor to be considered is

the shape of the catalyst, which will significantly affect its efficiency, mechanical strength and stability. In addition to these factors, the cost of the catalyst and the process must be lower than the product selling price. Another factor to be considered is that the catalyst must be environmentally friendly, minimising the level of toxic by-products of the reaction, while the catalyst itself must not release toxic chemicals into the environment.

1.2. Multifunctional catalysis

Multifunctional catalysts contain two or more different chemical functionalities (metal, acid, base, enzyme, etc.), which can act simultaneously to carry out a multistep chemical reaction in one step (one pot). In order to reduce waste, energy consumption, intermediate isolation steps and production cost, tandem (also known as cascade or domino) catalytic processes have been developed using multifunctional catalysis to provide environmentally friendly technologies with high selectivity for desirable products and high reactant conversion [11, 12]. Figure 1.2 illustrates a step-by-step reaction in which product D is obtained from reactant A through the formation of two intermediate compounds B and C via three steps. These intermediates should be isolated and purified, after each step, with a large quantity of waste formed (solid arrows), which makes the operation costly and time consuming. These disadvantages can be overcome by using tandem processes with multifunctional catalysts (dotted arrows) [13-15].

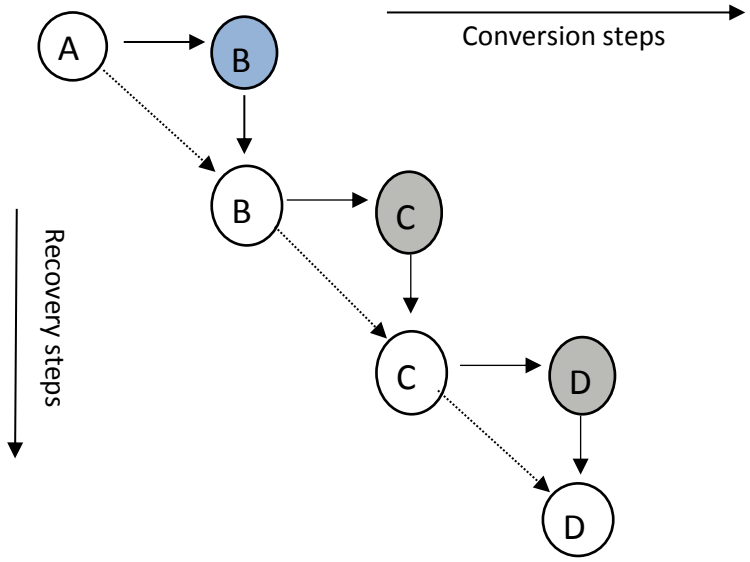

Figure 1.2. Tandem process versus traditional step-by-step process. Solid arrows represent recovery step after each conversion step in a traditional multistep organic reaction. Dotted arrows represent a tandem process to produce the final product without intermediate separation [13].

Tandem processes can overcome thermodynamic limitations for highly energetic intermediate compounds as shown in Figure 1.3. This can be achieved by balancing equilibrium-limited endothermic steps with exothermic steps to produce the target product [13, 16].

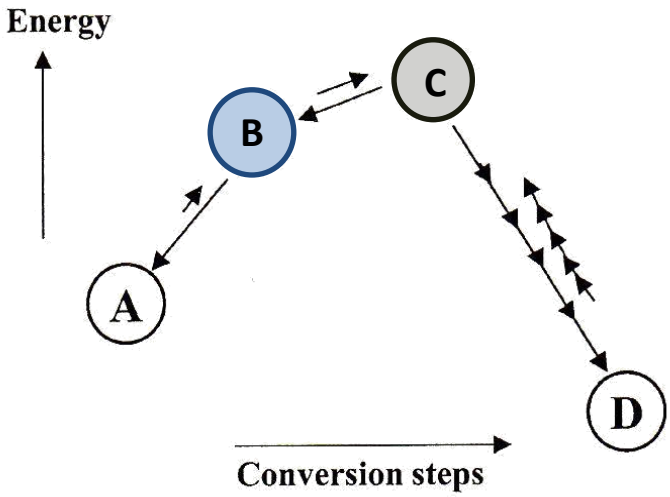

Figure 1.3. Potential energy diagram of tandem process to overcome thermodynamic barriers in multistep synthesis [13].

Designing and preparing a multifunctional catalysts, which can contain two or more active sites, is an important step to develop the tandem processes. The different active sites in such catalysts work simultaneously to effect one or more steps in sequential reactions in one-pot system. Nowadays, catalyst scientists are developing multifunctional catalysis that can be used to produce various organic chemicals via economically and environmentally sustainable processes [17].

Heterogeneous multifunctional catalysis has focussed extensively on developing catalysts made from transition metals on a support possessing acidic and/or basic sites. For instance, in early studies, Pt supported multifunctional catalysts were found to be efficient in the isomerisation of paraffins, hydroisomerisation of naphthenes and hydrocracking of paraffins [18-22]. Furthermore, multifunctional catalysts were widely investigated for one-pot synthesis of methyl isobutyl ketone (MIBK) from acetone [23-27]. This process involves a bifunctional catalyst comprising a metal supported on an acidic or basic support [28]. Firstly, acetone is transformed to diacetone alcohol (DA) on acid site, which is then dehydrated on the acid site to mesityl oxide (MO), followed by hydrogenation of MO to form MIBK on the metal site, as shown in Scheme 1.1.

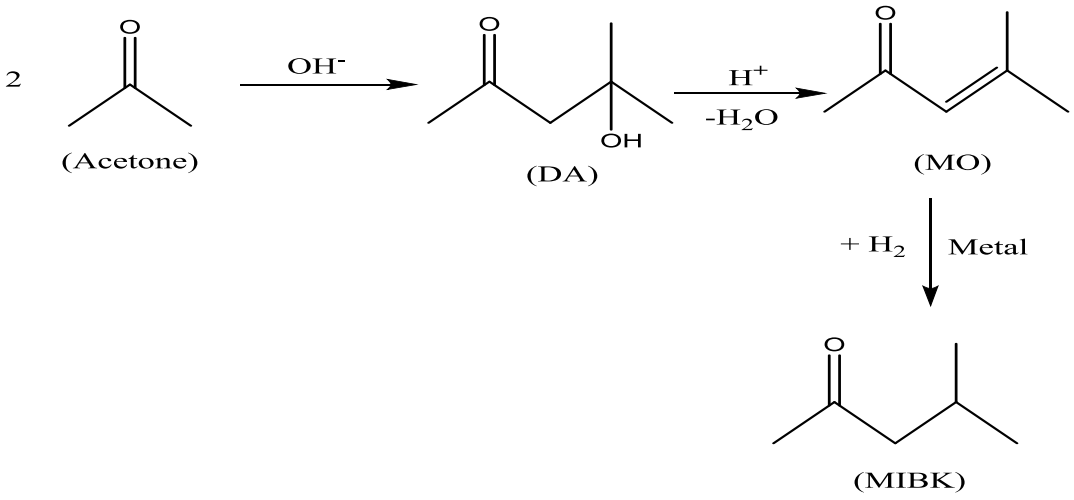

Scheme 1.1. Three-step production of MIBK from acetone over multifunctional catalysts [27]

1.3. Bifunctional metal-acid catalysts

These catalysts contain metal sites (e.g. Pt, Pd, etc.) and acid sites (Brønsted and/or Lewis acid sites). Metal-acid bifunctional catalysts are very important for several industrial processes, for example, alkane isomerisation. When using only metal catalyst or only acid catalyst for the isomerisation of n-hexane to isohexanes, the n-hexane conversion was < 1% at 373 °C and 1 atm. However, when using metal-acid bifunctional catalyst (Pt/SiO_2-Al_2O_3) the conversion increased to 6.8% [29].

Pt-HPA/ZrO_2 bifunctional catalysts (where HPA is a heteropoly acid, e.g., $H_3PW_{12}O_{40}$ or $H_4SiW_{12}O_{40}$) were used for glycerol hydrogenolysis to form 1-propanol and 2-propanol at 230 °C and atmospheric pressure in the gas phase, as shown in Scheme 1.2 [30].

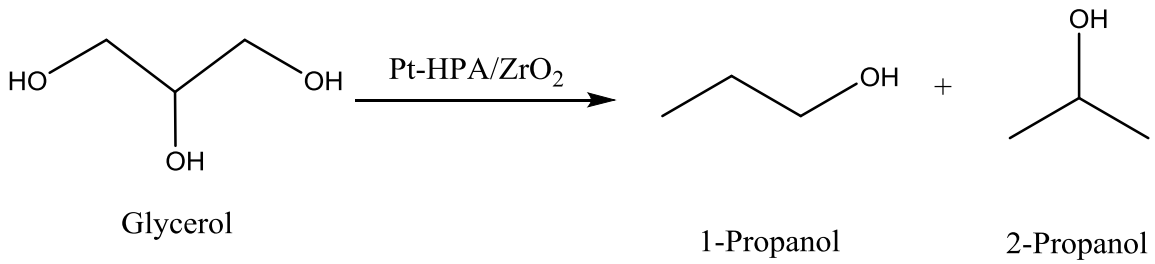

Scheme 1.2. Glycerol hydrogenolysis to form 1- and 2-propanol over metal-acid biltifunctional catalysts.

Poole et al. [31] studied ketone hydrodeoxygenation to form alkane over metal-acid bifunctional catalysts (metal = Pt and acid = $Cs_{2.5}H_{0.5}PW_{12}O_{40}$ (CsPW)) in the gas phase at 40-80 °C (Scheme 1.3).

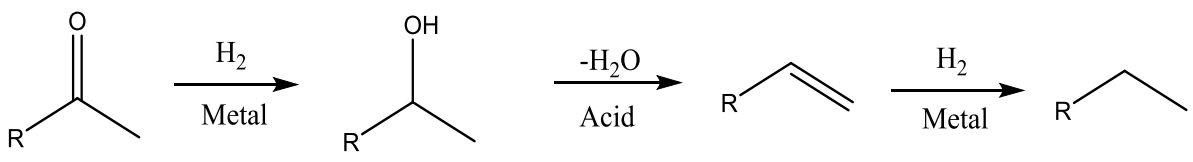

Scheme 1.3. Ketone hydrodeoxygenation to form alkane over metal-acid biltifunctional catalysts.

Pd-$H_3PW_{12}O_{40}/SiO_2$ has been used to produce (-)-menthol from (+)-citronellal in one-step process [32]. This reaction comprises two chemical steps as shows in Scheme 1.4. The first step uses the acid sites and the second step uses the metal sites.

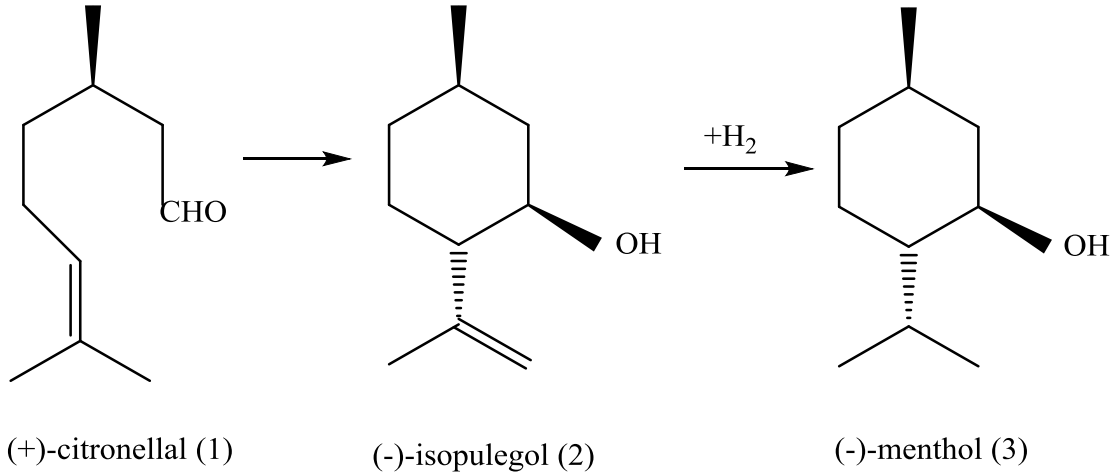

Scheme 1.4. One-step formation of (-)-menthol from (+)-citronellal over Pd-$H_3PW_{12}O_{40}/SiO_2$ [32].

1.4. Catalysis by heteropoly acids (HPAs)

HPAs are complex proton acids that comprise polyoxometalate anions (heteropolyanions), which have metal-oxygen octahedra in their structure [11]. The general chemical formula of herteropolyanions is $[X_xM_mO_y]^{q-}$ ($x \leq m$), where X is the heteroatom or central atom, M is the addenda atom (metal ion), and x, m and y are the number of atoms X, M and O, respectively. Typical heteroatoms are B^{3+}, Si^{4+}, Ge^{4+}, P^{5+} and As^{5+}. The most typical addenda atoms used are molybdenum (VI) and tungsten (VI), while vanadium (V) and niobium (V) are less frequently employed [11].

Heteropolyanions are commonly formed via a self-assembly process in an aqueous acidic solution as shown in equations 1.1-1.2 [33].

$$8H^+ + 7WO_4^{2-} \longrightarrow [W_7O_{24}]^{6-} + 4H_2O \quad (1.1)$$

$$23H^+ + HPO_4^{2-} + 12WO_4^{2-} \longrightarrow [PW_{12}O_{40}]^{3-} + 12H_2O \quad (1.2)$$

The scientist who discovered the first heteropoly compound was Berzelius in 1826. Since then, many studies have been conducted on the synthesis of heteropoly compounds and their structural characterisation [33]. Due to their unique physicochemical properties, they are widely used as homogeneous and heterogeneous acid and oxidation catalysts [11, 34].

HPAs in the solid state generally exist as ionic crystals and consist of large heteropolyanions, (primary structure), protons as the counter cations, water of crystallisation and other molecules (secondary structure). The constructive feature of the solid HPAs is their tertiary structure, which includes the particle size, the proton distribution within the particles and the pore structure as illustrated in Figure 1.4. [35].

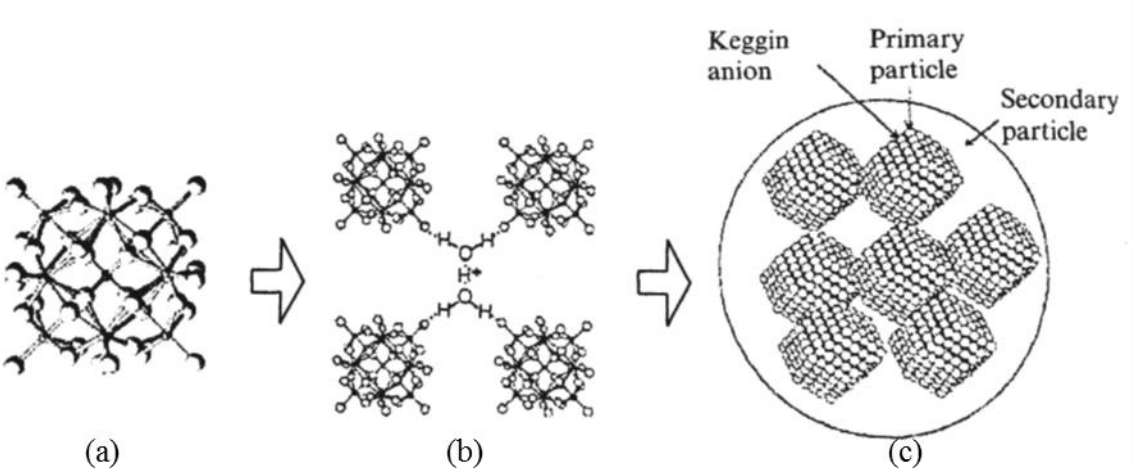

Figure 1.4. Primary, secondary and tertiary structures of heteropoly compounds: (a) primary structure (Keggin structure, $XM_{12}O_{40}$); (b) secondary structure ($H_3PW_{12}O_{40}.6H_2O$); (c) tertiary structure of bulk $Cs_{2.5}H_{0.5}PW_{12}O_{40}$ [33].

Structurally, there are many types of heteropoly acids, differing in atomic ratio of the heteroatom and metal atom present. Figure 1.5 shows the most common types of heteropolyanions.

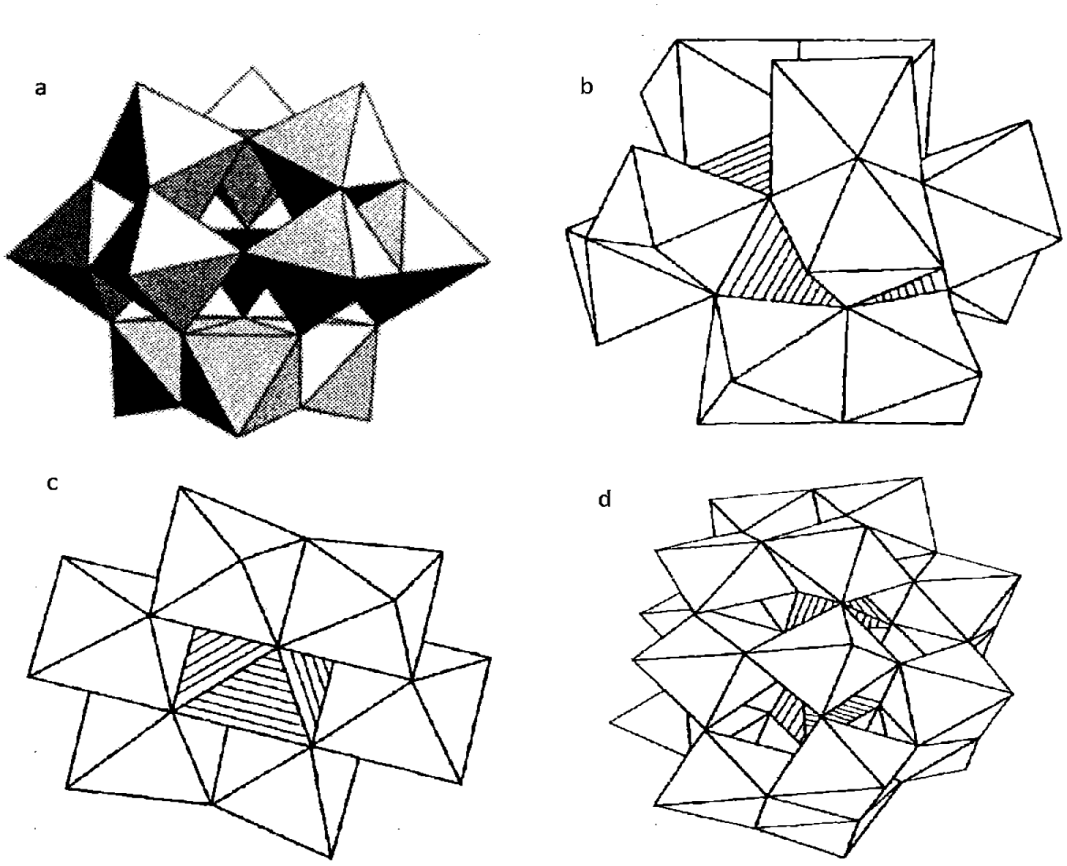

Figure 1.5. Different structural types of heteropolyanions: (a) Keggin structure, (b) Dexter-Silverton structure, (c) Anderson-Evans structure, (d) Wells-Dawson structure [33].

1.4.1. The Keggin structure

There are many structural types of HPAs [12]; however, the most common one is the Keggin structure. The Keggin heteropolyanion is typically represented by the formula $[XM_{12}O_{40}]^{x-8}$, where X is the central atom (Si^{4+}, P^{5+}, etc.), x is its oxidation state and M is the metal ion (usually W^{6+} or Mo^{6+}) [33, 36]. The structure of the Keggin anion is composed of a central tetrahedron (XO_4) surrounded by 12 edge- and corner-sharing metal-oxygen octahedra (MO_6), which are arranged into four groups of M_3O_{13}. Each group is made up of three octahedra sharing edges through a common oxygen atom, which is linked to the central

tetrahedron XO_4 as illustrated in Figure 1.6 [33]. The structure involves four types of oxygen atoms, which are:

- 12 terminal $M=O_t$
- 12 edge-sharing angular $M\text{-}O_{b1}\text{-}M$ shared by the octahedra within a M_3O_{13} group.
- 12 corner-bridging quasi-linear $M\text{-}O_{b2}\text{-}M$ connecting two M_3O_{13} groups.
- 4 internal $X\text{-}O_c\text{-}M$ [37].

It is possible to discriminate these types of oxygen atoms by ^{17}O NMR and Fourier transform infrared (FTIR) spectroscopy in the fingerprint range of 600-1100 cm^{-1} [11, 33].

Heteropolyanions of the Keggin structure are the most stable and most widely used for catalysis both homogeneous and heterogeneous. Typical Keggin HPAs, such as $H_3PW_{12}O_{40}$, $H_4SiW_{12}O_{40}$, $H_3PMo_{12}O_{40}$ and $H_4SiMo_{12}O_{40}$, are commercially available [12].

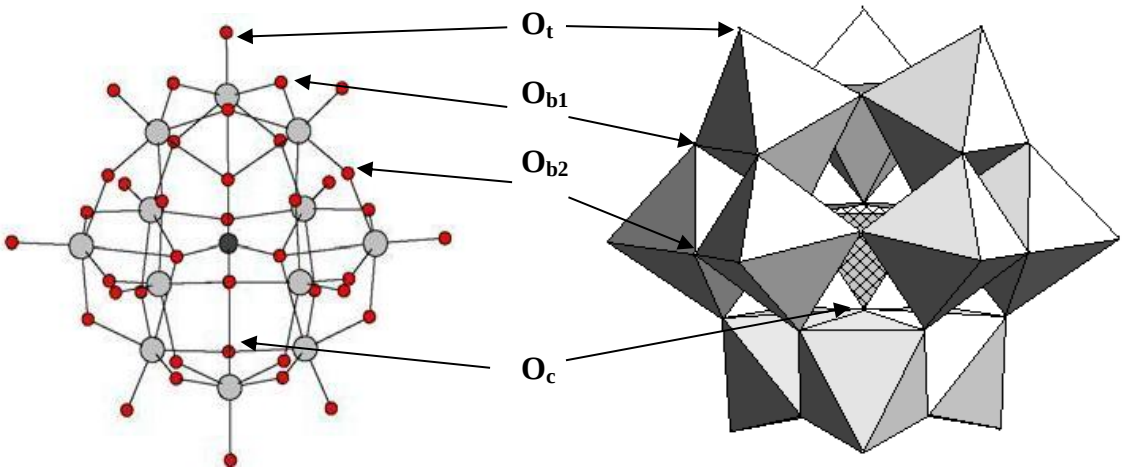

Figure 1.6. The Keggin structure of $[XM_{12}O_{40}]^{x-8}$ anion in ball-and-stick (left) and polyhedral (right) representations [33].

Heteropoly acids have a sufficiently high thermal stability which makes them suitable for use in heterogeneous catalytic reactions, which often operate at relatively high temperatures. The decomposition temperature of $H_4SiW_{12}O_{40}$ is 370 ºC, while $H_3PW_{12}O_{40}$

decomposes at 450 ºC and has the highest thermal stability among the Keggin type heteropoly acids.

The caesium salt of $H_3PW_{12}O_{40}$, $Cs_{2.5}H_{0.5}PW_{12}O_{40}$ ($Cs_{2.5}PW$), begins to decompose at a higher temperature of 500 ºC and is insoluble in water and most organic solvents. This makes it ideal material for use as a heterogeneous acid catalyst in solid/liquid and solid/gas systems.

1.4.2. Thermal stability of HPAs

The thermal stability of HPAs is a very important feature regarding their use in heterogeneous catalysis. As mentioned above, some HPAs are stable at relatively high temperatures, up to 450 °C ($H_3PW_{12}O_{40}$). However, there is an important issue of the thermal stability of HPAs regarding their regeneration, e.g., in catalyst decoking process, which is carried out at higher temperatures of 500-550 ^oC [33]. The thermal stability can be measured by thermogravimetric analysis (TGA), differential thermal analysis (DTA), differential scanning calorimetry (DSC), X-ray diffraction (XRD), infrared spectroscopy (IR) and solid state NMR. The most thermally stable type of HPA structure is the Kegging structure. The stability of Keggin HPAs can be measured in terms of their thermal decomposition temperature, when all acidic protons are lost, as shown in Scheme 1.5 [11, 12, 33]. The thermal stability (decomposition temperature) of commonly used Keggin HPAs, as estimated by the thermogravimetric analysis (TGA), decreases in the order: $H_3PW_{12}O_{40}$ (465 °C) > $H_4SiW_{12}O_{40}$ (445 °C) > $H_3PMo_{12}O_{40}$ (375 °C) > $H_4SiMo_{12}O_{40}$ (350 °C) [12, 29]. However, under reaction conditions, solid HPAs might be decomposed at lower temperatures then those measured by the TGA.

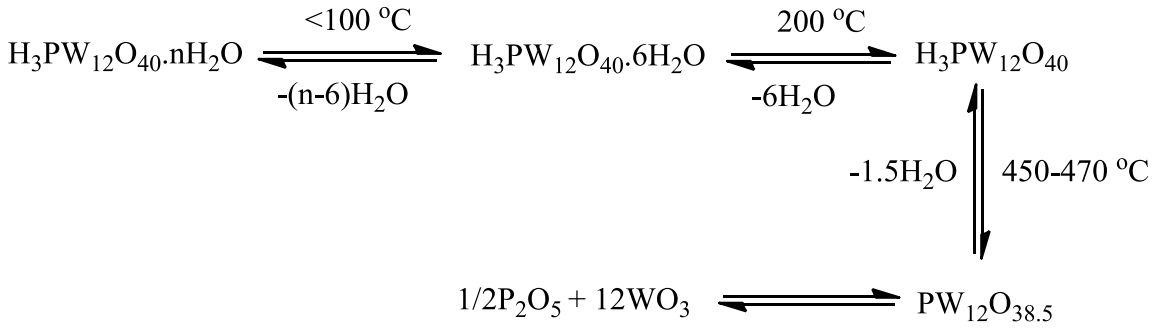

Scheme 1.5. Thermal decomposition of $H_3PW_{12}O_{40}$ hydrate.

1.4.3. Acidity of HPAs

HPAs have pure Brønsted acidity, which is stronger than the acidity of other solid acids such as zeolites and acidic oxides. The acid strength of Keggin HPAs decreases in the order: $H_3PW_{12}O_{40} > H_4SiW_{12}O_{40} > H_3PMo_{12}O_{40} > H_4SiMo_{12}O_{40}$ [20]. The acid sites in HPAs are more uniform and easier to control than those in other solid acid catalysts.

Two types of protons have been found in crystalline HPAs, as illustrated in Figure 1.7. The first type is hydrated protons (a), while the other one is non-hydrated protons (b) [11, 33]. The hydrated protons are highly mobile, which is responsible for the high proton conductivity of crystalline hydrated HPAs. The non-hydrated protons possess much less mobility and are localised on the outer oxygen atoms [33].

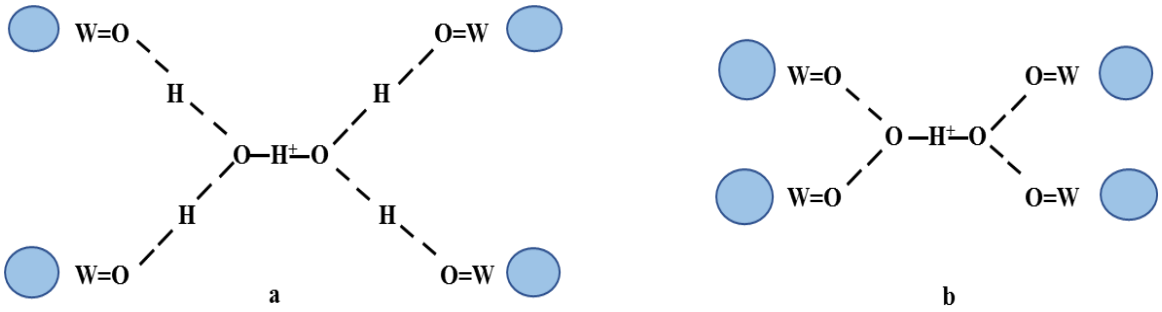

Figure 1.7. Schematic structure of proton sites in (a) $H_3PW_{12}O_{40}.6H_2O$ and (b) anhydrous $H_3PW_{12}O_{40}$.

In solid HPAs, the surface proton sites are stronger than the bulk ones; thus, they are more important for heterogeneous catalysis. The surface area and porosity of crystalline HPAs are generally low (< 5 m^2 g^{-1} and < 0.1 cm^3 g^{-1}, respectively) [11, 33, 36, 38]. The surface proton sites are localised at the bridging oxygen atoms in the surface Keggin units. In order to enhance the surface area and surface acidity, HPA is often supported on porous supports (e.g. silica) [11].

1.4.4. Acidity of supported HPAs

As mentioned above, bulk HPAs have a low surface area. So it is important for catalytic applications to support HPAs on high surface area support of acidic or neutral nature in order to increase the number of active acid sites as well as the thermal stability [11]. Both catalytic activity and acidity of supported HPAs are dependent on the nature of support, the HPA loading and pre-treatment conditions [11, 33]. The most common supports used for supporting HPAs are silica (SiO_2), active carbon, titania, zirconia, etc. [39-42].

The acid strength of the $H_3PW_{12}O_{40}$ (HPW), measured by microcalorimetry of NH_3 adsorption, decreased when HPW was supported on SiO_2, due to the chemical interaction between the HPW and support [43-45] (Figure 1.8). The thermal stability of HPW on silica seems to be comparable to or lower than that of bulk HPW without support [11, 33]. It has reported that at 20% or less of HPW loading on silica support, more than 80% of HPW proton sites are lost due to strong chemical interaction between HPW and SiO_2 [11, 39].

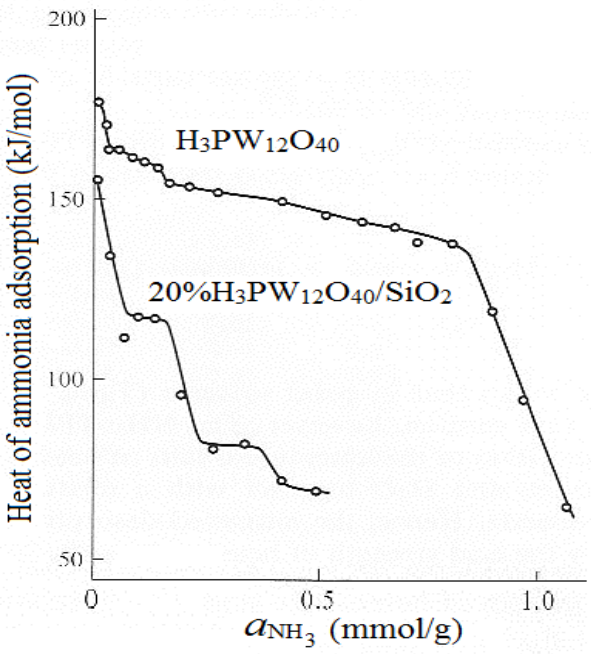

Figure 1.8. Differential heat of ammonia adsorption onto $H_3PW_{12}O_{40}$ and 20% $H_3PW_{12}O_{40}/SiO_2$ measured at 150 ^oC (pretreatment at 300 $^oC/10^{-3}$ mmHg) [33].

1.4.5. Metal-HPA multifunctional catalysts

The unique properties of HPAs, such as their acid and redox properties, allow for their use as multifunctional catalysts in combination with transition metals (Pt, Pd, Ru, etc.), which can be used effectively in multistep reactions [11, 33, 36, 46]. Some insoluble HPA acidic salts such as $Cs_{2.5}H_{0.5}PW_{12}O_{40}$ (CsPW) have strong proton acidity along with high surface area. Therefore, these compounds can serve as an acidic support for metal-acid bifunctional catalysts [47, 48]. For instance, supported Pd on CsPW was successfully utilised for one-pot synthesis of MIBK from acetone [46], which is shown in Section 1.2. Alhanash et al. [49] studied the hydrogenolysis of glycerol to form propanediol over Ru supported on CsPW. The deoxygenation of propanoic acid over metal-acid bifunctional catalysts was reported by Alotaibi et al. [50]. Additionally, Pd-HPW/SiO_2 was used for producing (-)-menthol from (+)-citronellal, as mentioned in Section 1.4 [32].

1.5. Catalysis by zeolites

Zeolites are natural or synthetic microporous crystalline materials with three-dimensional networks built from SiO_4 and AlO_4 tetrahedra that are linked by corner-shared oxygen atoms [29]. The general structural formula of zeolite is $A^{m+}_{y/m}[(SiO_4)_x(AlO_4)_y].wH_2O$, where m is the valence of cation A, x and y are the integers with $x/y \geq 1$, which is called the framework silica/alumina ratio and w is the number of water molecules per unit cell.

Zeolites are highly porous materials due to the extensive framework of channels that are characteristic of the zeolite structure and result in high surface area (400-800 $m^2\ g^{-1}$), which is a favourable property for catalysis. Water molecules and small cations, that counter the negative charge of tetrahedral AlO_4^-, fill the voids in the structure of zeolite. Zeolites are microporous materials with uniform pores of molecular dimensions (< 2 nm in diameter), which make them useful for shape selective catalysis.

There are three kinds of shape selectivity [51-53] (see Figure 1.9):

1. Reactant selectivity: only reactant molecules with the dimensions corresponding to the zeolite pore size can access the active sites.
2. Product selectivity: product molecules with certain dimensions can exit the pores of zeolite catalyst and leave the channels.
3. Restricted transition state selectivity: in certain reactions, the intermediates or transition states require more space than allows the pore size.

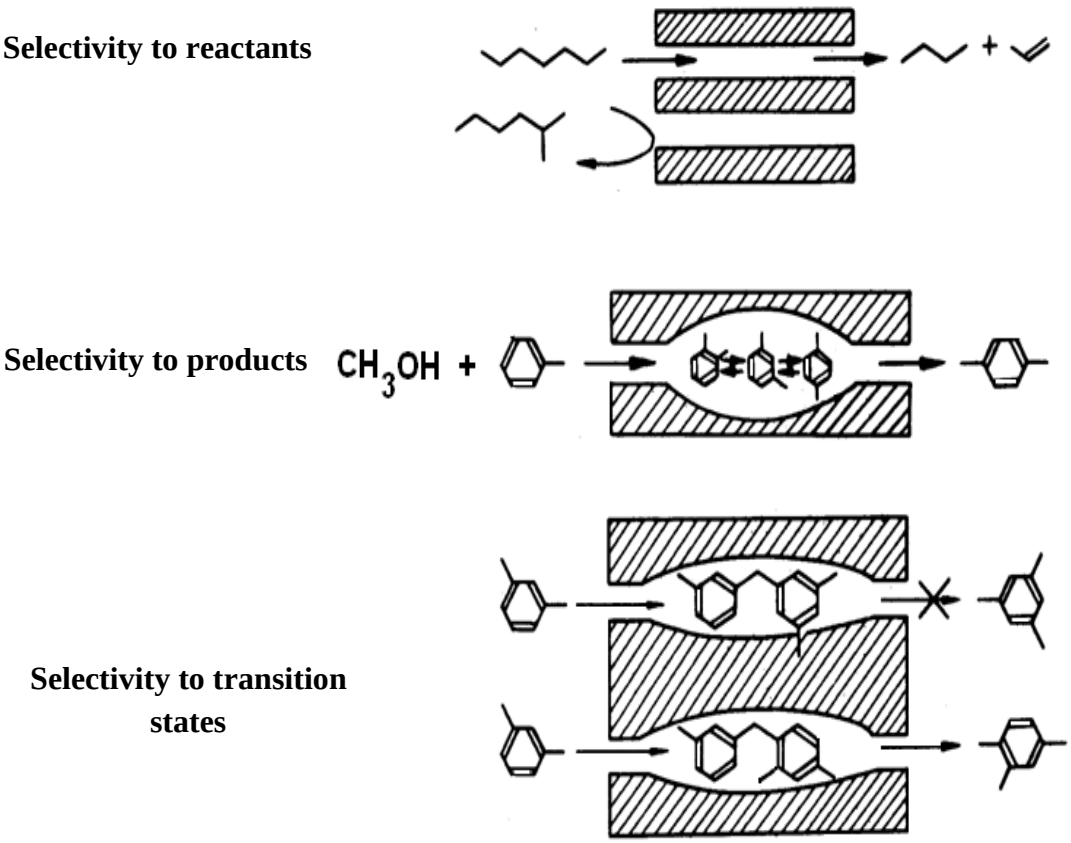

Figure 1.9. The three types of zeolites shape selectivity [51].

1.5.1. Acidity of zeolites

Acidity is one of the most important properties of zeolites regarding their catalytic applications. Synthetic zeolites are commonly prepared by using sodium ions to balance the framework charges. The sodium ions can be exchanged to generate Brønsted acid sites, which are required for most catalytic applications of zeolites. Brønsted acid sites are generated by introducing ammonium ions into the structure, followed by heat treatment. When the ammonia is removed, protons are introduced, which counter the tetrahedral aluminium atoms charge and are localised on the oxygen atoms in the lattice SiOAl groups. Further heat treatment (≥ 500 °C) leads to the creation of Lewis acid sites as a result of removing water molecules from the structure as seen in Figure 1.10 [54].

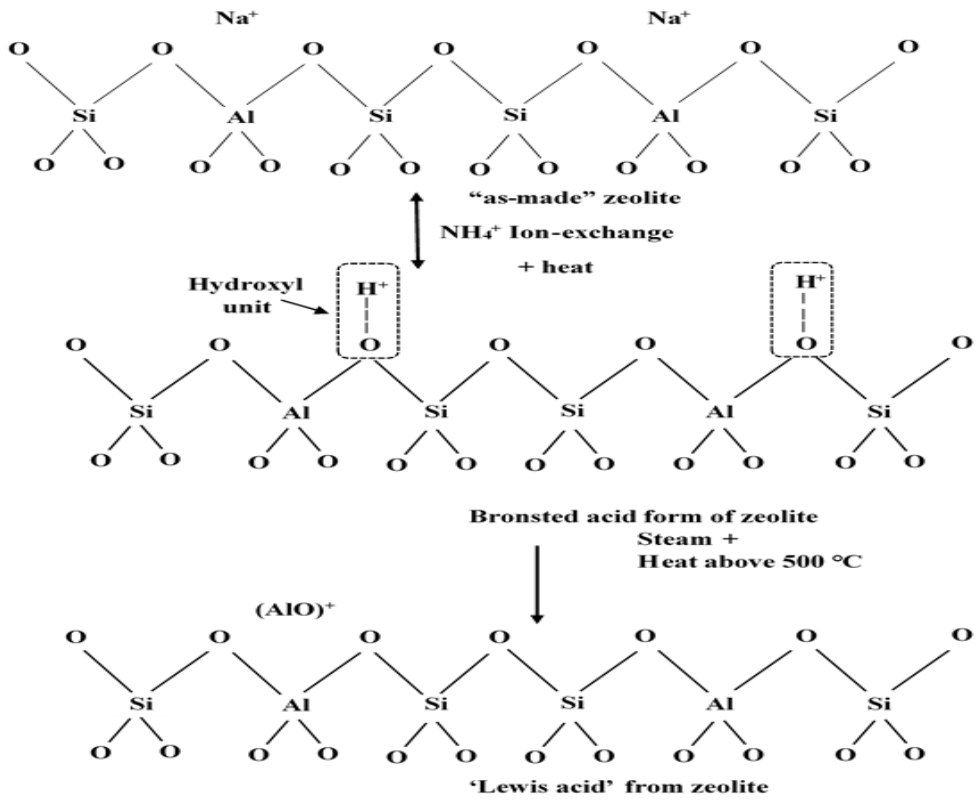

Figure 1.10. Development of internal acidity of zeolite by exchanging NH_4^+ cation [54].

The evaluation of zeolite acidity includes the total number of Brønsted and Lewis sites, their location and their strength distributions [52]. Adsorption of pyridine using FTIR spectroscopy is one of the commonly used techniques to determine the nature of acid sites of zeolites. Moreover, the ratio of Si/Al can be used to determine the zeolites acidity [52]. It has been found that the acid strength of Brønsted sites in zeolites with the same Si/Al ratio follows the order H-ZSM-5 > H-Mordenite > H-Beta > H-Y, which shows the effect of framework type on the acid strength [55-57]. Generally, the number of strong Brønsted sites increases with increasing the Si/Al ratio, whereas the total number of acid sites is reduced [52, 58-61]. It has been established that Brønsted acid sites are the main source of catalytic activity of zeolites [53].

Because of the unique properties of zeolites, they have been widely employed as catalysts for more than 40% of chemical and petrochemical industrial reactions [62]. By the end of 2014, 44 naturally occurring zeolites had been discovered and more than 160 zeolite frameworks had been synthetically produced [29].

ZSM-5 (Zeolite Socony-Mobil Five) is one of the most utilised zeolites in industry. Its strong acidity, which is introduced by the framework aluminium, is a major contributor to its catalytic activity. Changing the zeolite acidity (e.g., by varying the Si/Al ratio) may affect the reaction pathways and the product distribution [63]. One of industrial applications of ZSM-5 is the cracking of paraffins, where ZSM-5 forms carbonium ions via protonation of paraffins such as n-butane and n-hexane producing olefins, lower paraffins and hydrogen gas [51]. ZSM-5 is also used industrially to produce alkylbenzenes and alkyltoluenes as discussed in the next section.

1.6. Alkylation of aromatic compounds by alkanes

This section details the alkylation of aromatic compounds (benzene and toluene) by light alkanes over bifunctional metal-acid catalysts – the topic relevant to our research. But first, the conventional aromatic alkylation with alkenes over solid acid catalysts is discussed.

1.6.1. Conventional alkylation of aromatic compounds with alkenes

Acid-catalysed alkylation of aromatic compounds such as benzene and toluene with alkenes is an established commercial process for the manufacturing of a wide range of alkylbenzenes and alkyltoluenes. The alkylation of benzene and toluene with ethene and propene is used to produce ethylbenzene (EtPh), isopropylbenzene (iPrPh), p-ethyltoluene and p-isopropyltoluene (p-cymene), respectively, which are very important intermediates in the manufacturing of styrene, phenol, p-methylstyrene and p-cresol [64-66]. About 70% of the global demand for benzene (29.3 million tons) in 1999 was consumed in the alkylation

reaction with ethene and propene over acid catalysts (53 and 17% respectively) to produce EtPh and iPrPh [65].

The first solid catalyst used in the alkylation of benzene with light alkenes (ethene and propene) in the gas phase was amorphous silica-alumina in the 1940s [67]. In 1966, Venuto et al. [68] found that zeolites such as HY and REY, which are large pore zeolites, are more efficient catalysts as compared to the amorphous silica-alumina. In 1976, Mobil-Badger first used zeolite catalyst for industrial alkylation and it is still widely used. This process employs ZSM-5 (a medium pore zeolite) for benzene alkylation with ethene in the gas phase at 390-450 ºC [69]. Investigation of the alkylation of benzene with propene over zeolite dates back to 1965 [70]; however, it took a long time to commercialise this process.

Figure 1.11 shows the alkylation of benzene with ethene over acid catalyst to produce EtPh, which can react further with ethene producing diethylbenzene (DEB) and triethylbenzene (TEB).

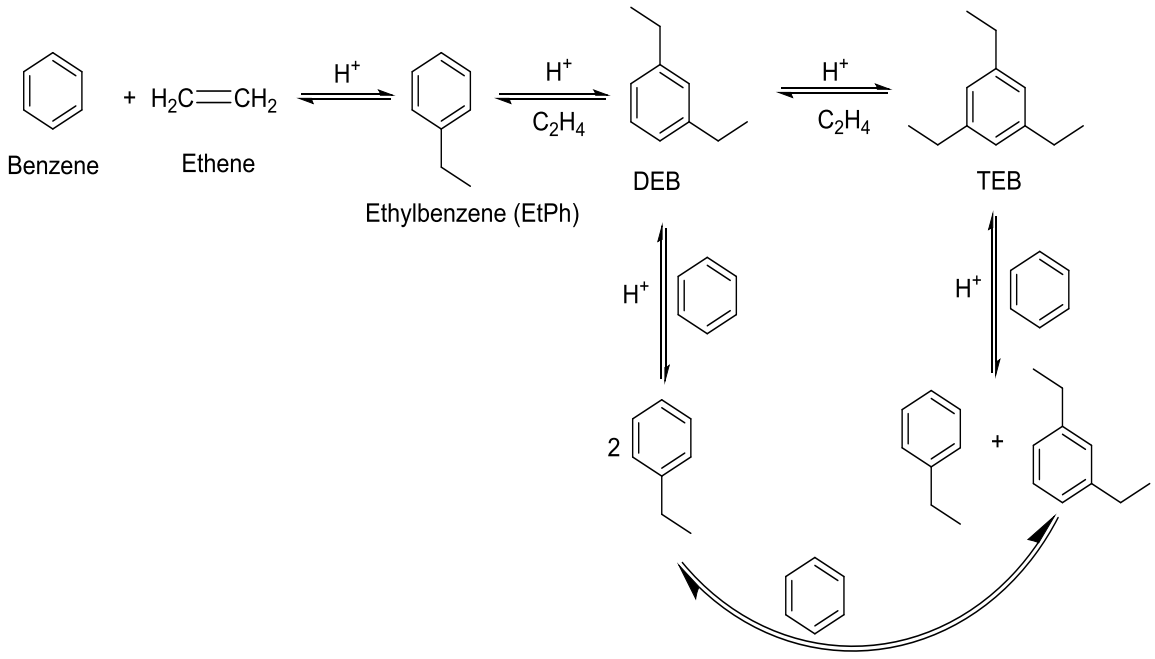

Figure 1.11. Alkylation of benzene with ethene over acid catalyst [65, 69].

Figure 2.12 illustrates the alkylation of benzene with propene over acid catalyst.

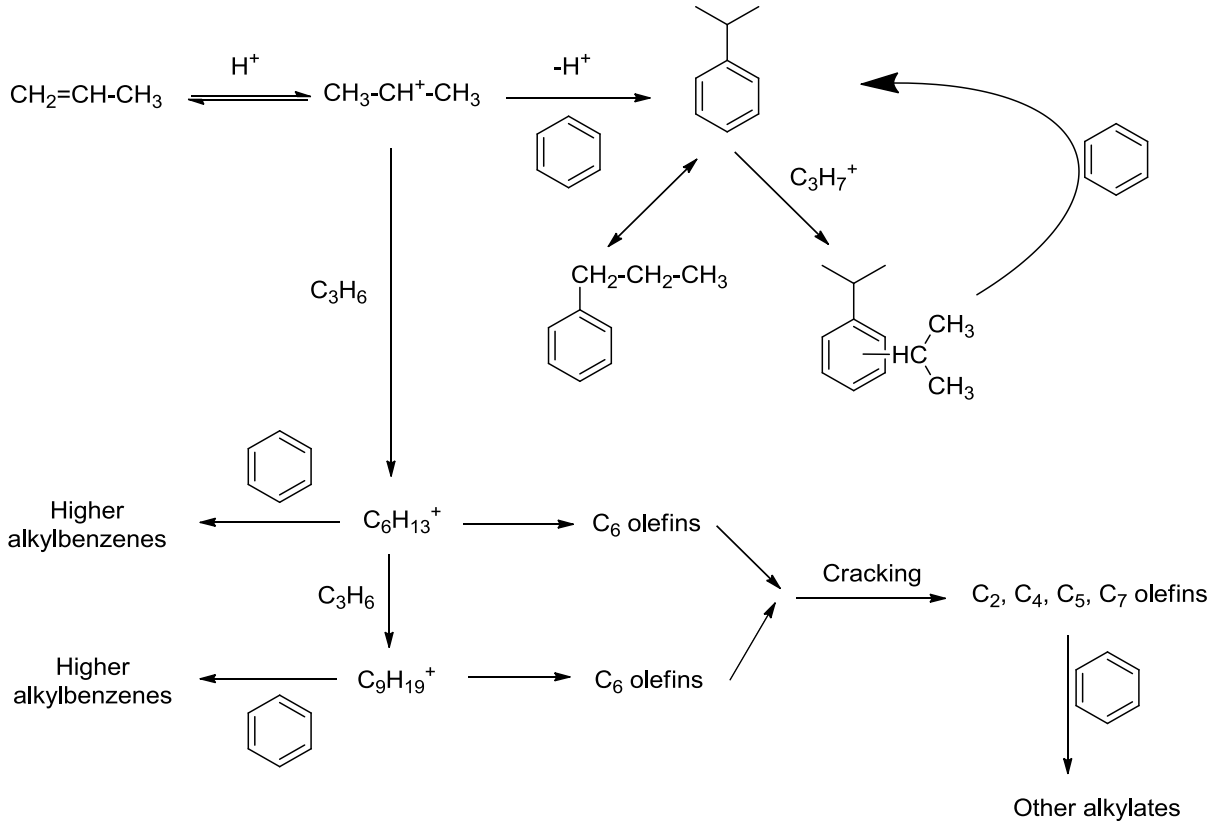

Figure 1.12. Alkylation of benzene with propene over acid catalyst [65].

Bohstrom et al. [71] reported the alkylation of toluene by ethene using the normal microporous HZSM-5 zeolite and a modified HZSM-5 that contained mesopores in addition to micropores. The zeolite containing mesopores gave higher overall conversion as well as higher yield of C9 product, which may be explained by higher mobility of molecules in mesopores. Cejka et al. [72] studied the alkylation of toluene with ethene over HY and HZSM-5 zeolites. High selectivity to p-ethyltoluene was achieved using HZSM-5 at 347 ºC. Engelhardt et al. [73] studied the alkylation of toluene with ethene over HZSM-5 at 400 ºC and atmospheric pressure.

Cejka et al. [74] studied the alkylation of toluene with propene using zeolite MCM-41. They achieved high selectivity to p-cymene (45.6%) using MCM-41 zeolite with a Si/Al ratio

of 35 at 247 ºC and toluene/propene molar ratio of 9.6. Even better p-cymene selectivity (49.9 %) was attained by using HPA/MCM-41 (HPA = $H_6PV_3Mo_9O_{12}$) [74]. Prokesova et al. [75] used Beta zeolites for the alkylation of toluene with propene in the gas phase (commercial zeolite Beta, micro/mesoporous composites and nanosized zeolite Beta). They found that toluene conversion depended on the size of zeolite crystals and the acidity of catalysts. The best result was achieved by using nanosized Beta with a Si/Al ratio of 33 and toluene/propene ratio of 2 at 250 ºC; this gave 20.2% toluene conversion with 88% cymene selectivity. The alkylation of toluene with propene in the gas phase was also studied over zeolites MCM-22 and MCM-58 [76]. It was reported that zeolite MCM-22 was more selective to cymenes. Rigoreau et al. [77] used H-MCM-22 (Si/Al = 15) in alkylation of toluene with propene at 200 ºC.

1.6.2. Alkylation of benzene with light alkanes

Effective functionalization of light alkanes found in natural gas, such as methane, ethane and propane, has long been and remains one of the greatest challenges of catalysis science [78,79]. Ethene and propene can be replaced in reactions with aromatic compounds by abundant and inexpensive alkanes like, ethane and propane, which can lead to cost-effective and environmentally benign production of these commodity chemicals. The direct alkylation of benzene with light alkanes to form EhPh and iPrPh has attracted particular interest [80]. As mentioned above, EtPh and iPrPh are the key intermediates in manufacturing styrene and phenol [64].

The direct benzene alkylation with light alkanes was first reported in 1975 by Olah et al. [81] in liquid superacid media to generate EtPh and iPrPh in low yields (1.0 and 1.4%) at 25 °C within 24 h reaction time [81]. Later, environment-friendly solid catalysts have been discovered for alkylation of benzene with ethane [82-90] and propane [91-96] in the gas phase. These catalysts comprise zeolites modified with metals such as Pt, Pd, Re, Ga or Zn

and operate via bifunctional pathway, which includes alkane dehydrogenation on metal sites to form the corresponding alkene and H_2 (step 1) followed by benzene alkylation with the alkene on acid sites (step 2). Scheme 1.6 shows the overall reaction for alkylation of benzene with propane. Best results have been achieved using Pt-modified HZSM-5 zeolites (MFI structure). Lukyanov et al. [85] have reported >90% EtPh selectivity at a close to equilibrium benzene conversion of 11.6% in the alkylation of benzene with ethane over 1%Pt/HZSM-5 (Si/Al = 36) at 370 ^{o}C, $[C_6H_6]/[C_2H_6]$ = 1:9 mol/mol and 1 bar pressure. The yield can be further increased by adding a hydrogen acceptor to shift equilibrium in step (1), however this effect decreases with time on stream due to saturation of acceptor capacity [88].

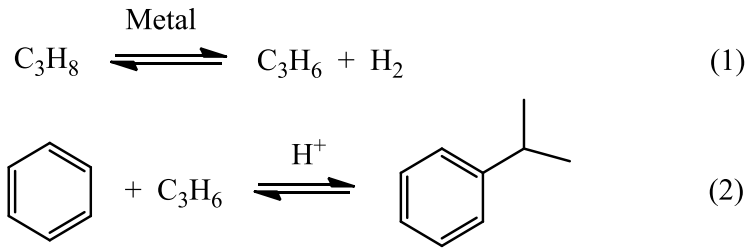

Scheme 1.6. Alkylation of benzene by propane via bifunctional catalysed pathway.

High selectivity alkylation of benzene with propane, in contrast to the reaction with ethane, has proven to be more difficult to achieve. Caeiro et al. [80] and Woltz et al. [97] reviewed the benzene alkylation by light alkanes over metal-acid bifunctional catalysts, where metal sites are responsible for hydrogenation/dehydrogenation steps and acid sites are responsible for the formation of carbenium ions. Ivanova et al. [91] and Bigey and Su [94] have studied benzene alkylation with propane by using Ga-containing ZSM-5 as the catalyst. Almost no activity was observed during benzene alkylation with propane over H-ZSM-5 catalyst at reaction temperatures lower than 500°C.

Smirnov et al. [92] reported the direct benzene alkylation with propane using a range of Pt/HZSM-5 catalysts (Si/Al = 25-160) with and without addition of Zr_2Fe as a hydrogen acceptor to shift propane dehydrogenation equilibrium. In the presence of Zr_2Fe, the conversion of benzene was 14.4% and iPrPh selectivity reached 32% (4.6% yield) over 0.22%Pt/HZSM-5 (Si/Al = 160) at 350 ^oC (1 bar pressure and $[C_6H_6]/[C_3H_8]$ = 1:1). On the other hand, the conversion dropped from 14.4 to 6.6% in the absence of Zr_2Fe while the iPrPh selectivity remained unchanged (2.1% yield). Moreover, the main product was nPrPh (50% selectivity) rather than iPrPh, which is the favourable product from the carbenium ion mechanism [84]. This could be due to product shape selectivity control imposed by HZSM-5, i.e., iPrPh formed initially could probably isomerize on HZSM-5 proton sites to nPrPh, which possesses higher diffusion mobility within zeolite micropores. Other products such as MePh, EtPh and unidentified C_9-C_{11} alkylarenes were also found. MePh and EtPh, which are thermodynamically more favourable than iPrPh, likely arise from cracking reactions on zeolite acid sites [92]. Therefore, the poor selectivity of benzene alkylation with propane on Pt/HZSM-5 is likely the result of the confinement of product molecules within zeolite micropores, causing their isomerization and cracking to produce primarily nPrPh together with the range of cracking by-products observed.

When a physical mixture of supported Pt/non-acid material and zeolite (HMFI) was used, the activity decreased in comparison with the supported Pt/HMFI, where Pt sites are close to acid sites [98]. This result agrees with Smirnov et al. [92] who found that using 1:1 w/w physical mixture of Pt/CeO_2 and HZSM-5 decreased the activity compared to Pt/HZSM-5 at 350 °C. This could also be explained by the decrease in Pt loading in the physical mixture as compared to the supported catalyst [92].

1.6.3. Alkylation of toluene with light alkanes

Ethene [71-73] and propene [74-77, 99] are commercially utilised in the alkylation of toluene to produce alkylaromatic compounds such as ethyltoluene and p-isopropyltoluene (p-cymene). The latter is an intermediate for p-cresol production by oxidation and acid cleavage [65]. Moreover, p-cymene is used to produce fungicides, flavours and perfumes [66].

The direct alkylation of toluene with ethane over bifunctional metal-acid catalysts based on Pt and HZSM-5 zeolite has been reported previously. Sealy et al. [100] described toluene alkylation with ethane to produce ethyltoluene isomers by using 0.9%Pd/HZSM-5 as the catalyst (Si/Al = 25) at 350 ^{0}C. The conversion of toluene reached 2% and the selectivity to ethyltoluenes increased from 30% at the beginning to 60% after 3 h on stream. Bressel et al. [101] have studied the alkylation of toluene by ethane over 0.9%Pd/HZSM-5 with different Si/Al ratios at 300-350 ^{0}C. Better results were achieved using the catalyst with a Si/Al ratio of 20 to obtain a toluene conversion around 5.5% and 60% ethyltoluene selectivity in 3 h on stream at 350 ^{0}C. Singer et al. [102] investigated the alkylation of toluene with ethane over 1%Pd/HZSM-5 (Si/Al = 20) as the catalyst at 350 ^{0}C and 1 bar pressure to achieve 6% toluene conversion and 3.4% ethyltoluene yield . They also reported that increasing the pressure lead to an increase in toluene conversion up to 27% at 50 bar with 29% ethyltoluene selectivity (7.8% yield). Alireza et al. [103] reported the alkylation of toluene with ethane by using 0.4%Pt/HZSM-5 (Si/Al = 28) as the catalyst at 350 ^{0}C and 30 bar. At 2 h on stream and with a contact time of 0.12 h, the conversion of toluene was 11% and the selectivity of ethyltoluene isomers was 20%. The toluene conversion decreased with increasing the time on stream, whereas the selectivity of ethyltoluene isomers increased, which made the ethyltoluene yield nearly constant. In contrast to toluene alkylation with ethane, the reaction with propane has not been studied, to the best of our knowledge.

1.7. Objectives and thesis outline

Effective functionalisation of light alkanes such as ethane and propane can be achieved by involving alkanes in reactions with aromatic hydrocarbons. The direct alkylation of benzene and toluene with propane to produce cumene and p-cymene has attracted particular interest [80]. Previous work indicates that the poor cumene selectivity obtained so far in the alkylation of benzene with propane over Pt/HZSM-5 catalyst results from the confinement of product molecules within zeolite micropores causing their isomerisation and cracking. It is, therefore, anticipated that the selectivity of aromatic alkylation with propane could be improved by using bifunctional metal-acid catalysts possessing larger pores. In this context, heteropoly acids supported on silica, HPA/SiO_2, can be considered as a promising alternative to zeolites in such catalysts due to the strong acidity of HPA and meso/macroporous structure of silica.

The aims of this study are:

- To study the alkylation of benzene with propane over bifunctional metal-acid catalysts in the gas phase using Pt and Pd as the metal components and silica-supported tungsten HPAs $H_3PW_{12}O_{40}$ and $H_4SiW_{12}O_{40}$ (the strongest Keggin HPAs) as the acid components in such catalysts.
- To study the alkylation of toluene with propane in the gas phase over the above bifunctional metal-acid catalysts in comparison with the corresponding catalysts based on zeolite HZSM-5.
- To investigate the effect of gold additives on the activity and stability of the above bifunctional metal-acid catalysts in the alkylation of benzene and toluene with propane.

The catalysts under study will be prepared using conventional procedures documented in the literature (mainly by wet impregnation) and characterised using different techniques such

as the Brunauer-Emmett-Teller (BET) texture analysis, thermogravimetric analysis (TGA), Fourier transform infrared spectroscopy (FTIR), powder X-ray diffraction (XRD) and others. The alkylation reactions will be carried out in a continuous flow fixed-bed microreactor with on-line gas-chromatographic analysis of reaction products.

The thesis presents the results of this investigation; it includes the following seven chapters.

Chapter 1 provides a review of the relevant literature that details the alkylation of aromatic compounds with alkanes. A general introduction to heterogeneous and bifunctional metal-acid catalysis is also provided, along with a brief discussion of the properties and structure of heteropoly acids and zeolites used in this study.

Chapter 2 describes the methods of catalyst preparation together with the techniques used for catalysts characterisation. It also describes catalyst testing in the gas-phase alkylation of aromatic compounds with alkanes including the reactor setup and product analysis.

Chapter 3 describes the results of catalyst characterisation.

Chapter 4 details the results obtained for the alkylation of benzene with propane over bifunctional Pt-heteropoly acid catalysts in comparison with Pt-zeolite catalysts.

Chapter 5 details the alkylation of benzene with propane over bifunctional Pd-heteropoly acid catalysts in comparison with Pt-heteropoly acid catalysts. This chapter also describes the effect of gold additives on the performance of the Pd-HPA catalysts.

Chapter 6 reports the alkylation of toluene with propane in the gas phase over bifunctional Pt-heteropoly acid catalysts in comparison with Pd-heteropoly acid catalysts, and Pt-zeolite catalysts.

Chapter 7 concludes the thesis by summarizing the findings from the previous chapters and gives some concluding comments.

References

1. Bond, G.C. *Heterogeneous Catalysis: Principles and Applications*, Clarendon Press, Oxford, **1974**.
2. Bowker, M. *The Basis and Applications of Heterogeneous Catalysis*, Oxford University Press Inc., New York, **1998**.
3. Michael, M. *Principles of Chemistry*, W.W. Norton & Company, **2000**.
4. Thomas, J.M.; Thomas, W.J. *Principles and Practice of Heterogeneous Catalysis*, VCH, Weinheim, **1997**.
5. Chang, C.D. *Catal. Rev. Sci. Eng.* **1984,** *26*, 323.
6. Chang, C.D.; Lang, W.H.; Silvestri, A.J. *US Patent 4062905*, **1977**.
7. Sheldon, R.A.; Bekkum, H.Van. *Fine Chemicals through Heterogeneous Catalysis*, Wiley, Chichester, **2001**.
8. Keim, W. *Green Chem.* **2003,** *5*, 105.
9. George, S.M. *Chem. Rev.* **1995,** *95*, 475.
10. Timofeeva, M.N. *Appl. Catal.* **2003,** *256*, 19.
11. Kozhevnikov, I.V. *Chem. Rev.* **1998,** *98*, 171.
12. Kozhevnikov, I.V. *J. Mol. Catal. A* **2007,** *262*, 86.
13. Bruggink, A.; Schoevaart, R.; Kieboom, T. *Org. Pro. Res. Dev.* **2003,** *7*, 622.
14. Wasilke, J.C.; Obrey, S.J.; Baker, R.T.; Bazan, G.C. *Chem. Rev.* **2005**, *105*, 1001.
15. Fogg, D.E.; dos Santos, E.N. Coord. *Chem. Rev.* **2004,** *248*, 2365.
16. Climent, M.J.; Corma, A.; Iborra, S. *Chem. Rev.* **2011,** *111*, 1072.
17. Brundtland, G.H. Our common future: *The World Commission on Environment and Development*, Oxford University Press, **1987**.
18. Kuhlmann, A.; Roessner, F.; Schwieger, W.; Gravenhorst, O.; Selvam, T. *Catal. Today*, **2004,** *97*, 303.
19. Ciapetta, F.G.; Hunter, J.B. *Ind. Eng. Chem.* **1953,** *45*, 147.
20. Ciapetta, F.G.; Hunter, J.B. *Ind. Eng. Chem.* **1953,** *45*, 155.
21. Haensel, V.; Donaldson, G.R. *Ind. Eng. Chem.* **1951,** *43*, 2102.
22. Heinemann, H.; Mills, G.A.; Hattman, J.B.; Kirsch, F.W. *Ind. Eng. Chem.* **1953,** *45*, 130.
23. Chen, P.Y.; Chu, S.J.; Chang, N.S.; Chuang, T.K.; Chen, L.Y. *Stud. Surf. Sci. Catal.* **1989,** *46*, 231.

24. Yang, P.P.; Shang, Y.C.; Yu, J.F.; Wang, J.; Zhang, M.L.; Wu, T.G. *J. Mol. Catal. A.* **2007,** *272*, 75.
25. Nicol, W.; du Toit, E.L. *Chem. Eng. Proc.* **2004,** *43*, 1539.
26. Kozhevnikova, E.F.; Kozhevnikov, I.V. *J. Catal.* **2006,** 238, 286.
27. Hetterley, R.D.; Mackey, R.; Jones, J.T.A.; Khimyak, Y.Z.; Fogg, A.M.; Kozhevnikov, I.V. *J. Catal.* **2008,** *258*, 250.
28. Winter, F.; van Dillen, A.J.; de Jong, K.P. *J. Mol. Catal. A* **2004,** *219*, 273.
29. Prins, R.; Wang, A.; Li, X. *Introduction to Heterogeneous Catalysis, World Scientific*, London, **2016**.
30. Priya, S.S.; Kumar, V.P.; Kantam, M.L.; Bhargava, S.K.; Periasamy, S.; Chary, K.V.R. *Appl. Catal. A* **2015,** *498*, 88.
31. Poole, O.; Alharbi, K.; Kozhevnikova, E.F.; Kozhevnikov, I.V. *Appl. Catal. B* **2017,** *202*, 446.
32. Rocha, K.A.D.; Robles-Dutenhefner, P.A.; Sousa, E.M.B.; Kozhevnikova, E.F.; Kozhevnikov, I.V.; Gusevskaya, E.V. *Appl. Catal. A* **2007,** *317*, 171.
33. Kozhevnikov, I.V. *Catalysts for Fine Chemical Synthesis, Catalysis by Polyoxometallates*, Wiley, Chichester, **2002**.
34. Rhule, J.T.; Hill, C.L.; Judd, D.A. *Chem. Rev.* **1998,** *98*, 327.
35. Mizuno, N.; Misono, M. *Chem. Rev.* **1998,** *98*, 199.
36. Okuhara, T.; Mizuno, N.; Misono, M. *Adv. Catal.* **1996,** *41*, 113.
37. Kozhevnikov, I.V. *Heterogeneous Catalysis By Heteropoly Compounds, in: J.J. Borras-Almenar (ED.), Polyoxometalate Molecular Science*, Kluwer Academic Publishers, Netherlands, **2003,** 351.
38. Moffat, J.B. *Metal-Oxygen Clusters: The Surface and Catalytic Properties of Heteropoly Oxometalates*, Kluwer, New York, **2001**.
39. Izumi, Y.; Hasebe, R.; Urabe, K. *J. Catal.* **1983,** *84*, 402.
40. Izumi, Y.; Urabe, K. *Chem. Lett.* **1981,** 663.
41. Schwegler, M.A.; van Bekkum; H. *Appl. Catal.* **1991,** *74*, 191.
42. Baba, T.; Ono, Y. *Appl. Catal.* **1986,** *22*, 321.
43. Kapustin, G.I.; Brueva, T.R.; Klyachko, A.L.; Timofeeva, M.N.; Kulikov, S.M.; Kozhevnikov, I.V. *Kinet. Catal.* **1990,** *31*, 1017.
44. Kapustin, G.I.; Brueva, T.R. *Thermochimica Acta.* **2001,** *379*, 71.
45. Bardin, B.B.; Davis, R.J. *Appl. Catal.* **2000,** *200*, 219.
46. Hetterley, R.D.; Kozhevnikova, E.F.; Kozhevnikov, I.V. *Chem. Comm.* **2006,** 782.

47. Okuhara, T. *Chem. Rev.* **2002,** *102*, 3641.
48. Misono, M. *Chem. Comm.* **2001,** 1141.
49. Alhanash, A.; Kozhevnikova, E.F.; Kozhevnikov, I.V. *Catal. Lett.* **2008,** *120*, 307.
50. Alotaibi, M.A.; Kozhevnikova, E.F.; Kozhevnikov, I.V. *Appl. Catal.* **2012,** *32*, 447.
51. Gates, B.C. *Catalytic Chemistry*, Wiley, Chichester, **1992**.
52. Ribeiro, F.R.; Alvarez, F.; Henriques, C.; Lemos,F.; Lopes, J.M.; Ribeiro, M.F. *J. Mol. Catal. A* **1995,** *96*, 245.
53. Weitkamp, J. *Solid State Ionics*, **2000,** *131*, 175.
54. Al-Dhiayan, D.M. *Ph.D Thesis, The synthesis and Characterisation of Metal Substituted Pentasil Zeolites*, Department of Chemistry, UMIST, UK, **1995**.
55. Hegde, S.G.; Kumar, R.; Bhat, R.N.; Ratnasamy,P. *Zeolites*, **1989,** *9*, 231.
56. Brandle, M.; Sauer, J. J. *Am. Chem. Soc.* **1998,** *120*, 1556.
57. Barthomeuf, D. *Mater. Chem. Phys.* **1987,** *17*, 49.
58. Mortier, W.J. *J. Catal.* **1978,** *55*, 138.
59. Kramer, G.J.; Vansanten, R.A. J. *Am. Chem. Soc.* **1993,** *115*, 2887.
60. Senchenya, I.N.; Kazansky, V.B.; Beran, S. *J. Phys. Chem.* **1986,** *90*, 4857.
61. Kato, S.; Nakagawa, K.; Ikenaga, N.; Suzuki, T. *Catal. Lett.* **2001,** *73*, 175.
62. Tanabe, K.; Holderich, W.F. *Appl. Catal. A* **1999,** *181*, 399.
63. Kouva, S.; Kanervo, J.; Schüβler, F.; Olindo, R.; Lercher, J.A. *Chem. Eng. Sci.* **2013,** *89*, 40.
64. Weissermel, K.; Arpe, H.-J. *Industrial Organic Chemistry;* Wiley-VCH: Weinheim, Germany, **2003**.
65. Perego, C.; Ingallina, P. *Catal. Today* **2002,** *73*, 3.
66. Parikh, P. A.; Subrahmanyam, N.; Bhat, Y. S.; Halgeri, A. B. *Appl. Catal. A* **1992,** *90*, 1.
67. O'Kelly, A.A.; Kellett, J.; Plucker, J. *Ind. Eng. Hem* **1947,** *39*, 154.
68. Venuto, P.B.; Hamilton, L.A.; Landis, P.S.; Wise, J.J. *J. Catal.* **1966,** *5*, 81.
69. Degnan, Jr T.F.; Smith, C.M.; Venkat, C.R. *Appl. Catal. A* **2001,** *221*, 283.
70. Minachev, Kr.M; Isakov, Ya.I.; Garanin, V.I.; Piguzova, L.I.;Bogomolov, V.I.; Vitukina, A.S. *Neftekhimiya* **1965,** *5*, 676.
71. Bohstrom, Z.; Harelind, B.G.; Andersson, S-L; Holmberg, K. *RSC Adv.* **2104,** *4*, 28786.
72. Cejka, J.; Wichterlova, B.; Bednarova, S. *Appl. Catal. A* **1991,** *79*, 215.
73. Engelhardt, J.; Lonyi, F. *React. Kinet. Catal. Lett.* **1987,** *34*, 355.
74. Cejka, J.; Krejci, A.; Zilkova, N.; Dedecek, J.; Hanika, J. *Micropor. Mesopor. Mater.* **2001,** *44-45*, 499.

75. Prokesova, P.; Zilkova, N.; Mintova, S.; Bein, T.; Cejka, J. *Appl. Catal. A* **2005,** *281*, 85.
76. Cejka, J.; Krejci, A.; Zilkova, N.; Kotrla, J.; Ernst, S.; Weber, A. *Micropor. Mesopor. Mater.* **2002,** *53*, 121.
77. Rigoreau, J.; Laforge, S.; Gnep, N.S.; Guisnet, M. *J. Catal.* **2005,** *236*, 45.
78. Shilov, A. E. *Activation of Saturated Hydrocarbons by Transition Metal Complexes*; Reidel: Dordrecht, **1984**.
79. Hashiguchi, B. G.; Bischof, S. M.; Konnick, M. M.; Periana, R. A. *Acc. Chem. Res.* **2012,** *45*, 885.
80. Caeiro, G.; Carvalho, R. H.; Wang, X.; Lemos, M. A. N. D. A.; Lemos, F.; Guisnet, M.; Ramoa Ribeiro, F. J. *Mol. Catal. A* **2006,** *255*, 131.
81. Olah, G. A.; Schilling, P.; Staral, J. S.; Halpern, Yu.; Olah, J. A. *J. Am. Chem. Soc.* **1975,** *97*, 6807.
82. Kato, S.; Nakagawa, K.; Ikenaga, N.; Suzuki, T. *Catal. Lett.* **2001,** *73*, 175.
83. Smirnov, A. V.; Mazin, E. V.; Ponomoreva, O. A.; Yuschenko, V. V.; Knyazeva, E. E.; Nesterenko, S. N.; Ivanova, I. I. *J. Catal.* **2001,** *135*, 153.
84. Bragin, O. V.; Shpiro, E. S.; Preobrazhensky, A. V.; Isaev, S. A.; Vasina, T. V.; Dyusenbina, B. B.; Antoshin, G. V.; Minachev, K. M. *Appl. Catal.* **1986,** *27*, 219.
85. Lukyanov, D. B.; Vazhnova, T. *J. Mol. Catal. A* **2008,** *279*, 128.
86. Lukyanov, D. B.; Vazhnova, T. *J. Catal.* **2008,** *257*, 382.
87. Chua, L. M.; Vazhnova, T.; Mays, T. J.; Lukyanov, D. B.; Rigby, S. P. *J. Catal.* **2010,** *271*, 401.
88. Ordomskiy, V. V.; Rodionova, L. I.; Ivanova, I. I.; Luck, F. *ChemCatChem* **2012,** *4*, 681.
89. Wong, K. S.; Vazhnova, T.; Rigby, S. P.; Lukyanov, D. B. *Appl. Catal. A* **2013,** *454*, 137.
90. Vazhnova, T.; Rigby, S. P.; Lukyanov, D. B. *J. Catal*. **2013,** *301*, 125.
91. Ivanova, I. I.; Blom, N.; Derouane, E. G. *J. Mol. Catal.* **1996,** *109*, 157.
92. Smirnov, A. V.; Mazin, E. V.; Yuschenko, V. V.; Knyazeva, E. E.; Nesterenko, S. N.; Ivanova, I. I.; Galperin, L.; Jensen, R.; Bradley, S. *J. Catal.* **2000,** *194*, 266.
93. Abasov, S. I.; Babayeva, F. A.; Zarbaliyev, R. R.; Abbasova, G. G.; Tagiyev, D. B.; Rustamov, M. I. *Appl. Catal. A* **2003,** *251*, 267.
94. Bigey, C.; Su, B-L. *J. Mol. Catal. A* **2004,** 209, 179.
95. Huang, X.; Sun. X.; Zhu, S.; Liu, Z. *React. Kinet. Catal. Lett.* **2007,** *91*, 385.
96. Babaeva, F. A.; Abasov, S. I.; Rustamov, M. I. *Petrol. Chem.* **2010,** *50*, 42.

97. Woltz, C.; Jentys, A.; Lercher, J. A., *J. Catal.* **2006,** 237, 337.
98. Guisnet, M.; Perot, G. *Zeolite Bifunctional Catalyst in: F.R. Ribeiro, et al. (Eds.), Zeolites: Science and Technology,* NATO ASI series, **1984,** *80*, 397.
99. Ya, C. C.; Tan, C. S. *Ind. Eng. Chem. Res.* **2007,** *46*, 4421.
100. Sealy, S.; Traa, Y. *Appl. Catal. A* **2005,** *294*, 273.
101. Bressel, A.; Donauer, T.; Sealy, S.; Traa, Y. *Micropor. Mesopor. Mater.* **2008,** *109,* 278.
102. Singer, D.; Alireza, S.; Rezai, S.; Sealy, S.; Traa, Y. *Ind. Eng. Chem. Res.* **2007,** *46,* 395.
103. Alireza, S.; Rezai, S.; Traa, Y. *Catal. Lett.* **2008,** *122,* 91.

Chapter 2: Experimental

In this chapter, the experimental techniques used in the alkylation of benzene and toluene with propane over metal-acid bifunctional catalysts in gas phase are described starting from catalyst preparation. The catalysts were studied using different techniques to characterise and determine their properties such as surface area, porosity, crystallinity, water content and metal dispersion. Additionally, techniques such as inductively coupled plasma atomic emission spectroscopy (ICP-AES) were employed to determine the elemental composition of catalysts. The alkylation reactions were studied using a fixed bed microreactor with online gas-chromatographic analysis, which is also described in detail in this chapter.

2.1. Chemicals and catalysts

Heteropoly acid hydrates $H_3PW_{12}O_{40}$ (HPW, 99%) and $H_4SiW_{12}O_{40}$ (HSiW, 99.9%) containing 20-28 H_2O molecules per Keggin unit were purchased from Sigma-Aldrich. The amount of crystallization water in heteropoly acids was determined by TGA. Zeolite NH_4^+-ZSM-5 (Si/Al = 18, specific surface area S_{BET} = 400 m^2g^{-1}) was from Zeolyst International. It was converted into the H^+ form by air calcination at 500 ^oC for 6 h. Carbon-supported platinum 10%Pt/C was from Johnson Matthey (7.0% Pt content in dried catalyst from inductively coupled plasma atomic emission spectroscopy (ICP-AES) analysis). Carbon-supported palladium 10%Pd/C was also from Johnson Matthey (7.1% Pd content in dried catalyst from ICP-AES analysis). Benzene (>99%) and toluene (>99%) were purchased from Sigma-Aldrich. $Pt(acac)_2$, $Pt(NH_3)_4(NO_3)_2$, $Pd(acac)_2$ and $HAuCl_4 \cdot 3H_2O$ were also purchased from Sigma-Aldrich. Propane, N_2 and H_2 gases (all >99% purity) were supplied by the British Oxygen Company. From GC analysis, the propane contained C_3H_8 (99.20%), C_2H_6 (0.76%), C_3H_6 (0.01%), C_4H_{10} (0.03%) and methane (0.004%).

2.2. Catalyst preparation

Acidic cesium heteropoly salt $Cs_{2.5}H_{0.5}PW_{12}O_{40}$ was prepared by adding dropwise the stoichiometric amount of aqueous cesium carbonate Cs_2CO_3 (0.47 M) to an aqueous solution of HPW (0.75 M) at 40 °C with stirring [1]. The precipitate formed was aged in the aqueous mixture for 24 h at room temperature. Then the catalyst was dried at 45 °C/3 kPa using a rotary evaporator, then dried in an oven at 150 °C/0.1 kPa under vacuum for 1.5 h.

Supported HPA catalysts were prepared by wet impregnation of oxide supports with an aqueous HPA solution (HPW or HSiW) and dried at 150 °C/10^{-3} kPa for 1.5 h [2, 3]. The oxide supports P25 titania (anatase/rutile = 3:1) and Aerosil 300 silica (S_{BET} = 300 m^2g^{-1}) were from Degussa. ZrO_2 and Nb_2O_5 oxides were prepared in-house and calcined at 400 °C in air for 5 h [2, 3].

Pt-HPA bifunctional catalysts were prepared by wet impregnation of acidic component, e.g., 25%HPA/SiO_2, with 0.02 M $Pt(acac)_2$ solution in benzene at room temperature for 1 h, followed by slow evaporation of benzene in a rotary evaporator at room temperature [4]. The catalyst was dried under vacuum at 150 °C/10^{-3} kPa and then reduced in oven by hydrogen flow at 250 °C for 2 h. 0.31%Pt/HZSM-5 was prepared by the literature procedure [5] involving adsorption of Pt(II) on to zeolite from 0.01 M aqueous solution of $Pt(NH_3)_4(NO_3)_2$ followed by washing with distilled water, air calcination at 450 °C for 2 h and reduction by H_2 at 400 °C for 2 h. The Pt loading quoted was determined by the ICP-AES analysis. 10%Pt/SiO_2 catalyst was prepared by impregnating Aerosil 300 silica with $Pt(acac)_2$ using the procedure described above.

Physical mixtures of 7%Pt/C with 25%HPA/SiO_2 or HZSM-5 containing 0.7% of Pt were prepared by grinding a 1:9 w/w mixture of these compounds.

Pd/HSiW/SiO_2 and Pd/HZSM-5 catalysts were prepared by the impregnation of 25%HSiW/SiO_2 or HZSM-5 with 0.02 M $Pd(acac)_2$ solution in benzene, followed by the slow rotoevaporation of benzene at room temperature, as described elsewhere [6]. The catalysts were dried under vacuum at 150 °C/10^{-3} kPa, then reduced in an oven by H_2 flow at 250 °C for 2 h.

The bimetallic 10%Au/6.0% Pd/C catalyst was prepared by the impregnation of 7.1%Pd/C with an aqueous solution of $HAuCl_4$, followed by drying and reduction by H_2 flow at 250 °C for 2 h. After reduction, Pd and Au loading in supported catalysts was confirmed by ICP-AES; this was in good agreement with the loading expected from the preparation stoichiometry (e.g., 10%Au/6.4%Pd/C from stoichiometry and 9.9%Au/6.0%Pd/C from ICP-AES analysis).

Physical mixtures of 7.1%Pd/C with 25%HSiW/SiO_2 or HZSM-5 containing a specified percentage of Pd were prepared by grinding mixtures of these components. Physical mixtures of 10%Au/6.0%Pd/C with 25%HSiW and HZSM-5 were prepared in the same way.

2.3. Catalyst characterisation techniques

2.3.1. Surface area and porosity analysis

Measuring surface area, pore volume and pore size distribution for heterogeneous catalysts is important because their activity, stability and selectivity depend on these parameters. The pores are classified into three groups regarding their size according to the IUPAC classification [7, 8, 9]:

1. Micropores (size < 2 nm)
2. Mesopores (size between 2 and 50 nm)
3. Macropores (size > 50 nm)

The most common heterogeneous catalysts have total surface areas in the range of 1-10^3 m^2 g^{-1}, whereas their external surface area is from 0.01 to 10 m^2 g^{-1} [7]. Therefore, porous solid catalysts have usually much higher total surface area than the external surface area as a result of the contribution of pore walls. Various techniques have been utilised to measure the surface area of catalysts and characterise their porous structure [7, 10, 11]. The most common technique used to determine the surface area and porosity of catalysts is nitrogen adsorption at its boiling temperature (-196 °C). This method, developed by Brunauer, Emmett and Teller (BET) in 1938 [7, 12], is widely used to calculate the monolayer volume of adsorbed N_2 gas (V_m) and the surface area of porous solid materials (A_s) by the following equation:

$$A_s = (V_m/22414)\, N_a \sigma \qquad (2.1)$$

In this equation, σ is the area covered by one nitrogen molecule (0.162 nm^2), N_a is the Avogadro number (6.022×10^{23} mol^{-1}) and the constant 22414 is the nitrogen molar volume (ml mol^{-1}) under standard conditions [11].

In this work, the characterisation of catalyst texture was carried out on a Micromeritics ASAP 2010 adsorption apparatus (Figure 2.1). All catalysts were first degassed externally at 150 °C under vacuum for 1.5 h. Typically, a sample (150-200 mg) was placed in a sample tube and evacuated at 250 °C on the Micromeritics ASAP 2010 until the vacuum reached 8 μmHg to remove adsorbed gasses. Then, the sample was allowed to cool to room temperature. After immersing sample tube in liquid nitrogen, the gas pressure was allowed to reach equilibrium before a number of nitrogen doses (usually 55 doses) was applied in order to obtain an adsorption isotherm.

Figure 2.1. Micromeritics ASAP 2010 adsorption apparatus.

The nitrogen physisorption at boiling temperature (-196 °C) was used to determine the catalyst surface area and to characterise the porous texture. To generate the nitrogen adsorption isotherm, the volume of nitrogen adsorbed was plotted versus the relative pressure. The unique shape of the isotherm depends on the texture of the solid catalyst. According to the IUPAC classification, six types of isotherm can be distinguished [13-15]. Figure 2.2 illustrates the isotherms, which are usually found in solid catalysts [7].

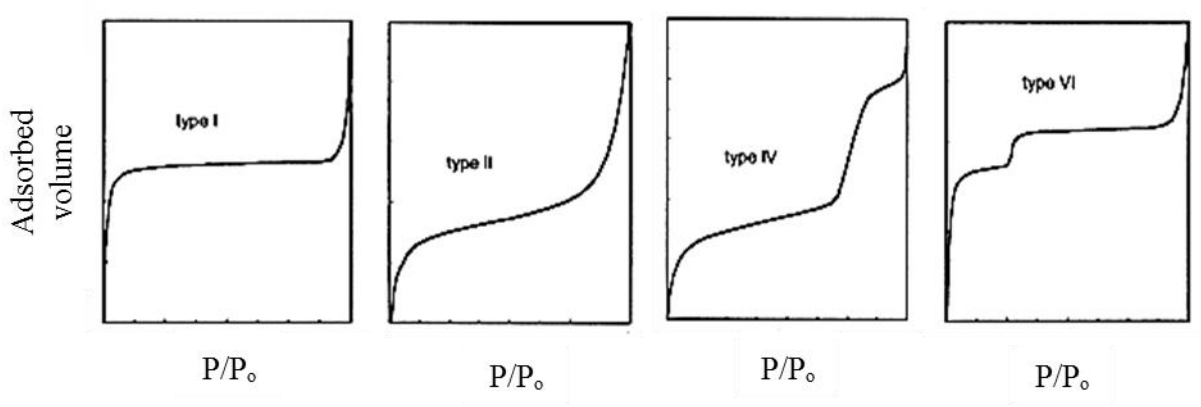

Figure 2.2. The four most typical types of nitrogen adsorption isotherm.

Type I, II and IV isotherms are representative of microporous, macroporous and mesoporous materials respectively.

(1) In microporous materials (type I), adsorption occurs at very low relative pressure, due to strong interaction between pore walls and the adsorbate molecules without capillary condensation in the medium relative pressure area (<0.3). At high relative pressures, the pores are completely filled and the adsorption is continued on the external surface. Zeolites are the typical example of microporous materials.

(2) In macroporous materials (type II), the formation of a monolayer of adsorbed molecules takes place at low relative pressure, while at high relative pressure multilayer adsorption occurs. The adsorbate thickness increases with increasing pressure until condensation pressure is reached.

(3) In mesoporous materials (type IV), the formation of the adsorption monolayer takes place at low relative pressure. At higher relative pressures, the capillary condensation takes place to fill the mesopores up, giving a sharp increase in the adsorption volume. The larger the mesopores in the solid catalyst, the higher the relative pressure for adsorption to take place. When the mesopores are filled, the

adsorption continues on the external surface. A typical example of mesoporous materials are supported HPA catalysts.

(4) When the surface of a catalyst is energetically uniform, the isotherm may have a step-like shape (type VI).

After measuring the adsorption isotherm by increasing the pressure until the adsorbate reaches saturation, desorption is measured by decreasing the pressure to evaporate the adsorbate from the pores and the surface. However, the evaporation in mesoporous materials takes place at a pressure lower than that of capillary condensation, which gives a hysteresis loop. There are four types of hysteresis for solid catalysts, according to the IUPAC classification (Figure 2.3).

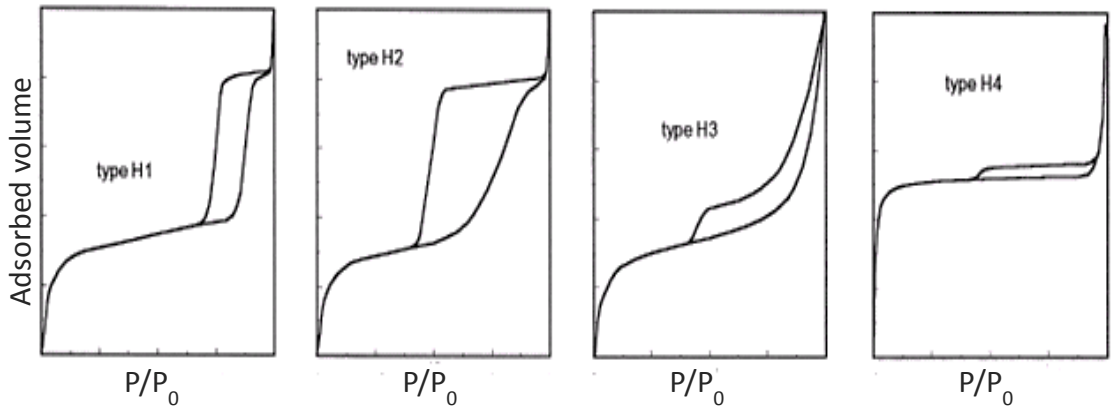

Figure 2.3. The four hysteresis shapes usually observed with N_2 adsorption.

Types H1 and H2 hysteresis are observed when analysed materials consist of particles with channels near to cylindrical in shape or made by aggregates (consolidated) or agglomerates (unconsolidated) spheroidal in shape. For materials showing type H1 hysteresis, pores may have uniform size and shape, while pores with non-uniform size and shape display type H2 hysteresis. Types H1 and H2 hysteresis are attributed to size differences between pore bodies and pore mouths (e.g. ink-bottle-shaped pores) or to different behaviour in

adsorption and desorption in nearly cylindrical pores. Most of the mesoporous materials display these two hysteresis isotherms [7].

Types H3 and H4 hysteresis are observed in with materials that consist of aggregates or agglomerate particles producing slit-shaped pores (plates or edged particles similar to cube shape). Pores with uniform size and/or shape display type H4 hysteresis, while pores with non-uniform size and/or shape display type H3. Zeolites and active carbons are examples of H3 and H4 isotherms, respectively.

In some cases, no hysteresis is observed and this indicates the materials with blind cylindrical, cone-shaped and wedge-shaped pores. However, because material pores are usually irregular in shapes and sizes, only isotherms with a much reduced hysteresis will be observed.

In this work, the total surface area of catalysts was determined using the BET method [12]. The pore size distribution and total pore volume were measured using the Barrett, Joyner and Halenda (BJH) method [16].

2.3.2. Powder X-ray diffraction (XRD)

Powder X-ray diffraction (XRD) is an important analytical technique used to provide information about phase structure of solid materials. X-rays have wavelengths equivalent to the spaces between atoms in crystalline materials, so that they can pass through these materials resulting in diffraction patterns. The angle of scattering of X-rays is affected by several factors, thus obeying Bragg's law (equation 2.2) [17]:

$$n\lambda = 2dSin\theta \qquad (2.2)$$

where n is the order of the reflection (an integer value), λ is the incident X-ray wavelength, d is the lattice planar spacing and θ is the diffraction angle.

Valuable information which can be achieved from the X-ray diffractogram includes the crystallinity of solid materials and the average particle size, which can be calculated using the Scherrer equation (2.3) [18]:

$$t = 0.9\lambda / B\ Cos\theta \qquad (2.3)$$

where t is the particle size, λ is the incident X-ray wavelength, B (rad) is the full width at half the maximum of the diffraction peak, and θ is the diffraction angle.

Powder X-ray diffraction studies were carried out on a Bruker D8 Advance diffractometer in Bragg-Brentano geometry equipped with a Ge monochromator giving Cu Kα radiation (λ = 1.542 Å), which is available in the Department of Chemistry at Liverpool University.

2.3.3. Temperature programmed reduction (TPR)

TPR is a commonly used technique to investigate the redox properties of catalysts by providing information about reduction conditions of the catalyst. Experimental parameters (sample weight, heating temperature rate, gas flow rate and catalyst particle size) affect the TPR profile [19].

In this study, H_2-TPR of catalysts was carried out on a Micromeritics TPD/TPR 2900 apparatus equipped with a thermal conductivity detector (TCD) (Figure 2.4). Catalyst samples (20-30 mg) were heated up to 800 °C at a rate of 5-10 °C/min in an H_2-N_2 (5:95) gas flow (60 ml min^{-1}).

Figure 2.4. Micromeritics TPD/TPR 2900 apparatus.

2.3.4. H_2 chemisorption

Measuring the metal dispersion on the surface of supported metal catalysts is an important technique to understand the catalyst activity. Hydrogen chemisorption usually increases with increasing the metal dispersion. The pulse hydrogen chemisorption technique, using H_2/O_2 titration, is a well-known method to measure the metal dispersion on supported catalysts due to its suitability and sensitivity [20, 21]. This technique has been employed widely to measure Pt [21] and Pd [20] dispersions. The metal dispersion (*D*) defined as the fraction of accessible metal at the surface of metal particles (M_s) to the total number of metal atoms (M_{total}) in the catalyst ($D = M_s/M_{total}$).

In this study, supported metal catalysts (e.g., Pt supported on active carbon, CsPW, 25%HSiW/SiO_2, 25%HPW/SiO_2 and HZSM-5) were reduced using H_2 flow for two hours at 250 °C to convert metal precursor M^{n+} to M^0. Then the catalyst sample (20 mg) was exposed to air at room temperature for several hours to allow oxygen to adsorb on the metal atoms on the catalyst surface [22]. After that, the sample was placed in a sample tube linked to a Micromeritics TPD/TPR 2900 instrument equipped with a thermal conductivity detector

(TCD) and stabilised at a specified temperature (room temperature for Pt and 100 °C for Pd) under a flow of nitrogen gas. A series of 20 µl pulses of pure H_2 (heated to 75 °C) were injected in the flow every 3 min until the catalyst was saturated with hydrogen. Equation (2.4) shows the stoichiometry of the H_2/O_2 titration [12, 18].

$$M_s\text{-}O + 3/2H_2 \longrightarrow M_s\text{-}H + H_2O \qquad (2.4)$$

The adsorbed volume of H_2 was calculated by integrating the areas under the detected TCD peaks, which were displayed on the screen. Pulses were applied until no more adsorption was observed, then the total adsorbed volume of H_2 (at 75 °C and each injection being 20 µl) was calculated.

The dispersion and the average metal particle diameter were calculated using equations (2.5-2.7) [23].

$$V_{348K}\,(\mu l) = \Sigma\{20 - [(PA_{ads}/PA_{av}) \times 20] \qquad (2.5)$$

In equation (2.5), V_{348K} is the total adsorbed volume of H_2 at 75 °C (348 K), PA_{ads} is the peak area of adsorbed hydrogen and PA_{av} is the average peak area for last 4-6 injections where no H_2 was adsorbed. Equation (2.6) gives the total adsorbed volume of H_2 at 0 °C (273 K).

$$V_{273\,K}\,(\mu l) = V_{348K} \times (273/348) \qquad (2.6)$$

$$D = \frac{V_{273}\ (\text{ml}) \times Ar\ (\text{g mol}^{-1})}{M_{cat}\ (\text{g}) \times 22414\ (\text{ml mol}^{-1}) \times C_M \times 1.5} \qquad (2.7)$$

In equation 2.7, D is the metal dispersion, A_r is the atomic weight of metal, M_{cat} is the mass of the catalyst used in the experiment, the constant 22414 is the volume of one mole of H_2 under standard conditions, C_M is the content of metal as a fraction of catalyst mass and 1.5 is the adsorption stoichiometry of H_2 adsorbed on the surface metal atoms.

The average diameter of metal particles, *d*, was calculated using the empirical equation (2.8) [20].

$$d\ (\text{nm}) = 0.9/D \qquad (2.8)$$

Figures 2.5 and 2.6 illustrate examples of the measurement of Pd dispersion by H_2/O_2 titration.

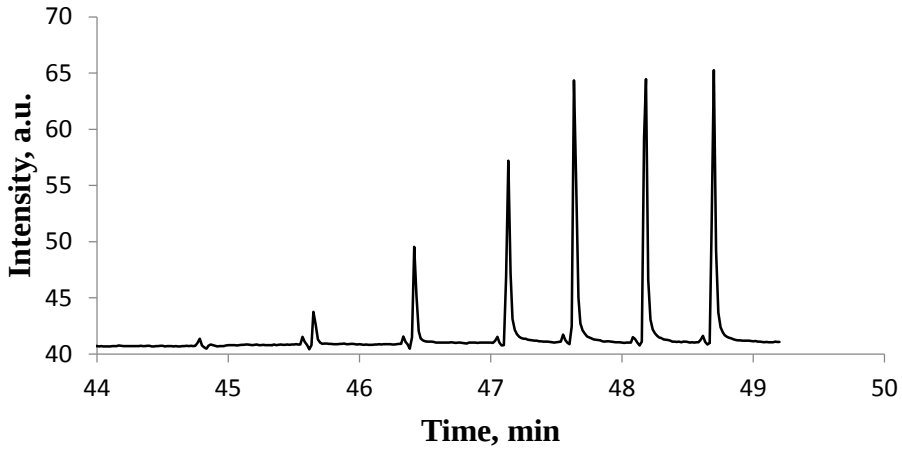

Figure 2.5. H_2 pulse adsorption on the surface of 2%Pd/25%HSiW/SiO_2, with H_2 signals detected during the pulsation.

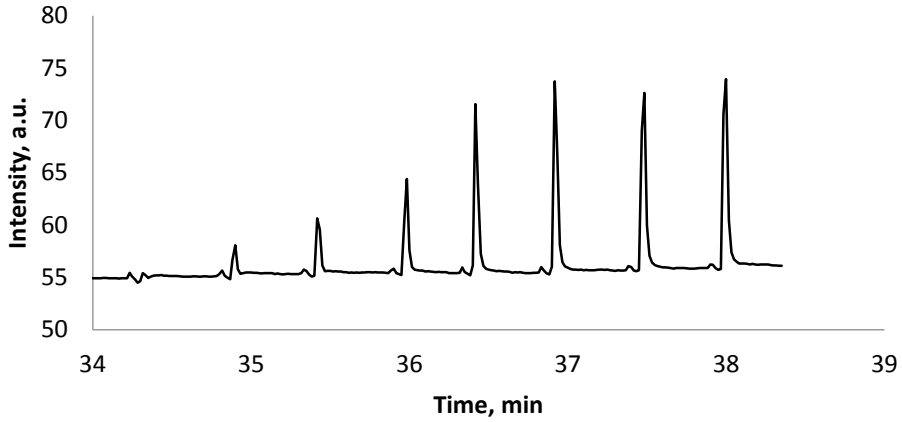

Figure 2.6. H_2 pulse adsorption on the surface of 7.1%Pd/C, with H_2 signals detected during the pulsation.

2.3.5. CO chemisorption

Pt dispersion was also measured by pulse chemisorption of CO in a helium flow at 50 °C by using Micromeritics TPD/TPR 2900 instrument. A catalyst sample (20 mg) was placed in the sample tube, then 50 μl pulses of pure CO were injected manually until the catalyst was saturated with CO (adsorption stoichiometry Pt_s: CO = 1).

2.3.6. Thermogravimetric analysis (TGA)

Thermogravimetric analysis (TGA) is widely used for catalyst characterisation by measuring the change in sample weight occurring upon increasing sample temperature. This weight change may have a chemical or physical origin, and can be calculated as a percentage value. The instrumentation consists of a precision balance and the sample holder placed inside the furnace, which is then heated electrically under a flow of nitrogen or air. Results are presented as a curve displaying the weight percentage of original material as a function of temperature. A derivative curve can be used to tell the point at which the weight loss is most apparent. TGA is a useful technique to measure the amount of physisorbed water in samples in order to use the correct amount of reactants in catalyst synthesis. It can also be used for the determination of thermal stability of catalysts.

A Perkin Elmer TGA 7 instrument was utilized in this work to perform the TGA of catalyst samples (20-50 mg) under flow of nitrogen gas using a heating rate between 10 to 20 $^{o}C\ min^{-1}$ to increase the temperature from room temperature to 700 ^{o}C.

2.3.7. Fourier transform infrared (FTIR) spectroscopy

FTIR spectroscopy is an analytical technique which is used to obtain information about bulk and surface properties of solid catalysts, for example, the nature of acid sites in solid acid catalysts [24].

In this work, the structure of Keggin HPAs was investigated by infrared spectroscopy in the fingerprint region of the spectrum (500 – 1200 cm^{-1}). Additionally, Brønsted and Lewis acid sites on the catalyst surface were determined by pyridine adsorption using diffuse reflectance infrared Fourier transform (DRIFT) spectroscopy in the range from 1540 cm^{-1} to 1450 cm^{-1}.

For the DRIFT measurements, catalyst samples were degassed under vacuum at 150 °C for two hours. Then 5 mg of the catalyst was diluted by 45 mg of dried KBr powder and ground thoroughly at room temperature under dry nitrogen flow. For the determination of acid sites using pyridine adsorption, samples were mixed with dried KBr (to dilute samples to 10 wt%), then degassed under vacuum at 150 °C/0.01 kPa for one hour. After that the samples were cooled to room temperature under dry nitrogen atmosphere, and 1-3 drops of pyridine were added onto each sample. The samples were exposed for an hour to pyridine at room temperature, then were degassed again under vacuum for one hour at 150 °C to remove physisorbed pyridine. Finally, the DRIFT spectrum of adsorbed pyridine was recorded at room temperature.

FTIR studies were carried out in transmission mode using a Nicolet NEXUS FTIR spectrometer.

2.3.8. Inductively coupled plasma atomic emission spectroscopy (ICP-AES)

An Inductively Coupled Plasma (ICP) source linked to Atomic Emission Spectroscopy (AES) is an atomic technique which is used to determine the amount of most elements in a sample at very low concentrations as small as a part per billion. This technique uses a plasma (a gas with a high proportion of ions and electrons, created by heating gases such as argon at a temperature >6000 K) as an excitation source. This technique can detect a significant number of elements over a wide range of concentrations [25].

ICP-AES was utilised to detect the amount of Pt, Pd and Au in our catalysts by dissolving 20-25 mg of the sample in an appropriate solution (aqua regia solution (HNO_3 + $HCl)_{(aq)}$ in this case) and heated at 30 °C for 1 hour. Then the solution was diluted in a 100 ml standard flask by distilled water. The ICP-AES analysis was performed by G. Miller using the Spectro Ciros emission spectrometer within the Department of Chemistry at University of Liverpool.

2.3.9. C, H, N analysis

Combustion analysis is an important technique for measuring the amount of C and H in solid catalysts [26]. Typically, a small amount of catalyst (~5 mg) was placed in the combustion reactor and heated up to 1000 °C under flowing He gas, then enriched with pure oxygen to cause the flash combustion to produce CO_2 and H_2O. By passing the gas mixtures to the GC detector, the combustion quantities were detected. This analysis was used in our study to measure the carbon content in spent catalysts to study the effect of coke on catalyst deactivation. For example, 1.2% of coke was found in the spent 1%Pt/25%HSiW/SiO_2 catalyst after alkylation of benzene by propane, which could block the metal and/or the acid sites in the catalyst.

Analysis of catalyst coking was carried out on the Thermo Flash EA 1112 series analyser, which is available in the Department of Chemistry at University of Liverpool.

2.3.10. Gas Chromatography

2.3.10.1. Introduction

Gas chromatography (GC) is an analytical technique which is widely used to separate and analyse volatile compounds in the gas phase [27]. Firstly, the sample is volatilised and transferred as a mixture of volatiles by a stream of an inert carrier gas such as He, Ar, H_2 or

N_2 through a heated column. The different components of the mixture pass through the GC column at different rates depending in their boiling points [28]. Figure 2.7 shows schematic diagram of a typical GC and the GC setup for this study is displayed in Figure 2.8.

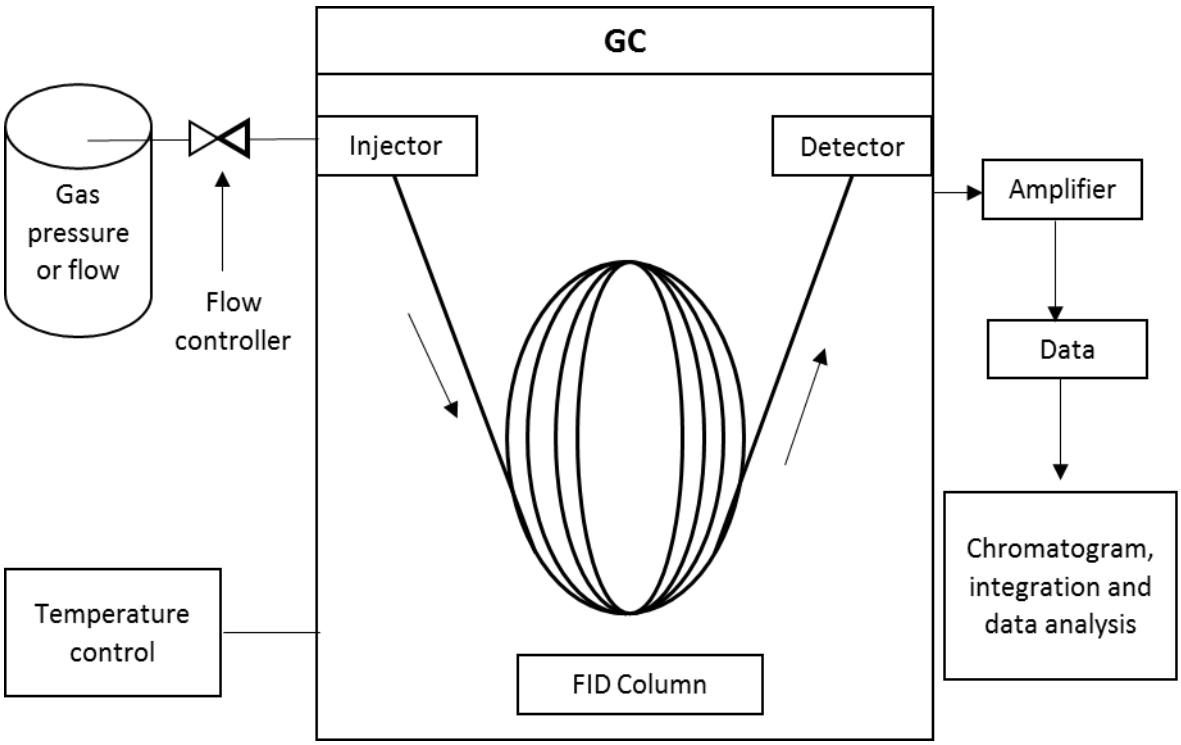

Figure 2.7. Schematic diagram of a typical GC.

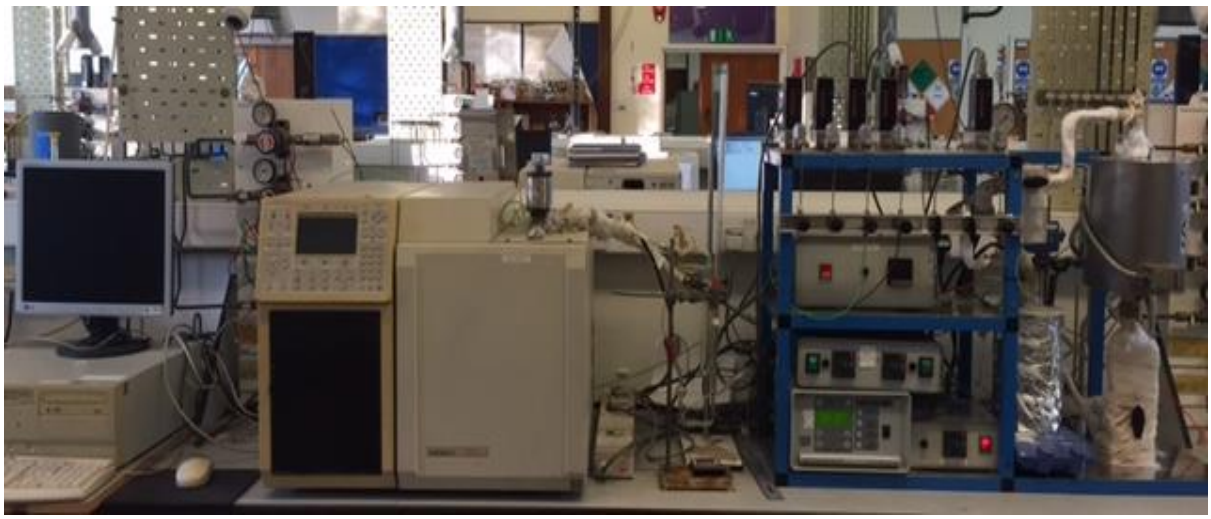

Figure 2.8. Varian 3800 GC connected to the fixed-bed reactor.

The GC column is a long capillary tube which has stationary phase bonded to its wall. The components of the gas mixture distribute between the stationary phase of the column and the mobile phase (carrier gas) due to a combination of volatility and the degree with which they interact with the stationary phase. Factors affecting the rate of passage of components include the boiling points and the polarity of each compound.

At the entrance of GC column, a split/splitless injector is used to inject a controlled quantity of samples into the column (Figure 2.9). The ratio of the spilt flow rate to the column flow rate is called the split ratio.

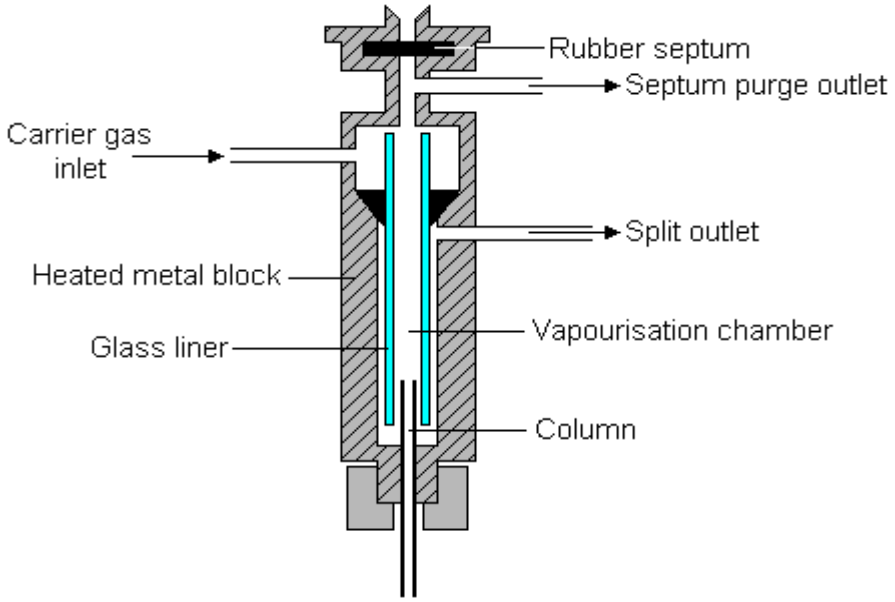

Figure 2.9. The split/splitless injector.

At the end of the column, there is a detector. In our case, a flame ionisation detector (FID) was used as shown in Figure 2.10. Within the FID detector, the analysed organic compounds are burned at high temperature flame, which is created by mixing H_2 and air at a small metal jet, to ionise the compounds with low ionisation potentials into charged particles. These charge particles migrate towards to the collector electrode. The quantity of charge produced is proportional to the amount of compound present. The resulting current is

amplified and plotted on the screen as a chromatogram. The time taken for each component to pass from the injector to the detector is called the retention time.

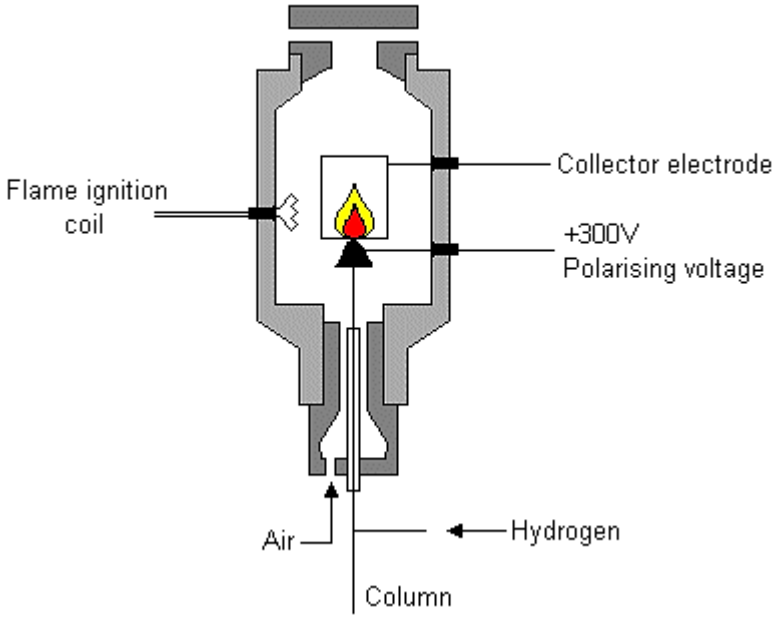

Figure 2.10. The flame ionisation detector [29].

In our analysis, a Varian 3800 gas chromatograph with a 30 m x 0.32 mm x 0.5 μm Zebron ZB-WAX capillary column and FID detector was used for on-line analysis of reaction products. The detector and injector temperature was set at 300 °C. The hydrogen flow rate was 30 ml min^{-1} while the air flow rate was 300 ml min^{-1}. The temperature of the column oven was programmed as shown in Figure 2.11 (a).

For off-line GC analysis of light hydrocarbons, a Varian 3800 GC with 60 m x 0.32 mm GS-GasPro capillary column and FID detector was used, which allowed for complete separation of these hydrocarbons. The detector and injector temperature was set at 300 °C. The temperature of the column oven was programmed as shown in Figure 2.11 (b).

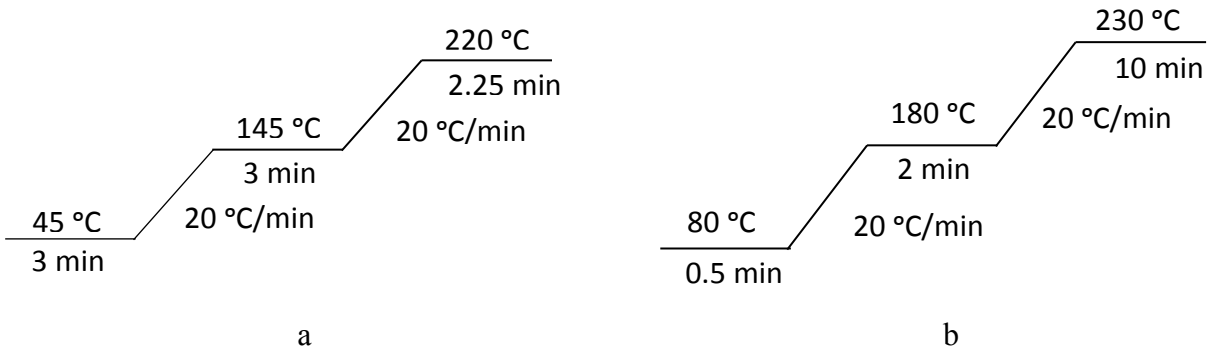

a b

Figure 2.11. The temperature program of the column oven a) ZB-WAX capillary column and b) GS-Gas Pro capillary column.

2.3.10.2. Product calibration

In the chromatogram, the equal peak areas for different compounds do not necessarily indicate equal concentrations of these compounds as the peak areas depend on the response characteristics of the detector. Moreover, there are other factors that might affect the peak area such as detector and column temperatures and the carrier gas flow rate. To eliminate the effect of these factors, the internal or external standard methods can be used. In this work, the internal standard, which is an inert compound to the sample and has similar chemical and physical characteristics to the sample, was used to calibrate the GC for the products of alkylation reactions. In each analysis, the internal standard (whose concentration was constant) and the analyte (whose concentration was varied) were added to the solvent for dilution. The ratio of the total area peak of the analyte (S) to the total area peak of the standard (S_o) was plotted against the ratio of the molar concentration of the analyte (M) to the molar concentration of the standard (M_o) (Equation 2.9).

$$\frac{M}{M_o} = K \times \frac{S}{S_o} \qquad (2.9)$$

Usually, decane and dodecane were used as internal standards while 1,2-dichloroethane was used as a solvent.

For alkylation of benzene by propane, Tables 2.1 and 2.2 give the molecular weights, boiling points, retention times and calibration factors for the main reaction products. If some of by-products were not available or had low area peaks, the calibration factors for similar compounds were used.

Table 2.1. Molecular weights, boiling points, retention times and calibration factors for the main products of benzene alkylation by propane using ZB-WAX capillary column[a].

Compound	MW ($g\ mol^{-1}$)	Boiling point (°C)	Retention time (min)	Calibration factor[a]
C_6H_6	78.11	81.1	1.4	1.00
MePh	92.14	110.6	2.4	0.89
EtPh	106.17	136.0	3.1	0.81
Cumene	120.19	152.4	4.2	0.74
nPrPh	120.19	159.0	4.7	0.74
P-cymene	134.22	177.0	5.2	0.64
Cymene isomers	134.22	175-178	5.6-5.8	0.64

[a]Calibration factor relative to benzene.

Table 2.2. Molecular weights, boiling points, retention times and calibration factors for light hydrocarbon products from the gas phase alkylation of benzene by propane using GS-Gas Pro capillary column[a].

Compound	MW (g mol^{-1})	Boiling point (°C)	Retention time (min)	Effective carbon number	Calibration factor
Methane	16.04	-161	4.40	1.0	1.00
Ethane	30.07	-89	4.70	2.0	0.50
Ethene	28.05	-103	4.77	1.9	0.53
Propane	44.10	-42	5.4	3	0.33
Propene	42.08	-47	5.7	2.9	0.34

[a]Calibration factors were estimated using the effective carbon number [30].

Figures from 2.12 to 2.14 illustrate the calibration plots for benzene and cumene.

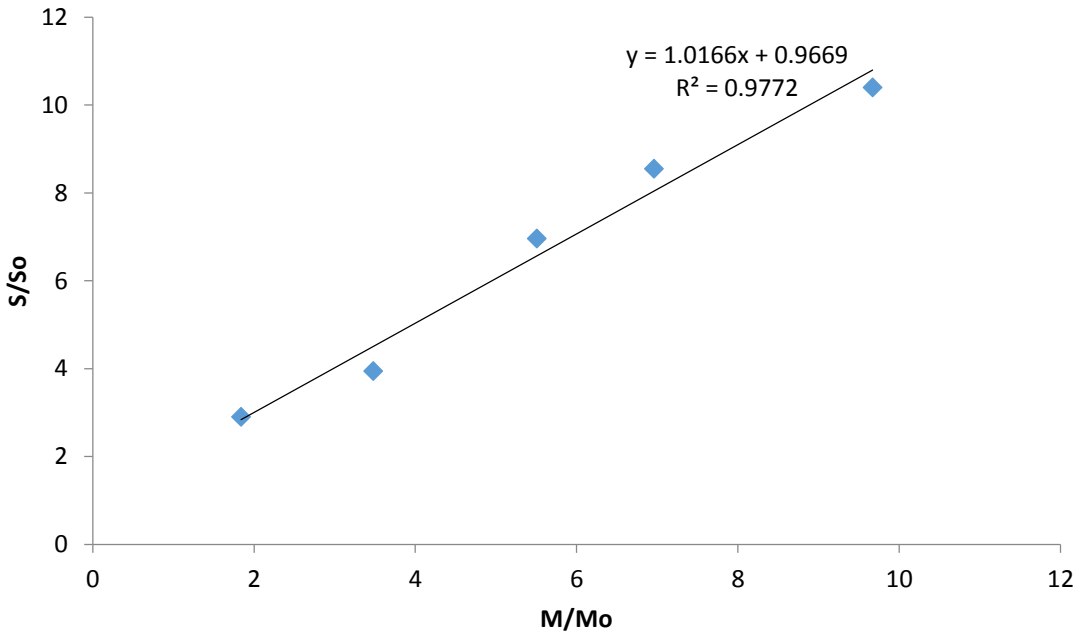

Figure 2.12. Calibration for benzene with decane as a standard.

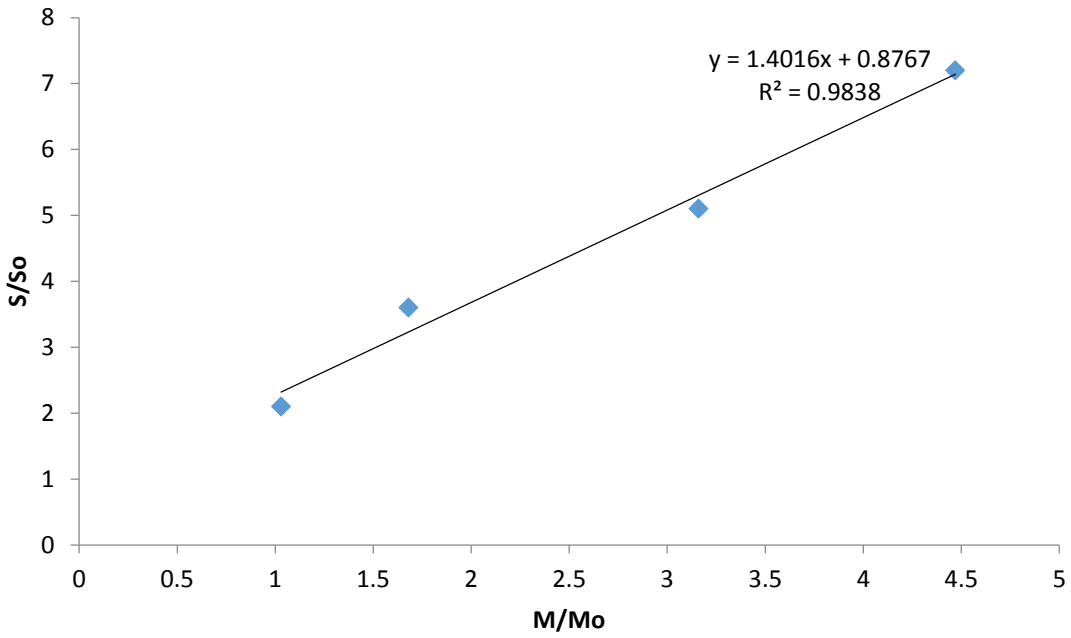

Figure 2.13. Calibration for cumene with decane as a standard.

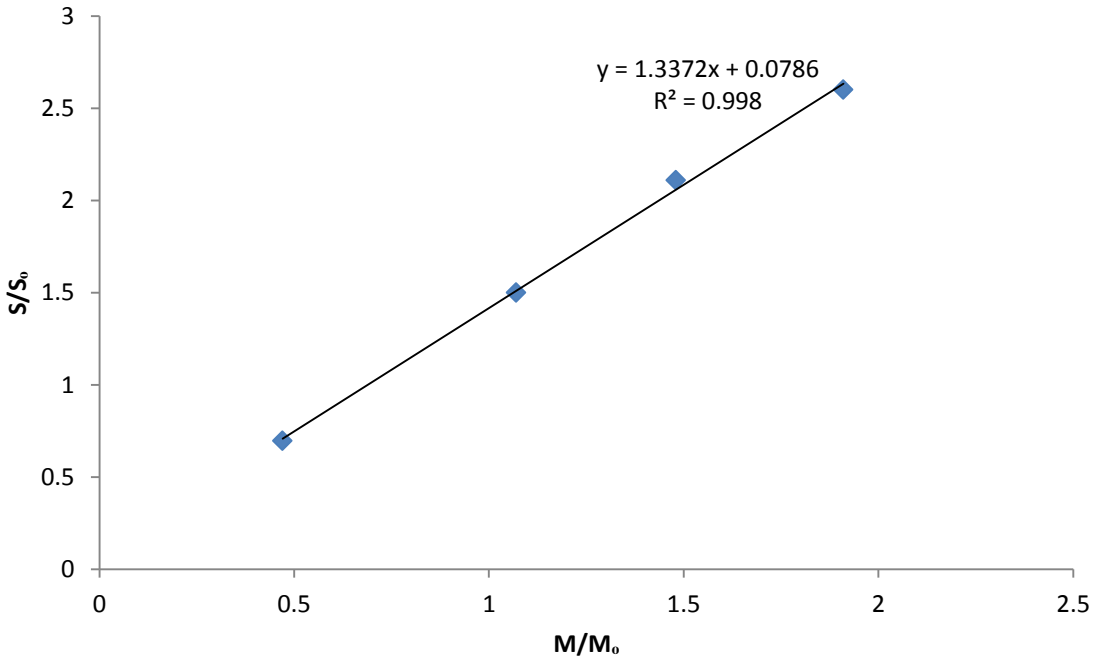

Figure 2.14. Calibration for cumene with benzene as a standard.

2.3.11. Catalyst testing

2.3.11.1. Alkylation of benzene by propane in the gas phase

The alkylation of benzene by propane was studied at 250-350 ºC and an inlet C_6H_6/C_3H_8 molar ratio of 1:9 under atmospheric pressure in a quartz fixed-bed down-flow reactor (9.0 mm internal diameter) (Figure 2.15). The reactor was fitted with online GC analysis (Varian 3800 instrument with a 30 m × 0.32 mm × 0.5 µm Zebron ZB-WAX capillary column and a flame ionization detector). For more accurate analysis of C_1-C_3 hydrocarbon, a 60 m × 0.32 mm GS-GasPro capillary column, which allowed for complete separation of these hydrocarbons, was used. The temperature in the reactor was controlled by a Eurotherm controller using a thermocouple placed at the top of the catalyst bed. Benzene was fed into the gas flow by passing propane flow controlled by a Brooks mass flow controller through a stainless steel saturator, which held liquid benzene at 20 ºC to maintain the chosen reactant partial pressure of 10 kPa [31]. The downstream gas lines and valves were heated to 150 ºC to prevent substrate and product condensation. The reactor was packed with 0.20 g catalyst powder of 45-180 µm particle size. The gas feed entered the reactor at the top at a flow rate of 10 mL min^{-1} (space time W/F = 80 g h mol^{-1}, where W (g) is the catalyst weight and F (mol h^{-1}) is the molar flow rate of benzene). Prior to reaction, the catalyst was pre-treated in H_2 for an hour at the reaction temperature. The online GC was employed to analyse the downstream gas flow then to measure benzene conversion and product selectivity.

2.3.11.2. Alkylation of toluene by propane in the gas phase

In this case, the above conditions were used except that the saturator held liquid toluene at 45.2 ºC to maintain the chosen reactant partial pressure of 10 kPa [31]. Figure 2.15 shows the schematic reactor setup.

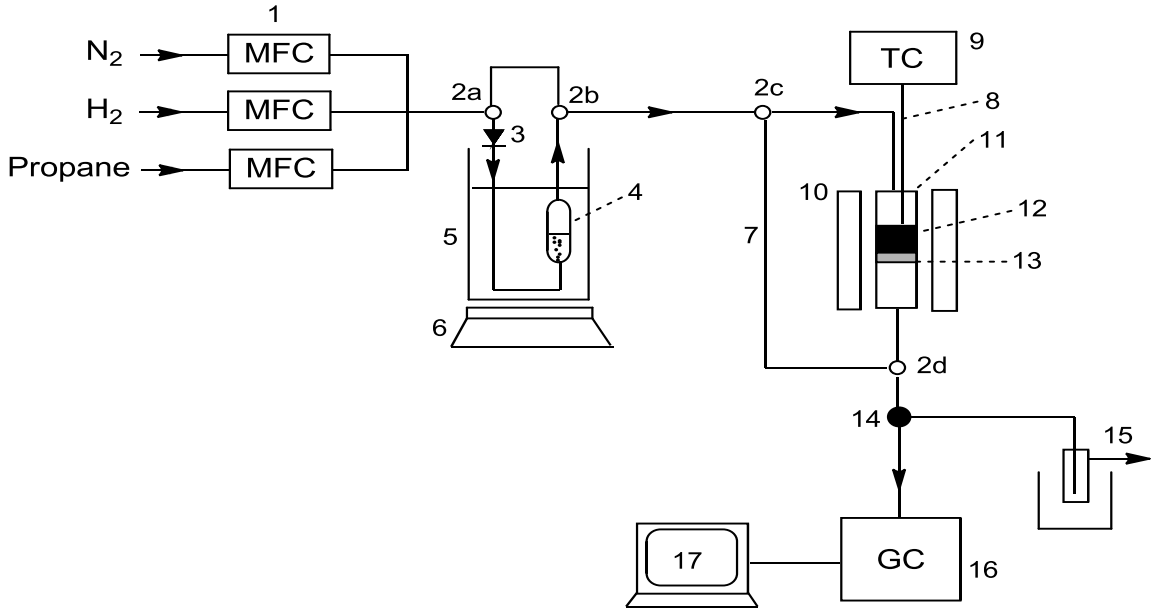

Figure 2.15. Continuous flow fixed-bed reactor setup for alkylation of benzene/toluene by propane: (1) Brooks mass flow controller, (2) 3-way valve, (3) check valve (non-return valve), (4) saturator containing liquid substrate, (5) temperature controlled water bath, (6) stirring hotplate, (7) bypass, (8) thermocouple, (9) Eurotherm temperature controller, (10) furnace, (11) quartz tubular reactor, (12) catalyst bed, (13) glass wool support, (14) Valco multiposition sampling valve with air actuator, (15) product trap, (16) Varian gas chromatograph, (17) computer.

Substrate conversion and product yield and selectivity were calculated using the following equations:

$$\text{Conversion of substrate (\%)} = \frac{\text{Moles of substrate reacted}}{\text{Moles of substrate fed}} \times 100 \qquad (2.10)$$

$$\text{Product yield (\%)} = \frac{\text{Moles of product}}{\text{Moles of substrate fed}} \times 100 \qquad (2.11)$$

The selectivity was defined as moles of product formed per mole of substrate converted and quoted in mole per cent. In this study, it was more convenient to calculate product selectivity from substrate conversion and product yield by the following equation:

$$\text{Product selectivity (\%)} = \frac{\text{Product yield}}{\text{Substrate conversion}} \times 100 \qquad (2.12)$$

Figures from 2.16 to 2.18 give examples of GC traces for alkylation of benzene and toluene with propane in gas phase.

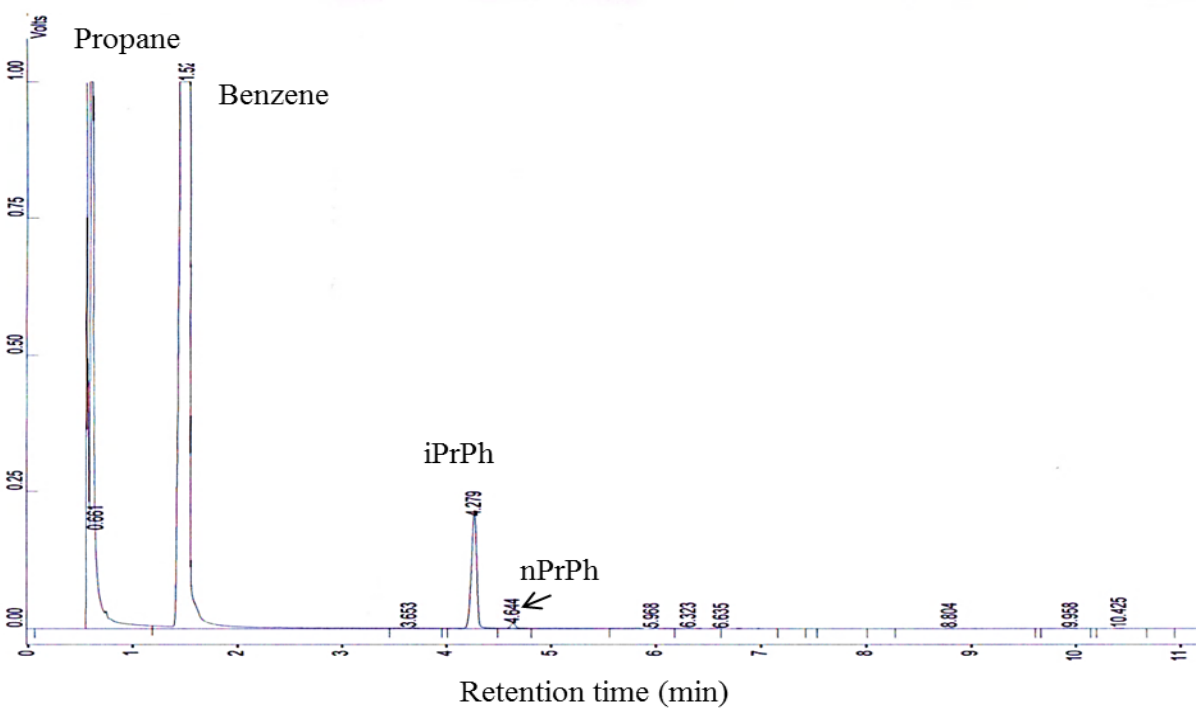

Figure 2.16. GC trace for alkylation of benzene with propane over 10%Pt/C + 25%HSiW/SiO_2 two-bed catalyst at 300°C, 10 ml min^{-1} flow rate.

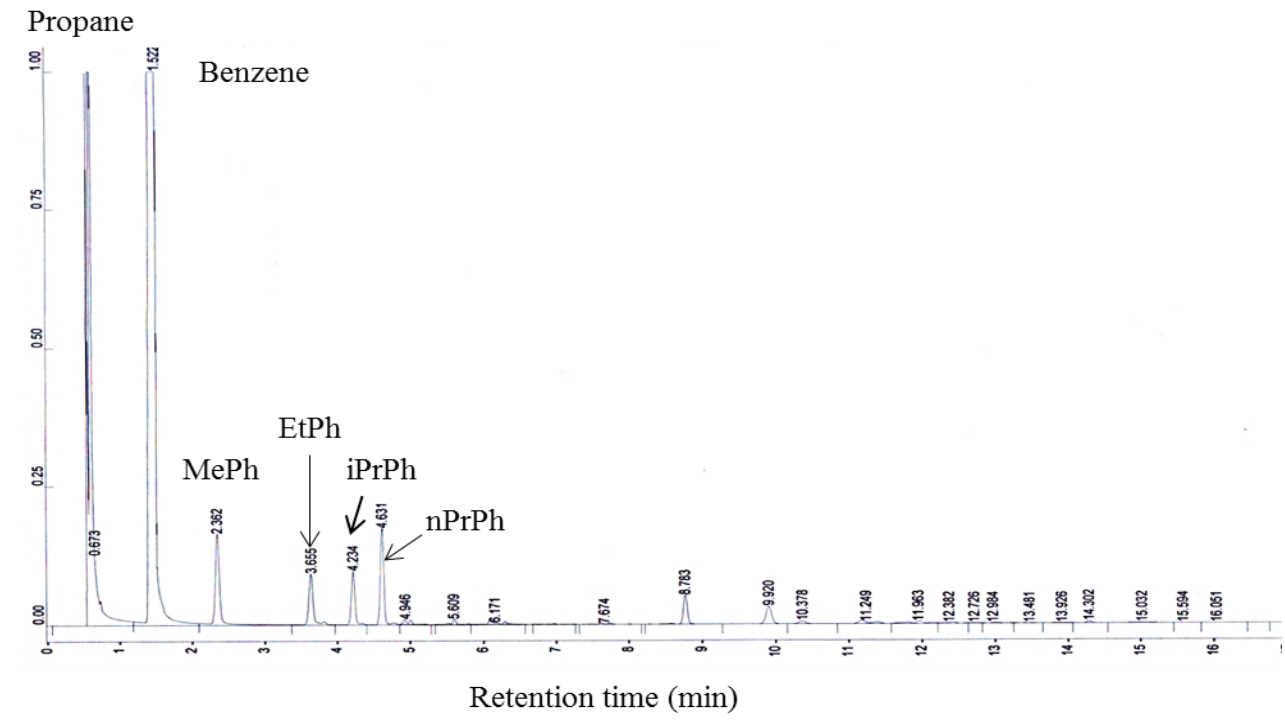

Figure 2.17. GC trace for alkylation of benzene with propane over HZSM-5 at 300°C, 10 ml min^{-1} flow rate.

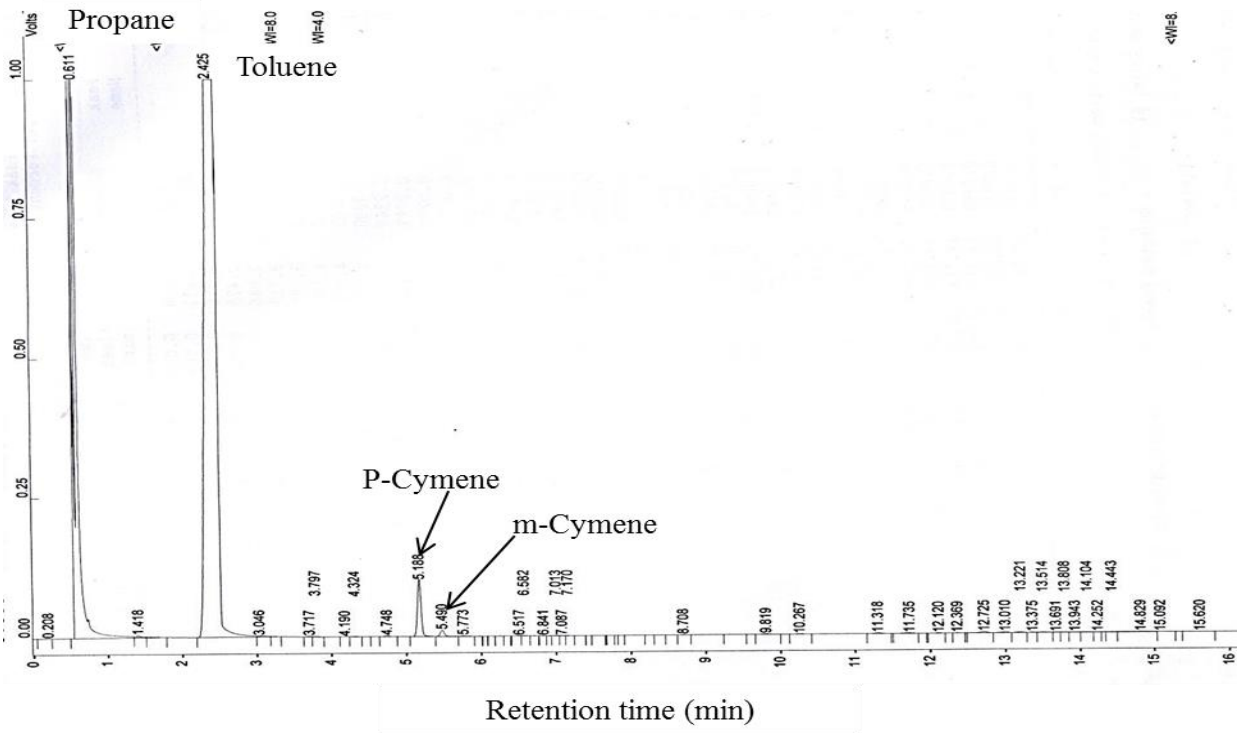

Figure 2.18. GC trace for alkylation of toluene with propane over mixed 5%Pt/C + 25%HSiW/SiO_2 catalyst (0.7%Pt) at 300 °C, 10 ml min^{-1} flow rate.

2.3.12. Gas chromatography-mass spectroscopy (GC-MS)

GC-MS is a powerful technique employed to identify reaction products. In this method, a substrate is vaporised using high vacuum, then bombarded by a beam of high-energy electrons. Many molecules undergo fragmentation and produce an array of ions of different size. Equation 2.13 illustrates this method, where M is the substrate to be ionised, e^- is the high-energy electron and $M^{\bullet+}$ is the charged ionised molecular radical [32].

$$M + e^- \longrightarrow M^{\bullet+} + 2e^- \qquad (2.13)$$

These ions are detected by acceleration in an electric field and then deflecting them in a magnetic field where they follow paths dictated by their mass/charge ratio. Each ion gives a peak in the mass spectrum. An example of GC-MS analysis of product mixture from the gas phase reaction of toluene alkylation with propane over 0.5%Pt/HZSM-5 catalyst is shown in Figure 6.3 (Chapter 6).

References

1. Tatematsu, S.; Hibi, T.; Okuhara, T.; Misono, M. *Chem. Lett.* **1984,** 865.
2. Alsalme, A. M.; Wiper, P. V.; Khimyak, Y. Z.; Kozhevnikova, E. F.; Kozhevnikov, I. V. *J. Catal.* **2010,** *276*, 181.
3. Alharbi, W.; Brown, E.; Kozhevnikova, E. F.; Kozhevnikov, I. V. *J. Catal.* **2014,** *319*, 174.
4. Alotaibi, M. A.; Kozhevnikova, E. F.; Kozhevnikov, I. V. *Appl. Catal. A* **2012,** *447-448*, 32.
5. Alotaibi, M. A.; Kozhevnikova, E. F.; Kozhevnikov, I. V. *J. Catal*. **2012,** *293*, 141.
6. Venesia, A. M.; La Parola, V.; Deganello, G.; Pawelec, B. J. G. Fierro, *J. Catal.* **2003,** *215*, 317.
7. Leofanti, G.; Padovan, M.; Tozzola, G.; Venturelli, B. *Catal. Today,* **1998,** *41*, 207.
8. Rouquerol, J.; Avnir, D.; Fairbridge, C.W.; Everett, D.H.; Haynes, J.H.; Pernicone, N.; Ramsay, J.D.F.; Sing, K.S.W.; Unger, K.K. *Pure Appl. Chem.* **1994,** *66*, 1739.
9. Rothenberg, G. *Catalysis: Concepts and Green Applications*, Wiley-VCH, Weinheim, **2008**.
10. Leofanti, G.; Tozzola, G.; Padovan, M.; Petrini, G.; Bordiga, S.; Zecchina, A. *Catal. Today*, **1997,** *34*, 329.
11. Leofanti, G.; Tozzola, G.; Padovan, M.; Petrini, G.; Bordiga, S.; Zecchina, A. *Catal. Today*, **1997,** *34*, 307.
12. Brunauer, S.; Emmett, P.H.; Teller, E. *J. Am. Chem. Soc.* **1938,** *60*, 309.
13. Gregg, S.J.; Sing, K.S.W. *Adsorption, Surface Area and Porosity,* Academic Press, London, **1982**.
14. Unger, K.K.; Roquerol, J.; Sing, K.S.W.; Kral H. (Eds.), *Characterisation of Porous Solids I*, Elsevier, Amsterdam, **1988**.
15. Roquerol, J.; Rodriguez-Reinoso, F.; Sing, K.S.W.; Unger, K.K. *Characterisation of Porous Solids III*, Elsevier, Amsterdam, **1994**.

16. Joyner, L.G.; Barrett, E.P.; Skold, R. *J. Am. Chem. Soc.* **1951,** *73*, 3155.
17. Atkins, P.W. *Physical Chemistry*, Oxford University Press, **1998**.
18. Burton, A.W. *Zeolite Characterization and Catalysis:* A **2009,** 1.
19. Pinna, F. *Catal. Today* **1998,** *41*, 129.
20. Benson, J.E.; Hwang, H.S.; Boudart, M. *J. Catal.* **1973,** *30*, 146.
21. Benson, J.E.; Boudart, M. *J. Catal.* **1965,** 4, 704.
22. Prelazzi, G.; Cerboni, M.; Leofanti, G. *J. Catal.* **1999,** *181*, 73.
23. TPD/TPR 2900 analyser, Operator's manual, *VI.* 02, April **1993**.
24. Schwedt, G. *The Essential Guide to Analytical Chemistry,* John Wiley and Sons, Chichester, England, **1997**.
25. Fifield, F.W.; Kealy, D. *Principles and practice of analytical chemistry*, (5^{th} ed), Blackwell Science Ltd, **2000**.
26. Mendham, J.; Denney, R.C.; Barnes, J.D.; Thomas, M.J.K. *Vogel's Textbook of Quantitative Chemical Analysis,* Preston Education Ltd, **2000**.
27. Fowis, I.A. *Gas Chromatography*, ACOL-Wiley, Chichester, **1995**.
28. Kealey, D.; Haines, D.J. *Analytical Chemistry, (1st ed),* Bio scientific, Oxford, **2002**.
29. http://teaching.shu.ac.uk/hwb/chemistry/totorials/chrom/gaschrm.htm (accessed 20 July 2017).
30. Robert, L.G.; Eugene, F.B. *Modern Practice of Gas Chromatography, (4th ed)*, Wiley Inter science, **2004**.
31. *CRC Handbook of Chemistry and Physics;* W.M. Haynes, ed.; CRC Press, **2012**.
32. Kealey, D.; Haines, D.J. *Analytical Chemistry, 1^{st} ed.*, Bio scientific, Oxford, **2002**.

Chapter 3: Catalyst characterisation

This chapter describes the results of catalyst characterisation, which determined the catalyst properties such as surface area, porosity, crystallinity, water content, metal dispersion, elemental composition and thermal stability. These properties were measured by various techniques detailed in Chapter 2.

3.1. Surface area and porosity analysis

As described in Chapter 2, section 2.3.1, the N_2 adsorption at -196 °C (77 K) was used to determine the surface area and porosity of the catalysts. The total surface area was measured using the BET method, while the BJH method was employed to measure pore size and pore volume of our catalysts.

3.1.1. Heteropoly acid catalysts

The surface area and porosity of bulk heteropoly acids, their Cs salts and silica-supported HPW and HSiW have been studied previously and well documented in the literature [1, 2]. The surface areas of bulk heteropoly acids, which have high solubility in water, are very low, in the range of 1 to 10 m^2g^{-1} [1, 2]. In contrast, the insoluble acidic salt CsPW has a large surface area (126-152 m^2g^{-1}) and low porosity [3, 4].

The BET surface area and porosity for most of catalysts employed in this study are listed in Table 3.1. It can be seen that the silica-supported HPW and HSiW have large surface areas (198 and 191 m^2g^{-1} respectively) and pore volumes (0.8 – 1.0 cm^3g^{-1}), as expected. Moreover, small platinum loadings (0.1-1%) had little effect on the surface area.

Table 3.1. Texture of HPA catalysts from N_2 adsorption.

Catalyst	S_{BET}[a] ($m^2\ g^{-1}$)	Pore volume[b] ($cm^3 g^{-1}$)	Pore size[c] (Å)
$Cs_{2.5}H_{0.5}PW_{12}O_{40}$	152.7	0.10	27
1.0%Pt/CsPW	141.5	0.09	24
0.3%Pt/CsPW	134.4	0.09	26
0.1%Pt/CsPW	126.4	0.08	25
25%HPW/SiO_2	198.4	1.00	203
1.0%Pt/25%HPW/SiO_2	188.7	0.92	195
0.3%Pt/25%HPW/SiO_2	190.9	0.85	178
0.1%Pt/25%HPW/SiO_2	196.2	0.85	174
25%HSiW/SiO_2	191.2	0.84	177
1.0%Pt/25%HSiW/SiO_2	174.6	0.88	194
0.3%Pt/25%HSiW/SiO_2	190.9	0.81	169
0.1%Pt/25%HSiW/SiO_2	189.4	0.88	187
40%HSiW/SiO_2	177.6	0.81	178
15%HSiW/SiO_2	208.2	0.98	181

a) BET surface area. b) Single point total pore volume. c) Average BET pore diameter.

Figure 3.1 shows the N_2 adsorption/desorption isotherm for 25%HPW/SiO_2, which is a type IV isotherm according to the IUPAC classification, indicating a mesoporous material. Also the isotherm has a type H3 hysteresis loop, which is indicative of non-uniform pores in size and/or shape. Figure 3.2 shows the pore size distribution for 25%HPW/SiO_2 obtained from desorption isotherm using the BJH method, which peaks at a 244 Å pore diameter. Similar results were obtained for 25%HSiW/SiO_2 catalyst (Figure 3.3 and 3.4).

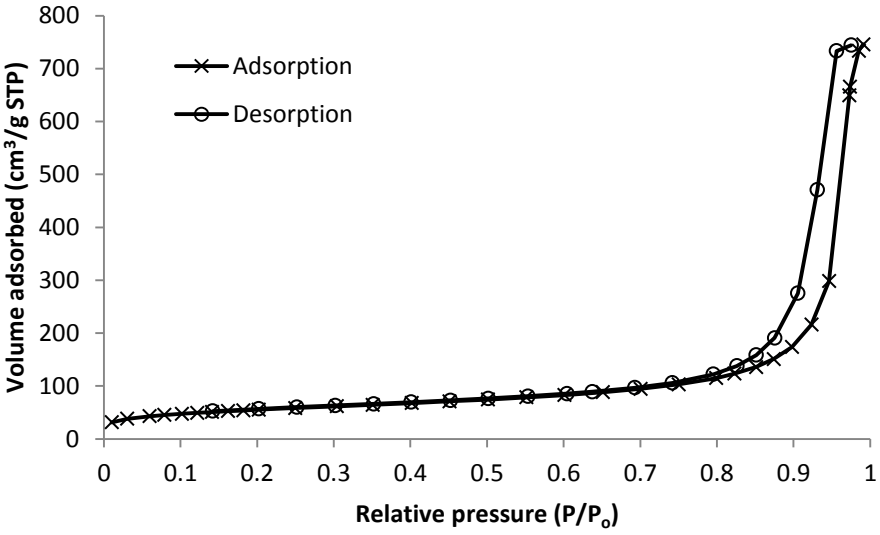

Figure 3.1. Nitrogen adsorption/desorption isotherm for 25%HPW/SiO_2.

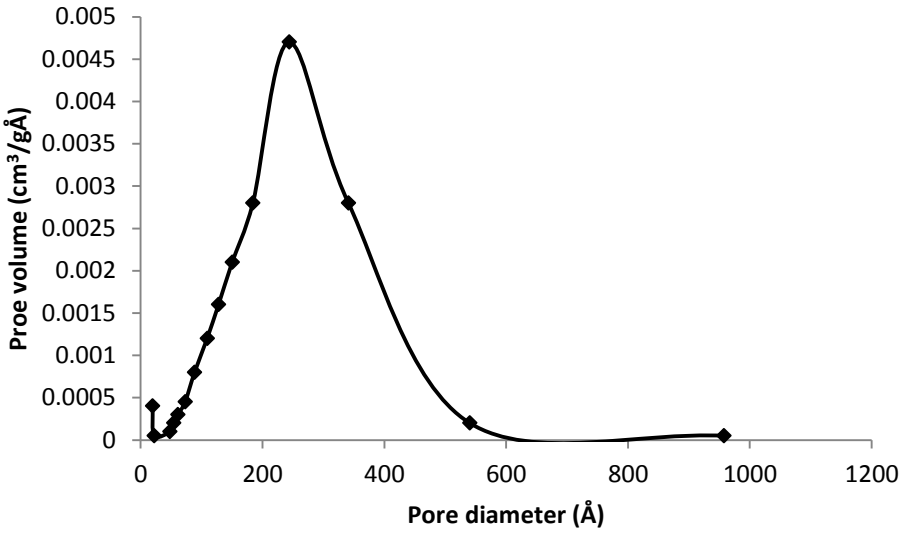

Figure 3.2. Pore size distribution for 25%HPW/SiO_2.

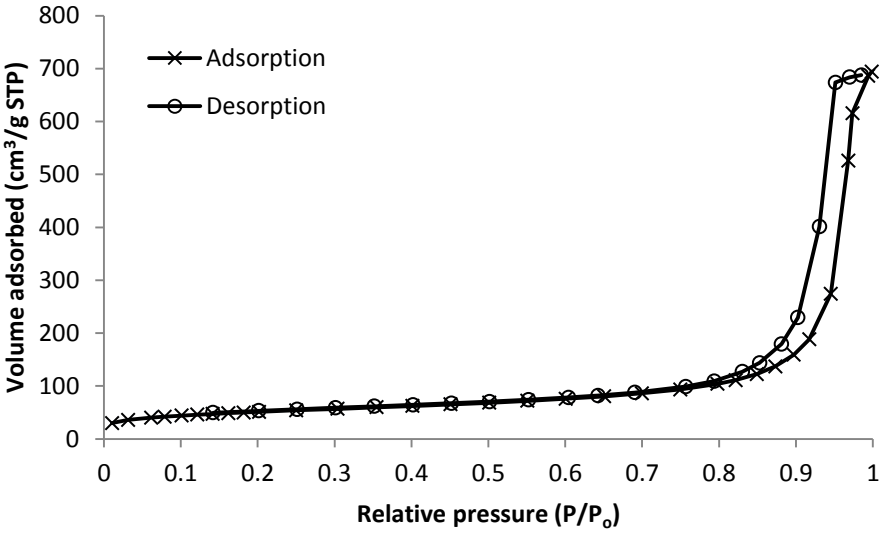

Figure 3.3. Nitrogen adsorption/desorption isotherm for 25%HSiW/SiO_2.

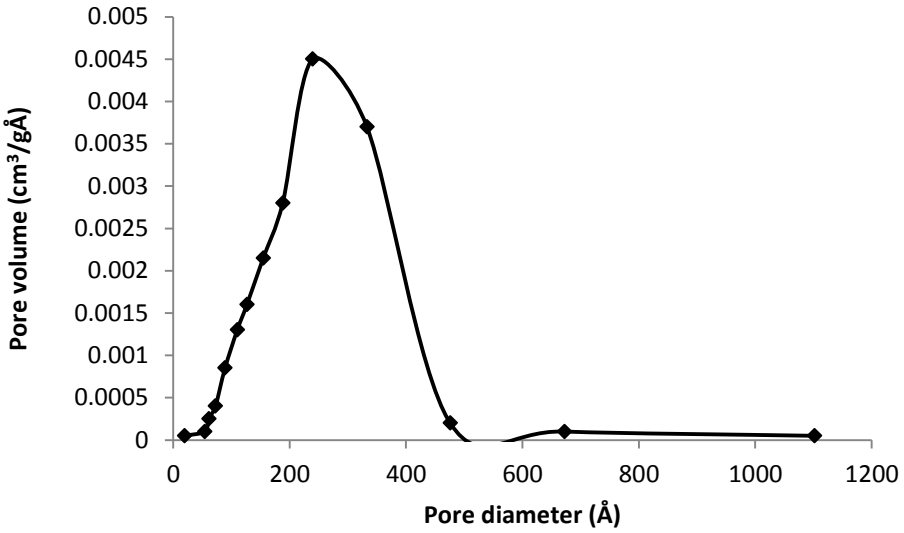

Figure 3.4. Pore size distribution for 25%HSiW/SiO_2.

The nitrogen adsorption/desorption isotherm of $Cs_{2.5}H_{0.5}PW_{12}O_{40}$ (CsPW) is shown in Figure 3.5. It is a type IV isotherm, with a type H2 hysteresis loop, representing a mesoporous material with non-uniform pore shape. However, from the pore size distribution (Figure 3.6), the steep increase in adsorption at low pressures indicates the presence of micropores in CsPW, which is in agreement with the previous reports [2, 5, 6]. Pores of 39 Å diameter dominate in CsPW, in agreement with the literature [7].

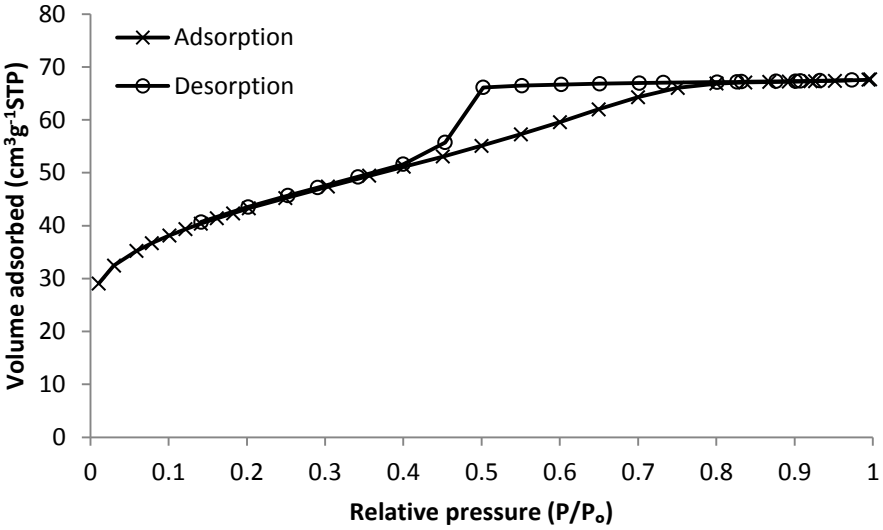

Figure 3.5. Nitrogen adsorption/desorption isotherm for $Cs_{2.5}H_{0.5}PW_{12}O_{40}$.

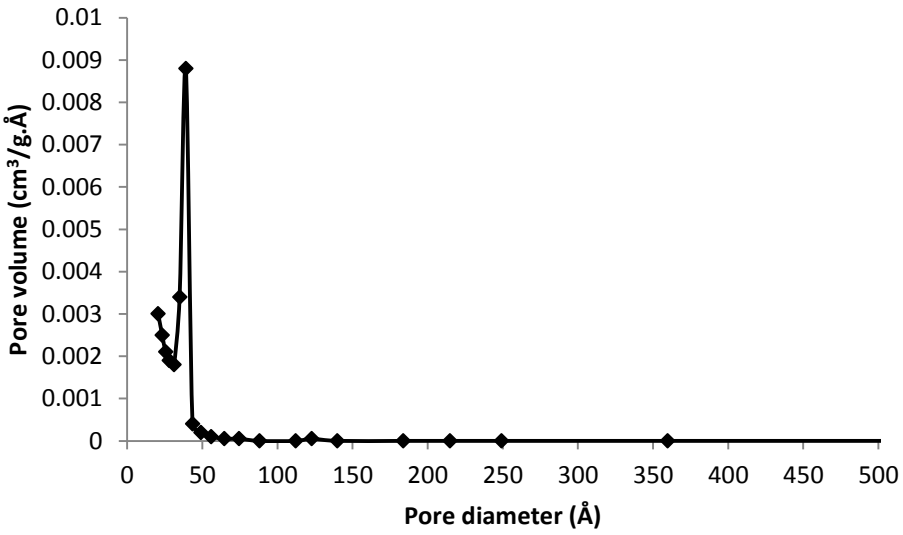

Figure 3.6. Pore size distribution for $Cs_{2.5}H_{0.5}PW_{12}O_{40}$.

3.1.2. Zeolite catalysts

Table 3.2 gives the texture of zeolite catalysts which were used in this study. The adsorption isotherms for zeolite catalysts are of type I with a H4 hysteresis loop, an indication of uniform microporous materials with slit shaped pores. Nitrogen adsorption isotherms for HZSM-5 (Si/Al =10), 0.5%Pt/HZSM-5 (Si/Al =10), 2%Pd/HZSM-5 (Si/Al =10), 1.0%Pt/HZSM-5 (Si/Al =30) and 0.5%Au/HZSM-5 (Si/Al =30) are shown in Figures 3.7-3.11.

Table 3.2. Texture of zeolite catalysts.

Catalyst	S_{BET}[a] ($m^2\ g^{-1}$)	Pore volume[b] ($cm^3 g^{-1}$)	Pore size[c] (Å)
HZSM-5 (Si/Al = 10)	294	0.23	31
0.5%Pt/HZSM-5 (Si/Al = 10)	302	0.22	29
0.5%Pt-0.5%Au/HZSM-5 (Si/Al = 10)	262	0.20	31
0.5%Au/HZSM-5 (Si/Al = 10)	269	0.21	32
2%Pd/HZSM-5 (Si/Al = 10)	255	0.20	31
0.5%Au/HZSM-5 (Si/Al = 30)	381	0.23	24
1%Pt/ZSM-5 (Si/Al = 30)	360	0.22	24

a) BET surface area. b) Single point total pore volume. c) Average BET pore diameter.

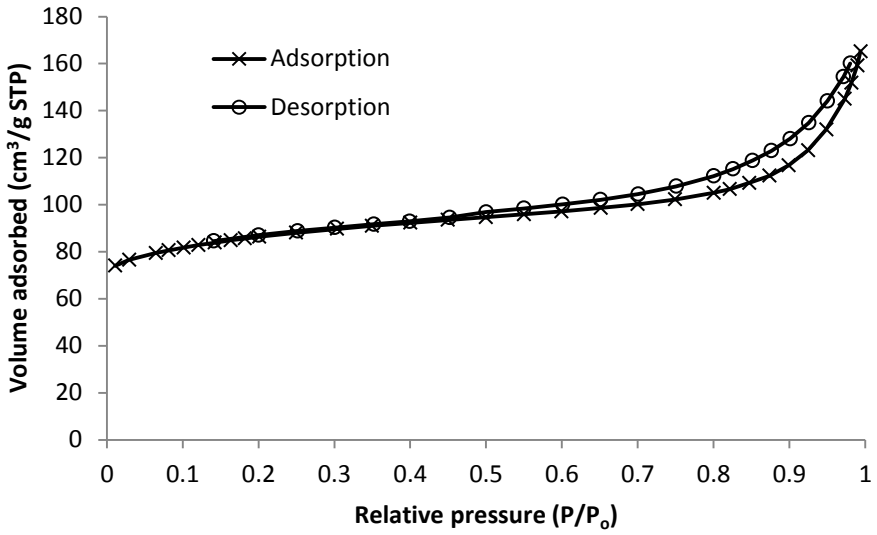

Figure 3.7. Nitrogen adsorption/desorption isotherm for HZSM-5 (Si/Al = 10).

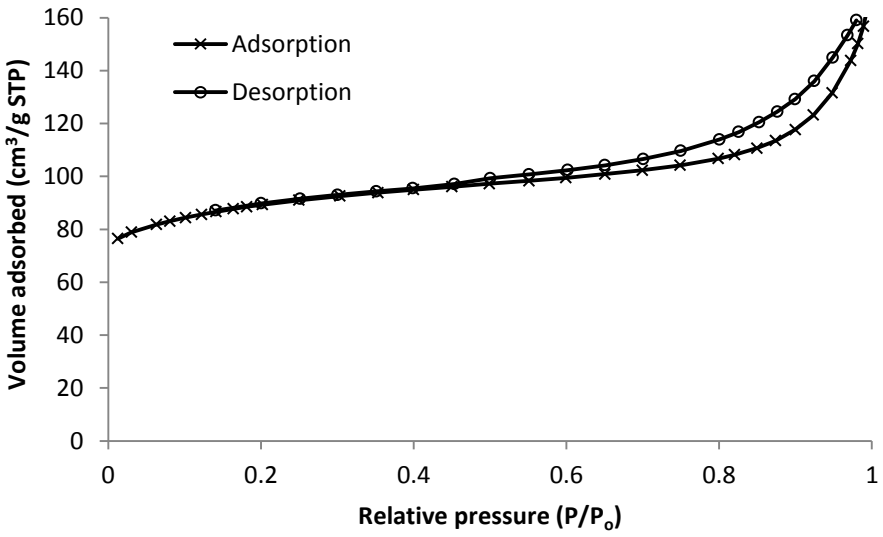

Figure 3.8. Nitrogen adsorption/desorption isotherm for 0.5%Pt/HZSM-5 (Si/Al = 10).

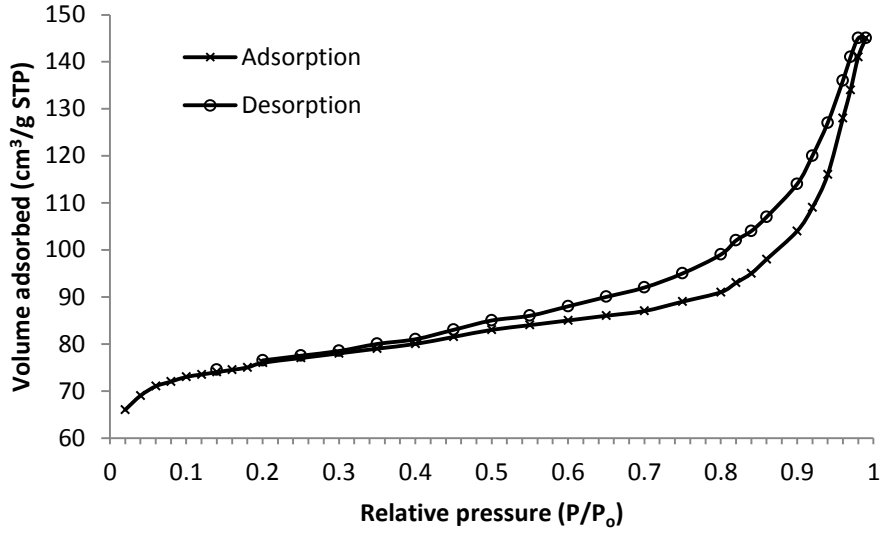

Figure 3.9. Nitrogen adsorption/desorption isotherm for 2%Pd/HZSM-5 (Si/Al = 10).

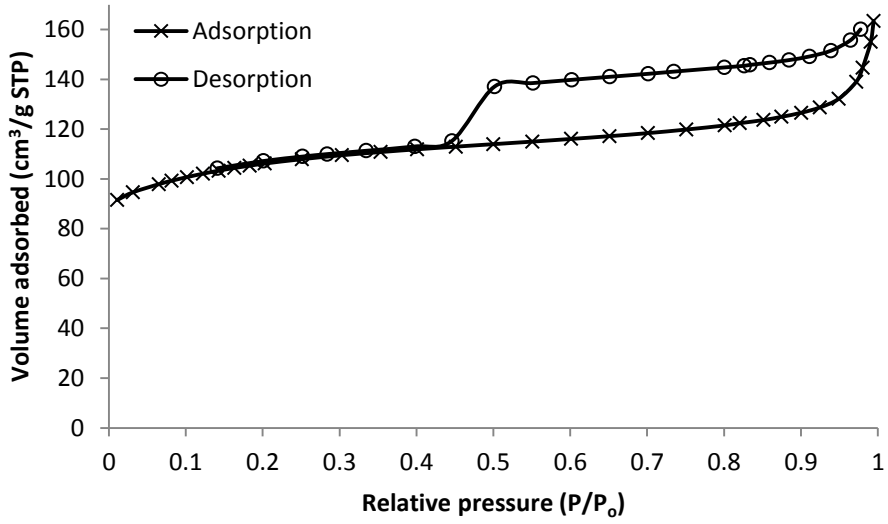

Figure 3.10. Nitrogen adsorption/desorption isotherm for 1%Pt/HZSM-5 (Si/Al = 30).

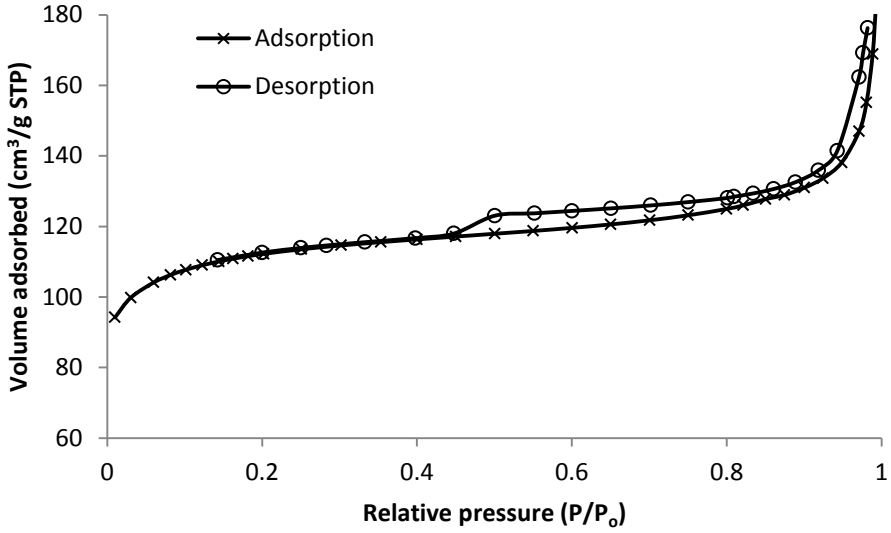

Figure 3.11. Nitrogen adsorption/desorption isotherm for 0.5%Au/HZSM-5 (Si/Al = 30).

The pore size distribution for these four zeolite catalysts is displayed in Figure 3.12; it shows mesopores of about 39 Å diameter as well as micropores.

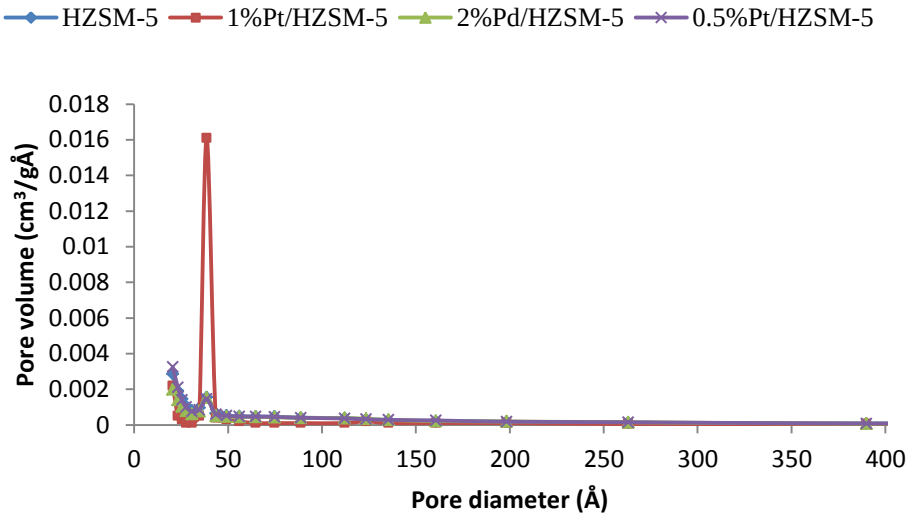

Figure 3.12. Pore size distribution for zeolite catalysts.

3.2. Powder X-ray diffraction (XRD)

The powder XRD described in chapter 2, section 2.3.2 was recorded for heteropoly acid and zeolite catalysts as well as carbon-supported metal catalysts. XRD patterns were attributed using the JCPDS database.

3.2.1. X-ray diffraction for heteropoly acid catalysts

The XRD pattern for $Cs_{2.5}PW$ is shown in Figure 3.13, which compares well with that in the literature [7, 8]. In Figure 3.14, no pattern of crystalline HPA can be seen for supported 25%HSiW/SiO_2 comparing to bulk HSiW. The XRD of 2%Pd/25%HSiW/SiO_2 shows the Pd (111) diffraction peak at 39.9°.

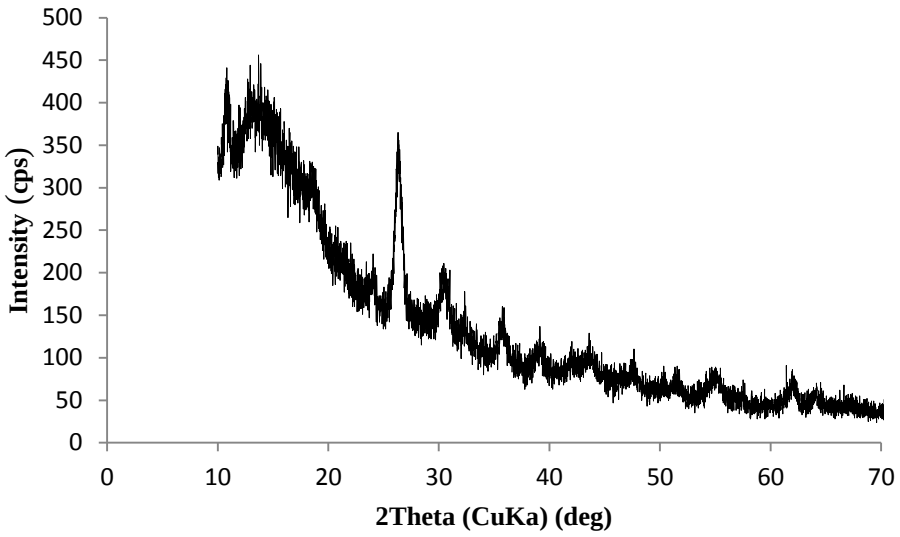

Figure 3.13. XRD pattern for $Cs_{2.5}H_{0.5}PW_{12}O_{40}$ catalyst (Cu Kα radiation).

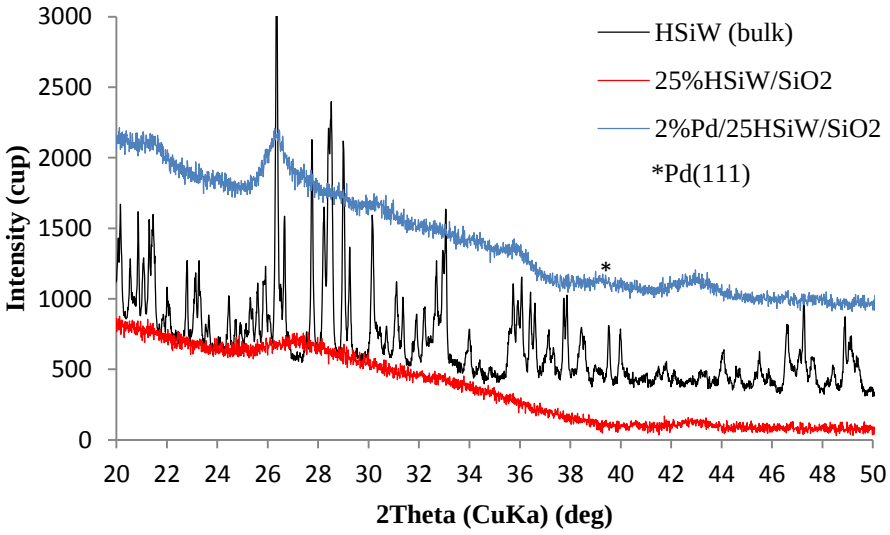

Figure 3.14. XRD patterns (Cu Kα radiation) for bulk HSiW (black), 25%HSiW/SiO_2 (red) and 2.0%Pd/25%HSiW/SiO_2 (blue).

Figure 3.15 shows the XRD for supported 25%HPW/SiO_2 and 25%HSiW/SiO_2. These catalysts are amorphous; no pattern of crystalline HPA can be seen. Figure 3.16 illustrates the XRD patterns for 0.5%Pt/25%HSiW/SiO_2, 0.5%Au/25%HSiW/SiO_2 and 0.5%Pt/0.5%Au/25%HSiW/SiO_2 catalysts. These catalysts are also HPA-amorphous, however the (111) diffraction peaks for Pt (39.9 ^{o}) and Au (38.2 ^{o}) are clearly seen.

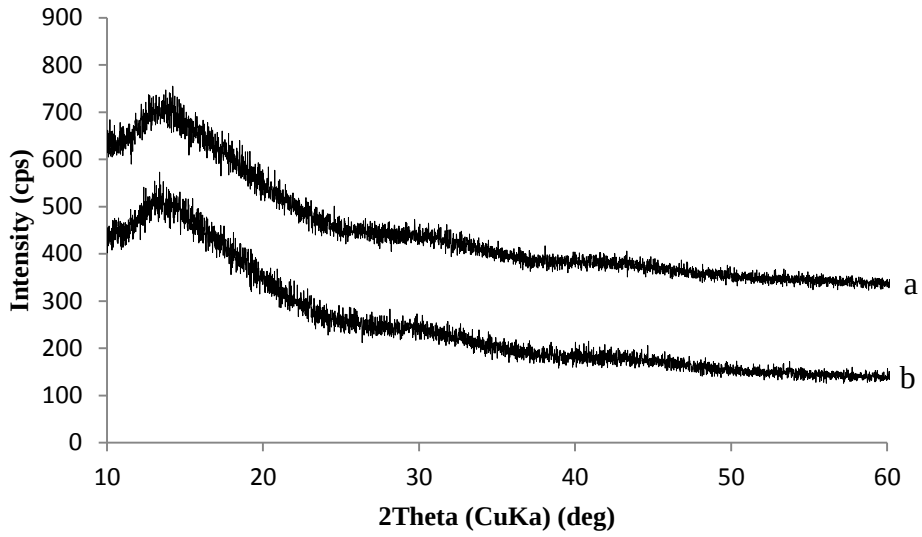

Figure 3.15. XRD patterns for silica-supported HPA catalysts (Cu Kα radiation): (a) 25%HSiW/SiO_2 and (b) 25%HPW/SiO_2.

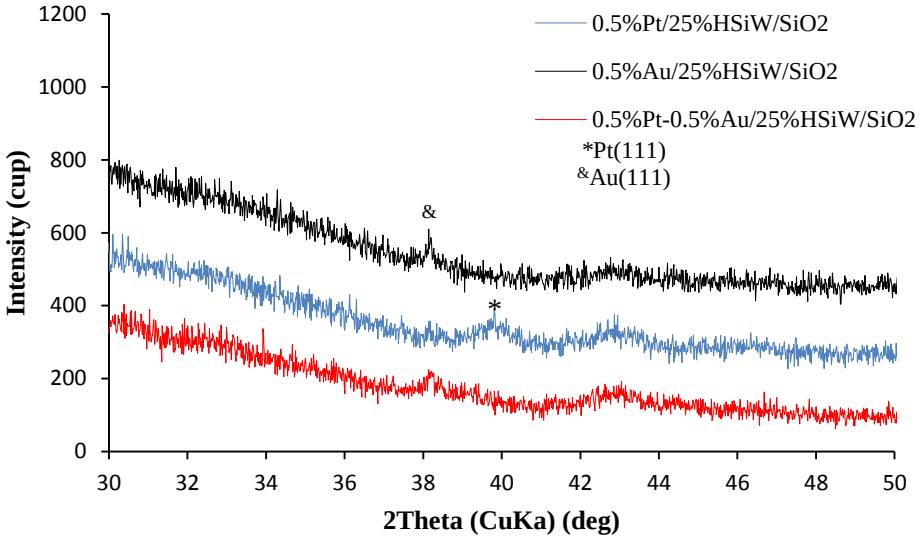

Figure 3.16. XRD patterns (Cu Kα radiation) for: 0.5%Pt/25%HSiW/SiO_2 (blue), 0.5%Au/25%HSiW/SiO_2 (black) and 0.5%Pt/0.5%Au/25%HSiW/SiO_2 (red).

3.2.2. X-ray diffraction for zeolite catalysts

Zeolites are crystalline materials which display XRD patterns characteristic of their structure [9]. Figure 3.17 illustrates the XRD patterns for HZSM-5 and 2%Pd/HZSM-5 (Si/Al = 10) catalysts. They had the typical pattern of MFI type zeolite, in agreement with the literature [10, 11]. The XRD of Pd/HZSM-5 clearly shows the Pd (111) diffraction peak at 39.9° [11]. This broad peak indicates high dispersion of Pd. The XRD for 0.5%Pt/HZSM-5 (Si/Al = 10), 0.5%Au/HZSM-5 and 0.5%Pt/0.5%Au/HZSM-5 are shown in Figure 3.18; these display the pattern of HZSM-5 together with (111) diffraction peaks of Pt and Au.

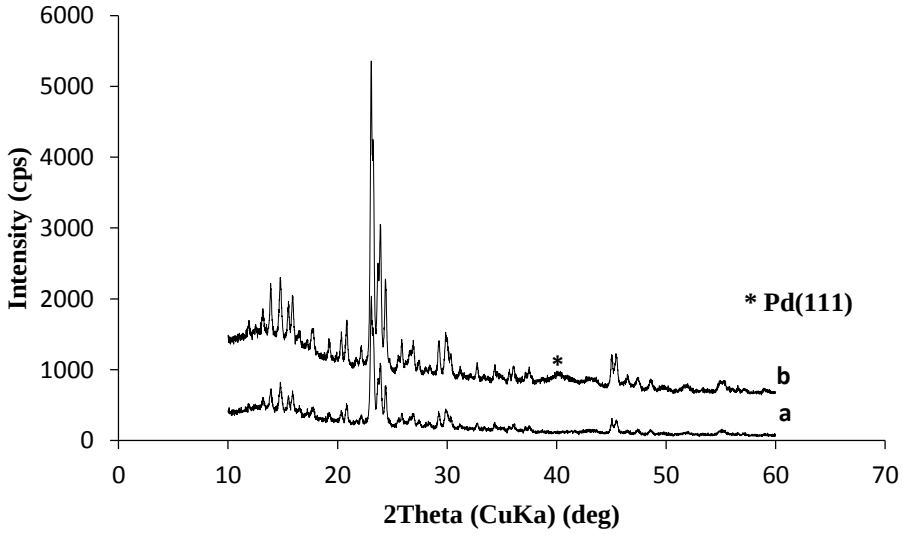

Figure 3.17. XRD patterns for zeolite catalysts: (a) HZSM-5 and (b) 2%Pd/HZSM-5 (Si/Al = 10).

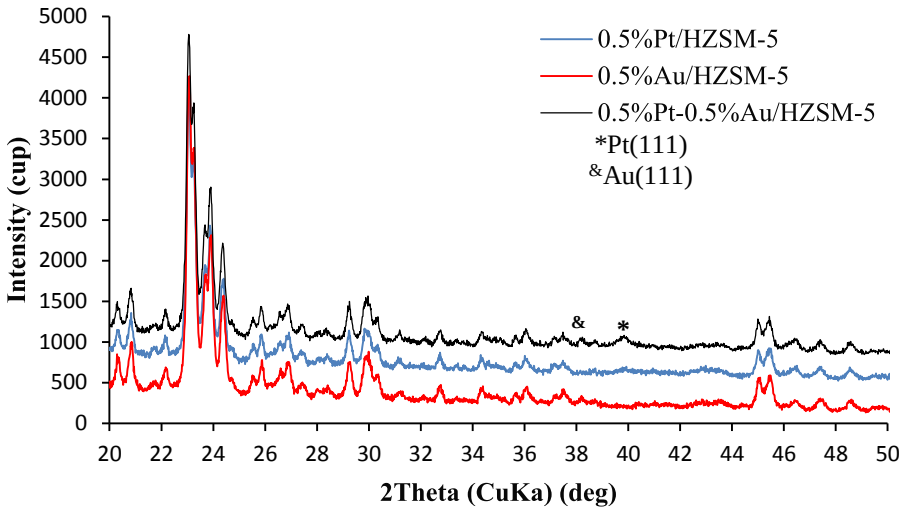

Figure 3.18. XRD patterns for 0.5%Pt/HZSM-5 (blue), 0.5%Au/HZSM-5 (red) and 0.5%Pt/0.5%Au/HZSM-5 (black) (Si/Al = 10).

3.2.3. Carbon-supported metal catalysts

The XRD patterns of carbon-supported Pt, Pd and Au catalysts are shown in Figure 3.19 and Figure 3.20. As expected, the most intense metal peaks are clearly observable; these include the diffraction peaks of Au(111), Au(200), Pt(111). The width of these peaks indicates much higher dispersion of Pd and Pt on carbon support as compared to Au. From these data, metal dispersion was estimated using the Scherrer equation (see below).

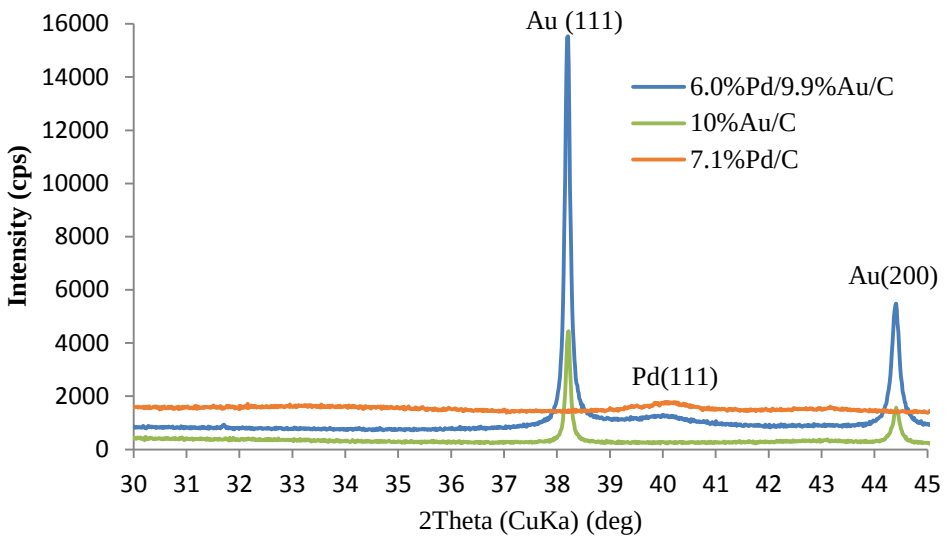

Figure 3.19. XRD of carbon-supported metal catalysts: 6.0%Pd/9.9%Au/C (blue), 10%Au/C (beige) and 7.1%Pd (green).

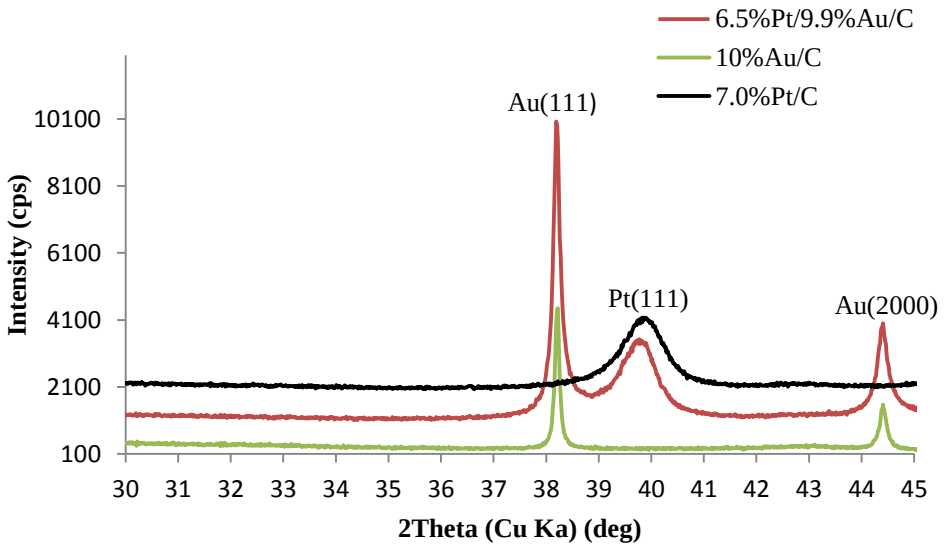

Figure 3.20. XRD of carbon-supported metal catalysts: 6.5%Pt/9.9%Au/C (red), 10%Au/C (green) and 7.0%Pt (black).

3.3. Temperature programmed reduction (TPR)

H_2-TPR for some catalysts used in this work was carried out on a Micromeritics TPD/TPR 2900 as described in Chapter 2, section 2.3.3. Figure 3.21 shows the H_2-TPR

profiles for 25%HSiW/SiO_2 and 1%Pt/25%HSiW/SiO_2 catalysts. The TPR profile for 25%HSiW/SiO_2 peaks at 690 °C, with a reduction onset at around 630 °C. For 1%Pt/25%HSiW/SiO_2, the corresponding temperatures are decreased to 630 and ~550 °C. The Keggin structure would probably collapse before the reduction took place as HSiW decomposes at 445 °C [1]. Since Pt is already reduced in this catalyst, it leaves W(VI) reduction as the source of the H_2-TPR uptake signals. Therefore, all Pt/HSiW catalysts should be resistant to reduction with H_2 upon pre-treatment at 300 °C, which otherwise could have caused the loss of HPA acidity.

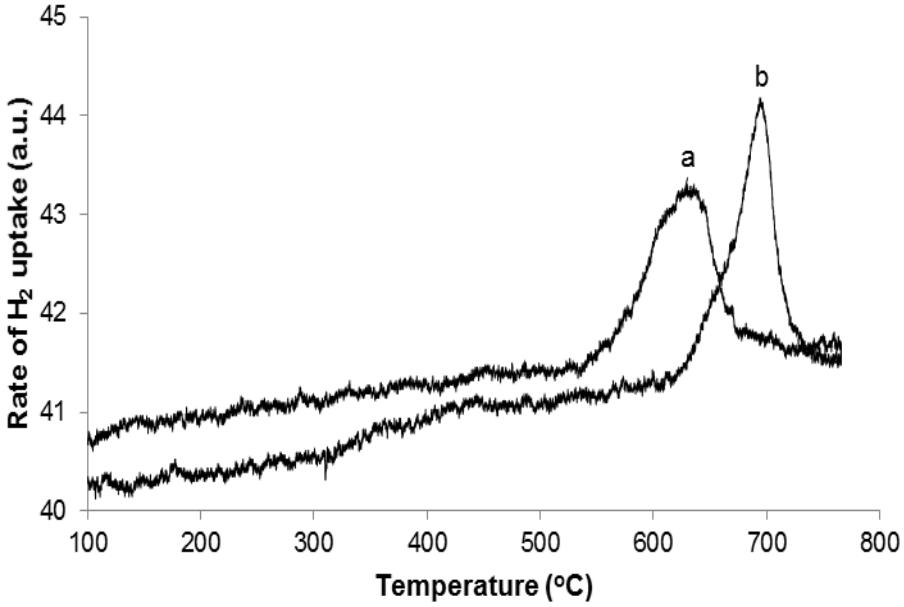

Figure 3.21. H_2-TPR for (a) 1%Pt/25%HSiW/SiO_2 and (b) 25%HSiW/SiO_2 (5 °C/min temperature ramp, catalysts pre-treated at 300 °C/1 h in N_2).

Figure 3.22 shows the H_2-TPR profiles for HPW, CsPW, 0.5%Pd/CsPW and 0.5%Pt/CsPW. The H_2-TPR profile for HPW peaks at 530 °C, with a reduction onset at ~400 °C. For CsPW, these temperatures were 750 and ~650 °C, respectively. These results are in agreement with previous reports [12, 13]. The TPR profiles for Pd/CsPW and Pt/CsPW peak at 710 and 730 °C, respectively, both with a reduction onset at ~600 °C.

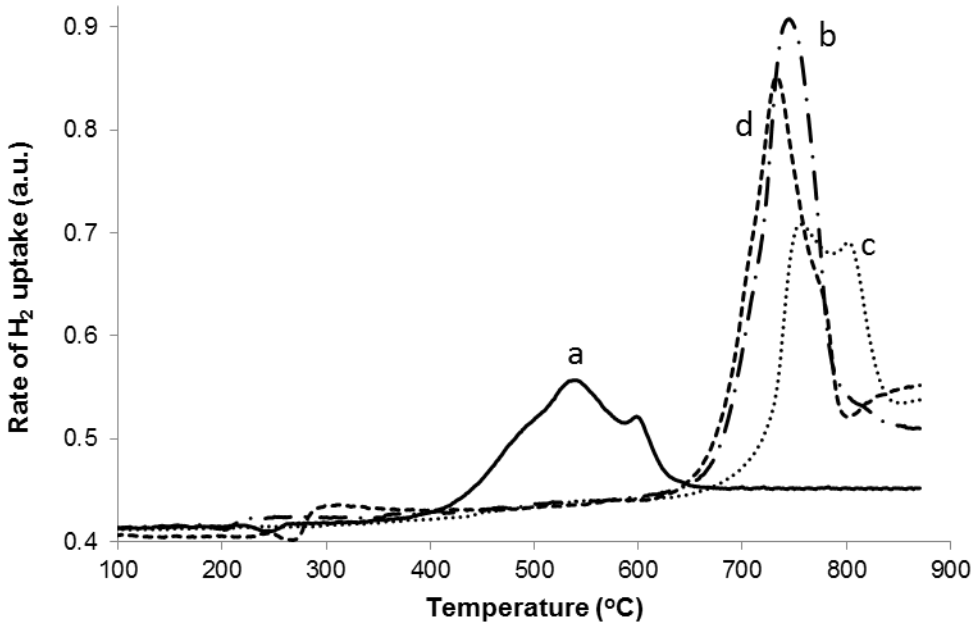

Figure 3.22. H_2-TPR for (a) HPW, (b) 0.5%Pt/CsPW, (c) CsPW and (d) 0.5%Pd/CsPW (catalysts pre-treated at 300 °C/1 h in N_2, 10 °C/min temperature ramp rate).

3.4. H_2 and CO chemisorption

In this work, the chemisorption of H_2 and CO was used to determine metal dispersion in supported metal catalysts (Chapter 3, sections 2.3.4 and 2.3.5). The results are given in Table 3.3. For comparison, are also given the values of metal dispersion obtained from XRD using the Scherrer equation.

Table 3.3. Metal dispersion.

Catalyst	Dispersion (%)		
	H_2/O_2 titration	CO titration	XRD
1%Pt/25%HSiW/SiO_2	25	24	24
1%Pt/25%HPW/SiO_2	28	27	--
2%Pd/25%HSiW/SiO_2	60	--	18
0.3%Pt/HZSM-5	--	60	--
2%Pd/HZSM-5	--	--	9.0
7.0%Pt/C	23	39	9.7
7.1%Pd/C	26	--	8.2
10%Au/C	0.7	--	1.0
9.9%Au/6.0%Pd/C	14 (Pd)	--	6.9 (Pd); 1.5 (Au)

3.5. Thermogravimetric analysis (TGA)

In this study, the TGA analysis was employed to measure the amount of water in catalysts and catalyst precursors as described in section 2.3.6.

3.5.1. HPA catalysts

TGA for bulk HPW hydrate is shown in Figure 3.23. This analysis gives 8.8% weight lost from 35 to 150 ºC due to the loss of hydration water. This water content was taken into account when preparing supported HPW catalysts. The second loss of weight (3.1%) appeared from 180 to 330 ºC, which due to the loss of six molecules of water bonded to the acidic protons in HPW without collapse of the Keggin structure [1].

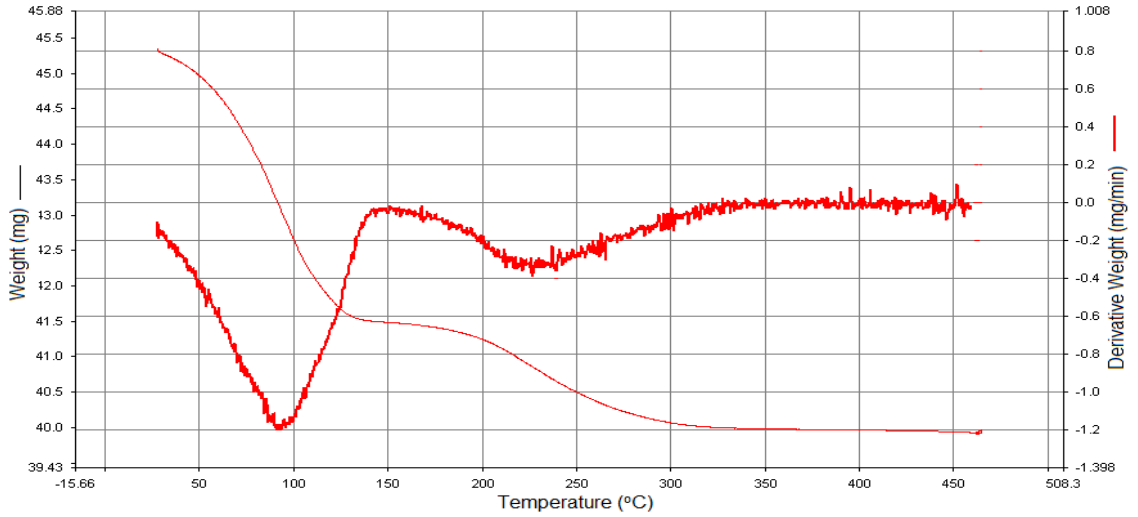

Figure 3.23. TGA analysis of HPW hydrate.

TGA for bulk HSiW hydrate shows a 15.0% weight loss from 30 to 450 ºC due to the loss of crystallization water as well as water molecules bound to acidic protons in HSiW (Figure 3.24).

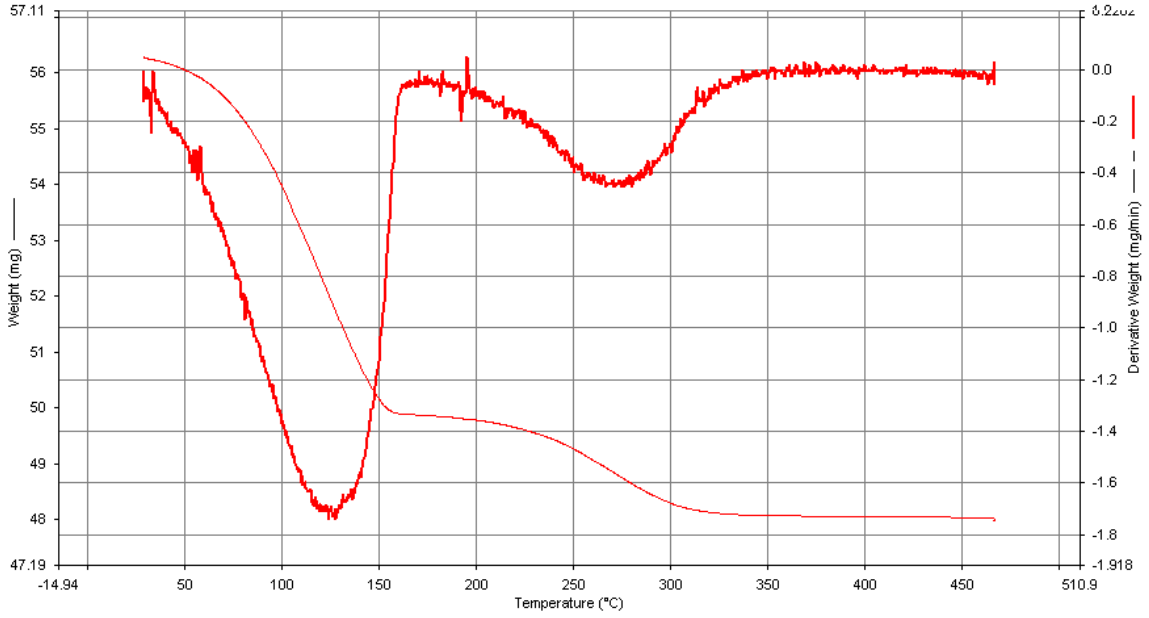

Figure 3.24. TGA analysis of HSiW hydrate.

3.5.2. Carbon-supported metal catalysts

Figure 3.25 shows the TGA for 7.0%Pt/C catalyst (from Johnson Matthey), which lost more than 25% of sample weight from 75 to 550 ºC due to the loss of water.

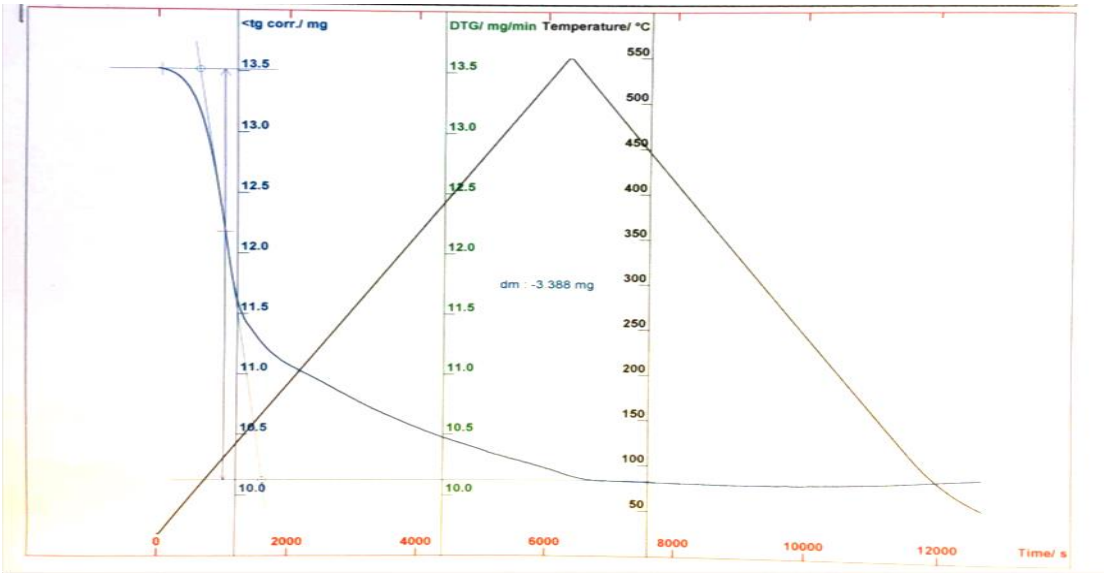

Figure 3.25. TGA analysis of 7.0%Pt/C.

3.6. Fourier transform infrared (FTIR) spectroscopy

FTIR analysis was used to confirm the structure of HPA and to determine the nature of acid sites (Brønsted or Lewis) in our catalysts as described in chapter 2, section 2.3.7.

3.6.1. FTIR study of HPA catalysts

The Keggin structure in heteropoly acid catalysts can be confirmed by FTIR in the fingerprint region between 1200 and 500 cm^{-1} [14]. Hydrous and anhydrous HSiW show the following infrared absorption bands characteristic of the structure of Keggin anion: 981 cm^{-1} (W=O), 928 cm^{-1} (Si-O), 880 cm^{-1} (W-O-W corner-sharing) and 787 cm^{-1} (W-O-W edge-sharing) [1, 15].

Figure 3.26 shows the DRIFT spectra for bulk HSiW (1) and fresh (2) and spent (3) 1%Pt/HSiW/SiO_2 catalyst after alkylation of benzene with propane at 300 °C. These spectra confirm the retention of Keggin structure in these catalyst. It should be noted that the band at 1018 cm^{-1} in (2) and (3) is obscured by strong silica band at 1100 cm^{-1}. Similarly, Figure 3.27 illustrates the retention of the Keggin structure in fresh and spent 2%Pd/25%HSiW/SiO_2 catalysts.

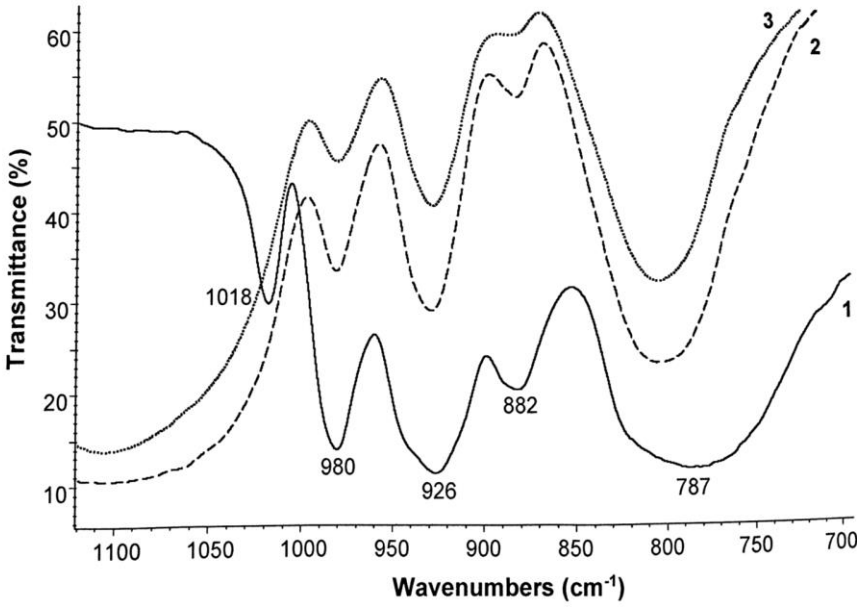

Figure 3.26. FTIR spectrum of bulk HSiW (1) and fresh (2) and spent (3) 1%Pt/25%HSiW/SiO_2 catalyst after alkylation of benzene by propane at 300 °C.

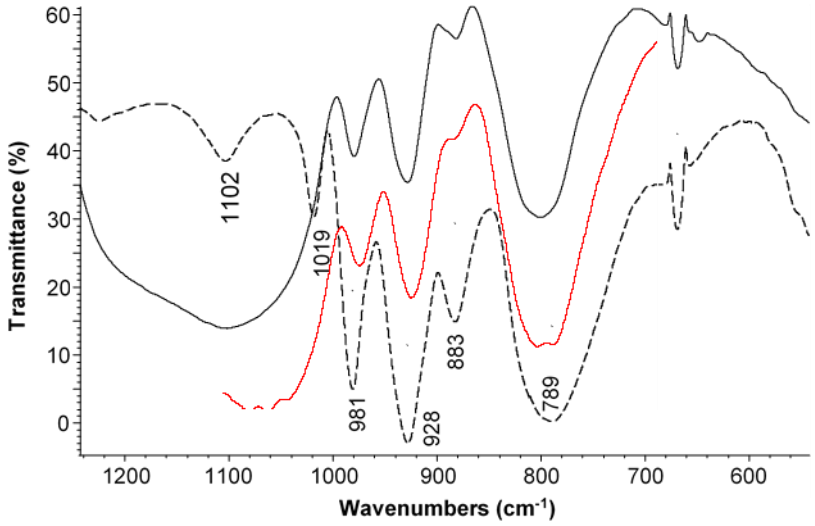

Figure 3.27. FTIR spectrum of bulk HSiW (dashed line), fresh 2%Pd/25%HSiW/SiO_2 (black solid line) and spent 2%Pd/25%HSiW/SiO_2 catalyst after alkylation of toluene by propane at 300 °C (red line).

3.6.2. FTIR of pyridine adsorption

The nature of acid sites on the catalyst surface can be characterised using infrared spectroscopy of adsorbed pyridine [16-18]. Lewis acid sites give an infrared band at about 1450 cm^{-1}, while Brønsted acid sites exhibit a vibration at about 1540 cm^{-1} [19]. The FTIR spectra of pyridine adsorption were examined for HSiW catalysts used in this study. Figure 3.28 shows the spectra of adsorbed pyridine on bulk HSiW and supported 25%HSiW/SiO_2 catalysts. Figure 3.29 illustrates the spectra of adsorbed pyridine on fresh 1%Pt/25%HSiW/SiO_2 catalyst, spent 1%Pt/25%HSiW/SiO_2 after alkylation of benzene by propane and spent 2%Pd/25%HSiW/SiO_2 catalyst after alkylation of toluene by propane. From these spectra, bulk and silica-supported HSiW catalysts have predominantly Brønsted acidity (compare the peaks at about 1540 and 1440 cm^{-1}). Addition of Pt increases the number of Lewis acid sites; the relative number of Brønsted and Lewis acid sites is practically the same in fresh and spent 1%Pt/25%HSiW/SiO_2 catalyst. In contrast, in spent

2%Pd/25%HSiW/SiO_2 catalyst, the number of Brønsted acid sites is significantly reduced, which may be caused by catalyst coking (see section 3.8).

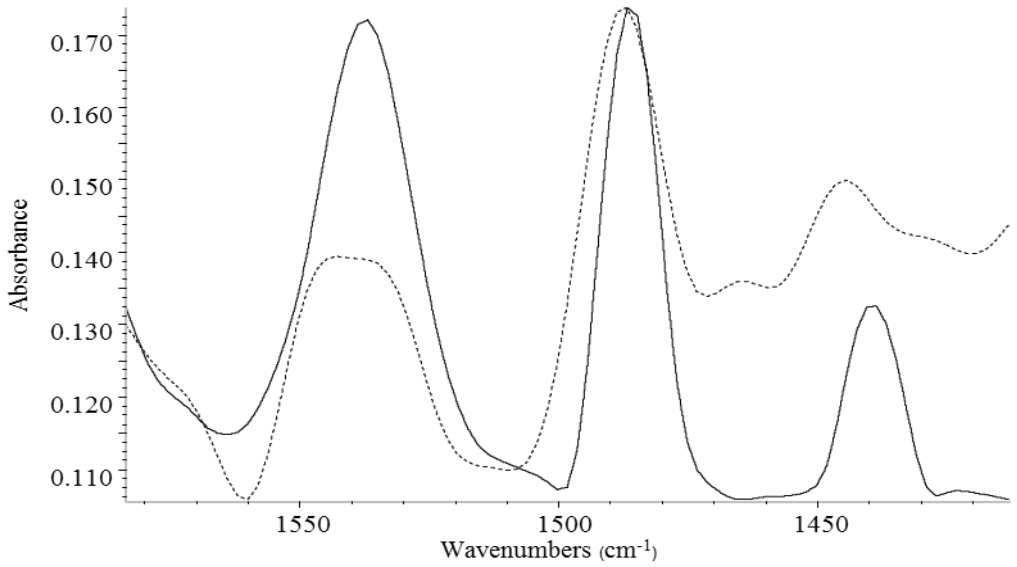

Figure 3.28. DRIFT spectra of pyridine adsorbed on bulk HSiW (solid line) and 25%HSiW/SiO_2 (dashed line).

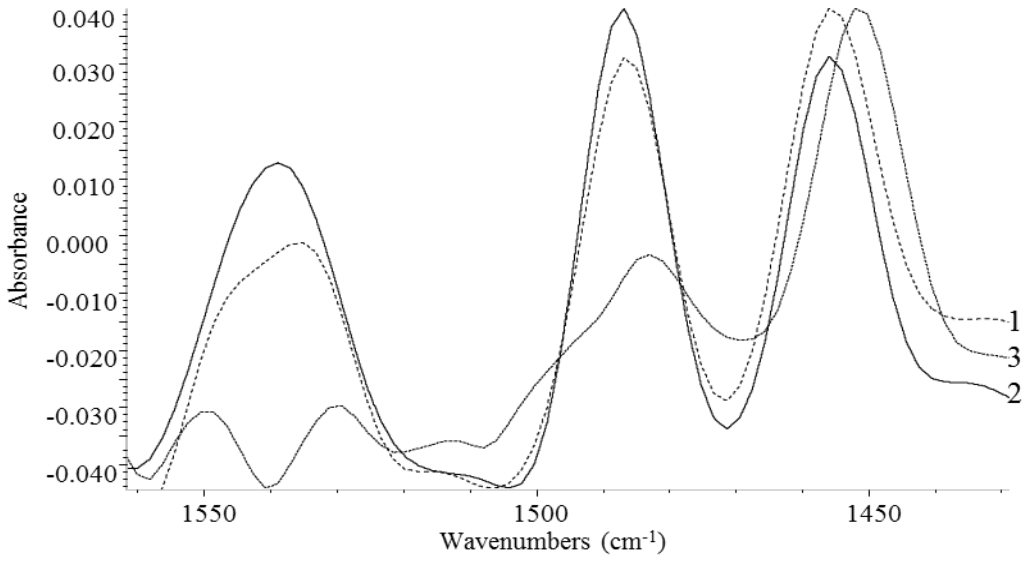

Figure 3.29. DRIFT spectra of pyridine adsorbed on fresh 1%Pt/25%HSiW/SiO_2 (1), spent 1%Pt/25%HSiW/SiO_2 after alkylation of benzene by propane (2) and spent 2%Pd/25%HSiW/SiO_2 after alkylation of toluene by propane (3).

3.7. Inductively coupled plasma atomic emission spectroscopy (ICP-AES)

The ICP-AES analysis was used in this study to determine metal content in catalysts as detailed in Chapter 2, section 2.3.8. Table 3.4 illustrates the calculated (from the preparation stoichiometry) and experimental amounts of Pt, Pd and Au in some of our catalysts. It can be seen that the two values are in good agreement with each other.

Table 3.4. ICP-AES analysis of Pt, Pd and Au content in supported metal catalysts.

Catalyst	Metal content (wt%)	
	Calculated	Experimental
10%Pt/C	10	7.0
10%Pd/C	10	7.1
5%Pt/C	5	4.3
5%Pd/C	5	4.7
10%Au/7.1%Pd/C	10(Au) and 7.1(Pd)	9.9(Au) and 6(Pd)
2%Pd/25%HSiW/SiO_2	2	2.2
0.5%Pt/ZSM-5	0.5	0.30
0.5%Au/HZSM-5	0.5	0.52
2%Pd/HZSM-5	2	2.6

3.8. Combustion C and H analysis

The combustion analysis was used in this study to measure the C and H content in spent catalysts as described in Chapter 2, section 2.3.9. Table 3.5 shows the results for some spent catalysts after use in alkylation of benzene and toluene with propane.

Table 3.5. C and H combustion analysis for spent catalysts after use in alkylation of (a) benzene and (b) toluene by propane.

Catalyst	C (wt%)	H (wt%)
1%Pt/25%HSiW/SiO_2[(a)]	1.2	0.4
1%Pt/25%HPW/SiO_2[(a)]	2.2	0.3
2%Pd/25%HSiW/SiO_2[(a)]	2.1	0.4
1%Pt/25%HSiW/SiO_2[(b)]	0.9	0.5
1%Pt/25%HPW/SiO_2[(b)]	1.7	0.5
3%Pd/25%HSiW/SiO_2[(b)]	2.4	0.6

References

1. Kozhevnikov, I.V. *Catalysis by Polyoxometalates*, Wiley & Sons: Chichester, England, **2002**.
2. Mizuno, N.; Misono, M. *Chem. Rev.* **1998,** *98*, 199.
3. Sun, P.; Yu, D.H.; Hu, Y.; Tang, Z.C.; Xia, J.J.; Li, H.; Huang, H. *Korean J. Chem. Eng.* **2011,** *28*, 99.
4. Alhanash, A.; Kozhevnikova, E.F.; Kozhevnikov, I.V. *Catal. Lett.* **2008,** *120*, 307.
5. Yamada, T.; Yoshinaga, Y.; Okuhara, T. *Bull. Chem. Soc. Jpn.* **1998,** *71*, 2727.
6. Nakato, T.; Toyoshi, Y.; Kimura, M.; Okuhara, T. *Catal. Today* **1999,** *52*, 23.
7. Okuhara, T.; Watanabe, H.; Nishimura, T.; Inumaru, K.; Misono, M. *Chem. Mater.* **2000,** *12*, 2230.
8. Dias, J.A.; Caliman, E.; Dias, S.C.L. *Micropor. Mesopor. Mater.* **2004,** *76*, 221.
9. Grieken, R. van; Sotelo, J.L.; Menendez, J.M.; Melero, J.A. *Micropor. Mesopor. Mater.* **2000,** *39*, 135.
10. Burton, A.W. *Zeolite Characterization and Catalysis:* A **2009**, 1.
11. Villegas, J.I.; Kumar, N.; Heikkila, T.; Lehto, V.P.; Salmi, T.; Murzin, D.Y. *Chem. Eng. J.* **2006,** *120*, 83.
12. Yoshida, S.; Nilyama, H.; Echigoya, E. *J. Phys. Chem.* **1982,** *86*, 3150.
13. Parida, K.M.; Rana, S.; Mallick, S.; Rath, D. J. *Colloid Interf. Sci.* **2010,** *350*, 132.
14. Moffat, J.B. *Metal-Oxygen Clusters: The Surfaces and Catalytic Properties of Heteropoly Oxometalates*, Klumer Academic/ Plenum Publishers, New York, **2001**.
15. Rocchioccioli-Deltcheff, C.; Fournier M.; Jeannin, Y. *J. Am. Chem. Soc.* **1982,** *104*, 3195.
16. Devassy, B.M.; Halligudi, S.B. *J. Catal.* **2005,** *236*, 313.
17. Devassy, B.M.; Lefebvre, F.; Halligudi, S.B. *J. Catal*. **2005,** *231*, 1.
18. Sachsenroder, H.; Brunner, E.; Koch, M.; Pfeifer, H. *B. Staudte, Micropo. Mater.* **1996,** *6*, 341.
19. Davis, B.H.; Keogh, R.A; Alerasool, S.; Zalewski, D.J.; Day, D.E.; Doolin, P.K. *J. Catal.* **1999,** *183*, 45.

Chapter 4: Selective alkylation of benzene with propane over bifunctional Pt-heteropoly acid catalyst

4.1. Introduction

Functionalization of light alkanes remains one of the greatest challenges for catalysis science [1,2]. In this context, the alkylation of benzene with ethane and propane to produce ethylbenzene (EtPh) and isopropylbenzene (iPrPh) has attracted much interest [3]. EtPh and iPrPh are the key intermediates in manufacturing styrene and phenol and produced commercially on a large scale by the well-established acid-catalysed alkylation of benzene by alkenes, i.e., ethene and propene [4]. The replacement of ethene and propene by ethane and propane, respectively, could lead to more cost effective and environmentally benign production of these commodity chemicals [4].

Previous research on the alkylation of benzene and toluene by ethane [5-14] and propane [15-20] is discussed in Chapter 1, section 1.6 of this thesis. Most promising catalysts reported so far for these reactions comprise zeolites modified with transition metals such as Pt, Pd, Re, Ga, etc. These catalysts operate via bifunctional pathway, which includes alkane dehydrogenation on metal sites to form alkene and H_2 followed by benzene alkylation with the alkene on acid sites (Scheme 4.1).

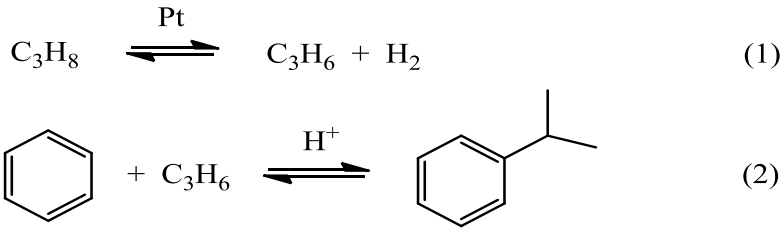

Scheme 4.1. Alkylation of benzene by propane via bifunctional catalyzed pathway.

The best results for the alkylation of benzene by ethane have been achieved using Pt-modified HZSM-5 zeolites (MFI structure). Thus, Lukyanov et al. [9] have reported >90% EtPh selectivity at a close to equilibrium benzene conversion of 11.6% in the alkylation of

benzene with ethane over 1%Pt/HZSM-5 (Si/Al = 36) at 370 ^{o}C, $[C_6H_6]/[C_2H_6]$ = 1:9 mol/mol and 1 bar pressure.

In contrast to the reaction with ethane, selective alkylation of benzene with propane has proved to be more difficult to achieve. Smirnov et al. [16] have studied this reaction with a range of Pt/HZSM-5 catalysts (Si/Al = 25-160). They have obtained iPrPh with 32% selectivity at 6.6% conversion (2.1% yield) using 0.22%Pt/HZSM-5 (Si/Al = 160) as the catalyst at 350 ^{o}C, 1 bar pressure and $[C_6H_6]/[C_3H_8]$ = 1:1, with the main product being nPrPh (50% selectivity) rather than iPrPh, which is the favourable product from the carbenium ion mechanism. This points to the product shape selectivity control imposed by HZSM-5, i.e., iPrPh formed initially possibly isomerised on HZSM-5 proton sites to nPrPh possessing higher diffusion mobility within zeolite micropores. Therefore, it is likely that the poor selectivity of benzene alkylation with propane on Pt/HZSM-5 is the result of the confinement of product molecules within zeolite micropores causing their isomerisation and cracking to form primarily nPrPh together with the range of by-products observed (MePh, EtPh, etc.). In this regard, it is conceivable that bifunctional catalysts based on strong solid acids possessing larger pores could improve reaction selectivity.

In the last decade, Kozhevnikov et al. in this group have investigated bifunctional heterogeneous catalysis by Keggin heteropoly acids (HPAs) modified with platinum group metals in a wide range of gas- and liquid-phase reactions [21-24]. HPAs are commercially available solid materials possessing very strong Brønsted acidity, stronger than zeolites and common mineral acids [25,26]. HPAs have found many applications in catalysis, including several industrial processes [26]. Supporting HPA on oxide supports provides solid acid catalysts with a wide range of pore geometries, e.g., SiO_2-supported HPAs possess both strong acidity and mesoporous structure [26]. In this work, we demonstrate highly efficient

bifunctional catalysis by Pt-modified Keggin HPAs for the alkylation of benzene with propane. Most efficiently the reaction occurs over $Pt/H_4SiW_{12}O_{40}/SiO_2$ catalyst at 300 ^oC, giving isopropylbenzene with 90-93% selectivity at 6-8% benzene conversion, significantly exceeding the efficiency of previously reported Pt/HZSM-5 catalyst.

4.2. Experimental

Experimental details including the chemicals used, catalyst preparation procedures, catalyst characterisation techniques, the description of the reactor setup for catalyst testing and data analysis are given in Chapter 2. A wide range of solid acid and bifunctional Pt-acid catalysts was tested for benzene alkylation with propane; these included supported heteropoly acids $H_3PW_{12}O_{40}$ (HPW) and $H_4SiW_{12}O_{40}$ (HSiW) and bifunctional metal-acid catalysts $Pt/HPW/SiO_2$, Pt/HSiW and Pt/HZSM-5. These catalysts were prepared using literature procedures [22, 24, 27, 28] or modifications thereof, as described in Chapter 2. They were characterised by a number of techniques such as, BET, XRD, FTIR, H_2-TPR, TGA, ICP-AES and chemisorption of H_2 and CO. The details of catalyst characterisation can be found in Chapters 2 and 3. Information about these catalysts is summarised in Table 4.1; it includes catalyst texture (surface area, pore volume and pore diameter), platinum dispersion and platinum particle size and the strength of acid sites represented by the initial enthalpies of ammonia adsorption (ΔH) taken from previous studies of this group [27,28].

Table 4.1. Catalyst characterisation.

Catalyst	S_{BET}[a] m^2g^{-1}	Pore volume[b] cm^3g^{-1}	Pore size[c] Å	D[d] %	d[e] nm	ΔH[f] kJ mol^{-1}
7%Pt/C	-	-	-	39	2.3	-
25%HPW/SiO_2	198	1.00	203	-	-	-
25%HSiW/SiO_2	191	0.84	177	-	-	-
1%Pt/25%HPW/SiO_2	189	0.92	195	27	3.3	-
1%Pt/25%HSiW/SiO_2	181	0.88	194	24	3.8	-
0.31%Pt/HZSM-5	369	0.21	24	60	1.5	-
15%HSiW/SiO_2	221	1.02	185	-	-	-154
15%HPW/SiO_2	202	1.00	169	-	-	-154
15%HPW/TiO_2	45	0.20	174	-	-	-143
15%HPW/Nb_2O_5	126	0.11	34	-	-	-132
15%HPW/ZrO_2	109	0.09	36	-	-	-121

[a]BET surface area. [b]Single point total pore volume. [c]Average BET pore diameter. [d]Pt dispersion in catalysts determined from CO chemisorption. [e]Pt particle size calculated from equation d (nm) = 0.9/D [29]. [f]Initial enthalpy of ammonia adsorption at 150 °C (±3 kJ mol^{-1}) [27,28].

The alkylation of benzene with propane was carried out in the gas phase at 250-350 °C and an inlet C_6H_6/C_3H_8 molar ratio of 1:9 under atmospheric pressure in a quartz fixed-bed down-flow reactor (9.0 mm internal diameter) with online GC analysis as described in Chapter 2, section 2.3.11. The reactor was packed with 0.20 g catalyst powder of 45-180 μm particle size. The gas feed entered the reactor at the top at a flow rate of 10 mL min^{-1} (space time W/F = 80 g h mol^{-1}, where W (g) is the catalyst weight and F (mol h^{-1}) is the molar flow rate of benzene). Benzene was fed into the gas flow by passing the propane flow controlled by a Brooks mass flow controller through a stainless steel saturator, which held liquid

benzene at 20 ^{o}C to maintain the chosen reactant partial pressure of 10 kPa [30]. Prior to reaction, the catalyst was pre-treated in H_2 for 1 h at the reaction temperature. The downstream gas flow was analysed by the on-line GC to obtain benzene conversion and product selectivity. The selectivity to alkylbenzenes was defined as moles of product formed per one mole of benzene converted and quoted in mole per cent. The mean absolute percentage error in conversion and selectivity was ≤ 10% and the carbon balance was maintained within 95%.

4.3. Results and discussion

4.3.1. Thermodynamic calculations

The thermodynamic analysis includes calculation of the Gibbs free energy (ΔG) and equilibrium conversion (x) for dehydrogenation of ethane and propane and benzene alkylation with ethane, propane and propene in the ideal gas system at 1 bar pressure. Initial thermodynamic data on the formation Gibbs energy $\Delta_f G^o$ and enthalpy $\Delta_f H^o$ together with the entropy S^o and heat capacity C_p at standard conditions (298.15 K and 1 bar) are presented in Table 4.2.

Table 4.2. Initial thermodynamic data (298.15 K, 1 bar).

Compound	$\Delta_f G^o$ kJ mol^{-1}	$\Delta_f H^o$ kJ mol^{-1}	S^o J mol^{-1} K^{-1}	C_p J mol^{-1} K^{-1}	Reference
H_2	0	0	130.68	28.82	[31]
C_2H_6	-32.82	-84.68	229.60	52.63	[32]
C_2H_4	68.15	52.26	219.56	43.56	[33]
C_3H_8	-23.56	-103.85	270.20	73.60	[32]
C_3H_6	62.84	20.42	266.60	64.31	[33]
EtPh		29.80	360.60	127.40	[34]
iPrPh	137.15	3.93	388.68	151.71	[35]

4.3.1.1. Dehydrogenation of ethane and propane

The stoichiometry of these reactions is represented equations (4.1) and (4.2).

$$C_2H_6 = C_2H_4 + H_2 \quad (4.1)$$

$$C_3H_8 = C_3H_6 + H_2 \quad (4.2)$$

Equations used for the thermodynamic calculations are given below, where K_p (bar) is the equilibrium constant, x (unitless) is the equilibrium fractional conversion of ethane, T is the absolute temperature (in K), P (bar) is the pressure and R is the gas constant (8.314 J mol^{-1} K^{-1}). ΔC_p was assumed to be independent of the temperature, i.e., $\Delta C_p = \Delta C_p^o$. The results are presented in Tables 4.3 and 4.4.

$$\Delta H = \Delta H^o + \Delta C_p^o (T - 298.15) \quad (4.3)$$

$$\Delta S = \Delta S^o + \Delta C_p^o \ln(T/298.15) \quad (4.4)$$

$$\Delta G = \Delta H - T\Delta S \quad (4.5)$$

$K_p = \exp\{-\Delta G/RT\} = x^2P/(1-x^2)$, where P is the pressure. (4.6)

$$x = \sqrt{K_p/(P + K_p)} \quad (4.7)$$

Table 4.3. Thermodynamics of ethane dehydrogenation.[a]

T	T	ΔH	ΔS	ΔG	K_p	x
^{o}C	K	kJ mol^{-1}	J mol^{-1} K^{-1}	kJ mol^{-1}	bar	
25	298.15	136.94	120.64	100.97	2.04E-18	1.43E-09
100	373.15	138.42	125.07	91.75	1.43E-13	3.78E-07
200	473.15	140.40	129.76	79.00	1.90E-09	4.35E-05
300	573.15	142.37	133.56	65.84	9.95E-07	9.98E-04
370	643.15	143.75	135.83	56.41	2.61E-05	5.11E-03
400	673.15	144.35	136.72	52.32	8.71E-05	9.33E-03
500	773.15	146.32	139.46	38.50	2.51E-03	5.01E-02
600	873.15	148.30	141.86	24.43	3.46E-02	1.83E-01
700	973.15	150.27	144.00	10.14	2.86E-01	4.72E-01
800	1073.15	152.25	145.93	-4.35	1.63E+00	7.87E-01

[a]At 1 bar, ΔC_p^o = 19.75 J mol^{-1} K^{-1}.

Table 4.4. Thermodynamics of propane dehydrogenation.[a]

T	T	ΔH	ΔS	ΔG	K_p	x
^{o}C	K	kJ mol^{-1}	J mol^{-1} K^{-1}	kJ mol^{-1}	bar	
25	298.15	124.27	127.08	86.40	7.290E-16	2.70E-08
100	373.15	125.73	131.46	76.68	1.844E-11	4.29E-06
200	473.15	127.69	136.10	63.29	1.030E-07	3.21E-04
300	573.15	129.64	139.84	49.49	3.070E-05	5.54E-03
350	623.15	130.62	141.48	42.33	2.828E-04	1.68E-02
400	673.15	131.59	142.98	35.34	1.810E-03	4.25E-02
500	773.15	133.55	145.69	20.91	3.870E-02	1.93E-01
600	873.15	135.50	148.07	6.21	4.250E-01	5.46E-01
700	973.15	137.45	150.18	-8.70	2.931E+00	8.63E-01
800	1073.15	139.41	152.09	-23.81	1.442E+01	9.67E-01

[a]At 1 bar, ΔC_p^{o} = 19.53 J mol^{-1} K^{-1}.

4.3.1.2. Alkylation of benzene with ethane and propane

In this case, the reaction stoichiometry is represented by equations (4.8) and (4.9). The equilibrium constant K_p was calculated using equation (4.10); the equilibrium conversion x was calculated for C_6H_6/C_2H_6 molar ratio of 1:1 and 1:9 using equations (4.11) and (4.13), respectively. The results are presented in Tables 4.5 and 4.6.

$$C_6H_6 + C_2H_6 = EtPh + H_2 \quad (4.8)$$

$$C_6H_6 + C_3H_8 = iPrPh + H_2 \quad (4.9)$$

Table 4.5. Thermodynamics of benzene alkylation with ethane.[a]

T	T	ΔH	ΔS	ΔG	K_p	x C_6H_6/C_2H_6=	x C_6H_6/C_2H_6=
^oC	K	kJ mol^{-1}	J mol^{-1} K^{-1}	kJ mol^{-1}		1:1	1:9
25	298.15	31.55	-7.33	33.74	1.23E-06	1.11E-03	0.00331
100	373.15	33.14	-2.58	34.10	1.68E-05	4.09E-03	0.0123
200	473.15	35.25	2.44	34.10	1.72E-04	1.29E-02	0.0385
300	573.15	37.37	6.49	33.65	8.57E-04	2.84E-02	0.0836
370	643.15	38.85	8.93	33.11	2.05E-03	4.33E-02	0.125
400	673.15	39.48	9.89	32.82	2.84E-03	5.06E-02	0.146
500	773.15	41.60	12.82	31.69	7.23E-03	7.83E-02	0.222
600	873.15	43.71	15.40	30.26	1.55E-02	1.11E-01	0.305
700	973.15	45.83	17.69	28.61	2.91E-02	1.46E-01	0.391
800	1073.15	47.94	19.76	26.73	5.00E-02	1.83E-01	0.474

[a]At 1 bar, ΔC_p^o = 21.15 J mol^{-1} K^{-1}.

$$K_p = \exp\{-\Delta G/RT\} = x^2/(1-x)^2 \text{ at } C_6H_6/C_2H_6 = 1{:}1. \quad (4.10)$$

$$x = \sqrt{K_p/(1+\sqrt{K_p})} \quad (4.11)$$

$$K_p = \exp\{-\Delta G/RT\} = x^2/(1-x)(9-x) \text{ at } C_6H_6/C_2H_6 = 1{:}9. \quad (4.12)$$

$$x = \frac{5K_p}{K_p-1} + \sqrt{\frac{25K_p^2}{(K_p-1)^2} - \frac{9K_p}{K_p-1}} \quad (4.13)$$

Table 4.6. Thermodynamics of benzene alkylation with propane.[a]

T	T	ΔH	ΔS	ΔG	K_p	x C_6H_6/C_3H_8=	x C_6H_6/C_3H_8=
^oC	K	kJ mol^{-1}	J mol^{-1} K^{-1}	kJ mol^{-1}		1:1	1:9
25	298.15	24.85	-20.15	30.86	3.92E-06	1.98E-03	0.00592
100	373.15	26.74	-14.48	32.14	3.17E-05	5.60E-03	0.0167
200	473.15	29.27	-8.48	33.28	2.12E-04	1.43E-02	0.0426
300	573.15	31.80	-3.64	33.89	8.16E-04	2.78E-02	0.0816
350	623.15	33.06	-1.53	34.01	1.41E-03	3.62E-02	0.106
400	673.15	34.32	0.42	34.04	2.28E-03	4.56E-02	0.132
500	773.15	36.85	3.92	33.82	5.19E-03	6.72E-02	0.190
600	873.15	39.37	6.99	33.27	1.02E-02	9.18E-02	0.253
700	973.15	41.90	9.73	32.43	1.81E-02	1.19E-01	0.315
800	1073.15	44.43	12.2	31.34	2.98E-02	1.47E-01	0.394

[a]At 1 bar, ΔC_p^o = 25.26 J mol^{-1} K^{-1}.

4.3.1.3. Alkylation of benzene with propene

$$C_6H_6 + C_3H_6 = \text{iPrPh} \qquad (4.14)$$

The Gibbs free energy for this reaction was obtained as the difference between the ΔG values for benzene alkylation with propane (Table 4.6) and propane dehydrogenation (Table 4.4).

Table 4.7. Thermodynamics of benzene alkylation with propene.[a]

T	*T*	Δ*G*
°C	K	kJ mol^{-1}
25	298.15	-55.54
100	373.15	-44.54
200	473.15	-30.01
300	573.15	-15.6
350	623.15	-8.32
400	673.15	-1.30
500	773.15	12.91
600	873.15	27.06
700	973.15	41.13
800	1073.15	55.15

4.3.2. Thermodynamic analysis

The alkylation of benzene with propane via bifunctional pathway combines propane-to-propene dehydrogenation (1) and benzene alkylation with propene thus formed (2) (Scheme 4.1). Step (1) is thermodynamically unfavourable, whereas step (2) is favourable one. Tungsten HPAs are active catalysts for the alkylation of benzene with propene (step (2)) [36] as well as for the reverse reaction of iPrPh cracking [37].

Figure 4.1 shows the Gibbs free energy (Δ*G*) for these steps as a function of temperature calculated from thermodynamic data [31-33, 35] (Tables 4.2 – 4.7) . It can be seen that at 300 °C and 1 bar pressure, equilibrium conversion of propane in step (1) is only 0.55%. For benzene alkylation with propane, Δ*G* is positive at 30-35 kJ mol^{-1} in the

temperature range of 25-800 ^{o}C. Equilibrium conversion of benzene at 300 ^{o}C and $[C_6H_6]/[C_3H_8]$ molar ratio of 1:1 is 2.8%. At the ratio $[C_6H_6]/[C_3H_8]$ = 1:9 applied in this work, it increases to 8.2% (Figure 4.1).

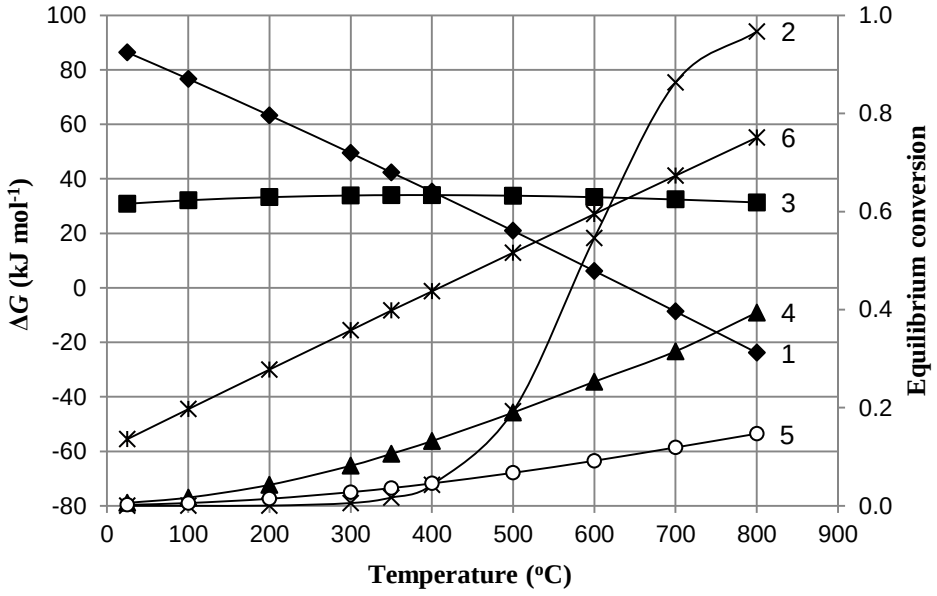

Figure 4.1. Gibbs free energy (ΔG) and equilibrium conversion (x) for dehydrogenation of propane (undiluted C_3H_8) and alkylation of benzene with propane as a function of temperature at 1 bar pressure: (1) ΔG and (2) x for $C_3H_8 = C_3H_6 + H_2$; (3) ΔG and (4) x at $[C_6H_6]/[C_3H_8]$ = 1:9 and (5) x at $[C_6H_6]/[C_3H_8]$ = 1:1 for $C_6H_6 + C_3H_8$ = iPrPh + H_2; (6) ΔG for $C_6H_6 + C_3H_6$ = iPrPh.

Table 4.8 shows the experimental conversion values for propane dehydrogenation (1) over bifunctional catalyst 1%Pt/25%HSiW/SiO_2 at 300-400 ^{o}C under typical reaction conditions applied for benzene alkylation in this work. It is evident that the experimental values of propane conversion are practically equal, within the accuracy of measurement, to the calculated equilibrium values, which indicates that the dehydrogenation reaction is fast in this system. On top of that, the amount of methane and ethane present in propane flow did not

change hence propane cracking did not occur in this temperature range. Propane aromatization did not occur either, as no aromatic compounds were found amongst the products.

Table 4.8. Propane dehydrogenation over 1%Pt/25%HSiW/SiO_2.[a]

Temperature (^oC)	300	350	400
Experimental propane conversion (%)[b]	0.48	1.93	4.56
Calculated equilibrium conversion (%)	0.55	1.68	4.25

[a]Catalyst (0.20 g) pre-treated in situ at 300 ^oC/1 h in H_2 flow, 10 mL min^{-1} propane flow rate, *W/F* = 80 g h mol^{-1}, 1 bar pressure, 1 h time on stream. [b]Inlet gas contained propane (99.20%), propene (0.01%), ethane (0.76%), butane (0.03%) and methane (0.004%); methane and ethane content did not change in the downstream flow.

4.3.3. Alkylation of benzene over Pt/HZSM-5

It is essential to compare new Pt/HPA and previously reported Pt/HZSM-5 catalysts under the same reaction conditions. Therefore, first we tested Pt/HZSM-5 for benzene alkylation with propane in our system at 300 ^oC, contact time *W/F* = 80 g h mol^{-1} and $[C_6H_6]/[C_3H_8]$ = 1:9. Representative results are given in Table 4.9. Supported bifunctional catalyst 0.31%Pt/HZSM-5 gave 16.4% iPrPh selectivity at 19.9% conversion (3.3% benzene-based yield), with nPrPh (33.8%) and MePh (21.5%) formed as the main products. It should be noted that this catalyst showed stable performance for over 8 h on stream (Figure 4.2). In the absence of Pt, HZSM-5 gave only 1.1% benzene conversion with a similar iPrPh selectivity of 14.2%, which is in agreement with the previous report [16]. The reaction with

Pt-free catalyst probably occurs through carbonium ion intermediate or transition state formed by propane protonation with the zeolite [16].

Table 4.9. Alkylation of benzene with propane via bifunctional catalysed pathway.[a]

Catalyst	Conversion[b]	Aromatic selectivity (%)[c]				
	(%)	MePh	EtPh	iPrPh	nPrPh	C_{9+}
HZSM-5	1.1 (2)	25.5	22.8	14.2	24.6	12.9
7%Pt/C+SiO_2[d]	0.1 (2)	0	0	37.2	54.6	8.2
0.31%Pt/HZSM-5	19.9 (8)	21.5	6.0	16.4	33.8	22.4
7%Pt/C+HZSM-5 (0.7%Pt)[d]	19.0 (6)	30.8	16.5	12.8	24.3	15.7
7%Pt/C+HZSM-5 (0.7%Pt)[e]	5.1 (7)	26.5	31.2	12.8	22.6	6.9

[a]Reaction conditions: 300 ^oC, 1 bar pressure, 0.20 g catalyst, inlet molar ratio C_6H_6/C_3H_8 = 1:9, 10 mL min^{-1} flow rate, *W/F* = 80 g h mol^{-1}; in situ catalyst pre-treatment at 300 ^oC/1 h in H_2 flow, 10 mL min^{-1}). [b]Average conversion of benzene since steady state reached during time on stream (h) given in round brackets. [c]Selectivity to aromatic products including unidentified C_{9+} alkylbenzenes. [d]Uniform physical mixture 7%Pt/C (0.02 g) + HZSM-5 or SiO_2 (0.18 g). [e]Two catalyst beds: 7%Pt/C (0.02 g, top bed) and 25%HSiW/SiO_2 or HZSM-5 (0.18 g, bottom bed).

A uniform physical mixture 7%Pt/C + HZSM-5 (1:9 w/w) with 0.7% Pt content showed practically the same activity as the 0.31%Pt/HZSM-5 catalyst at 19.0% conversion and 12.8% iPrPh selectivity (Figure 4.3), with MePh (30.8%), nPrPh (24.3%) and EtPh (16.5%) formed as the main products (Table 4.9). This disagrees with Smirnov et al. who found a 4-fold decrease in catalyst activity when using a 1:1 w/w physical mixture of 0.3%Pt/CeO_2 and HZSM-5 (Si/Al = 25-160) instead of 0.22-0.29%Pt/HZSM-5 at 350 ^oC and

$[C_6H_6]/[C_3H_8]$ = 1:1 [16]. At least partly, this may be explained by the decrease in Pt loading in the Pt/CeO_2 + HZSM-5 physical mixture in comparison with the supported Pt/HZSM-5 catalyst. Only when we used two catalyst beds, 7%Pt/C (top) and HZSM-5 (bottom) (1:9 w/w) separated by ~1 mm layer of silica, a 4-fold drop in benzene conversion was predictably observed, although the selectivity pattern did not change (Table 4.9, Figure 4.4). This supports the view that the selectivity of benzene alkylation with propane over Pt/HZSM-5 catalyst is controlled by acid-catalyzed transformations within zeolite microporous structure.

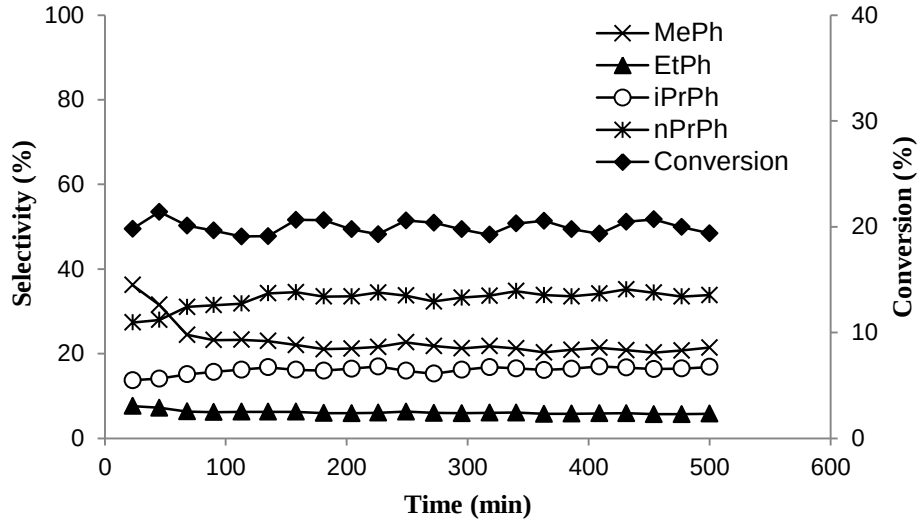

Figure 4.2. Time course for alkylation of benzene with propane over 0.31%Pt/HZSM-5 (Si/Al = 18) (0.2 g catalyst, 300 ^oC, 1 bar pressure, inlet molar ratio C_6H_6/C_3H_8 = 1:9, 10 mL min^{-1} flow rate, *W/F* = 80 g h mol^{-1}; in-situ catalyst pre-treatment at 300 ^oC/1 h in H_2 flow, 10 mL min^{-1}).

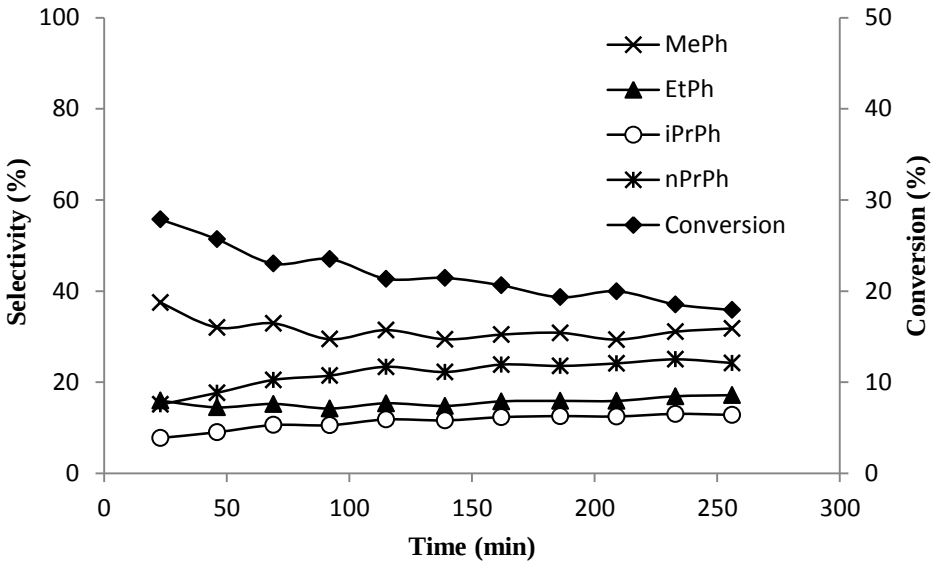

Figure 4.3. Time course for alkylation of benzene with propane over 7%Pt/C (0.02 g) + HZSM-5 (0.18 g, Si/Al = 18) physical mixture (0.2 g total catalyst weight, 0.7% Pt; 300 ^{o}C, 1 bar pressure, inlet molar ratio C_6H_6/C_3H_8 = 1:9, 10 mL min^{-1} flow rate, *W/F* = 80 g h mol^{-1}; in-situ catalyst pre-treatment at 300 ^{o}C/1 h in H_2 flow, 10 mL min^{-1}).

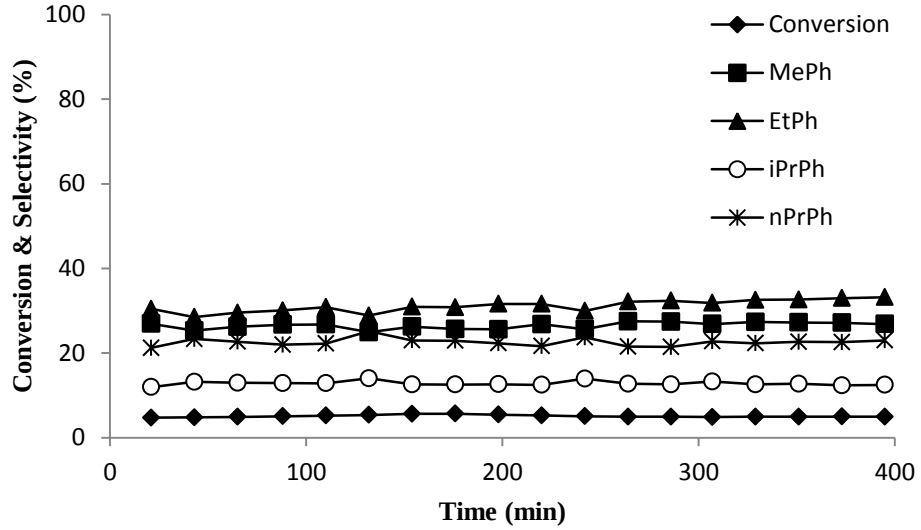

Figure 4.4. Time course for alkylation of benzene with propane over two-bed catalyst 7%Pt/C (0.02 g, top bed) + HZSM-5 (0.18 g, Si/Al = 18, bottom bed) separated with ~1 mm SiO_2 layer (0.2 g total catalyst weight, 0.7% Pt; 300 ^{o}C, 1 bar pressure, inlet molar ratio C_6H_6/C_3H_8 = 1:9, 10 mL min^{-1} flow rate, *W/F* = 80 g h mol^{-1}; in situ catalyst pre-treatment at 300 ^{o}C/1 h in H_2 flow, 10 mL min^{-1}).

4.3.4. Alkylation of benzene over Pt/HPA catalysts

Bulk tungsten HPAs possess very strong proton sites [25,26]. The initial enthalpies of ammonia adsorption (ΔH) for bulk HPW and HSiW have been reported to be -197 and -171 [27,28 and 38] kJ mol^{-1}, respectively. The acid sites of MFI zeolites are weaker, ΔH = -131 to -150 kJ mol^{-1} (Si/Al = 20-70) from ammonia adsorption microcalorimetry and NH_3-TPD [39]. However, supporting HPA reduces the acid strength because of HPA-support interaction [27,28] (Table 4.1).

Initial testing of supported HPA catalysts modified with platinum group metals showed that Pt catalysts were more active than Pd ones in the alkylation of benzene with propane, in agreement with previous studies [3]. Amongst Keggin HPAs tested, $H_4SiW_{12}O_{40}$ (HSiW) gave the best performance, followed by $H_3PW_{12}O_{40}$ (HPW). Bulk acidic Cs salt $C_{2.5}H_{0.5}PW_{12}O_{40}$, which is widely used as a strong solid acid catalyst [25,26] showed very low activity. Predictably, the best catalyst support was found to be SiO_2; other oxide supports such as TiO_2, Nb_2O_5 and ZrO_2 gave lower benzene conversions (Table 4.11) probably due to decreasing the acid strength of HPA as shown by NH3 adsorption microcalorimetry [27].

Best performance in benzene alkylation with propane gave the catalysts comprising 0.5-1% Pt metal and 25%HSiW/SiO_2. These were mesoporous materials with S_{BET} = 181-191 m^2g^{-1} and pore diameters of 177-194 Å (Table 4.1). For 1%Pt/25%HSiW/SiO_2, the N_2 adsorption isotherm and pore size distribution are shown in Figures 4.5 and 4.6. Benzene conversion increased with temperature from 250 to 300 ^oC. Further temperature increase to 350 ^oC did not produce any increase in conversion probably due to catalyst deactivation by coking. Therefore, further catalyst testing was carried out at 300 ^oC. Representative results are shown in Table 4.10.

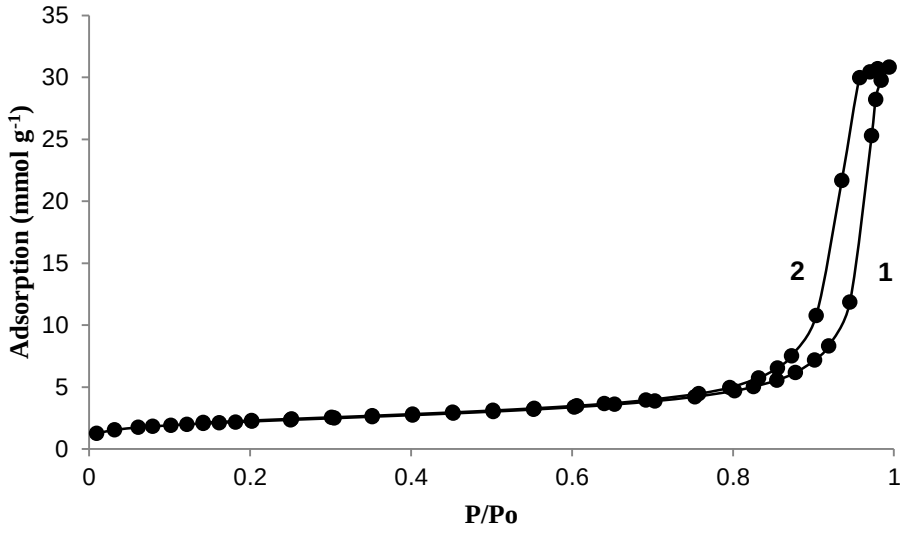

Figure 4.5. Nitrogen adsorption (1) and desorption (2) isotherms for 1%Pt/25%HSiW/SiO_2.

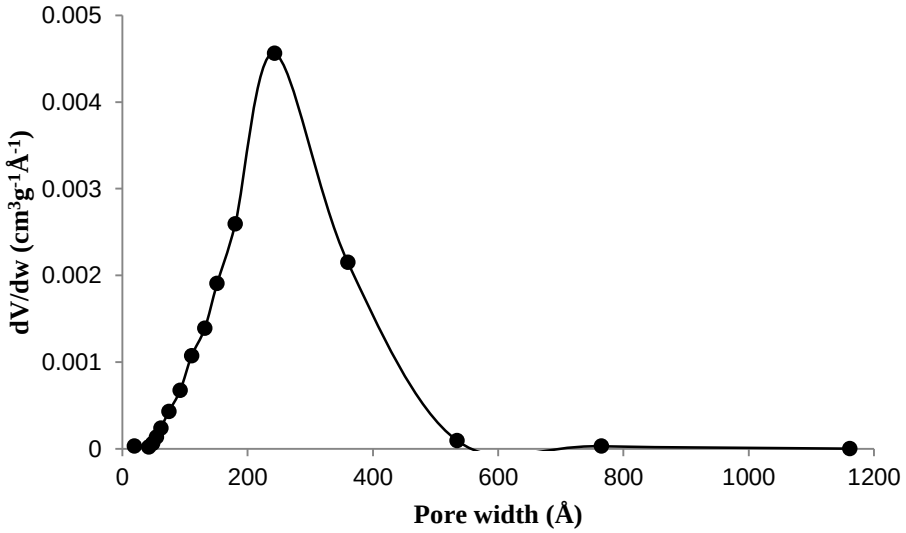

Figure 4.6. BJH desorption pore size distribution for 1%Pt/25%HSiW/SiO_2.

Table 4.10. Alkylation of benzene with propane via bifunctional catalysed pathway.[a]

Catalyst	Conversion[b]	Aromatic selectivity (%)[c]				
	(%)	MePh	EtPh	iPrPh	nPrPh	C_{9+}
25%HSiW/SiO_2	0.2 (2)	0	1.5	81.0	3.1	14.4
7%Pt/C+SiO_2[d]	0.1 (2)	0	0	37.2	54.6	8.2
1%Pt/25%HPW/SiO_2	3.1 (3)	0	0.8	75.7	2.1	21.4
1%Pt/25%HSiW/SiO_2[f]	4.0 (3)	0	0.8	81.6	2.9	14.7
1%Pt/25%HSiW/SiO_2[g]	2.0 (3)	0	3.0	81.9	2.2	12.9
7%Pt/C+25%HPW/SiO_2 (0.7%Pt)[d]	3.8 (4)	0	1.6	85.7	2.6	10.2
7%Pt/C+25%HSiW/SiO_2 (0.7%Pt)[d]	5.5 (6)	0	0.5	89.2	2.4	7.8
7%Pt/C+25%HSiW/SiO_2 (0.7%Pt)[e]	7.6 (9)	0	0.5	90.4	3.0	6.0
7%Pt/C+25%HSiW/SiO_2 (0.7%Pt)[h]	6.2 (15)	0	0.7	92.6	2.7	4.2

[a]Reaction conditions: 300 ^oC, 1 bar pressure, 0.20 g catalyst, inlet molar ratio C_6H_6/C_3H_8 = 1:9, 10 mL min^{-1} flow rate, W/F = 80 g h mol^{-1}; in situ catalyst pre-treatment at 300 ^oC/1 h in H_2 flow, 10 mL min^{-1}). [b]Average conversion of benzene since steady state reached during time on stream (h) given in round brackets. [c]Selectivity to aromatic products including unidentified C_{9+} alkylbenzenes. [d]Uniform physical mixture 7%Pt/C (0.02 g) + 25%HSiW/SiO_2 or SiO_2 (0.18 g). [e]Two catalyst beds: 7%Pt/C (0.02 g, top bed) and 25%HSiW/SiO_2 or HZSM-5 (0.18 g, bottom bed). [f]1.2% coke content in the catalyst after reaction. [g]At 250 ^oC. [h]Two catalyst beds: 7%Pt/C (0.02 g, top bed) and 0.18 g 25%HSiW/SiO_2 (0.18 g, bottom bed) separated with ca. 1 mm SiO_2 layer.

The reaction with either Pt or HSiW as monofunctional catalysts gave a very low benzene conversion of only 0.1-0.2% (Table 4.10). This clearly demonstrates that the

alkylation of benzene with propane over Pt/HPA catalysts occurs through bifunctional metal-acid catalysis as represented in Scheme 4.1.

The most striking feature of the alkylation over Pt/HPA catalysts is its high selectivity to iPrPh, which is the preferred alkylation product from the classical carbenium ion mechanism. For the Pt/HSiW/SiO_2 catalysts, the iPrPh selectivity was in the range of 83-93% (cf. 13-16% with Pt/HZSM-5, Table 4.9). The main by-products were unidentified C_{9+} alkylarenes, with only small amounts of EtPh (0.5-1.6%) and nPrPh (2.1-3.0%) formed. MePh was not observed at all amongst the products. This is in agreement with the results on the alkylation of benzene by propene over supported HPA, which gives high selectivity to iPrPh with only negligible amount of nPrPh formed [36]. The difference in reaction selectivity between Pt/HPA/SiO_2 and Pt/HZSM-5 catalysts indicates that with Pt/HZSM-5 the alkylation is controlled by zeolite shape selectivity, whereas with Pt/HPA/SiO_2 the reaction is likely to occur under kinetic control. It is worth noting that Pt-free monofunctional acid catalysts HSiW/SiO_2 (Table 4.10) and HZSM-5 (Table 4.9) also exhibited this selectivity pattern, which further strengthens the point about shape selectivity control in zeolite catalysts.

1%Pt/25%HSiW/SiO_2 catalyst gave 81.6% iPrPh selectivity, with benzene conversion gradually decreasing from 7.5% to less than 4% over 3 h on stream. This can be explained by catalyst coking; 1.2% of coke was found in the spent catalyst (Table 3.5, Chapter 3), which could block Pt and/or HPA proton sites in the catalyst. The loss of acidity due to HPA reduction can be ruled out as the cause of catalyst deactivation since the HPA reduced only above 500 ^{o}C (see the H_2-TPR in Figure 3.21 and 3.22, Chapter 3). The structural integrity of the HPA was also maintained during reaction as evidenced by the DRIFT spectra of fresh and spent catalysts, showing that the Keggin structure remained intact (Figure 3.26, Chapter 3). The fact that HPW despite its acid strength was a less efficient partner in the Pt/HPA catalyst than HSiW may be the result of relatively more intense coking of HPW.

The physical mixture of 7%Pt/C + 25%HSiW/SiO_2 (1:9 w/w) with 0.7% Pt content exhibited more stable performance with a higher average conversion of 5.5% over 6 h on stream and 85.7% iPrPh selectivity. Figure 4.7 shows the time course for this reaction, which is typical of Pt/HSiW bifunctional catalysts. It is seen that iPrPh selectivity increases during first 2 h on stream to reach steady-state value at about 90%. At the same time, benzene conversion gradually decreases to level off at about 5%. This behaviour may be explained by catalyst coking.

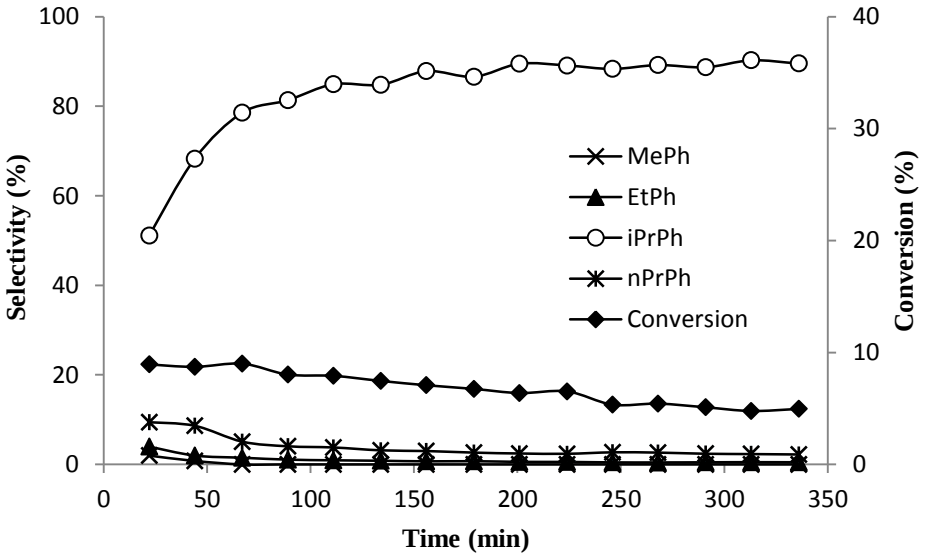

Figure 4.7. Time course for alkylation of benzene with propane over 7%Pt/C (0.02 g) + 25% HSiW/SiO_2 (0.18 g) physical mixture (0.2 g total catalyst weight, 0.7% Pt; 300 ^oC, 1 bar pressure, inlet molar ratio C_6H_6/C_3H_8 = 1:9, 10 mL min^{-1} flow rate, *W/F* = 80 g h mol^{-1}; in-situ catalyst pre-treatment at 300 ^oC/1 h in H_2 flow, 10 mL min^{-1}).

Even better conversion stability and higher iPrPh yield gave two-bed catalysts comprising 7%Pt/C and 25%HSiW/SiO_2 beds either unseparated or separated with ~1 mm layer of SiO_2 (Table 4.10). The unseparated two-bed catalyst gave 7.6% conversion over 9 h on stream (Figure 4.8) with 90.4% iPrPh selectivity (6.9% yield). This yield is quite close to the equilibrium value (8.2%) and significantly higher than that reported so far (cf. 4.6% yield

with hydrogen acceptor and 2.1% without it [16]). The catalyst with silica-separated beds exhibited stable 6.2% benzene conversion for 13 h on stream with iPrPh selectivity of 92.6%, the highest achieved in this work (Figure 4.9). The high activity of mixed and two-bed catalysts indicates that the reaction is not limited by migration of intermediates between metal and acid sites. The better performance stability of these catalysts in comparison to the supported 1%Pt/25%HSiW/SiO_2 catalyst may be explained by their better resistance to coking.

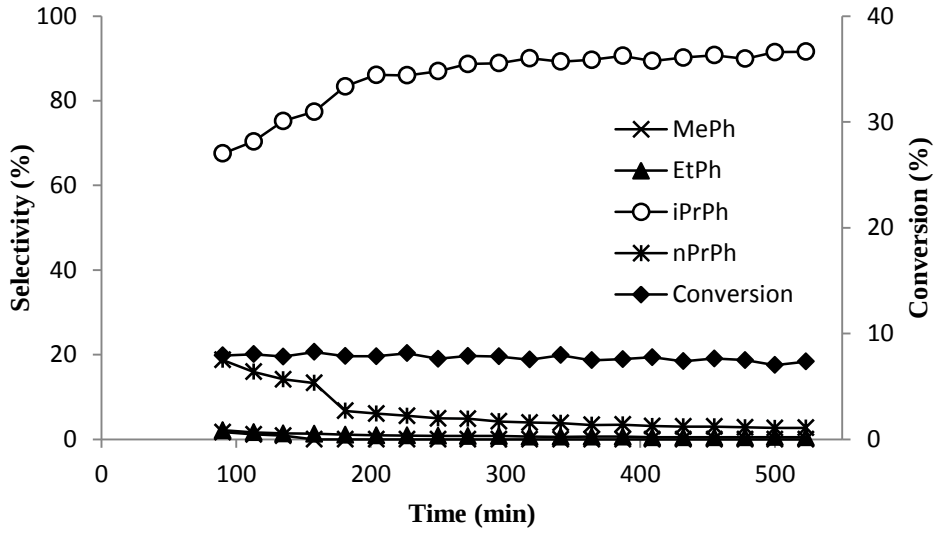

Figure 4.8. Time course for alkylation of benzene with propane over two-bed catalyst 7%Pt/C (0.02 g, top bed) + 25% HSiW/SiO_2 (0.18 g, bottom bed) (0.2 g total catalyst weight, 0.7% Pt; 300 ^{o}C, 1 bar pressure, inlet molar ratio C_6H_6/C_3H_8 = 1:9, 10 mL min^{-1} flow rate, *W/F* = 80 g h mol^{-1}; in-situ catalyst pre-treatment at 300 ^{o}C/1 h in H_2 flow, 10 mL min^{-1}).

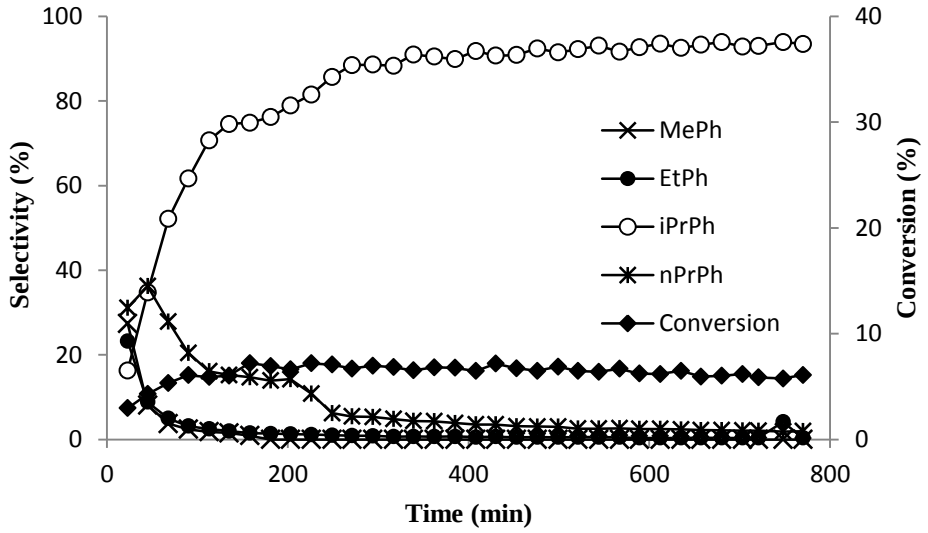

Figure 4.9. Time course for alkylation of benzene with propane over two-bed catalyst 7%Pt/C (0.02 g, top bed) + 25% HSiW/SiO_2 (0.18 g, bottom bed) separated with 1 mm SiO_2 layer (0.2 g total catalyst weight, 0.7% Pt; 300 ^{o}C, 1 bar pressure, inlet molar ratio C_6H_6/C_3H_8 = 1:9, 10 mL min-1 flow rate, *W/F* = 80 g h mol^{-1}; in situ catalyst pre-treatment at 300 ^{o}C/1 h in H_2 flow, 10 mL min^{-1}).

The apparent activation energy for benzene alkylation with 1%Pt/25%HSiW/SiO_2 was roughly estimated to be 50 kJ mol^{-1} (from the results at 250 and 300 ^{o}C, Table 4.10). This value indicates that the reaction was not affected by mass transport limitations, thus supporting the view that the reaction selectivity was not controlled by pore diffusion.

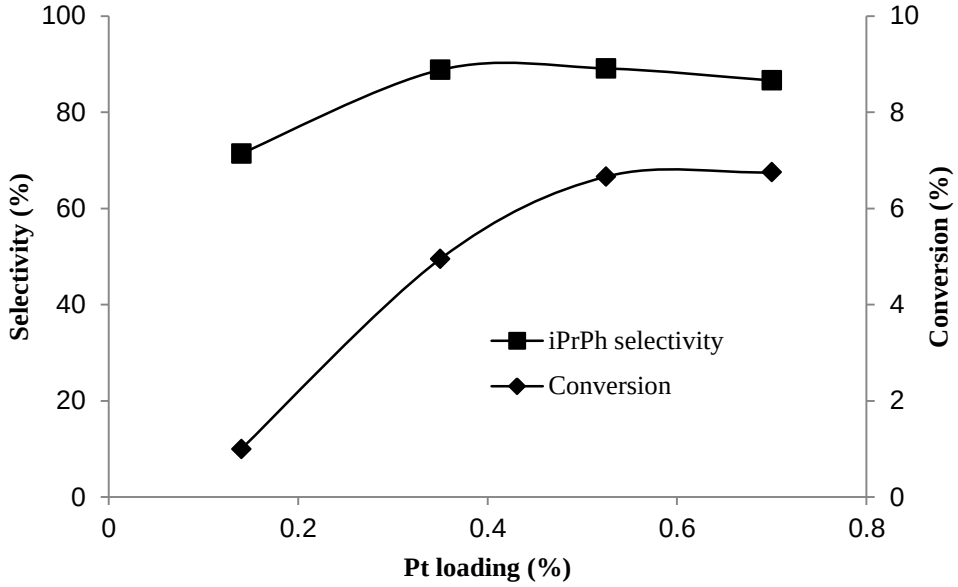

Figure 4.10. Effect of Pt loading on conversion and iPrPh selectivity of benzene alkylation over 7%Pt/C+25%HSiW/SiO_2 catalyst at 300 ^oC.

Further mechanistic evidence was obtained from examination of effects of Pt loading and HPA acid strength on the rate of benzene alkylation. Figure 4.10 shows the effect of Pt loading on benzene conversion and iPrPh selectivity for the reaction over mixed catalyst 7%Pt/C + 25%HSiW/SiO_2. Both parameters increase with Pt loading and reach a plateau at a Pt loading of 0.5%. This indicates that at Pt loading above 0.5% propane dehydrogenation step (1) is at fast quasi-equilibrium. It should be noted that Pt dispersion was not varied here since the same 7%Pt/C catalyst was used in these experiments.

The catalytic activity of HPA in the conventional alkylation of benzene by propene has been found to increase with HPA acid strength [31]. Here the effect of HPA acid strength on catalyst activity in benzene alkylation by propane was assessed using mixed catalysts 7%Pt/C + 15%HPA/Support (1:9 w/w) at 0.7% Pt and 15% HPA loading and SiO_2, TiO_2, Nb_2O_5 and ZrO_2 as the HPA supports (Table 4.11). We used the mixed rather than two-bed

catalysts because the former allowed better reproducible conversions to be obtained. The acid strength of the 15%HPA/Support catalysts has been determined previously by microcalorimetry of ammonia adsorption [27,28]; it decreases in the order of supports SiO_2 > TiO_2 > Nb_2O_5 > ZrO_2 (Table 4.1) owing to increasing interaction between HPA and support in this series [27]. As seen from Table 4.11, the conversion of benzene also decreases in this order, although reaction selectivity remains unchanged. The number of surface proton sites in these catalysts can be assumed to be equal to the total number of HPA protons (0.156 mmol g^{-1} for HPW and 0.208 mmol g^{-1} for HSiW) [28]. This allows for turnover frequencies (TOF) to be obtained. The TOF values (h^{-1}) were calculated as reaction rate per single proton site. The reaction rate (r) was determined as $r = XF/W$ (mol $h^{-1}g^{-1}$), where X is the fractional conversion of benzene and W/F = 80 g h mol^{-1} is the contact time. Figure 4.11 shows the plot of ln(TOF) versus ΔH for benzene alkylation, which demonstrates a fairly good correlation between the turnover reaction rate and the catalyst acid strength. This backs up the reaction mechanism through steps (1) and (2) (Scheme 4.1) and also supports the conclusion that at Pt loading above 0.5% the reaction is limited by step (2) of benzene alkylation with propene whereas step (1) is at fast quasi-equilibrium.

Mechanism of formation of alkylated aromatic by-products in the alkylation of benzene by ethane and propane over Pt/HZSM-5 has been discussed in detail elsewhere [9-11,16]. MePh and EtPh, the main by-products in the alkylation with propane, are more favourable thermodynamically than the desired iPrPh [4,16]. These have been suggested to arise from acid-catalyzed cracking of propane as well as cracking and transalkylation of propylbenzenes (iPrPh and nPrPh) [16]. In the reaction with Pt/HSiW, only small amounts of EtPh (0.5-3%) and nPrPh (2.1-3%) were formed together with unidentified C_{9+} aromatics (Table 4.10). As no propane cracking was observed (Table 4.8) and no MePh found amongst the products (Table 4.10), the formation of EtPh may be viewed as the result of iPrPh

cracking, which would also produce methane. The latter was indeed found amongst the alkylation products. As to the nPrPh is concerned, it is likely to come from acid-catalyzed isomerization of iPrPh.

Table 4.11. Effect of support on alkylation of benzene with propane via bifunctional catalyzed pathway.[a]

Catalyst[b]	Conversion[c]	Aromatic selectivity (%)[c]				
	(%)	MePh	EtPh	iPrPh	nPrPh	C_{9+}
7%Pt/C+15%HSiW/SiO_2	7.3	0	1.0	85.8	3.5	9.7
7%Pt/C+15%HPW/SiO_2	4.0	0.6	1.6	82.5	3.2	12.1
7%Pt/C+15%HPW/TiO_2	2.4	0	1.9	82.9	2.1	13.2
7%Pt/C+15%HPW/Nb_2O_5	3.0	0.8	2.7	82.3	2.8	11.4
7%Pt/C+15%HPW/ZrO_2	2.4	0.5	2.5	83.6	2.2	11.2

[a]Reaction conditions: 300 ^oC, 1 bar pressure, 0.20 g catalyst, inlet molar ratio C_6H_6/C_3H_8 = 1:9, 10 mL min^{-1} flow rate, *W/F* = 80 g h mol^{-1}, 2 h time on stream; in situ catalyst pre-treatment at 300 ^oC/1 h in H_2 flow, 10 mL min^{-1}). [b]Uniform physical mixture 7%Pt/C (0.02 g) + 15%HPA/Support (0.18 g) with 0.7% Pt content. [c]Conversion and selectivity values at 2 h time on stream.

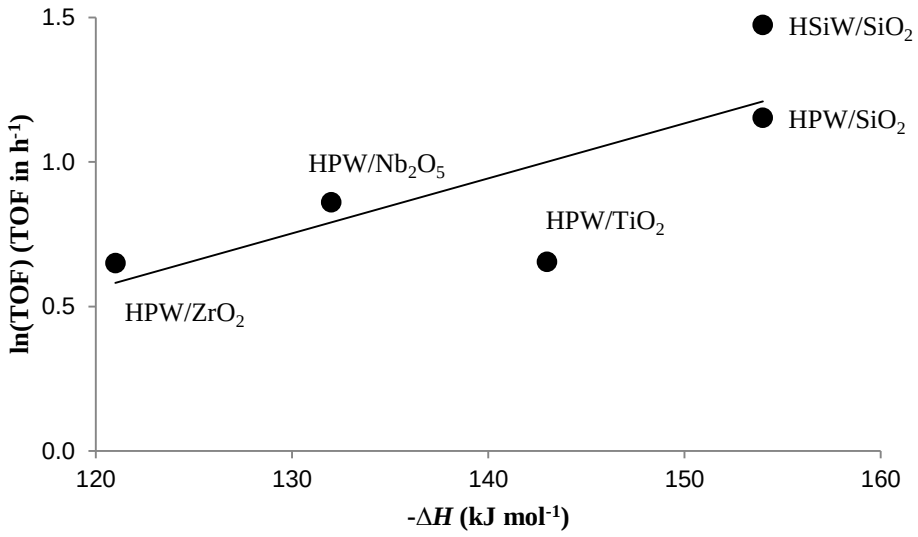

Figure 4.11. Plot of ln(TOF) vs. Δ*H* for benzene alkylation over 1:9 w/w mixture 7%Pt/C + 15%HPA/Support at 300 ^{o}C.

4.4. Conclusions

The alkylation of benzene with propane to yield isopropylbenzene proceeds with high selectivity over bifunctional metal-acid catalysts comprising Pt and Keggin heteropoly acid in a fixed-bed reactor at 250-350 ^{o}C and 1 bar pressure. Most efficiently the reaction occurs over Pt/$H_4SiW_{12}O_{40}$/SiO_2 catalyst, giving isopropylbenzene with 90-93% selectivity at 6-8% benzene conversion at 300 ^{o}C and an inlet C_6H_6/C_3H_8 molar ratio of 1:9. This significantly exceeds the efficiency of previously reported Pt/HZSM-5 catalyst [16]. The alkylation proceeds through the bifunctional reaction pathway (Scheme 4.1) including dehydrogenation of propane to propene (1) on Pt sites followed by benzene alkylation with propene (2) on acid sites. At Pt loadings above 0.5%, step (1) is at fast quasi-equilibrium, and step (2) is the rate-limiting one. There is important difference in performance between Pt/HPA/SiO_2 and Pt/HZSM-5 catalysts. With the Pt/HZSM-5, reaction selectivity is controlled by acid-catalysed transformations within zeolite microporous structure (product shape selectivity), leading to preferential formation of nPrPh together with cracking and transalkylation

products such as MePh and EtPh rather that the desired iPrPh. In contrast, the mesoporous Pt/HPA/SiO_2 catalyst gives selectively iPrPh, i.e., the alkylation product favoured from the carbenium ion mechanism. The preferred reactor design is a two-bed configuration involving Pt/C top (upstream) and HSiW/SiO_2 bottom (downstream) catalyst bed, providing better catalyst stability to deactivation as well as higher iPrPh selectivity.

References

1. Shilov, A. E. *Activation of Saturated Hydrocarbons by Transition Metal Complexes*; Reidel: Dordrecht, **1984**.

2. Hashiguchi, B. G.; Bischof, S. M.; Konnick, M. M.; Periana, R. A. *Acc. Chem. Res.* **2012**, *45*, 885.

3. Caeiro, G.; Carvalho, R. H.; Wang, X.; Lemos, M. A. N. D. A.; Lemos, F.; Guisnet, M.; Ramoa Ribeiro, F. *J. Mol. Catal. A: Chem*. **2006,** *255*, 131.

4. Weissermel, K.; Arpe, H.-J. *Industrial Organic Chemistry*; Wiley-VCH: Weinheim, Germany, **2003**.

5. Olah, G. A.; Schilling, P.; Staral, J. S.; Halpern, Yu.; Olah, J. A. *J. Am. Chem. Soc.* **1975,** *97*, 6807.

6. Bragin, O. V.; Shpiro, E. S.; Preobrazhensky, A. V.; Isaev, S. A.; Vasina, T. V.; Dyusenbina, B. B.; Antoshin, G. V.; Minachev, K. M. *Appl. Catal*. **1986,** *27*, 219.

7. Smirnov, A. V.; Mazin, E. V.; Ponomoreva, O. A.; Yuschenko, V. V.; Knyazeva, E. E.; Nesterenko, S. N.; Ivanova, I. I. *J. Catal.* **2001,** *135*, 153.

8. Kato, S.; Nakagawa, K.; Ikenaga, N.; Suzuki, T. *Catal. Lett*. **2001,** *73*, 175.

9. Lukyanov, D. B.; Vazhnova, T. *J. Mol. Catal. A: Chem*. **2008,** *279*, 128.

10. Lukyanov, D. B.; Vazhnova, T. *J. Catal*. **2008,** *257*, 382.

11. Chua, L. M.; Vazhnova, T.; Mays, T. J.; Lukyanov, D. B.; Rigby, S. P. *J. Catal*. **2010,** *271*, 401.

12. Ordomskiy, V. V.; Rodionova, L. I.; Ivanova, I. I.; Luck, F. *ChemCatChem* **2012,** *4*, 681.

13. Wong, K. S.; Vazhnova, T.; Rigby, S. P.; Lukyanov, D. B. *Appl. Catal. A* **2013,** *454*, 137.

14. Vazhnova, T.; Rigby, S. P.; Lukyanov, D. B. *J. Catal.* **2013,** *301*, 125.

15. Ivanova, I. I.; Blom, N.; Derouane, E. G. *J. Mol. Catal*. **1996,** *109*, 157.

16. Smirnov, A. V.; Mazin, E. V.; Yuschenko, V. V.; Knyazeva, E. E.; Nesterenko, S. N.; Ivanova, I. I.; Galperin, L.; Jensen, R.; Bradley, S. *J. Catal.* **2000,** *194*, 266.

17. Abasov, S. I.; Babayeva, F. A.; Zarbaliyev, R. R.; Abbasova, G. G.; Tagiyev, D. B.; Rustamov, M. I. *Appl. Catal. A* **2003,** *251*, 267.

18. Bigey, C.; Su, B-L. *J. Mol. Catal. A* **2004,** *209*, 179.

19. Huang, X.; Sun. X.; Zhu, S.; Liu, Z. *React. Kinet. Catal. Lett.* **2007,** *91*, 385.

20. Babaeva, F. A.; Abasov, S. I.; Rustamov, M. I. *Petrol. Chem.* **2010,** *50*, 42.

21. Hetterley, R. D. ; Kozhevnikova, E. F.; Kozhevnikov, I. V. *Chem. Commun.* **2006**, 782.

22. Alotaibi, M. A.; Kozhevnikova, E. F.; Kozhevnikov, I. V. *J. Catal*. **2012,** *293*, 141.

23. Alotaibi, M. A.; Kozhevnikova, E. F.; Kozhevnikov, I. V. *Chem. Commun*. **2012,** *48*, 7194.

24. Alotaibi, M. A.; Kozhevnikova, E. F.; Kozhevnikov, I. V. *Appl. Catal*. *A* **2012,** *447-448*, 32.

25. Okuhara, T.; Mizuno, N.; Misono, M. *Adv. Catal*. **1996,** *41*, 113.

26. Kozhevnikov, I. V. *Catalysis by Polyoxometalates*; Wiley & Sons: Chichester, England, **2002.**

27. Alsalme, A. M.; Wiper, P. V.; Khimyak, Y. Z.; Kozhevnikova, E. F.; Kozhevnikov, I. V. *J. Catal.* **2010,** *276*, 181.

28. Alharbi, W.; Brown, E.; Kozhevnikova, E. F.; Kozhevnikov, I. V. *J. Catal.* **2014,** *319*, 174.

29. Benson, J. E.; Hwang, H. S.; Boudart, M. *J. Catal*. **1973,** *30*, 146.

30. *CRC Handbook of Chemistry and Physics;* Haynes, W. M., ed.; CRC Press, **2012**.

31. Wagman, D. D.; Evans, W. H.; Parker, V. B.; Schumm, R. H.; Halow, I.; Bailey, S. M.; Churney, K. L.; Nuttall, R. L. *J. Phys. Chem. Ref. Data* **1982,** *11*, 1.

32. Chao, J.; Wilhoit, R. C.; Zwolinski, B. J. *J. Phys. Chem. Ref. Data* **1973,** *2*, 427.

33. Chao, J.; Zwolinski, B. J. *J. Phys. Chem. Ref. Data* **1975,** *4*, 251.

34. NIST Chemistry WebBook *htt://webbook.nist.gov/chemistry/thermo/* (accessed May 14, **2015**).

35. Alberty, R. A. *J. Phys. Chem. Ref. Data* **1985,** *14*, 177.

36. De Angelis, A.; Amarilli, S.; Berti, D.; Montanari, L.; Perego, C. *J. Mol. Catal. A* **1999,** *146*, 37.

37. Nowinska, K.; Fiedorow, R.; Adamiec, J. *J. Chem. Soc. Faraday Trans.* **1991,** *87*, 749.

38. Bardin, B. B.; Bordawekar, S. V.; Neurock, M.; Davis, R. J. *J. Phys. Chem. B* **1998,** *102*, 10817.

39. Brandle, M; J. Sauer, J. *J. Am. Chem. Soc.* **1998**, *120*, 1556.

Chapter 5: Alkylation of Benzene with Propane over Bifunctional Pd-Acid Catalysts

5.1. Introduction

Acid-catalysed alkylation of benzene with alkenes is an established commercial process to manufacture a wide range of alkylbenzenes. The alkylation of benzene with ethene and propene is used to produce ethylbenzene (EtPh) and isopropylbenzene (iPrPh), which are the intermediates in styrene and phenol production, respectively [1]. As discussed in Chapter 1, section 1.6, it has been demonstrated that ethene and propene can be replaced by abundant and inexpensive alkanes, ethane and propane, which would lead to more cost effective and environmentally benign production of these commodity chemicals [2-18]. The alkylation of benzene with light alkanes occurs in the gas phase in the presence of solid bifunctional metal-acid catalysts, which operate via a pathway shown in Scheme 1.6 (section 1.6) including alkane dehydrogenation on metal sites to form alkene and H_2 (step 1) followed by benzene alkylation with the alkene on acid sites (step 2).

Pt-zeolite bifunctional catalysts have been shown to be most active for benzene alkylation with ethane [2-17]. Best results have been achieved using Pt-modified HZSM-5 zeolite to obtain >90% EtPh selectivity at a close to equilibrium benzene conversion of 12% [6]. In contrast, the alkylation of benzene with propane has proved to be more difficult, giving only 32% iPrPh selectivity at 6.6% conversion using Pt/HZSM-5 [13]. The main product was nPrPh (50% selectivity) rather than iPrPh [13], which would be the favourable product from the carbenium ion mechanism. This may be due to the shape selectivity control imposed by zeolite (HZSM-5) microporous environment (Chapter 4, section 4.1).

We have reported a much more selective alkylation of benzene by propane (90-93% iPrPh selectivity) using a mesoporous silica-supported Pt-heteropoly acid catalyst, $Pt/H_4SiW_{12}O_{40}/SiO_2$, based on the Keggin-type 12-tungstosilicic acid $H_4SiW_{12}O_{40}$ (HSiW) [18] (Chapter 4). Notably HSiW is superior to its stronger analogue $H_3PW_{12}O_{40}$ in this

reaction probably due to the larger number of proton sites and better resistance to coking (Chapter 4, section 4.3.3).

We now investigate the alkylation of benzene by propane using less expensive bifunctional catalysts based on palladium. Similar to platinum, palladium is an active catalyst for alkane dehydrogenation hence capable of promoting the alkylation process. The bifunctional Pd catalysts under study comprise HSiW and HZSM-5 as the acid components. In general, regardless of their formulation, these catalysts are denoted herein Pd-HSiW and Pd-HZSM-5, respectively. Both supported and physically mixed bifunctional catalysts are used in this work; the supported ones are denoted Pd/HSiW/SiO_2 and Pd/HZSM-5 and the mixed ones Pd/C + HSiW/SiO_2 and Pd/C + HZSM-5. Also we looked at the effect of gold additives on catalyst performance by testing the corresponding PdAu-HSiW and PdAu-HZSM-5 bimetallic catalysts. It is demonstrated that in benzene alkylation with propane the Pd-HSiW and Pd-HZSM-5 catalysts perform similarly to their Pt counterparts, Pt-HSiW and Pt-HZSM-5, reported previously (Chapter 4, Tables 4.9 and 4.10). Addition of gold to Pd-HSiW is shown to enhance the activity of this catalyst, although the Au-HSiW without Pd is inert.

5.2. Materials and Methods

5.2.1. Chemicals and catalysts

Information about the sources and purity of chemicals used in this work is given in Chapter 2, section 2.1.

Silica-supported HSiW catalysts were prepared by wet impregnation of Aerosil 300 silica by an aqueous HSiW solution and dried at 150°C/10^{-3} kPa for 1.5 h [19, 20]. Pd/HSiW/SiO_2 and Pd/HZSM-5 bifunctional catalysts were prepared by wet impregnation of acidic component (25%HSiW/SiO_2 or HZSM-5) with 0.02 M Pd(acac)$_2$ solution in benzene

at room temperature for 1 h, followed by slow evaporation of benzene in a rotary evaporator at room temperature, as described elsewhere [21]. The catalysts were dried under vacuum at 150 $^{o}C/10^{-3}$ kPa and then reduced in oven by hydrogen flow at 250 ^{o}C for 2 h. The integrity of HSiW Keggin structure on the silica surface in the Pd/HSiW/SiO_2 catalysts was confirmed by infrared spectroscopy (Figure 3.27, Chapter 3). Bimetallic 6.0%Pd/10%Au/C catalyst was prepared by wet impregnation of 7.1%Pd/C with an aqueous solution of $HAuCl_4$ followed by drying and reduction by H_2 flow at 250 ^{o}C for 2 h. Pd and Au loading in supported catalysts was confirmed by the ICP-AES; it was in good agreement with the loading expected from the preparation stoichiometry (e.g. 6.4%Pd/10%Au/C from stoichiometry and 6.0%Pd/9.9%Au/C from ICP-AES analysis). Physical mixtures of 7.1%Pd/C with 25%HSiW/SiO_2 or HZSM-5 containing a specified percentage of Pd were prepared by grinding mixtures of these components. Physical mixtures of 6.0%Pd/10%Au/C with 25%HSiW and HZSM-5 were prepared in the same way.

5.2.2. Techniques

The catalysts prapared were characterised by a number of techniques such as, BET surface area, XRD, FTIR, H_2-TPR, TGA, ICP-AES and chemisorption of H_2 and CO. The details of catalyst characterisation are given in Chapters 2 and 3. Most of results on catalyst characterisation are presented in Chapter 3. Some additional results are also given in this chapter.

Nitrogen adsorption isotherms and pore size distribution for Pd-HSiW and Pd-HZSM-5 catalysts are shown in Figures 5.1-5.4. Powder X-ray diffraction (XRD) patterns of these catalysts recorded on a PANalytical Xpert diffractometer with CuKα radiation (λ = 1.542 Å) are shown in Figures 3.14 and 3.17 (Chapter 3).

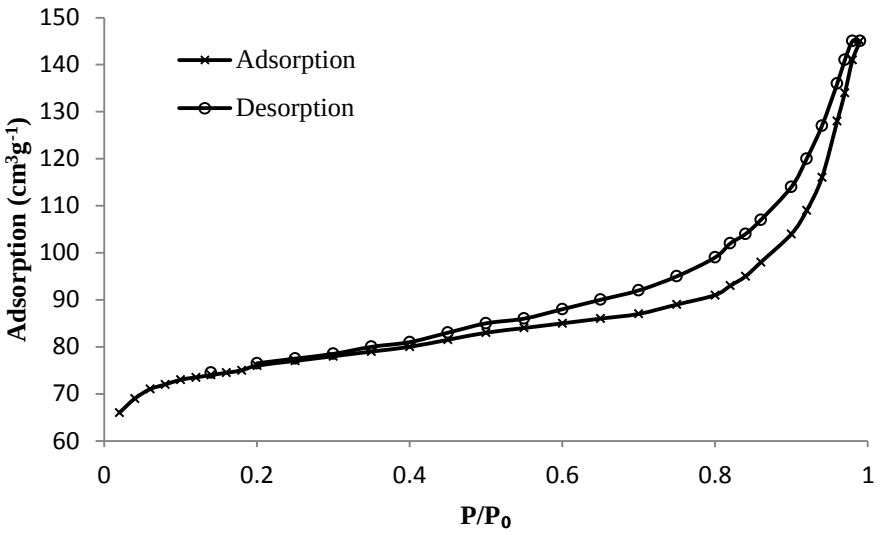

Figure 5.1. Nitrogen adsorption (×) and desorption (○) isotherms for 2%Pd/HZSM-5.

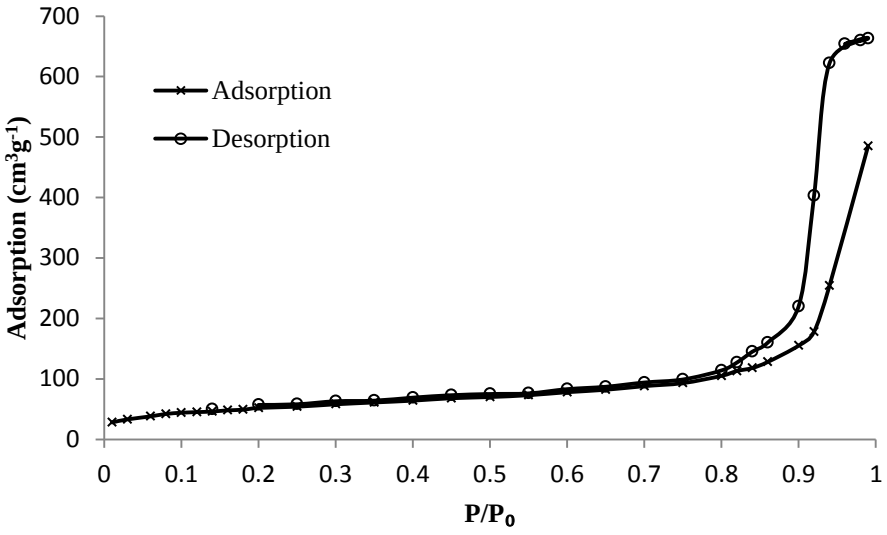

Figure 5.2. Nitrogen adsorption (×) and desorption (○) isotherms for 2%Pd/25%HSiW/SiO_2.

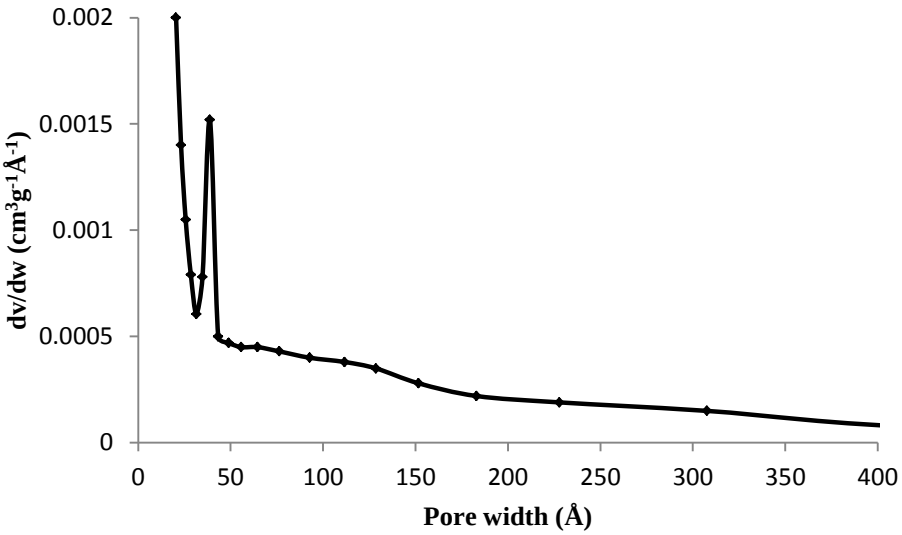

Figure 5.3. BJH desorption pore size distribution for 2%Pd/HZSM-5.

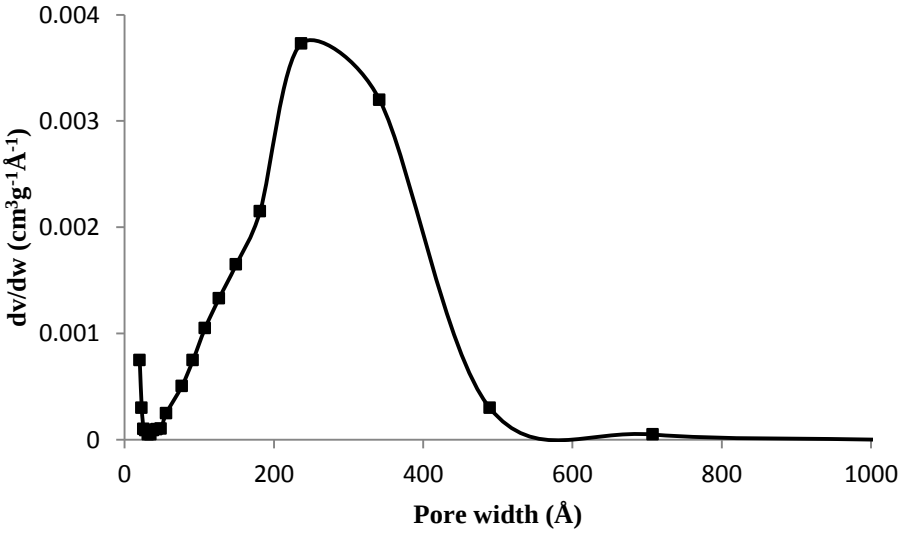

Figure 5.4. BJH desorption pore size distribution for 2%Pd/25%HSiW/SiO_2.

Average metal particle size, *d*, in supported catalysts was estimated from XRD using the Scherrer equation, with line broadening assessed as the full width at half maximum intensity (FWHM). Metal dispersion, *D*, defined as the metal (M) fraction at the surface, $D = M_s/M_{total}$, was calculated from the empirical equation $D = 0.9/d$ (nm) [22]. XRD patterns of supported Pd and Au catalysts are shown in Figures 3.14, 3.16-3.17 in Chapter 3. The acid strength of heteropoly acids, including HSiW, has been characterised previously using ammonia adsorption microcalorimetry [18, 19].

Information about the Pd and Au catalysts used in this chapter is summarised in Table 5.1. It includes catalyst texture (surface area, pore volume and pore diameter), Pd and Au dispersion and particle size.

Table 5.1. Catalyst characterisation.

Catalyst	S_{BET}[a] (m^2g^{-1})	Pore volume[b] (cm^3g^{-1})	Pore diameter[c] (Å)	d[d] (nm)	D[e]
25%HSiW/SiO_2	215	0.95	171		
2%Pd/25%HSiW/SiO_2	189	0.75	159	5	0.18
HZSM-5	301	0.22	31		
2%Pd/HZSM-5	262	0.20	31	10	0.090
7.1%Pd/C				11	0.082
10%Au/C				89	0.010
6.0%Pd/9.9%Au/C				13 (Pd)	0.069 (Pd)
				62 (Au)	0.015 Au)

[a]BET surface area. [b]Single point pore volume. [c]Average BET pore diameter. [d]Metal particle size from XRD. [e]Metal dispersion calculated from the empirical equation $D = 0.9/d$ (nm).

5.2.3. Catalyst testing

The alkylation of benzene with propane was carried out in the gas phase at 300 ^{o}C and an inlet C_6H_6/C_3H_8 molar ratio of 1:9 under atmospheric pressure in a quartz fixed-bed down-flow reactor (9.0 mm internal diameter) with online GC analysis (Varian 3800 instrument with a 30 m x 0.32 mm x 0.5 μm Zebron ZB-WAX capillary column and a flame ionisation detector), as described elsewhere (Chapter 4, section 4.2.). The reactor was packed with 0.20 g catalyst powder of 45-180 μm particle size. The gas feed containing propane (90 kPa) and benzene (10 kPa) entered the reactor at the top at a flow rate of 10 mL min^{-1} (space time W/F = 80 g h mol^{-1}, where W is the catalyst weight and F is the molar flow rate of benzene). Prior to reaction, the catalysts were pre-treated in situ in H_2 flow (10 mL min^{-1}) for 1 h at the reaction temperature. The selectivity to alkylbenzenes was defined as moles of alkylbenzene formed per one mole of benzene converted and quoted in mole per cent. The mean absolute percentage error in conversion and selectivity was ≤ 10% and the carbon balance was maintained within 95%.

5.3. Results and Discussion

It is essential to compare the bifunctional Pd catalysts under study with previously reported Pt catalysts (Chapter 4) at the same reaction conditions. Therefore, the Pd catalysts were tested in benzene alkylation with propane in the same system at 300 ^{o}C, contact time W/F = 80 g h mol^{-1} and $[C_6H_6]/[C_3H_8]$ = 1:9 mol/mol without dilution of the gas feed with an inert gas, as described previously (Chapter 4, section 4.2). At such conditions, equilibrium conversion of benzene to iPrPh was calculated to be 8.2% (Chapter 4, section 4.3.4).

5.3.1. Alkylation of benzene over Pd-HZSM-5

Representative results are given in Table 5.2. Monofunctional catalysts HZSM-5 and Pd/C + SiO_2 showed very low activity (entries 1 and 2). In contrast, bifunctional catalysts containing Pd and zeolite HZSM-5, both mixed and supported, were active in benzene alkylation with propane. This confirms the view that the reaction occurs through bifunctional metal-acid catalysis (Scheme 4.1, Chapter 4). With mixed catalysts Pd/C + HZSM-5, benzene conversion increased with Pd loading, levelling off at about 2% Pd loading (Figure 5.5; Table 5.2, entries 3-7). This indicates that propane dehydrogenation step (1) reaches quasi-equilibrium at ≥ 2% Pd loading, and the alkylation process becomes limited by acid-catalysed step (2) of benzene alkylation with propene (Scheme 4.1).

With Pd-HZSM-5 catalysts, the selectivity to the desired product iPrPh was 11-18%, the main reaction products being MePh, EtPh and nPrPh. Similar results have been obtained previously with Pt-HZSM-5 (Chapter 4, Table 4.9). Predominant formation of nPrPh rather than iPrPh, which would be the favourable product from the carbenium ion mechanism, has been explained (Chapter 4, section 4.3.3) by product shape selectivity control imposed by HZSM-5 microporous environment. This implies that iPrPh formed initially could isomerize on HZSM-5 proton sites to form nPrPh possessing higher diffusivity in zeolite micropores. MePh and EtPh, which are thermodynamically more favourable products than iPrPh, probably arise from cracking of nPrPh and iPrPh on zeolite acid sites [13].

Supported catalyst 2%Pd/HZSM-5 exhibited the best performance, giving 17.7% iPrPh selectivity at 19.5% benzene conversion (3.5% iPrPh yield) (Table 5.2, entry 8). This catalyst also showed good performance stability on stream (Figure 5.6). Its platinum counterpart, Pt/HZSM-5, gave similar results: 16.4% iPrPh selectivity at 19.9% conversion, i.e. 3.3% iPrPh yield (Chapter 4, Table 4.9). Overall, in benzene alkylation with propane, Pd-HZSM-5 and Pt-HZSM-5 catalysts perform similarly regarding the selectivity to iPrPh.

Table 5.2. Alkylation of benzene with propane over Pd-HZSM-5 catalysts.[a]

Catalyst	Conversion[b]	Aromatic selectivity (%)[c]				
	(%)	MePh	EtPh	iPrPh	nPrPh	C_{9+}
1) HZSM-5	0.2	25.5	22.8	14.2	24.6	12.9
2) Pd/C+SiO_2 (0.7%Pd)[d]	0.6	88.7	0	0	0	11.3
3) Pd/C+HZSM-5 (0.1%Pd)[d]	1.1	19.3	31.6	15.0	28.9	5.3
4) Pd/C+HZSM-5 (0.4%Pd)[d]	2.5	25.2	23.9	16.4	28.2	6.4
5) Pd/C+HZSM-5 (0.7%Pd)[d]	3.8	27.9	20.8	14.2	25.6	11.6
6) Pd/C+HZSM-5 (1.4%Pd)[d]	9.2	34.9	21.8	12.0	19.2	12.2
7) Pd/C+HZSM-5 (2.1%Pd)[d]	10.9	35.6	21.1	10.7	19.1	13.6
8) 2.0%Pd/HZSM-5	19.5	13.0	8.4	17.7	29.9	31.1

[a]Reaction conditions: 300 ^{o}C, 1 bar pressure, 0.20 g catalyst, inlet molar ratio C_6H_6/C_3H_8 = 1:9, 10 mL min^{-1} flow rate, *W/F* = 80 g h mol^{-1}; in situ catalyst pre-treatment at 300 ^{o}C/1 h in H_2 flow, 10 mL min^{-1}). [b]Benzene conversion at 3 h time on stream. [c]Selectivity to aromatic products including unidentified C_{9+} alkylbenzenes at 3 h time on stream. [d]Uniform physical mixture of 7.1%Pt/C with HZSM-5 or SiO_2.

It should be noted that supported 2.0%Pd/HZSM-5 catalyst is twice as active as Pd/C + HZSM-5 mixed catalyst (2.1% Pd loading) (Table 5.2, entries 7, 8). Since the distances between metal and acid sites in these catalysts differ greatly (nanometer scale in the first one and micrometer scale in the second), this indicates that the reaction may be limited by migration of alkene intermediates between the metal and acid sites within zeolite micropores. A different picture was observed in the case of mesoporous Pd/HSiW/SiO_2 catalysts (section 5.3.2).

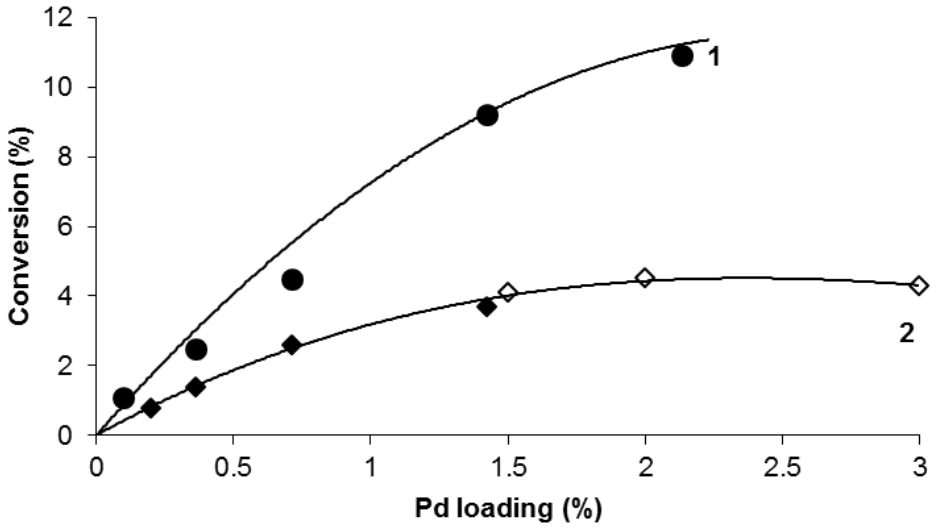

Figure 5.5. Effect of Pd loading on benzene conversion for benzene alkylation at 300 ^{o}C over (1) 7.1%Pd/C+HZSM-5 catalysts and (2) Pd-HSiW including physically mixed catalysts 7.1%Pd/C+25%HSiW/SiO_2 (solid diamonds) and supported catalysts Pd/25%HSiW/SiO_2 (open diamonds) (for reaction conditions, see Tables 5.2 and 5.3).

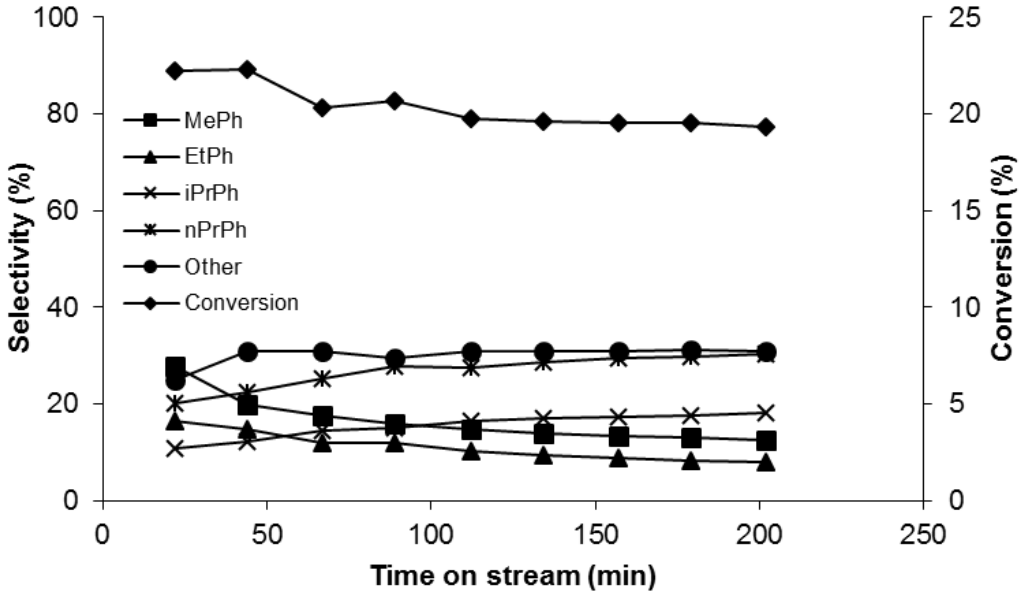

Figure 5.6. Time course for benzene alkylation by propane over 2%Pd/HZSM-5 (Si/Al = 10) (0.2 g catalyst, 1 bar pressure, inlet molar ratio C_6H_6/C_3H_8 = 1:9, 10 mL min^{-1} flow rate, *W/F* = 80 g h mol^{-1}; in-situ catalyst pre-treatment at 300 ^{o}C/1 h in H_2 flow).

5.3.2. Alkylation of benzene over Pd-HSiW

Silica-supported Pd-HSiW catalysts differ from Pd-HZSM-5 catalysts in two aspects: (i) they are mesoporous rather than microporous and (ii) HSiW heteropoly acid possesses stronger proton sites than HZSM-5 (Chapter 4). Therefore, the Pd-HSiW catalysts can be expected to be much more selective to iPrPh than Pd-HZSM-5, similar to the previously reported Pt-HSiW catalysts (Chapter 4).

The results for benzene alkylation with propane over Pd-HSiW are given in Table 5.3 for both mixed Pd/C + 25%HSiW/SiO_2 and supported Pd/25%HSiW/SiO_2 catalysts. As expected, the 25%HSiW/SiO_2 acid catalyst in the absence of Pd was practically inert (entry 1), whereas the bifunctional Pd-HSiW metal-acid catalysts showed good activity in the alkylation reaction. In stark contrast to Pd-HZSM-5, the reaction with the Pd-HSiW catalysts occurred with high selectivity to iPrPh, up to 88.1% (entry 9), as anticipated for the alkylation unaffected by shape selectivity effects. Supported catalysts 1.5-3%Pd/25%HSiW/SiO_2 showed the best results to give 85-88% iPrPh selectivity at 4.1-4.5% benzene conversion (up to 3.8% iPrPh yield) (entries 8 and 9). Therefore, with comparable yields, the Pd-HSiW catalysts are much more selective to iPrPh than the Pd-HZSM-5 ones. It can be seen that Pd-HSiW and Pt-HSiW catalysts perform similarly (cf. entries 7 and 10), with the Pt catalysts predictably more active than Pd ones per metal loading. This, however, is compensated for by the lower price (by a factor of ~1.5) of Pd as compared to Pt.

Like with Pd-HZSM-5 catalysts, benzene conversion was found to increase with Pd loading in Pd-HSiW catalysts to level off at ≥ 1.5% Pd loading (Figure 5.5; Table 5.3, entries 2-5). This indicates that propane dehydrogenation step (1) reached quasi-equilibrium at 1.5% Pd loading. Similar trend was observed for Pt-HSiW (Chapter 4, Figure 4.10).

Table 5.3. Alkylation of benzene with propane over Pd-HSiW catalysts.[a]

Catalyst	Conversion[b]	Aromatic selectivity (%)[c]				
	(%)	MePh	EtPh	iPrPh	nPrPh	C_{9+}
1) 25%HSiW/SiO_2	0.2					
2) Pd/C+HSiW/SiO_2 (0.2%Pd)[d]	0.8	0	5.9	44.3	18.8	31.0
3) Pd/C+HSiW/SiO_2 (0.4%Pd)[d]	1.4	0	2.7	67.3	10.0	20.0
4) Pd/C+HSiW/SiO_2 (0.7%Pd)[d]	2.6	3.6	1.4	69.6	6.4	18.9
5) Pd/C+HSiW/SiO_2 (1.4%Pd)[d]	3.7	2.0	2.0	74.2	6.7	15.1
6) Pd/C+HSiW/SiO_2 (1.4%Pd)[e]	5.2	4.4	3.1	70.6	15.9	6.0
7) 1.5%Pd/25%HSiW/SiO_2	4.1	0	0.8	86.3	3.0	9.9
8) 2.0%Pd/25%HSiW/SiO_2[f]	4.5	0	0.8	85.4	3.6	10.4
9) 3.0%Pd/25%HSiW/SiO_2	4.3	0	0.9	88.1	3.4	7.6
10) 1%Pt/25%HSiW/SiO_2 [18]	4.0	0	0.8	81.6	2.9	14.7

[a]Reaction conditions: 300 ^oC, 1 bar pressure, 0.20 g catalyst, inlet molar ratio C_6H_6/C_3H_8 = 1:9, 10 mL min^{-1} flow rate, *W/F* = 80 g h mol^{-1}; in situ catalyst pre-treatment at 300 ^oC/1 h in H_2 flow, 10 mL min^{-1}). [b]Benzene conversion at 3 h time on stream. [b]Selectivity to aromatic products including unidentified C_{9+} alkylbenzenes at 3 h time on stream. [d]Uniform physical mixture 7.1%Pt/C with 25%HSiW/SiO_2. [e]Two catalyst beds: 7.1%Pd/C (0.04 g, top bed) and 25%HSiW/SiO_2 (0.16 g, bottom bed). [f]2.1% coke content in the catalyst after reaction.

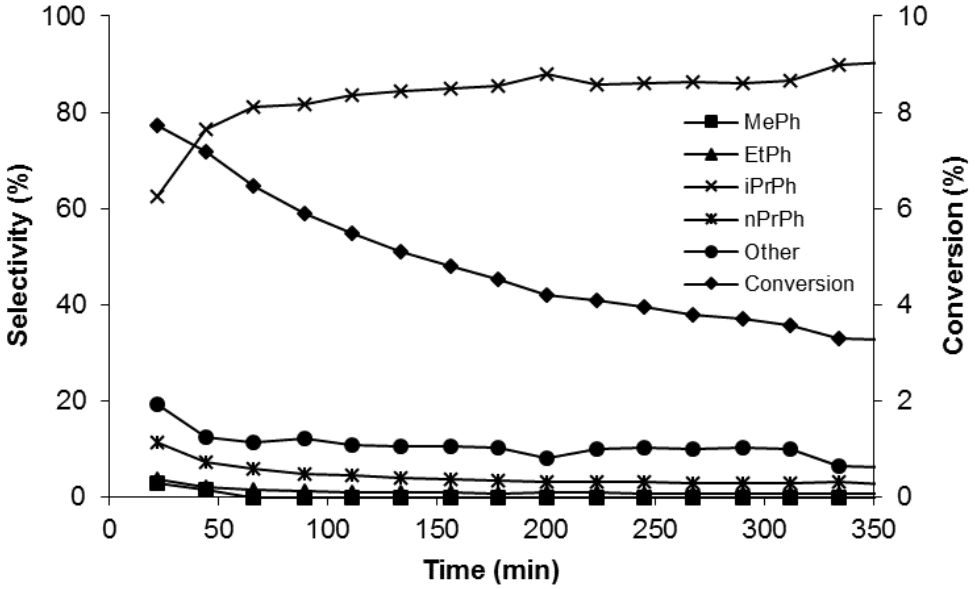

Figure 5.7. Time course for benzene alkylation by propane over 2%Pd/25%HSiW/SiO_2 (0.2 g catalyst, 300 ^{o}C, 1 bar pressure, inlet molar ratio C_6H_6/C_3H_8 = 1:9, 10 mL min^{-1} flow rate, *W/F* = 80 g h mol^{-1}; in-situ catalyst pre-treatment at 300 ^{o}C/1 h in H_2 flow).

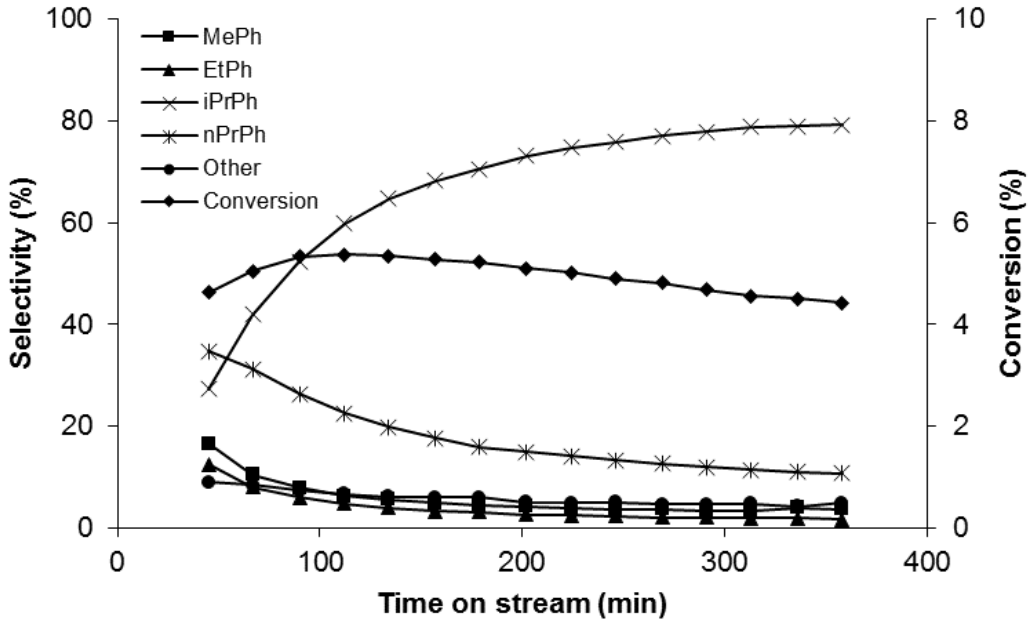

Figure 5.8. Time course for benzene alkylation by propane over two-bed catalyst 7.1%Pd/C (0.04 g, top bed) + 25%HSiW/SiO_2 (0.16 g, bottom bed) (0.2 g total catalyst weight, 1.4% Pd, 300 ^{o}C, 1 bar pressure, inlet molar ratio C_6H_6/C_3H_8 = 1:9, 10 mL min^{-1} flow rate, *W/F* = 80 g h mol^{-1}; in-situ catalyst pre-treatment at 300 ^{o}C/1 h in H_2 flow).

Similar to supported Pt-HSiW catalysts (Chapter 4, section 4.3.4), the supported Pd-HSiW catalysts suffered from deactivation, as shown in Figure 5.7. This may be explained by catalyst coking (Table 5.3, entry 8). In contrast, the mixed and especially two-bed Pd/C + 25%HSiW/SiO_2 catalysts were more stable on stream (Figure 5.8), albeit with a lower iPrPh selectivity of 70-74% (Table 5.3, entries 4-6). Similar performance has also been observed for their Pt counterparts (Chapter 4, Table 4.10). The high activity of mixed and two-bed catalysts indicates no reaction limitation by migration of alkene intermediates between metal and acid sites within these mesoporous catalysts. This is different from the microporous Pd-HZSM-5 catalysts (section 5.3.1.). The better performance stability of these catalysts in comparison to the supported Pd/25%HSiW/SiO_2 catalyst may be due to their better resistance to coking (Chapter 4, section 4.3.4).

5.3.3. Effect of gold additives

Bimetallic PdAu and PtAu catalysts have attracted much interest because of their enhanced performance in comparison to monometallic counterparts ([23-32] and references therein). For example, addition of gold to bifunctional Pt/CsPW catalyst (CsPW = $Cs_{2.5}H_{0.5}PW_{12}O_{40}$) for hydrodeoxygenation of 3-pentanone has been found to increase both catalyst hydrogenation activity (turnover rate at Pt sites) and catalyst stability to deactivation, although the Au itself was inert in this reaction [30]. Gold enhancement of catalyst performance is usually attributed to Au alloying through ensemble (geometric) and ligand (electronic) effects of the constituent elements [28, 29]. Previously reported STEM-EDX and XRD analysis of PtAu/CsPW catalysts indicates the presence of bimetallic nanoparticles with a wide range of Pt/Au atomic ratios in such catalysts [30].

Table 5.4. Alkylation of benzene with propane over PdAu-HZSM-5 and PdAu-HSiW catalysts.[a]

Catalyst	Conv.[b]	Aromatic selectivity (%)[c]				
	(%)	MePh	EtPh	iPrPh	nPrPh	C_{9+}
1) 0.5%Au/HZSM-5	0.5	0	35.4	12.9	23.7	28.0
2) 5.0%Au/C+HZSM-5 (2.0%Au)[d]	0.4	0	30.0	18.3	36.5	15.2
3) PdAu/C+HZSM-5 (1.2%Pd, 2.0%Au)[d]	8.8	34.2	23.3	10.6	18.4	13.5
4) Pd/C+HZSM-5 (1.4%Pd)[d]	9.2	34.9	21.8	12.0	19.2	12.2
5) 10%Au/C+HSiW/SiO_2 (2.0%Au)[d]	0.4	0	22.6	18.0	28.4	31.0
6) PdAu/C+HSiW/SiO_2 (1.2%Pd, 2.0%Au)[d]	3.8	2.9	1.6	72.3	5.7	16.7
7) Pd/C+HSiW/SiO_2 (1.4%Pd)[d]	3.7	0	2.0	74.2	6.7	17.1
8) PdAu/C+HSiW/SiO_2 (1.2%Pd, 2.0%Au)[e]	5.8	6.5	2.7	70.9	14.3	5.6
9) Pd/C+HSiW/SiO_2 (1.4%Pd)[e]	5.2	4.4	3.1	70.6	15.9	6.0

[a]Reaction conditions: 300 ^oC, 1 bar pressure, 0.20 g catalyst, inlet molar ratio C_6H_6/C_3H_8 = 1:9, 10 mL min^{-1} flow rate, W/F = 80 g h mol^{-1}; in situ catalyst pre-treatment at 300 ^oC/1 h in H_2 flow, 10 mL min^{-1}). [b]Benzene conversion at 3 h time on stream. [c]Selectivity to aromatic products including unidentified C_{9+} alkylbenzenes at 3 h time on stream. [d]Uniform physical mixture 7.1%Pt/C or 6.0%Pd/9.9%Au/C with HZSM-5 or 25%HSiW/SiO_2. [e]Two catalyst beds: 7.1%Pd/C or 6.0%Pd/9.9%Au/C (0.04 g, top bed) and 25%HSiW/SiO_2 (0.16 g, bottom bed).

Here we looked at the effect of gold additives on the performance of Pd-HZSM-5 and Pd-HSiW catalysts in the alkylation of benzene by propane. The results, including benzene conversions and product selectivities, are shown in Table 5.4. Supported and mixed gold catalysts in the absence of Pd (0.5%Au/HZSM-5, 5%Au/C + HZSM-5 (2% Au) and 10%Au/C + HSiW/SiO_2 (2% Au)) showed very low activity (0.4-0.5% benzene conversion).

No enhancing effect of gold was found in the case of mixed Pd/C + HZSM-5 catalysts. Thus, Pd/C + HZSM-5 (1.4% Pd) and PdAu/C + HZSM-5 (1.2% Pd, 2% Au) gave similar benzene conversions of 9.2 and 8.8%, respectively, with the same product selectivity. In contrast, the HSiW-based mixed catalysts PdAu/C + HSiW/SiO_2 (1.2% Pd, 2.0% Au) showed a small enhancement of benzene conversion in comparison to Pd/C + HSiW (1.4% Pd) (Table 5.4). Even better activity enhancement was observed in the case of two-bed catalysts PdAu/C + HSiW/SiO_2 (1.2% Pd, 2.0% Au) versus Pd/C + HSiW/SiO_2 (1.4% Pd) (5.8 and 5.2% conversion, respectively, with product selectivity unchanged) (Figure 5.9). Given the difference in Pd loading, the enhancement of benzene conversion amounts to about 20%. Similar results were obtained for these two-bed catalysts with lower metal loadings (Pd/C + HSiW/SiO_2 (0.71% Pd) and Pd/Au/C + HSiW/SiO_2 (0.60% Pd, 1.0% Au)).

Although clearly discernible, this Au enhancement is considerably smaller than that reported previously for the hydrodeoxygenation of octanoic acid (PdAu/SiO_2 catalyst) [28] and 3-pentanone (Pt/CsPW catalyst) [30]. This may be explained by the reaction conditions of benzene alkylation. The relatively small Au effect on the dehydrogenation activity of Pd-HSiW catalyst can be attributed to the propane dehydrogenation step being close to equilibrium (Figure 5.9). Therefore, any enhancement of Pd activity would not cause significant increase in benzene conversion.

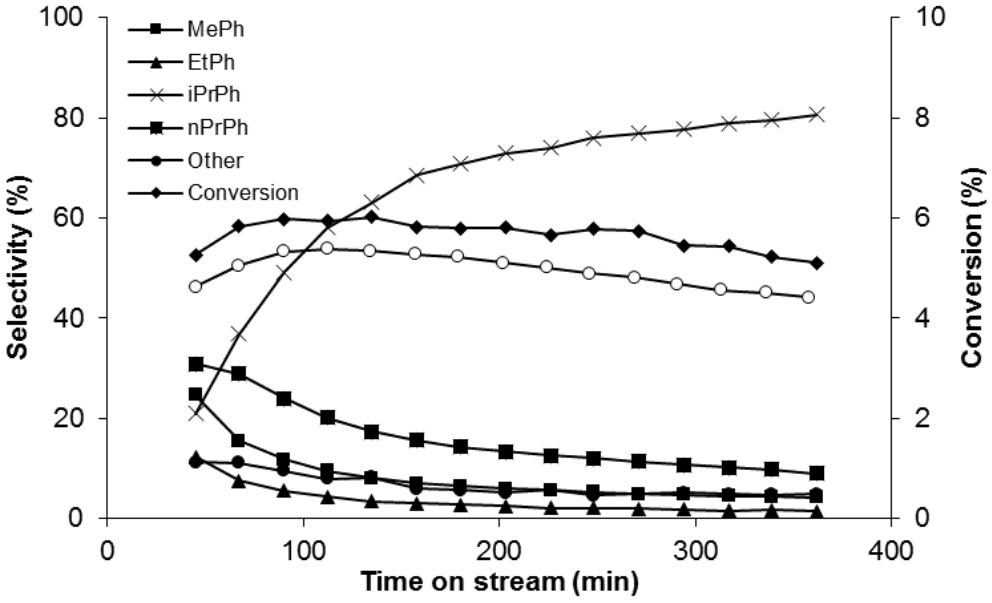

Figure 5.9. Time course for benzene alkylation by propane over two-bed catalyst 6.0%Pd/9.9%Au/C (0.04 g, top bed) + 25%HSiW/SiO_2 (0.16 g, bottom bed) (0.2 g total catalyst weight, 2%Au, 1.2% Pd, 300 ^{o}C, 1 bar pressure, inlet molar ratio C_6H_6/C_3H_8 = 1:9, 10 mL min^{-1} flow rate, *W/F* = 80 g h mol^{-1}; in-situ catalyst pre-treatment at 300 ^{o}C/1 h in H_2 flow). Open circles show the conversion with Pd/C + 25%HSiW/SiO_2 from Figure 5.8 for comparison.

5.4. Conclusions

It has been demonstrated that bifunctional Pd-acid catalysts (Pd-heteropoly acid and Pd-zeolite) are active in the alkylation of benzene by propane to yield isopropylbenzene (iPrPh). Keggin-type tungstosilicic acid $H_4SiW_{12}O_{40}$ (HSiW) and zeolite HZSM-5 have been used as the acid components in these catalysts. The mesoporous catalyst Pd/HSiW/SiO_2 is much more selective to iPrPh (up to 88%) than the microporous catalyst Pd/HZSM-5, which gives only 11-18% iPrPh selectivity. The reaction proceeds via the bifunctional reaction pathway including Pd-catalysed dehydrogenation of propane to propene followed by acid-

catalysed alkylation of benzene with the propene thus formed. Evidence has been provided that the first step reaches quasi-equilibrium at 1.5 – 2% Pd loading, and the second step becomes rate limiting. Addition of gold to Pd-HSiW has been found to slightly enhance the activity of this catalyst.

References

1. Weissermel, K.; Arpe, H.-J. *Industrial Organic Chemistry*; Wiley-VCH: Weinheim, Germany, **2003**.

2. Caeiro, G.; Carvalho, R. H.; Wang, X.; Lemos, M. A. N. D. A.; Lemos, F.; Guisnet, M.; Ramoa Ribeiro, F. *J. Mol. Catal. A* **2006,** *255*, 131.

3. Bragin, O. V.; Shpiro, E. S.; Preobrazhensky, A. V.; Isaev, S. A.; Vasina, T. V.; Dyusenbina, B. B.; Antoshin, G. V.; Minachev, K. M. *Appl. Catal*. **1986,** *27*, 219.

4. Smirnov, A. V.; Mazin, E. V.; Ponomoreva, O. A.; Yuschenko, V. V.; Knyazeva, E. E.; Nesterenko, S. N.; Ivanova, I. I. *J. Catal.* **2001,** *135*, 153.

5. Kato, S.; Nakagawa, K.; Ikenaga, N.; Suzuki, T. *Catal. Lett*. **2001,** *73*, 175.

6. Lukyanov, D. B.; Vazhnova, T. *J. Mol. Catal. A* **2008,** *279*, 128.

7. Lukyanov, D. B.; Vazhnova, T. *J. Catal*. **2008,** *257*, 382.

8. Chua, L. M.; Vazhnova, T.; Mays, T. J.; Lukyanov, D. B.; Rigby, S. P. *J. Catal*. **2010,** *271*, 401.

9. Ordomskiy, V. V.; Rodionova, L. I.; Ivanova, I. I.; Luck, F. *ChemCatChem* **2012,** *4*, 681.

10. Wong, K. S.; Vazhnova, T.; Rigby, S. P.; Lukyanov, D. B. *Appl. Catal. A* **2013,** *454*, 137.

11. Vazhnova, T.; Rigby, S. P.; Lukyanov, D. B. *J. Catal.* **2013,** *301*, 125.

12. Ivanova, I. I.; Blom, N.; Derouane, E. G. *J. Mol. Catal*. **1996,** *109*, 157.

13. Smirnov, A. V.; Mazin, E. V.; Yuschenko, V. V.; Knyazeva, E. E.; Nesterenko, S. N.; Ivanova, I. I.; Galperin, L.; Jensen, R.; Bradley, S. *J. Catal.* **2000,** *194*, 266.

14. Abasov, S. I.; Babayeva, F. A.; Zarbaliyev, R. R.; Abbasova, G. G.; Tagiyev, D. B.; Rustamov, M. I. *Appl. Catal. A* **2003,** *251*, 267.

15. Bigey, C.; Su, B-L. *J. Mol. Catal. A* **2004,** *209*, 179.

16. Huang, X.; Sun. X.; Zhu, S.; Liu, Z. *React. Kinet. Catal. Lett.* **2007,** *91*, 385.

17. Babaeva, F. A.; Abasov, S. I.; Rustamov, M. I. *Petrol. Chem.* **2010,** *50*, 42.

18. Alotaibi, A.; Bayahia, H.; Kozhevnikova, E. F.; Kozhevnikov, I. V. *ACS Catalysis*, **2015,** *5*, 5512.

19. Alsalme, A. M.; Wiper, P. V.; Khimyak, Y. Z.; Kozhevnikova, E. F.; Kozhevnikov, I. V. *J. Catal.* **2010,** *276*, 181.

20. Alharbi, W.; Brown, E.; Kozhevnikova, E. F.; Kozhevnikov, I. V. *J. Catal.* **2014,** *319*, 174.

21. Alotaibi, M. A.; Kozhevnikova, E. F.; Kozhevnikov, I. V. *Appl. Catal. A* **2012,** *447-448*, 32.

22. Benson, J. E.; Hwang, H. S.; Boudart, M. *J. Catal*. **1973,** *30*, 146.

23. Hutchings, G. J. *Chem. Commun.* **2008,** 1148.

24. Sun, K.; Wilson, A. R.; Thompson, S. T.; Lamb, H. H. *ACS Catal.* **2015,** *5*, 1939.

25. Han, Y. F.; Wang, J. H.; Kumar, D.; Yan, Z.; Goodman, D. W. *J. Catal.* **2005,** *232*, 467.

26. Hanrieder, E. K.; Jentys, A.; Lercher, J. A. *J. Catal.* **2016,** *333*, 71.

27. Xu, J.; White, T.; Li, P.; He, C.; Yu, J.; Yuan, W.; Han, Y. F. *J. Am. Chem. Soc.* **2010,** *132*, 10398.

28. Coq, B.; Figueras, F. *J. Mol. Catal. A* **2001,** *173*, 117.

29. Gao, F. Goodman, D. W. *Chem. Soc. Rev.* **2012,** *41*, 8009.

30. Poole, O.; Alharbi, K.; Belic, D.; Kozhevnikova, E. F.; Kozhevnikov, I. V. *Appl. Catal. B* **2017,** *202*, 446.

31. Venesia, A. M.; Parola, V. La; Nicoli, V.; Deganello, G. *J. Catal.* **2002,** *212*, 56.

32. Venesia, A. M.; Parola, V. La; Deganello, G.; Pawelec, B.; Fierro, J. G. *J. Catal.* **2003,** *215*, 317.

Chapter 6: Alkylation of toluene with propane over bifunctional metal-acid catalysts

6.1. Introduction

Ethene and propene are commercially utilised in the acid-catalysed alkylation of toluene to produce alkylaromatic compounds such as ethyltoluene and p-isopropyltoluene (p-cymene) [1-8]. The latter is the intermediate for the production of p-cresol by oxidation and acid cleavage [9]. p-Cymene is also used to produce fungicides, flavours, and perfumes [10]. This study focuses on the use of alkanes as the alkylating agents, which are more abundant and less expensive than the corresponding alkenes. This chapter describes the alkylation of toluene by propane using M-HZSM-5 and M-HPA bifunctional metal-acid catalysts, where M = Pt, Pd and Au. Previous studies on the alkylation of toluene by alkanes over bifunctional Pt-HZSM-5 and Pd-HZSM-5 catalysts [11-14] are reviewed in Chapter 1, section 1.6.3.

6.2. Experimental

6.2.1. Chemicals and materials

p-Cymene (99%), heteropoly acid hydrates $H_3PW_{12}O_{40}$ (HPW, 99%) and $H_4SiW_{12}O_{40}$ (HSiW, 99.9%) containing 20-28 H_2O molecules per Keggin unit were purchased from Sigma-Aldrich. The amount of crystallization water in heteropoly acids was determined by TGA. Zeolites NH_4^+-ZSM-5 (Si/Al = 10, 30 and 120 specific surface area S_{BET} = 400 m^2g^{-1}) were from Zeolyst International. These were converted into the H^+ form by air calcination at 500 ^oC for 6 h. Carbon-supported platinum 10%Pt/C and 10%Pd/C were from Johnson Matthey (7.0% Pt and 7.1% Pd content in dried Pt/C and Pd/C catalysts, respectively, from ICP-AES analysis). $H_2PtCl_6{\cdot}nH_2O$, $Pt(acac)_2$, $Pd(acac)_2$ and $HAuCl_4{\cdot}3H_2O$ were purchased from Sigma-Aldrich. Aerosil 300 silica (S_{BET} = 300 m^2g^{-1}) was from Degussa and Darco KB-B activated carbon from Sigma-Aldrich. Propane, N_2 and H_2 gases (all >99% purity) were

supplied by the British Oxygen Company. From our GC analysis, the propane contained C_3H_8 (99.20%), C_2H_6 (0.76%), C_3H_6 (0.01%), C_4H_{10} (0.03%) and methane (0.004%).

6.2.2. Catalyst preparation

Silica-supported HPAs were prepared by wet impregnation of Aerosil 300 silica by an aqueous HPA solution and dried at 150°C/10^{-3} kPa for 1.5 h [15-18]. Pt-HPA and Pd-HPA bifunctional catalysts were prepared by wet impregnation of acidic component, e.g., 25%HSiW/SiO_2, with 0.02 M $Pt(acac)_2$ and $Pd(acac)_2$ solution in benzene, respectively, at room temperature for 1 h, followed by slow evaporation of benzene in a rotary evaporator at room temperature [19]. The catalysts were dried under vacuum at 150 $^oC/10^{-3}$ kPa and then reduced in an oven by hydrogen flow at 250 ^oC for 2 h. Carbon-supported Au catalysts 10%Au/C, 0.5%Au/HZSM-5 and 0.5%Au/25%HSiW/SiO_2 were prepared by wet impregnation of Darco KB-B activated carbon, HZSM-5 or 25%HSiW/SiO_2, respectively, with an aqueous solution of $HAuCl_4$ at 50 ^oC for 2 h followed by rotary evaporation to dryness and reduction by H_2 flow as above. Bimetallic Au/(Pd/C) and Au/(Pt/C) catalysts were prepared by wet impregnation of 7.1%Pd/C and 7.0%Pt/C with an aqueous solution of $HAuCl_4$ followed by drying and reduction by H_2 flow at 250 ^oC for 2 h. Bimetallic Pt/(0.5%Au/HZSM-5) catalysts were prepared by wet impregnation of 0.5%Au/HZSM-5 with 0.02 M $Pt(acac)_2$ solution in benzene at room temperature for 1 h, followed by rotary evaporation to dryness and reduction by H_2 flow at 250 ^oC for 2 h. Bimetallic PtAu/25%HSiW/SiO_2 catalysts were prepared by co-impregnation of 25%HSiW/SiO_2 with an aqueous solution of H_2PtCl_6 and $HAuCl_4$ followed by drying and reduction by H_2 flow at 250 ^oC for 2 h. Physical mixtures of Pt/C and Pd/C with 25%HSiW/SiO_2 or HZSM-5 were prepared by grinding mixtures of these compounds in a specified ratio. Physical mixtures of

AuPd/C and AuPt/C with 25%HSiW and HZSM-5 were prepared in the same way. These catalysts are designated as, for example, Pt/C + HZSM-5, with metal loading indicated in round brackets, e.g. Pt/C + HZSM-5 (Si/Al = 10, 1% Pt loading).

6.2.3. Characterisation techniques

BET surface area, single point total pore volume and average BET pore diameter of the prepared catalysts were determined from N_2 physisorption using a Micromeritics ASAP 2010 instrument at -196 ^{o}C. The samples were pre-treated and out-gassed at 240 ^{o}C for 2 h. ICP-AES elemental analysis of metal content in the catalysts was carried out on a Spectro Ciros emission spectrometer.

Metal (Pt and Pd) dispersion, *D*, defined as the fraction of accessible metal at the surface of metal particles, $D = M_s/M_{total}$, was determined by H_2/O_2 titration using Micromeritics TPD/TPR 2900 instrument as described previously (20 mg catalyst sample, 20 μL pulses of H_2, adsorption stoichiometry M_s:H_2 = 1.5) (chapter 2, section 2.3.4). The average diameter of metal particles, *d*, was calculated from the empirical equation d (nm) = 0.9/D [20].

6.2.4. Catalyst testing

The alkylation of toluene with propane was carried out in the gas phase at 200-350 ^{o}C and an inlet toluene/C_3H_8 molar ratio of 1:9 under atmospheric pressure in a quartz fixed-bed down-flow reactor (9.0 mm internal diameter) with online GC analysis (Varian 3800 instrument with a 30 m x 0.32 mm x 0.5 μm Zebron ZB-WAX capillary column and a flame ionisation detector), as described elsewhere (Chapter 4, section 4.2). A schematic reactor

setup is shown in Figure 2.15 in Chapter 2. A Eurotherm controller was used to control the temperature within the reactor by using a thermocouple fixed at the top of the catalyst bed. The reactor was packed with 0.20 g catalyst powder of 45-180 μm particle size. The gas feed containing propane (90 kPa) and toluene (10 kPa) entered the reactor at the top at a flow rate of 10 mL min^{-1} (space time W/F = 80 g h mol^{-1}, where W (g) is the catalyst weight and F (mol h^{-1}) is the molar flow rate of toluene). Toluene was fed by passing propane flow controlled by a Brooks mass flow controller through a stainless steel saturator, which held liquid toluene at 45.2 ^{o}C to give the toluene partial pressure of 10 kPa in the gas flow. Prior to reaction, the catalysts were pre-treated in H_2 for 1 h at the reaction temperature. The alkylation products (alkylbenzenes) were identified by GC and GC-MS. The selectivity to aromatic products was defined as moles of product formed per one mole of toluene converted and quoted in mole per cent. The mean absolute percentage error in conversion and selectivity was ≤ 10% and the carbon balance was maintained within 95%.

6.3. Results and discussion

6.3.1. Catalyst characterisation

The BET surface area and porosity of HZSM-5 and HPA catalysts used in this study are given in Table 6.1. The surface area of metal-modified HZSN-5 and HPA/SiO_2 catalysts was smaller than that of HZSM-5 and HPA/SiO_2, as expected.

Table 6.1. Catalyst texture from BET analysis.

Catalyst	S_{BET}[a] (m^2g^{-1})	Pore volume[b] (cm^3g^{-1})	Pore diameter[c] (Å)
25%HSiW/SiO_2	215	0.95	171
1%Pt/25%HSiW/SiO_2	181	0.88	194
2%Pd/25%HSiW/SiO_2	189	0.75	159
HZSM-5	301	0.22	31
2%Pd/HZSM-5	262	0.20	31

[a]BET surface area, [b]Single point pore volume, [c]Average pore diameter.

Table 6.2 shows the metal dispersion and metal particle size of our bifunctional metal-zeolite and metal-HPA catalysts. These were estimated from H_2/O_2 titration and XRD.

Table 6.2. Metal particle size and dispersion.

Catalyst	Dispersion (%)		Particle size (nm)
	H_2/O_2 titration	XRD	
1%Pt/25%HSiW/SiO_2	24	24	3.8
2%Pd/25%HSiW/SiO_2	60	18	5.1
2%Pd/HZSM-5	--	9.0	10
7.0%Pt/C	23	9.7	9.3
7.1%Pd/C	26	7.9	11
10%Au/7.0%Pt/C	6.4 (Pt)	6.9 (Pt); 1.5 (Au)	13 (Pt); 62 (Au)
10%Au/7.1%Pd/C	14 (Pd)	6.8 (Pd); 1.4 (Au)	13 (Pd); 63 (Au)
10%Au/C	0.7	1.0	89

6.3.2. Alkylation of toluene with propane over Pt-HZSM-5

Figures 6.1 and 6.2 give examples for GC traces of products for the alkylation of toluene by propane over Pt-HZSM-5 catalysts, which show poor reaction selectivity to p-cymene in the case of these catalysts. The main products formed are benzene together with C_8 and C_9 alkylarenes. Figure 6.3 shows the GC-MS analysis of product mixture from the gas phase reaction of toluene alkylation with propane over 0.5%Pt/HZSM-5 (Si/Al = 10). This analysis clearly identifies p-cymene as the reaction product.

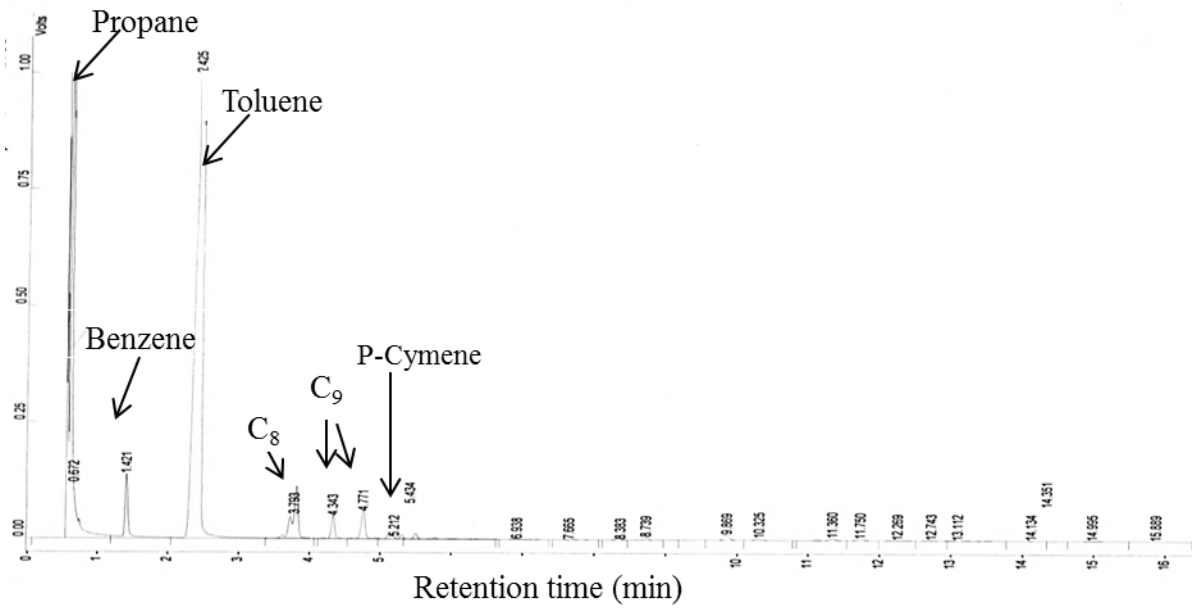

Figure 6.1. GC trace for alkylation of toluene alkylation with propane over mixed 7%Pt/C + HZSM-5 (Si/Al =10, Pt loading = 1.4%) at 300 °C, 10 ml/min flow rate.

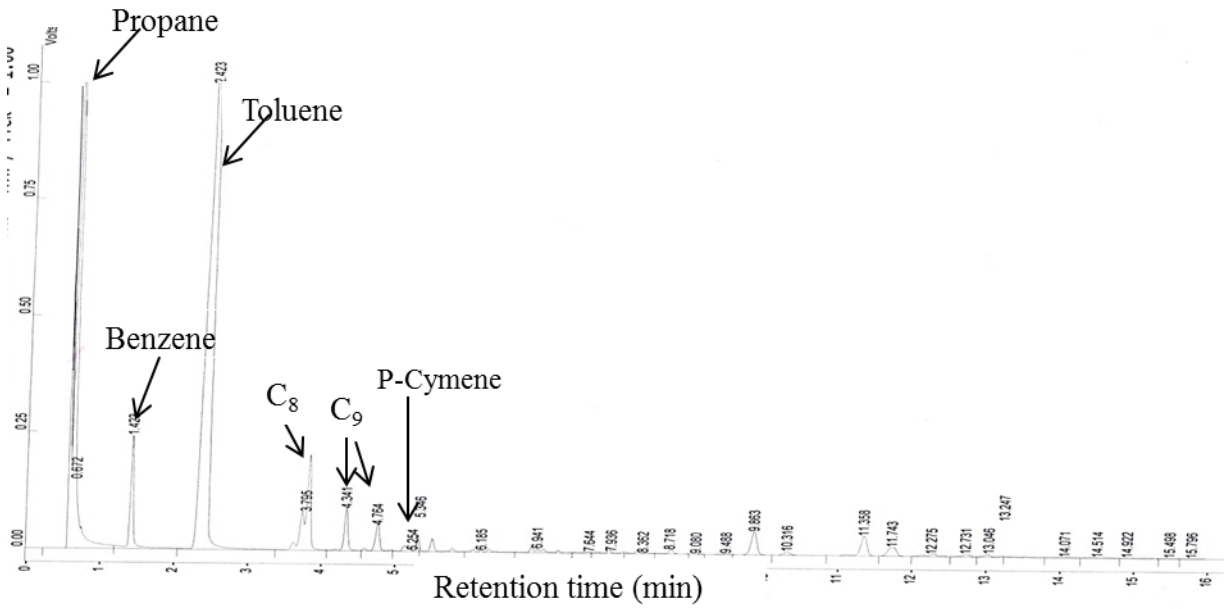

Figure 6.2. GC trace for alkylation of toluene alkylation with propane over 0.5%Pt/HZSM-5 (Si/Al =10) at 300 °C, 10 ml/min flow rate.

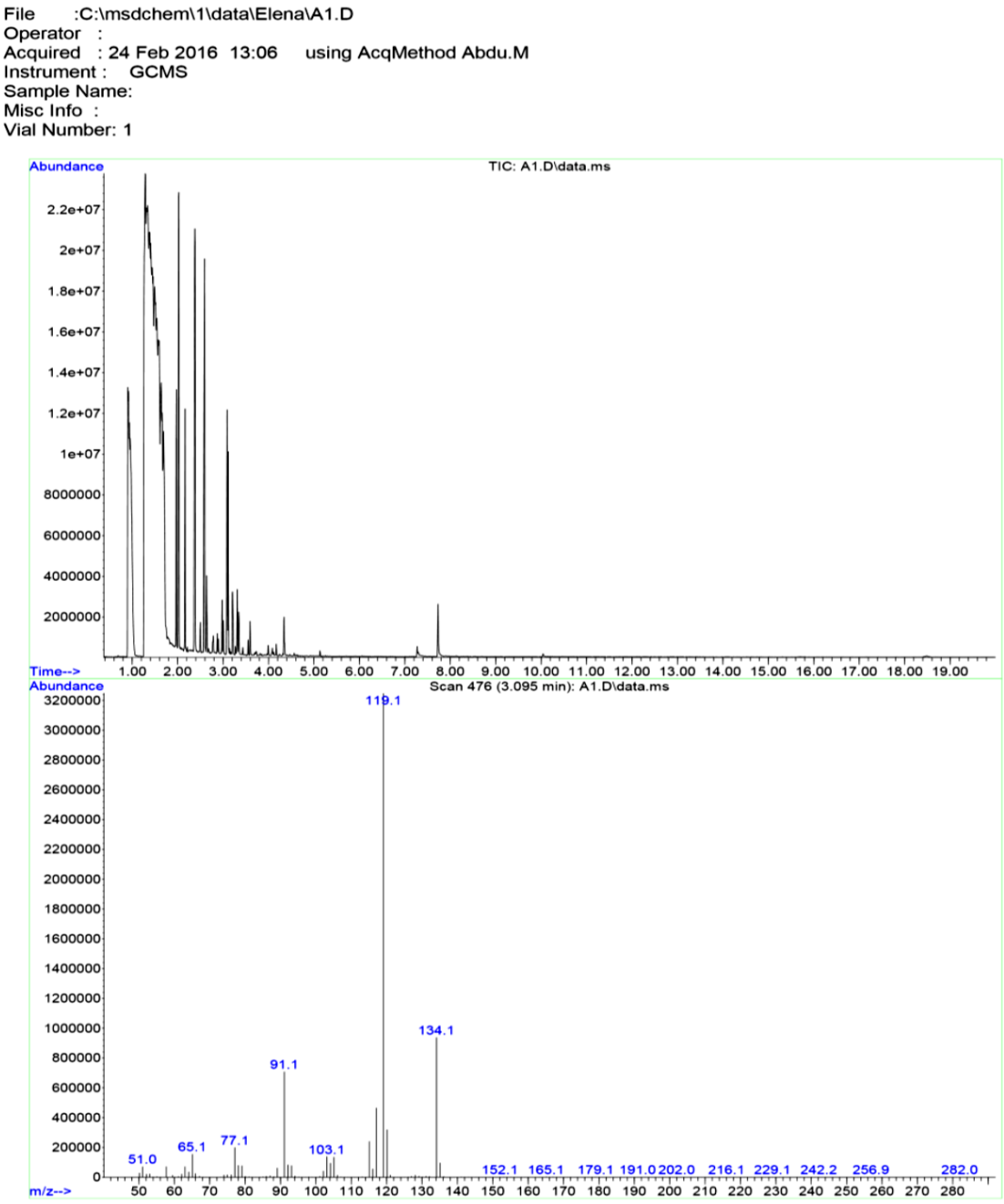

Figure 6.3. Mass spectrum of p-cymene detected by GC-MS analysis of product mixture from the gas phase reaction of toluene alkylation with propane over 0.5%Pt/HZSM-5 (Si/Al = 10): GC trace (top) and MS analysis (bottom).

6.3.2.1. Toluene alkylation over monofunctional Pt and HZSM-5 catalysts versus bifunctional Pt-HZSM-5 catalyst

The reaction with monofunctional Pt and HZSM-5 catalysts gave low toluene conversion compared to bifunctional Pt-HZSM-5 catalyst as shown in Table 6.3 and Figures 6.4 and 6.5. The toluene conversion for HZSM-5 as the monofunctional catalyst was higher than that for Pt, which could be explained by the cracking of toluene over the acid sites in HZSM-5.

Figure 6.6 illustrates the toluene alkylation with the mixed catalyst 7%Pt/C + HZSM-5 (0.7 %Pt) by using N_2 instead of propane as a carrier gas, which gave 2.4% toluene conversion at 3 h time on stream without any p-cymene formed. In this case, only toluene disproportionation to form benzene, xylenes and trimethylbenzenes was observed, as expected.

Table 6.3. Alkylation of toluene with propane over HZSM-5, Pt/C and Pt-HZSM-5.[a]

Catalyst	Conv.[b]	Aromatic selectivity[c] (%)				
	(%)	C_6H_6	C_8[d]	C_9[e]	p-Cymene	Other[f]
HZSM-5	3.6	29.8	28.0	34.8	4.7	2.7
Pt/C+SiO_2 (0.7%Pt)[g]	0.1	0.0	0.0	0.0	16.7	83.3
Pt/C+HZSM-5 (0.7%Pt)[g]	16.5	37.8	30.4	19.6	3.1	9.1
Pt/C+HZSM-5 (1.4%Pt)[g]	18.6	33.9	31.8	19.7	3.2	11.4

[a]Reaction conditions: 350 ^oC, 1 bar pressure, 0.20 g catalyst, inlet molar ratio toluene/C_3H_8 = 1:9, 10 mL min^{-1} flow rate, *W/F* = 80 g h mol^{-1}; in situ catalyst pre-treatment at 350 ^oC/1 h in H_2 flow, 10 mL min^{-1}. [b]Toluene conversion at 3 h time on stream. [c]Selectivity to aromatic products. [d]The mixture of xylenes and ethylbenzene. [e]The mixture of trimethyl-, methylethyl-

and propylbenzenes. [f]Other products include ortho- and meta-cymene and unidentified alkylbenzenes. [g]Uniform physical mixture 7.0%Pt/C with HZSM-5 or SiO_2.

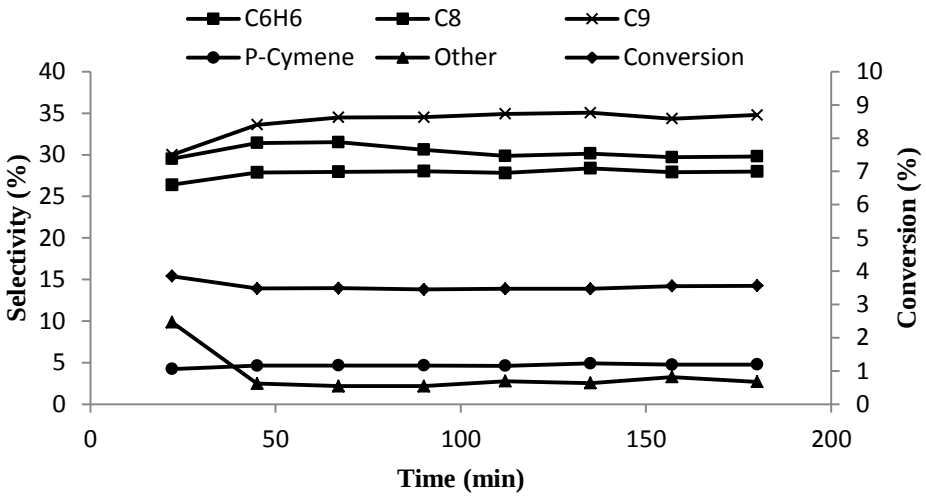

Figure 6.4. Time course for toluene alkylation by propane over HZSM-5 (Si/Al = 10) (0.2 g catalyst, 350 ^{o}C, 1 bar pressure, inlet molar ratio toluene/C_3H_8 = 1:9, 10 mL min^{-1} flow rate, *W/F* = 80 g h mol^{-1}; in-situ catalyst pre-treatment at 350 ^{o}C/1 h in H_2 flow).

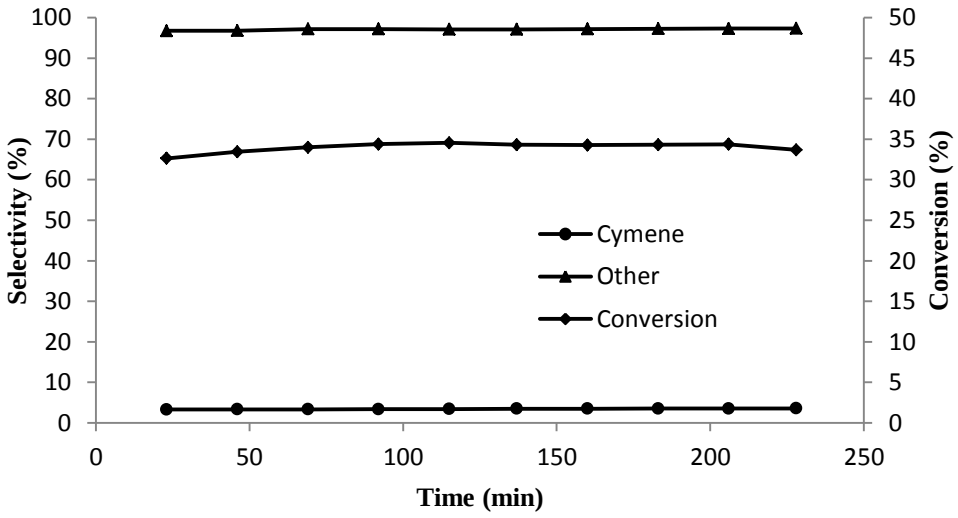

Figure 6.5. Time course for toluene alkylation by propane over 0.5%Pt/HZSM-5 (Si/Al = 10) (0.2 g catalyst, 350 ^{o}C, 1 bar pressure, inlet molar ratio toluene/C_3H_8 = 1:9, 10 mL min^{-1} flow rate, *W/F* = 80 g h mol^{-1}; in-situ catalyst pre-treatment at 350 ^{o}C/1 h in H_2 flow).

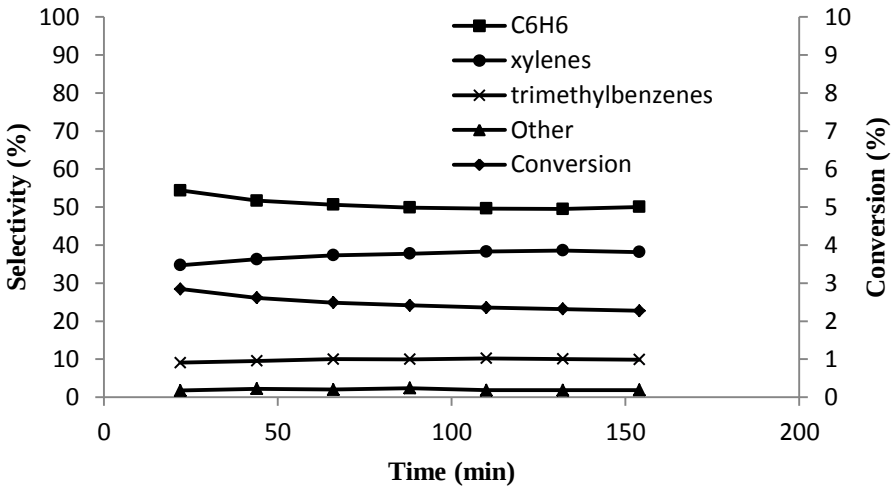

Figure 6.6. Blank test using N_2 instead of propane in reaction of toluene interaction with 7%Pt/C + HZSM-5 (Si/Al = 10) catalyst (0.2 g catalyst, 0.7% Pt loading, 350 ^{o}C, 1 bar pressure, inlet molar ratio toluene/N_2 = 1:9, 10 mL min^{-1} flow rate, *W/F* = 80 g h mol^{-1}; in-situ catalyst pre-treatment at 350 ^{o}C/1 h in H_2 flow).

6.3.2.2. Effect of temperature and Si/Al ratio

The alkylation of toluene by propane over mixed catalysts 7%Pt/C + HZSM-5 (Si/Al = 10) was studied at 250, 300 and 350 °C. The results are given in Table 6.4. Toluene conversion predictably increased with increasing reaction temperature, whereas p-cymene selectivity decreased. (Table 6.4, entries 1-3). It is also evident from the results in Table 6.4 that the alkylation of toluene by propane over Pt-HZSM-5 correlates with the number of proton (H^+) sites in HZSM-5 zeolite showing decreasing toluene conversion as the Si/Al ratio increases: HZSM-5(10) > HZSM-5(30) >> HZSM-5(120).

Table 6.4. Alkylation of toluene with propane over Pt-HZSM-5: effect of temperature and Si/Al ratio.[a]

Catalyst	Temp. (˚C)	Conversion[b] (%)	Selectivity (%)	
			p-Cymene	Other[c]
7%Pt/C + HZSM-5 (Si/Al = 10)[d]	250	3.44	13.7	86.3
7%Pt/C + HZSM-5 (Si/Al = 10)[d]	300	7.50	4.5	95.5
7%Pt/C + HZSM-5 (Si/Al = 10)[d]	350	16.50	3.1	96.9
7%Pt/C + HZSM-5 (Si/Al = 30)[d]	250	0.59	57.0	43.0
7%Pt/C + HZSM-5 (Si/Al = 30)[d]	300	1.92	26.5	73.5
7%Pt/C + HZSM-5 (Si/Al = 30)[d]	350	2.81	10.0	90.0
7%Pt/C + HZSM-5 (Si/Al = 120)[d]	300	1.04	38.8	61.2

[a]Reaction conditions: 1 bar pressure, 0.20 g catalyst, 0.7%Pt loading, inlet molar ratio toluene/C_3H_8 = 1:9, 10 mL min^{-1} flow rate, *W/F* = 80 g h mol^{-1}; in situ catalyst pre-treatment at 350 ^oC/1 h in H_2 flow, 10 mL min^{-1}. [b]Toluene conversion at 3 h time on stream. [c]Other products include xylenes, ethylbenzene, trimethylbenzenes, methylethylbenzenes, propylbenzenes, ortho- and meta-cymene and unidentified alkylbenzenes. [d]Uniform physical mixture 7.0%Pt/C with HZSM-5.

Figure 6.7 shows the Arrhenius plot for toluene alkylation over 7.0%Pt/C + HZSM-5 (Si/Al = 10, 0.7%Pt loading) catalyst in the temperature range of 250-350 ^oC. It gives an apparent activation energy of 40 kJ mol^{-1}. Figure 6.8 shows similar plot for the reaction over 7.0%Pt/C + HZSM-5 (Si/Al = 30, 0.7%Pt loading) catalyst with an apparent activation energy of 44 kJ mol^{-1}.

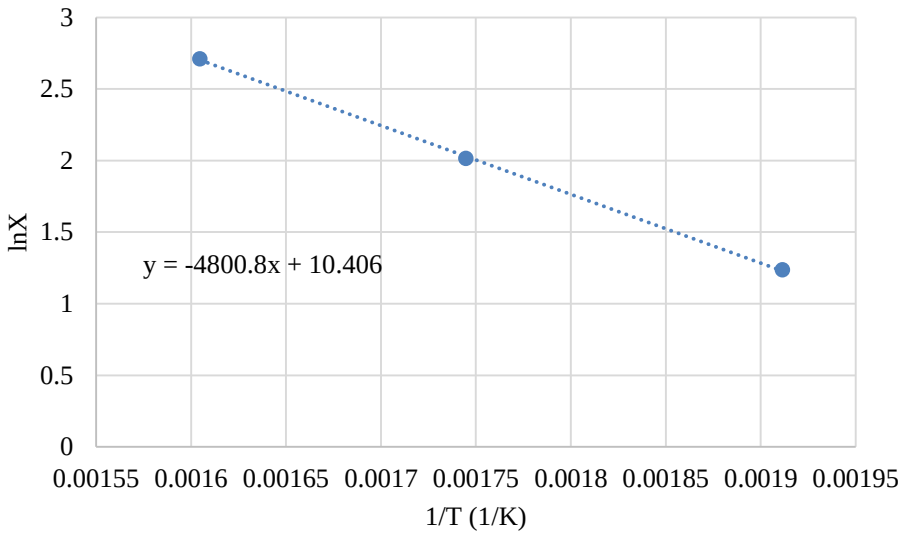

Figure 6.7. Arrhenius plot for toluene alkylation over mixed catalyst 7.0%Pt/C + HZSM-5 (Si/Al = 10) (*X* is the toluene conversion; 0.2 g catalyst, 0.7% Pt loading, 1 bar pressure, inlet molar ratio toluene/C_3H_8 = 1:9, 10 mL min^{-1} flow rate, *W/F* = 80 g h mol^{-1}).

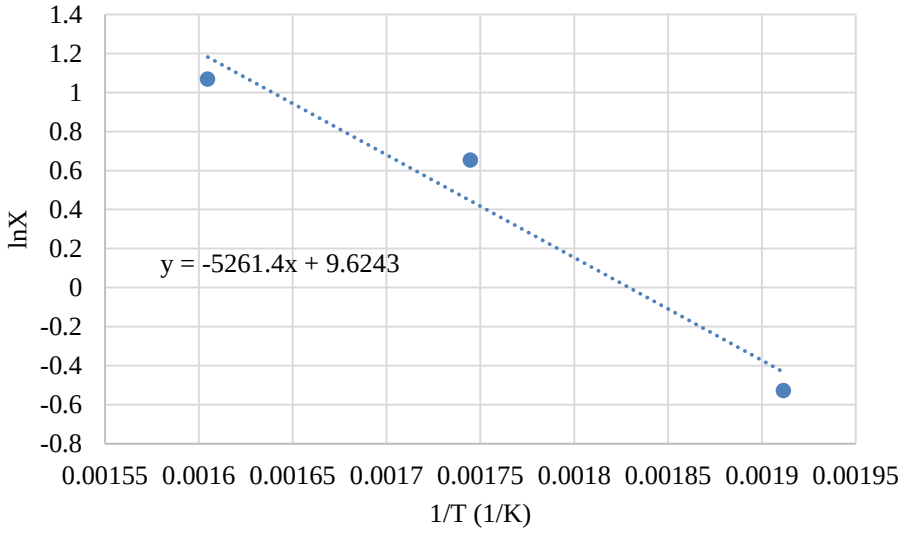

Figure 6.8. Arrhenius plot for toluene alkylation over mixed catalyst 7.0%Pt/C + HZSM-5 (Si/Al = 30) (*X* is the toluene conversion; 0.2 g catalyst, 0.7% Pt loading, 1 bar pressure, inlet molar ratio toluene/C_3H_8 = 1:9, 10 mL min^{-1} flow rate, *W/F* = 80 g h mol^{-1}).

6.3.2.3. Effect of toluene/propane ratio

Two different toluene partial pressures were tested in this study, namely 10.26 and 3.55 kPa, which correspond to the toluene/propane molar ratios of 1:9 and 1:27, respectively (Table 6.5). Toluene conversion decreased from 15.0% to 10.8% with decreasing toluene pressure from 10.26 to 3.55 kPa. At the same time, the selectivity to p-cymene increased from 2.9 to 3.7%. Further experiments were carried at the toluene/propane ratio of 1:9, which gave higher toluene conversions.

Table 6.5. Alkylation of toluene with propane over Pt-HZSM-5: effect of toluene pressure.[a]

Catalyst	Toluene/C_3H_8	Conversion[b] (%)	Selectivity (%)	
			p-Cymene	Other[c]
7%Pt/C + HZSM-5 [d]	1:9	15.0	2.9	97.1
7%Pt/C + HZSM-5 [d]	1:27	10.8	3.7	96.3

[a]Reaction conditions: 350 ^oC, 1 bar pressure, 0.20 g catalyst, 0.7%Pt loading, 10 mL min^{-1} flow rate, W/F = 80 g h mol^{-1}; in situ catalyst pre-treatment at 350 ^oC/1 h in H_2 flow, 10 mL min^{-1}. [b]Toluene conversion at 3 h time on stream. [c]Other products include xylenes, ethylbenzene, trimethylbenzenes, methylethylbenzenes, propylbenzenes, ortho- and meta-cymene and unidentified alkylbenzenes. [d]Uniform physical mixture 7.0%Pt/C with HZSM-5.

6.3.2.4. Effect of Pt loading

The results shown in Table 6.6 and Figure 6.9 illustrate that the toluene conversion, for the reaction over mixed (7.0%Pt/C + HZSM-5 (Si/Al =10)) catalysts, increased with increasing Pt loading and reached a plateau at ≥ 0.7% Pt content. This indicates that at Pt loading above 0.7% propane dehydrogenation step (Scheme 4.1, Chapter 4) is at fast quasi-equilibrium.

Table 6.6. Alkylation of toluene with propane over Pt-HZSM-5 (Si/Al = 10): effect of Pt loading.[a]

Catalyst	Conv.[b]	Aromatic selectivity[c] (%)				
	(%)	C_6H_6	C_8[d]	C_9[e]	p-Cymene	Other[f]
HZSM-5	3.6	29.8	28.0	34.8	4.7	2.7
Pt/C+HZSM-5 (0.1%Pt)[g]	5.4	30.6	30.5	32.6	4.2	2.1
Pt/C+HZSM-5 (0.5%Pt)[g]	13.4	41.3	30.9	20.5	2.9	4.4
Pt/C+HZSM-5 (0.7%Pt)[g]	16.5	37.8	30.4	19.6	3.1	9.1
Pt/C+HZSM-5 (1.4%Pt)[g]	18.6	33.9	31.8	19.7	3.2	11.4

[a]Reaction conditions: 350 ^oC, 1 bar pressure, 0.20 g catalyst, inlet molar ratio toluene/C_3H_8 = 1:9, 10 mL min^{-1} flow rate, *W/F* = 80 g h mol^{-1}; in situ catalyst pre-treatment at 350 ^oC/1 h in H_2 flow, 10 mL min^{-1}. [b]Toluene conversion at 3 h time on stream. [c]Selectivity to aromatic products. [d]A mixture of xylenes and ethylbenzene. [e]A mixture of trimethyl-, methylethyl- and propylbenzenes. [f]Other products include ortho- and meta-cymene and unidentified alkylbenzenes. [g]Uniform physical mixture 7.0%Pt/C with HZSM-5.

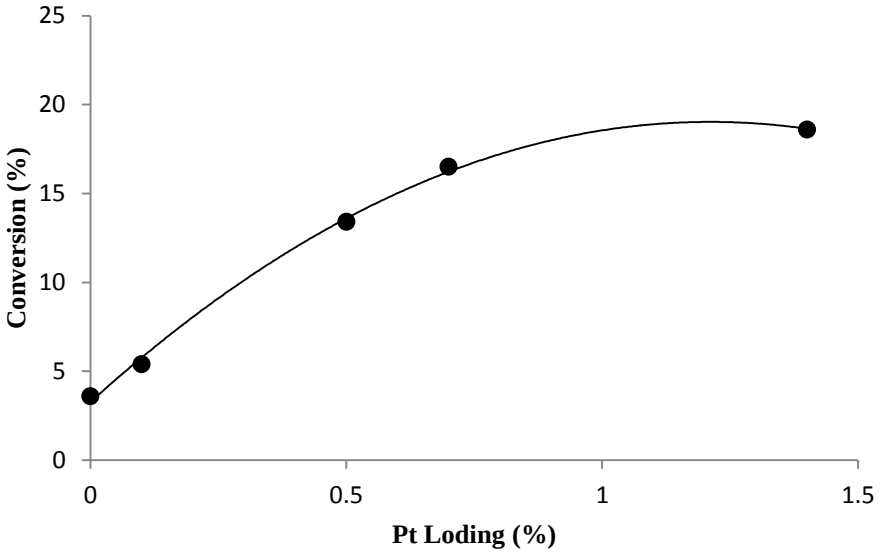

Figure 6.9. Effect of Pt loading on toluene conversion for toluene alkylation at 350 ^{o}C over 7.0%Pt/C+HZSM-5 (Si/Al = 10) catalysts (for reaction conditions, see Table 6.6).

6.3.2.5. Effect of catalyst composition: mixed versus supported catalysts

Supported catalysts were found to be more active than the mixed ones as shown in Table 6.7 and Figure 6.6 for 0.5%/Pt/HZSM-5 catalyst and Figure 6.10 for mixed (7.0%Pt/C + HZSM-5) catalyst. This may indicate that the distance between the Pt and proton active sites (which is longer for the mixed catalysts) affects the catalyst performance.

Table 6.7. Alkylation of toluene with propane over Pt-HZSM-5.[a]

Catalyst	Conv.[b]	Aromatic selectivity[c] (%)				
	(%)	C_6H_6	C_8[d]	C_9[e]	p-Cymene	Other[f]
Pt/C + HZSM-5 (0.5%Pt)[g]	13.4	41.3	30.9	20.5	2.9	4.4
0.5%Pt/HZSM-5	34.3	25.2	29.1	13.4	3.5	28.8

[a]Reaction conditions: 350 ^{o}C, 1 bar pressure, 0.20 g catalyst, inlet molar ratio toluene/C_3H_8 = 1:9, 10 mL min^{-1} flow rate, *W/F* = 80 g h mol^{-1}; in situ catalyst pre-treatment at 350 ^{o}C/1 h in H_2 flow, 10 mL min^{-1}. [b]Toluene conversion at 3 h time on stream. [c]Selectivity to aromatic

products. [d]A mixture of xylenes and ethylbenzene. [e]A mixture of trimethyl-, methylethyl- and propylbenzenes. [f]Other products include ortho- and meta-cymene and unidentified alkylbenzenes. [g]Uniform physical mixture 7.0%Pt/C with HZSM-5.

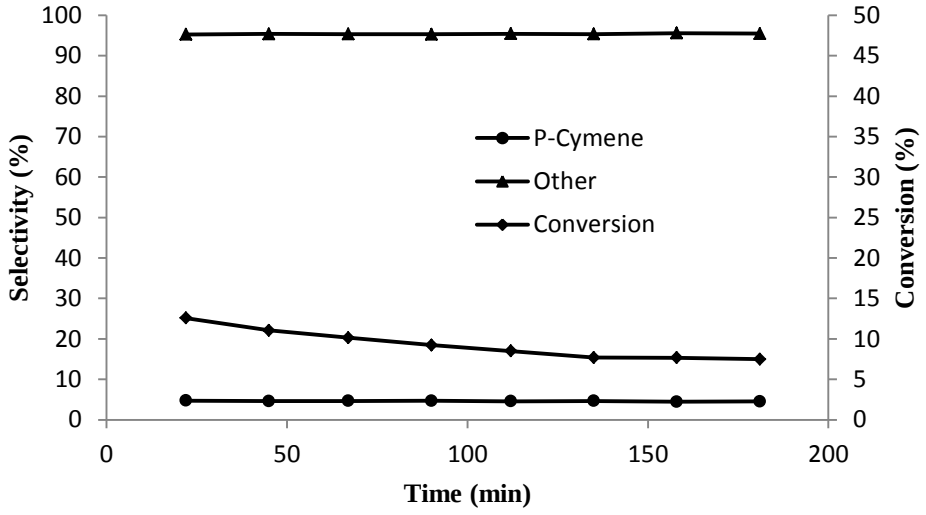

Figure 6.10. Time course for toluene alkylation by propane over 7.0%Pt/C + HZSM-5 (Si/Al = 10, 0.7%Pt loading) (0.2 g catalyst, 350 ^{o}C, 1 bar pressure, inlet molar ratio toluene/C_3H_8 = 1:9, 10 mL min^{-1} flow rate, *W/F* = 80 g h mol^{-1}; in-situ catalyst pre-treatment at 350 ^{o}C/1 h in H_2 flow).

6.3.2.6. Effect of gold additives

Bimetallic PdAu and PtAu catalysts have attracted much interest because of their enhanced performance in comparison to monometallic counterparts ([23-30] and references therein), as discussed in Chapter 5, section 5.3.3.

Here we examined the effect of gold additives on the performance of Pt-HZSM-5 catalysts in the alkylation of toluene by propane. The results (toluene conversions and product selectivities) are shown in Table 6.8. Supported gold catalyst in the absence of Pt (0.5%Au/HZSM-5 (Si/Al=10)) showed low activity (7.2% toluene conversion at 350˚C). No

enhancing effect of gold was found in the case of 0.5%Pt/HZSM-5 (Si/Al=10) catalyst at 350 and 250 ^{o}C. Thus, 0.5%Pt/HZSM-5 and 0.5%Pt/0.5%Au/HZSM-5 gave similar toluene conversions of 34.3 and 32.3%, respectively, at 350 ^{o}C (Figure 6.5 for 0.5%/Pt/HZSM-5 catalyst and Figure 6.11 for 0.5%Pt/0.5%Au/HZSM-5). However, at 200 ^{o}C the conversion of toluene increased from 0.7% over 0.5%Pt/HZSM-5 to 1.7% over 0.5%Pt/0.5%Au/HZSM-5 with a slight decrease in p-cymene selectivity from 32.5% to 26.8% (Figure 6.12 for 0.5%/Pt/HZSM-5 catalyst and Figure 6.13 for 0.5%Pt/0.5%Au/HZSM-5).

Table 6.8. Alkylation of toluene with propane over Pt-HZSM-5: effect of Au additives.[a]

Catalyst	Temp.	Conv.[b]	Aromatic selectivity[c] (%)				
	(˚C)	(%)	C_6H_6	C_8[d]	C_9[e]	p-Cymene	Other[f]
0.5%Au/HZSM-5	350	7.2	31.6	31.4	30.4	4.1	2.5
0.5%Pt/HZSM-5	350	34.3	25.2	29.1	13.4	3.5	28.8
0.5%Pt/0.5%Au/HZSM-5	350	32.3	28.4	31.5	16.2	3.9	20.5
0.5%Pt/HZSM-5	250	4.0	22.0	23.8	10.0	13.5	30.7
0.5%Pt/0.5%Au/HZSM-5	250	5.1	18.7	20.0	9.7	14.9	36.7
0.5%Pt/HZSM-5	200	0.7	0.0	9.6	3.4	31.5	55.5
0.5%Pt/0.5%Au/HZSM-5	200	1.7	13.6	8.8	6.5	26.8	43.3

[a]Reaction conditions: 1 bar pressure, 0.20 g catalyst, inlet molar ratio toluene/C_3H_8 = 1:9, 10 mL min^{-1} flow rate, *W/F* = 80 g h mol^{-1}; in situ catalyst pre-treatment at reaction temperature/1 h in H_2 flow, 10 mL min^{-1}. [b]Toluene conversion at 3 h time on stream. [c]Selectivity to aromatic products. [d]A mixture of xylenes and ethylbenzene. [e]A mixture of trimethyl-, methylethyl- and propylbenzenes. [f]Other products include ortho- and meta-cymene and unidentified alkylbenzenes.

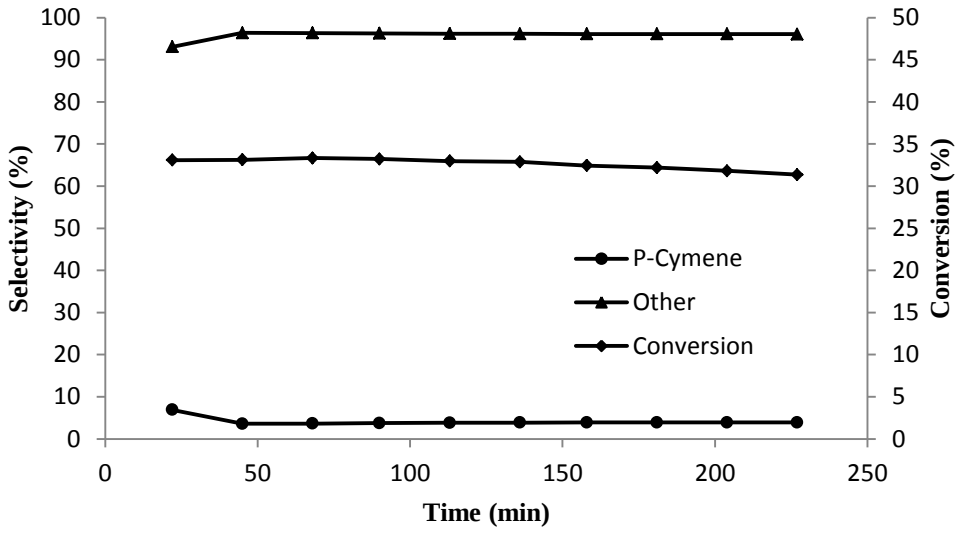

Figure 6.11. Time course for toluene alkylation by propane over 0.5%Pt/0.5%Au/HZSM-5 (Si/Al = 10) (0.2 g catalyst, 350 ^{o}C, 1 bar pressure, inlet molar ratio toluene/C_3H_8 = 1:9, 10 mL min^{-1} flow rate, *W/F* = 80 g h mol^{-1}; in-situ catalyst pre-treatment at 350 ^{o}C/1 h in H_2 flow).

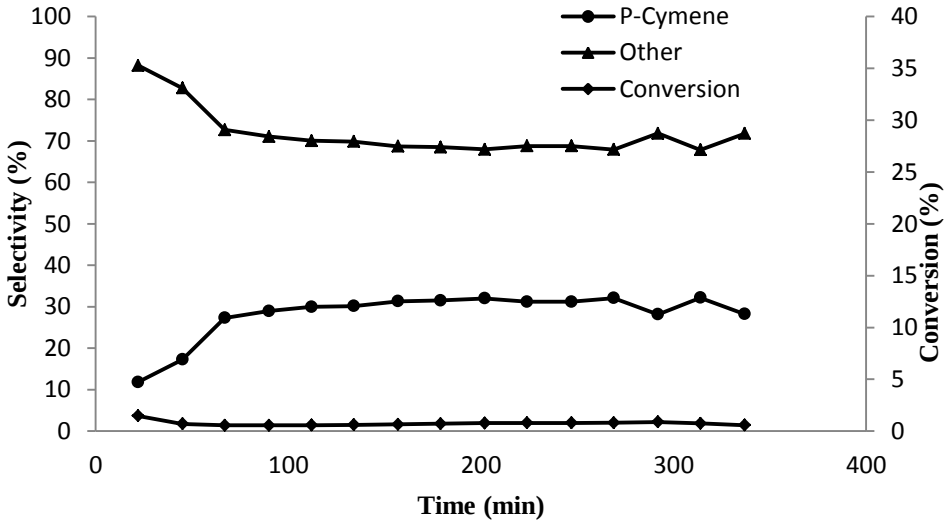

Figure 6.12. Time course for toluene alkylation by propane over 0.5%Pt/HZSM-5 (Si/Al = 10) (0.2 g catalyst, 200 ^{o}C, 1 bar pressure, inlet molar ratio toluene/C_3H_8 = 1:9, 10 mL min^{-1} flow rate, *W/F* = 80 g h mol^{-1}; in-situ catalyst pre-treatment at 200 ^{o}C/1 h in H_2 flow).

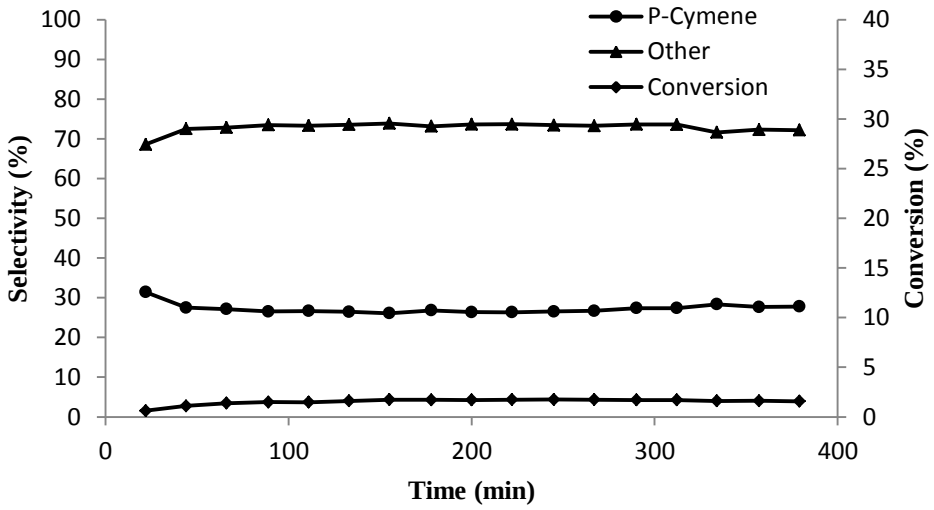

Figure 6.13. Time course for toluene alkylation by propane over 0.5%Pt/0.5%Au/HZSM-5 (Si/Al = 10) (0.2 g catalyst, 200 ^{o}C, 1 bar pressure, inlet molar ratio toluene/C_3H_8 = 1:9, 10 mL min^{-1} flow rate, *W/F* = 80 g h mol^{-1}; in-situ catalyst pre-treatment at 200 ^{o}C/1 h in H_2 flow).

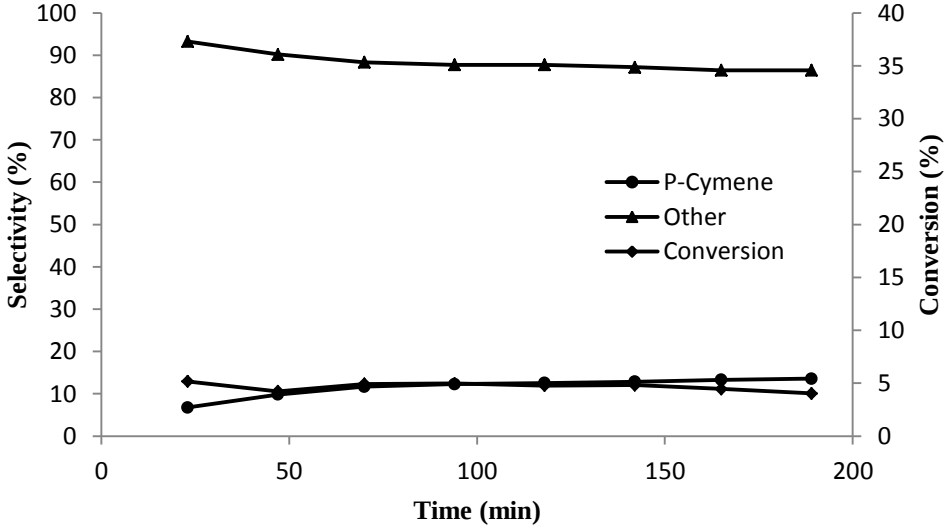

Figure 6.14. Time course for toluene alkylation by propane over 0.5%Pt/HZSM-5 (Si/Al = 10) (0.2 g catalyst, 250 ^{o}C, 1 bar pressure, inlet molar ratio toluene/C_3H_8 = 1:9, 10 mL min^{-1} flow rate, *W/F* = 80 g h mol^{-1}; in-situ catalyst pre-treatment at 250 ^{o}C/1 h in H_2 flow).

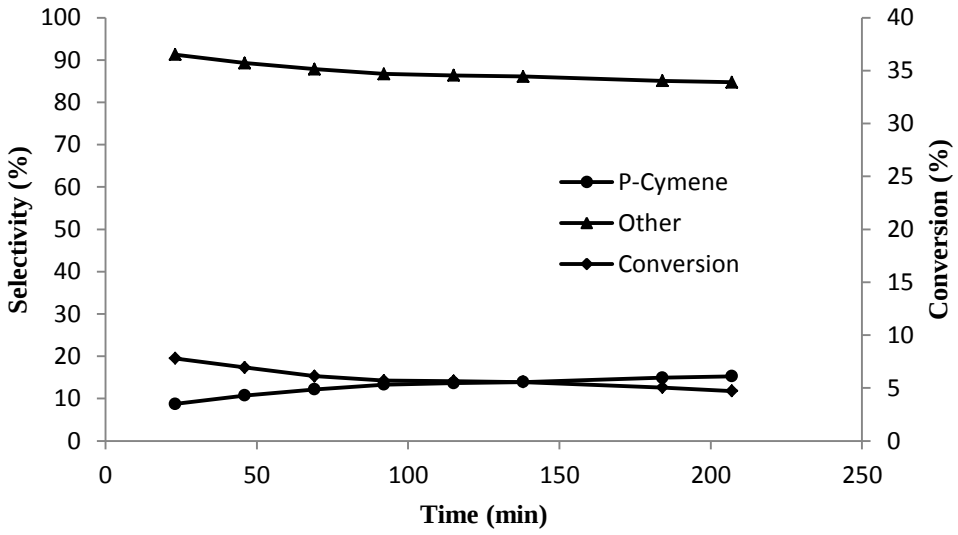

Figure 6.15. Time course for toluene alkylation by propane over 0.5%Pt/0.5%Au/HZSM-5 (Si/Al = 10) (0.2 g catalyst, 250 ^{o}C, 1 bar pressure, inlet molar ratio tpoluene/C_3H_8 = 1:9, 10 mL min^{-1} flow rate, *W/F* = 80 g h mol^{-1}; in-situ catalyst pre-treatment at 250 ^{o}C/1 h in H_2 flow).

6.3.3. Alkylation of toluene with propane over Pt-HPA/SiO_2

6.3.3.1. Effect of Pt loading

Figure 6.16 shows an example of GC trace for product analysis for the alkylation of toluene by propane over Pt/HPA/SiO_2 catalyst. This clearly demonstrates much higher p-cymene selectivity of the Pt/HPA/SiO_2 catalyst compared to Pt/HZSM-5. Similar results were obtained for the alkylation of benzene with propane (Chapter 4). Table 6.9 gives p-cymene selectivities for mixed 5.0%Pt/C + 25%HSiW/SiO_2 catalysts with varying Pt loading; these selectivities are significantly higher than those for Pt-zeolite catalysts.

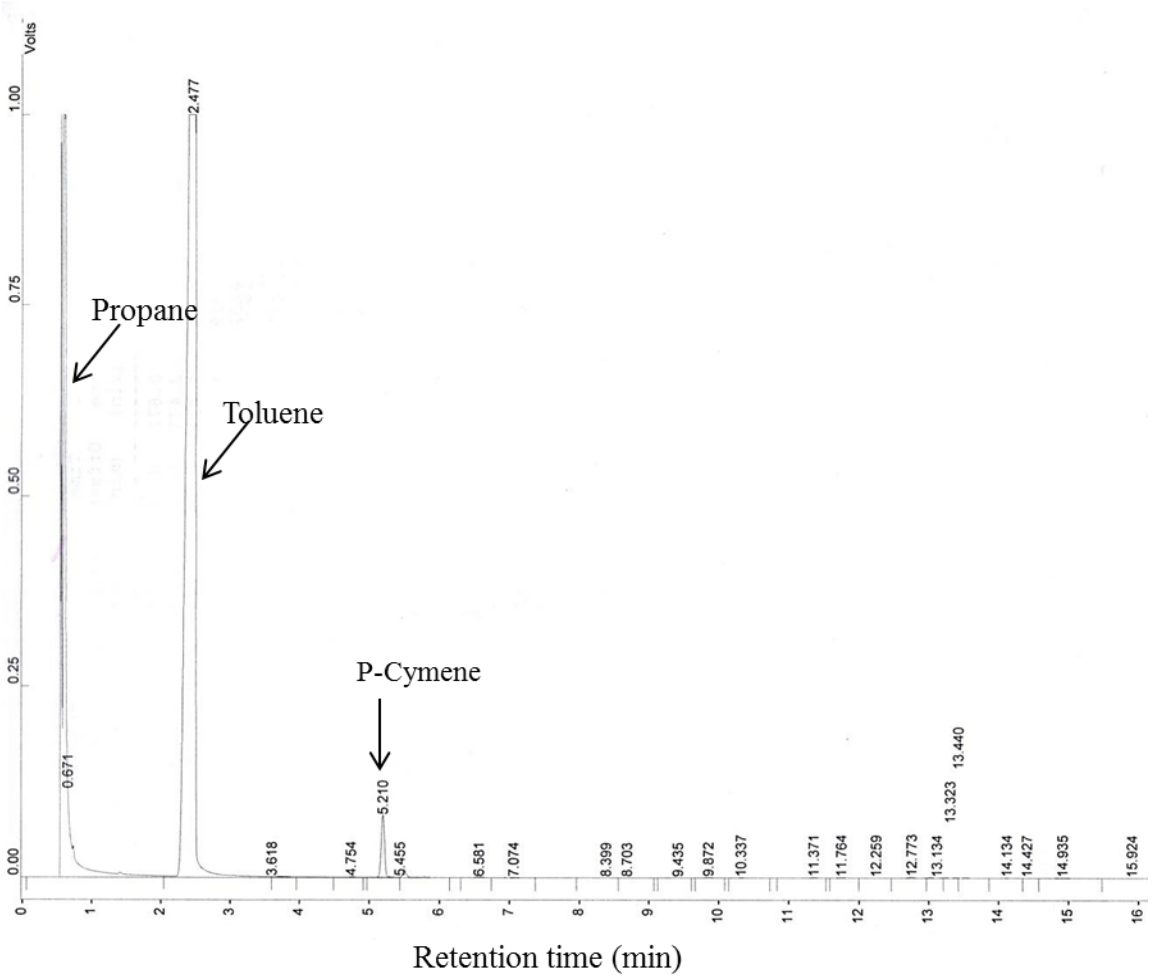

Figure 6.16. GC trace for alkylation of toluene with propane over 1%Pt/25%HSiW/SiO_2 at 300 °C, 10 ml/min flow rate.

Table 6.9 and Figure 6.17 illustrate that the toluene conversion, for the reaction over mixed 5.0%Pt/C + 25%HSiW/SiO_2 catalysts, increases with increasing Pt loading and reaches a plateau at ≥1.0% Pt loading. This indicates that at Pt loading above of 1.0% propane dehydrogenation is at fast quasi-equilibrium (Scheme 4.1, Chapter 4).

Table 6.9. Alkylation of toluene with propane over Pt/25%HSiW/SiO_2: effect of Pt loading.[a]

Catalyst	Conv.[b]	Aromatic selectivity[c] (%)				
	(%)	C_6H_6	C_8[d]	C_9[e]	p-Cymene	Other[f]
Pt/C+25%HSiW/SiO_2 (0.1%Pt)[g]	1.0	14.6	15.9	6.0	32.3	31.2
Pt/C+25%HSiW/SiO_2 (0.3%Pt)[g]	1.7	5.5	6.8	2.1	56.1	29.5
Pt/C+25%HSiW/SiO_2 (0.5%Pt)[g]	2.4	4.5	5.3	2.9	58.5	28.8
Pt/C+25%HSiW/SiO_2 (0.7%Pt)[g]	3.0	2.1	2.2	1.9	70.0	23.8
Pt/C+25%HSiW/SiO_2 (1.0%Pt)[g]	3.5	1.8	1.9	2.4	69.4	24.5
Pt/C+25%HSiW/SiO_2 (1.5%Pt)[g]	3.5	1.3	1.5	2.3	68.3	26.6

[a]Reaction conditions: 300 ^oC, 1 bar pressure, 0.20 g catalyst, inlet molar ratio toluene/C_3H_8 = 1:9, 10 mL min^{-1} flow rate, *W/F* = 80 g h mol^{-1}; in situ catalyst pre-treatment at 300 ^oC/1 h in H_2 flow, 10 mL min^{-1}. [b]Toluene conversion at 3 h time on stream. [c]Selectivity to aromatic products. [d]A mixture of xylenes and ethylbenzene. [e]A mixture of trimethyl-, methylethyl- and propylbenzenes. [f]Other products include ortho- and meta-cymene and unidentified alkylbenzenes. [g]Uniform physical mixture 5.0%Pt/C with 25%HSiW/SiO_2.

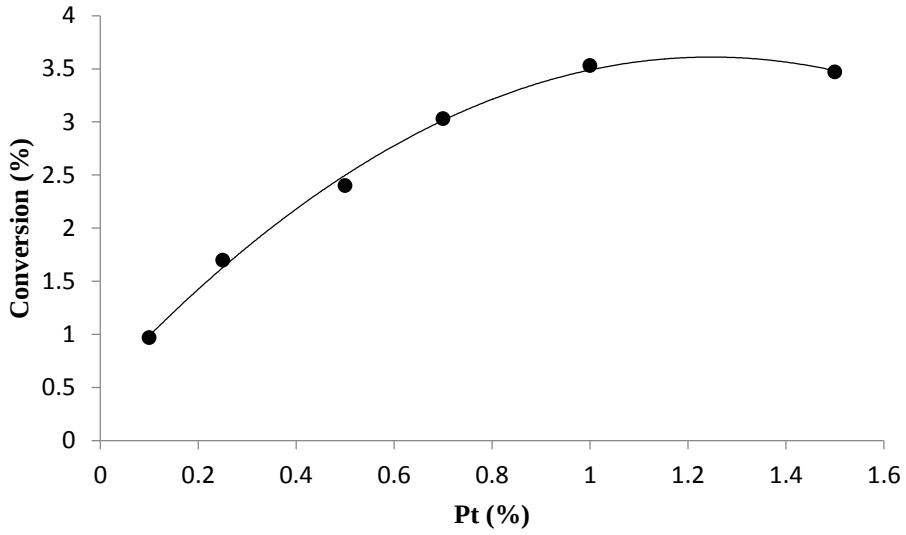

Figure 6.17. Effect of Pt on toluene conversion for toluene alkylation at 300 ^{o}C over 5.0%Pt/C+25%HSiW/SiO_2 catalysts (for reaction conditions, see Table 6.9).

6.3.3.2. Mixed catalysts Pt/C + HPA/SiO_2

Table 6.10 shows the effect of HSiW loading on SiO_2 (15, 20, 25 and 40%) and also compares the performance of HSiW and HPW within the mixed 5%Pt/C + HPA/SiO_2 catalysts (1% Pt loading). It can be seen that 5%Pt/C + 25%HSiW/SiO_2 had a better activity amongst the HSiW-based catalysts (entries 2-5). It had also slightly better activity compared to 5%Pt/C + 25%HPW/SiO_2 (entries 4 and 6). Similar results were obtained for 7.0%Pt/C + 25%HSiW/SiO_2 catalysts. Figures 6.18 and 6.19 show that 5%Pt/C + 25%HSiW/SiO_2 catalysts gave higher toluene conversion than 5%Pt/C + 25%HPW/SiO_2.

Table 6.10. Alkylation of toluene with propane over 5%Pt/C + HPA/SiO_2.[a]

Catalyst	Conv.[b]	Aromatic selectivity[c] (%)				
	(%)	C_6H_6	C_8[d]	C_9[e]	p-Cymene	Other[f]
1) 25%HSiW/SiO_2	1.5	42.0	33.8	11.5	2.8	9.9
2) Pt/C+15%HSiW/SiO_2 (1.0%Pt)[g]	3.1	1.2	1.4	1.5	69.9	26.0
3) Pt/C+20%HSiW/SiO_2 (1.0%Pt)[g]	3.2	1.4	1.5	2.0	67.7	27.4
4) Pt/C+25%HSiW/SiO_2 (1.0%Pt)[g]	3.5	1.8	1.9	2.4	69.4	24.5
5) Pt/C+40%HSiW/SiO_2 (1.0%Pt)[g]	3.4	1.5	2.3	2.0	67.1	27.1
6) Pt/C+25%HPW/SiO_2 (1.0%Pt)[g]	2.9	1.6	1.3	2.4	69.3	25.4

[a]Reaction conditions: 300 ^oC, 1 bar pressure, 0.20 g catalyst, inlet molar ratio toluene/C_3H_8 = 1:9, 10 mL min^{-1} flow rate, *W/F* = 80 g h mol^{-1}; in situ catalyst pre-treatment at 300 ^oC/1 h in H_2 flow, 10 mL min^{-1}. [b]Toluene conversion at 3 h time on stream. [c]Selectivity to aromatic products. [d]A mixture of xylenes and ethylbenzene. [e]A mixture of trimethyl-, methylethyl- and propylbenzenes. [f]Other products include ortho- and meta-cymene and unidentified alkylbenzenes. [g]Uniform physical mixture 5.0%Pt/C with HPA/SiO_2.

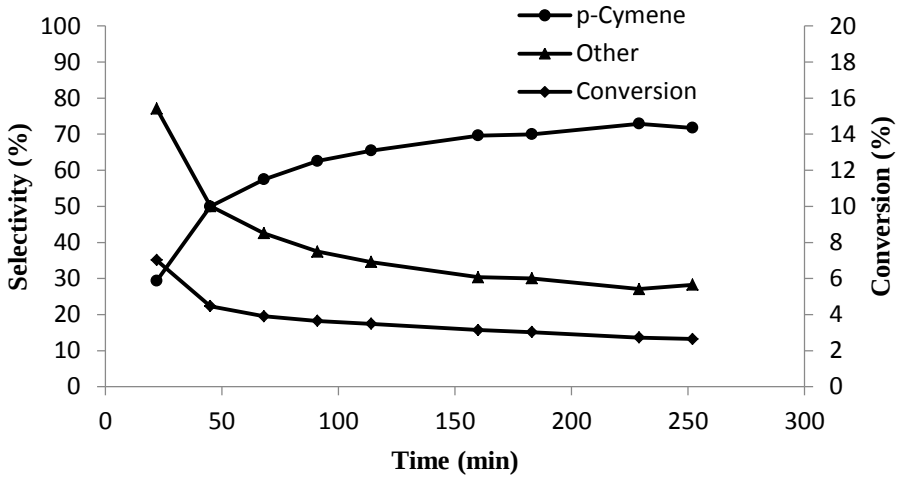

Figure 6.18. Time course for toluene alkylation by propane over 5.0%Pt/C + 25%HSiW/SiO_2 (0.2 g catalyst, 0.7%Pt loading, 300 ^{o}C, 1 bar pressure, inlet molar ratio toluene/C_3H_8 = 1:9, 10 mL min^{-1} flow rate, *W/F* = 80 g h mol^{-1}; in-situ catalyst pre-treatment at 300 ^{o}C/1 h in H_2 flow).

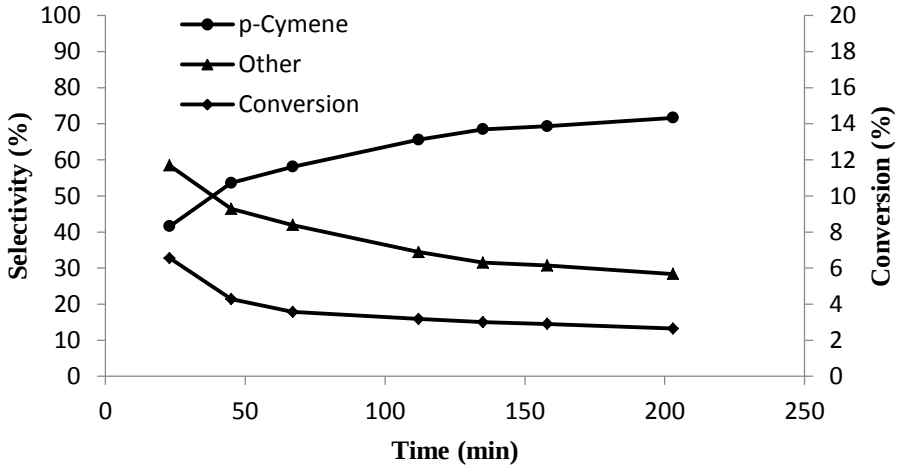

Figure 6.19. Time course for toluene alkylation by propane over 5.0%Pt/C + 25%HPW/SiO_2 (0.2 g catalyst, 0.7%Pt loading, 300 ^{o}C, 1 bar pressure, inlet molar ratio toluene/C_3H_8 = 1:9, 10 mL min^{-1} flow rate, *W/F* = 80 g h mol^{-1}; in-situ catalyst pre-treatment at 300 ^{o}C/1 h in H_2 flow).

6.3.3.3. Supported catalysts Pt/HPA/SiO_2

When using HPA-based catalysts, physically mixed catalysts were found to be more active than supported ones as can be seen from the results in Table 6.9 and Table 6.11. For example, toluene conversion was 2.1% with supported 1%Pt/25%HSiW/SiO_2 catalyst, while for mixed 5%Pt/C + 25%HSiW/SiO_2 (1% Pt loading) catalyst, toluene conversion was 3.5%. This indicates that in the case of mesoporous Pt-HPA/SiO_2 catalyst the reaction is not limited by migration of intermediates between the metal and acid sites. A different picture was observed in the case of microporous HZSM-5-based catalysts (section 6.3.2.5). The higher activity of the mixed catalysts compared to the supported ones may be explained by a better stability of the former to deactivation (coking). Figure 6.20 shows that toluene conversion over 1%Pt/25%HSiW/SiO_2 catalyst decreases from 4% to 2% over 3 h on stream, which could be explained by catalyst coking. Indeed, 0.9% of coke was found in the spent catalyst. Physical mixture of 5%Pt/C + 25%HSiW/SiO_2 (1%Pt, 1:4 w/w) shows less catalyst deactivation (from 4.7% to 3.5%) over 3 h on stream (Figure 6.21).

Table 6.11. Alkylation of toluene with propane over Pt/HPA/SiO_2.[a]

Catalyst	Conv.[b]	Aromatic selectivity[c] (%)				
	(%)	C_6H_6	C_8[d]	C_9[e]	p-Cymene	Other[f]
0.5%Pt/25%HSiW/SiO_2	0.9	0.0	19.9	7.0	37.2	35.9
1%Pt/25%HSiW/SiO_2	2.1	0.0	1.3	1.7	70.4	26.6
1%Pt/25%HPW/SiO_2	1.4	0.0	0.0	0.9	75.1	24.0
3%Pt/25%HSiW/SiO_2	2.3	0.0	0.0	1.1	74.0	24.9

[a]Reaction conditions: 300 ^oC, 1 bar pressure, 0.20 g catalyst, inlet molar ratio toluene/C_3H_8 = 1:9, 10 mL min^{-1} flow rate, *W/F* = 80 g h mol^{-1}; in situ catalyst pre-treatment at 300 ^oC/1 h in H_2 flow, 10 mL min^{-1}. [b]Toluene conversion at 3 h time on stream. [c]Selectivity to aromatic products. [d]A mixture of xylenes and ethylbenzene. [e]A mixture of trimethyl-, methylethyl- and propylbenzenes. [f]Other products include ortho- and meta-cymene and unidentified alkylbenzenes.

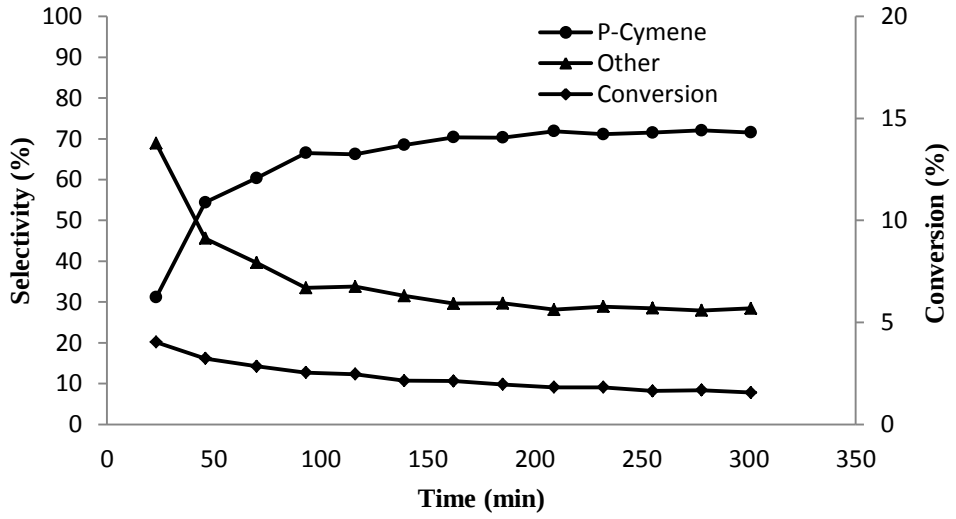

Figure 6.20. Time course for toluene alkylation by propane over 1%Pt/25%HSiW/SiO_2 (0.2 g catalyst, 300 ^oC, 1 bar pressure, inlet molar ratio toluene/C_3H_8 = 1:9, 10 mL min^{-1} flow rate, *W/F* = 80 g h mol^{-1}; in-situ catalyst pre-treatment at 300 ^oC/1 h in H_2 flow).

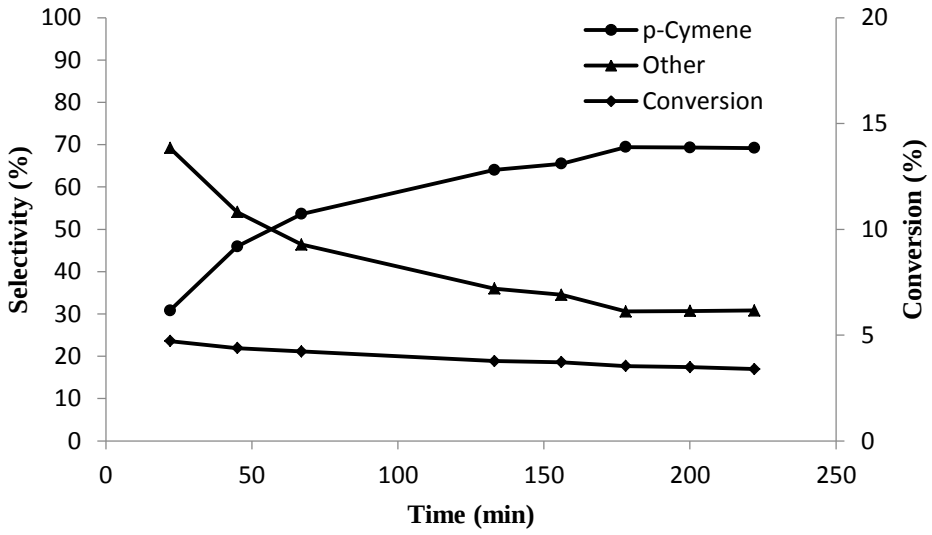

Figure 6.21. Time course for toluene alkylation by propane over 5.0%Pt/C + 25%HSiW/SiO_2 (0.2 g catalyst, 1.0%Pt loading, 300 ^{o}C, 1 bar pressure, inlet molar ratio toluene/C_3H_8 = 1:9, 10 mL min^{-1} flow rate, *W/F* = 80 g h mol^{-1}; in-situ catalyst pre-treatment at 300 ^{o}C/1 h in H_2 flow).

Even better conversion stability was reached by using two-bed catalysts comprising 5%Pt/C and 25%HSiW/SiO_2 beds either unseparated or separated with ~1 mm layer of SiO_2. The unseparated two-bed catalyst gave toluene conversion from 3.5% to 3.3% over 8.5 h on stream (Figure 6.22). The catalyst with silica-separated beds gave toluene conversion from 3.5% to 3.1% over 12 h on stream (Figure 6.23).

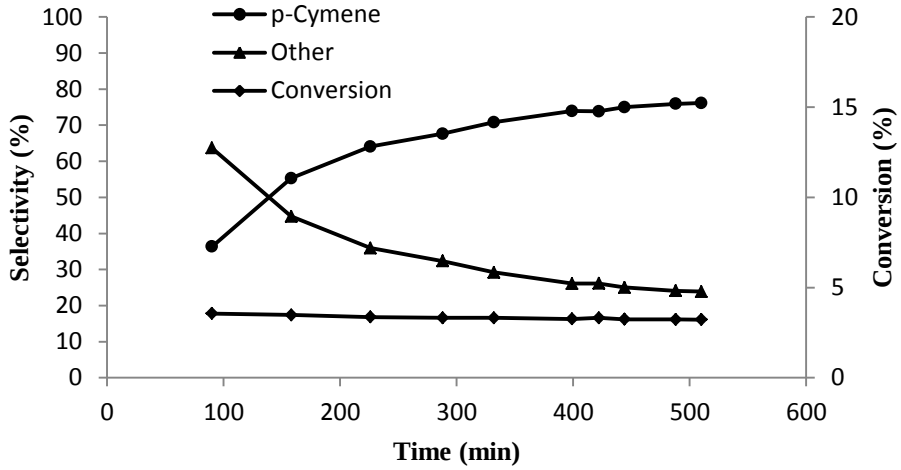

Figure 6.22. Time course for toluene alkylation by propane over 5.0%Pt/C (0.04 g, top bed) + 25%HSiW/SiO_2 (0.16 g, bottom bed) (0.2 g total catalyst weight, 1.0%Pt loading, 300 ^{o}C, 1 bar pressure, inlet molar ratio toluene/C_3H_8 = 1:9, 10 mL min^{-1} flow rate, *W/F* = 80 g h mol^{-1}; in-situ catalyst pre-treatment at 300 ^{o}C/1 h in H_2 flow).

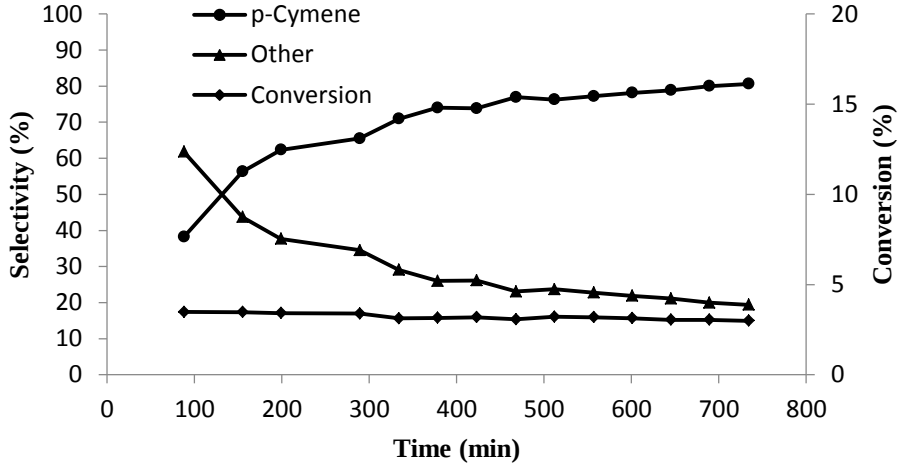

Figure 6.23. Time course for toluene alkylation by propane over 5.0%Pt/C (0.04 g, top bed) + 25%HSiW/SiO_2 (0.16 g, bottom bed) separated with ~1 mm layer of SiO_2 (0.2 g total catalyst weight, 1.0%Pt loading, 300 ^{o}C, 1 bar pressure, inlet molar ratio toluene/C_3H_8 = 1:9,

10 mL min^{-1} flow rate, *W/F* = 80 g h mol^{-1}; in-situ catalyst pre-treatment at 300 ^{o}C/1 h in H_2 flow).

6.3.3.4. Effect of gold additives

In Table 6.12, mixed AuPt/C + 25%HSiW/SiO_2 catalyst (0.7% Pt, 1.0% Au loading) showed a lower toluene conversion in comparison to Pt/C + 25%HSiW/SiO_2 (0.7% Pt). Some activity enhancement was observed in the case of AuPt/C + 25%HSiW/SiO_2 (0.7% Pt, 2.0% Au) versus Pd/C + 25%HSiW/SiO_2 (0.7% Pt) (2.9 and 2.6% conversion, respectively, with product selectivity unchanged) (Figure 6.24). This difference, however, is likely to be within the experimental error.

Table 6.12. Alkylation of toluene with propane over Pt-HPA/SiO_2: effect of Au additives.[a]

Catalyst	Temp. (˚C)	Conv.[b] (%)	Aromatic selectivity[c] (%)				
			C_6H_6	C_8[d]	C_9[e]	p-Cymene	Other[f]
0.5%Au/25%HSiW/SiO_2	300	0.3	0	12.0	0	15.7	72.3
Pt/C+25%HSiW/SiO_2 (0.7%Pt)[g]	300	2.6	0	1.7	2.0	64.5	31.8
AuPt/C+25%HSiW/SiO_2 (0.7%Pt, 1%Au)[g]	300	1.1	0	16.7	6.6	37.5	39.2
AuPt/C+25%HSiW/SiO_2 (0.7%Pt, 2%Au)[g]	300	2.9	0	3.0	2.7	64.8	29.5
1%Pt/25%HSiW/SiO_2	300	2.1	0	1.3	1.7	70.4	26.6
1%Pt/1%Au/25%HSiW/SiO_2[h]	300	1.9	0	0	1.3	72.1	26.6
1%Pt/0.5%Au/25%HSiW/SiO_2[h]	300	1.7	0	0	0.8	74.1	25.1
1%Pt/0.5%Au/25%HSiW/SiO_2[h]	280	1.5	0	0	0.8	77.5	21.7
0.5%Pt/25%HSiW/SiO_2	280	1.0	14.8	22.6	6.0	32.5	24.1
0.5%Pt/0.5%Au/25%HSiW/SiO_2[h]	280	0.9	0	0	1.4	62.2	36.4

[a]Reaction conditions: 1 bar pressure, 0.20 g catalyst, inlet molar ratio toluene/C_3H_8 = 1:9, 10 mL min^{-1} flow rate, *W/F* = 80 g h mol^{-1}; in situ catalyst pre-treatment at reaction temperature/1 h in H_2 flow, 10 mL min^{-1}. [b]Toluene conversion at 3 h time on stream. [c]Selectivity to aromatic products. [d]A mixture of xylenes and ethylbenzene. [e]A mixture of trimethyl-, methylethyl- and propylbenzenes. [f]Other products include ortho- and meta-cymene and unidentified alkylbenzenes. [g]Uniform physical mixture 7.0%Pt/C with HPA/SiO_2 or. [h]Co-impregnation catalysts.

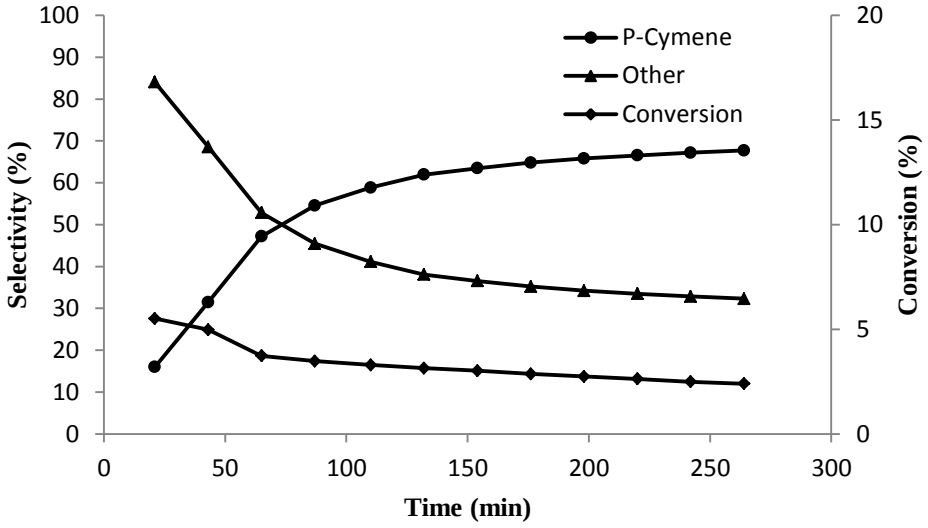

Figure 6.24. Time course for toluene alkylation by propane over AuPt/C + 25%HSiW/SiO_2 (0.2 g catalyst, 2% Au and 0.7% Pt loading, 300 ^oC, 1 bar pressure, inlet molar ratio toluene/C_3H_8 = 1:9, 10 mL min^{-1} flow rate, *W/F* = 80 g h mol^{-1}; in-situ catalyst pre-treatment at 300 ^oC/1 h in H_2 flow).

The effect of gold additives was also studied on the supported Pt/25%HSiW/SiO_2 catalysts in the alkylation of toluene by propane. The results (toluene conversions and product selectivities) are shown in Table 6.12 and Figures 6.25 and 6.26. Supported 1%Pt/25%HSiW/SiO_2 and 1%Pt/1%Au/25%HSiW/SiO_2 co-impregnation catalysts gave similar toluene conversion of 2.1 and 1.9%, respectively, with almost the same product selectivity. However, the toluene conversion slightly decreased with decreasing the amount of Au from 1% to 0.5% (1%Pt/0.5%Au/25%HSiW/SiO_2 co-impregnation catalyst) with increasing p-cymene selectivity from 72.1 to 74.1.% Better p-cymene selectivity (77.5%) was achieved for toluene alkylation over 1%Pt/0.5%Au/25%HSiW/SiO_2 co-impregnation catalyst at 280 ^oC.

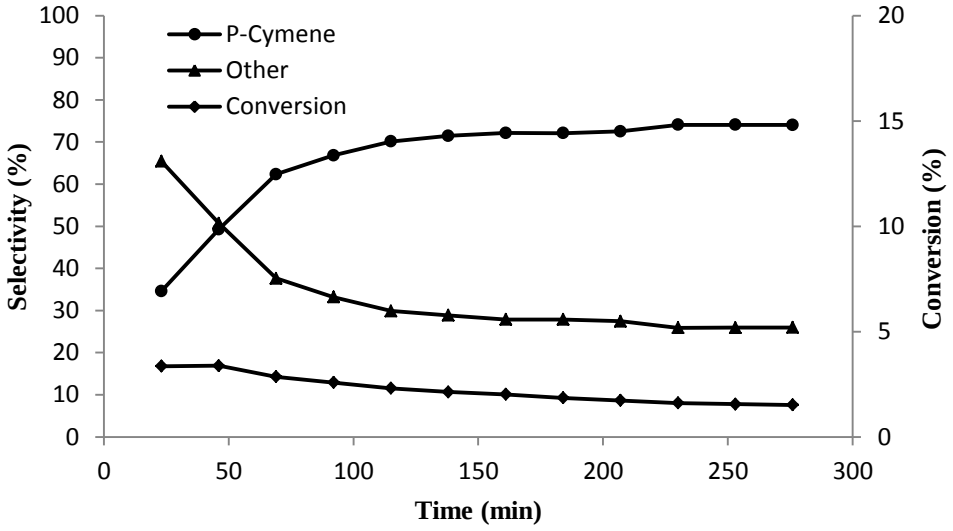

Figure 6.25. Time course for toluene alkylation by propane over 1%Pt/1%Au/25%HSiW/SiO_2 co-impregnation catalyst (0.2 g catalyst, 300 ^oC, 1 bar pressure, inlet molar ratio toluene/C_3H_8 = 1:9, 10 mL min^{-1} flow rate, *W/F* = 80 g h mol^{-1}; in-situ catalyst pre-treatment at 300 ^oC/1 h in H_2 flow).

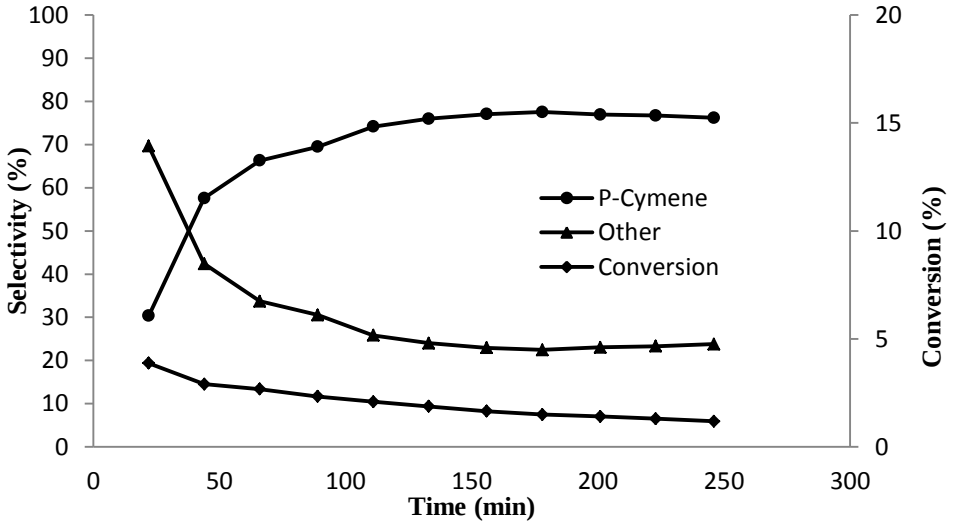

Figure 6.26. Time course for toluene alkylation by propane over 1%Pt/0.5%Au /25%HSiW/SiO_2 co-impregnation catalyst (0.2 g catalyst, 280 ^oC, 1 bar pressure, inlet molar ratio toluene/C_3H_8 = 1:9, 10 mL min^{-1} flow rate, *W/F* = 80 g h mol^{-1}; in-situ catalyst pre-treatment at 280 ^oC/1 h in H_2 flow).

6.3.3.5. Comparison of Pt-HPA/SiO_2 and Pt-HZSM-5 catalysts

As for the alkylation of benzene with propane (Chapter 4), the striking feature of toluene alkylation over Pt/HPA catalysts is its high selectivity to p-cymene. For the 1%Pt/25%HSiW/SiO_2 catalyst, the p-cymene selectivity was almost 70% while for 1%Pt/HZSM-5 (Si/Al =10) catalyst, the p-cymene selectivity only reached 5.5% (Table 6.13). The zeolite-based catalysts give higher toluene conversion than the HPA-based ones, but the latter give 1.7 to 3.6 times higher yield of the desired p-cymene (Table 6.13).

Table 6.13. Alkylation of toluene with propane over Pt-HPA/SiO_2 or Pt-HZSM-5.[a]

Catalyst	Conv.[b]	Aromatic selectivity[c] (%)				
	(%)	C_6H_6	C_8[d]	C_9[e]	p-Cymene	Other[f]
Pt/C+HZSM-5 (1.0%Pt)[g]	12.2	12.5	22.2	12.8	5.4	47.1
1%Pt/HZSM-5	15.6	18.8	24.6	8.0	5.5	43.1
Pt/C+25%HSiW/SiO_2 (1.0%Pt)[g]	3.5	1.8	1.9	2.4	69.4	24.5
1%Pt/25% HSiW/SiO_2	2.1	0.0	1.3	1.7	70.4	26.6

[a]Reaction conditions: 300 ^oC, 1 bar pressure, 0.20 g catalyst, inlet molar ratio toluene/C_3H_8 = 1:9, 10 mL min^{-1} flow rate, *W/F* = 80 g h mol^{-1}; in situ catalyst pre-treatment at 300 ^oC/1 h in H_2 flow, 10 mL min^{-1}. [b]Toluene conversion at 3 h time on stream. [c]Selectivity to aromatic products. [d]A mixture of xylenes and ethylbenzene. [e]A mixture of trimethyl-, methylethyl- and propylbenzenes. [f]Other products include ortho- and meta-cymene and unidentified alkylbenzenes. [g]Uniform physical mixture 5.0%Pt/C with HZSM-5 or 25%HSiW/SiO_2.

6.3.4. Alkylation of toluene with propane over Pd-HZSM-5 and Pd-HPA catalysts

6.3.4.1. Pd-HZSM-5 catalysts

Pd-HZSM-5 catalysts are active in toluene alkylation by propane. 2%Pd/HZSM-5 catalyst gave 36.3% conversion of toluene (Table 6.14, entry 3), which is similar to 0.5%Pt/HZSM-5 (34.3% toluene conversion, section 6.3.2.5). We found that Pd-HZSM-5 and Pt-HZSM-5 perform similarly in the alkylation of toluene with propane, albeit the Pd-HZSM-5 catalyst has considerably lower activity per metal weight. Figures 6.27 and 6.28 show the reaction time courses for 2%Pd/HZSM-5 catalyst at 350 and 300 ^{o}C, respectively. At 300 ^{o}C, p-cymene selectivity is notably higher (7.6%) than at 350 ^{o}C (2.2%).

Table 6.14. Alkylation of toluene with propane over Pd-HZSM-5.[a]

Catalyst	Conv.[b]	Aromatic selectivity[c] (%)				
	(%)	C_6H_6	C_8[d]	C_9[e]	p-Cymene	Other[f]
Pd/C+SiO_2 (1.4%Pd)[g]	0.4	54.0	39.7	0.0	0.0	6.3
Pd/C + HZSM-5 (0.5%Pd)[g]	6.2	32.8	35.4	24.3	5.3	2.2
2%Pd/HZSM-5	36.3	9.8	20.3	5.8	2.2	61.9
2%Pd/HZSM-5 (at 300˚C)	13.2	10.4	20.7	9.7	7.6	61.9

[a]Reaction conditions: 350 ^{o}C, 1 bar pressure, 0.20 g catalyst, inlet molar ratio toluene/C_3H_8 = 1:9, 10 mL min^{-1} flow rate, *W/F* = 80 g h mol^{-1}; in situ catalyst pre-treatment at 350 ^{o}C/1 h in H_2 flow, 10 mL min^{-1}. [b]Toluene conversion at 3 h time on stream. [c]Selectivity to aromatic products. [d]A mixture of xylenes and ethylbenzene. [e]A mixture of trimethyl-, methylethyl- and propylbenzenes. [f]Other products include ortho- and meta-cymene and unidentified alkylbenzenes. [g]Uniform physical mixture 7.0%Pd/C with HZSM-5.

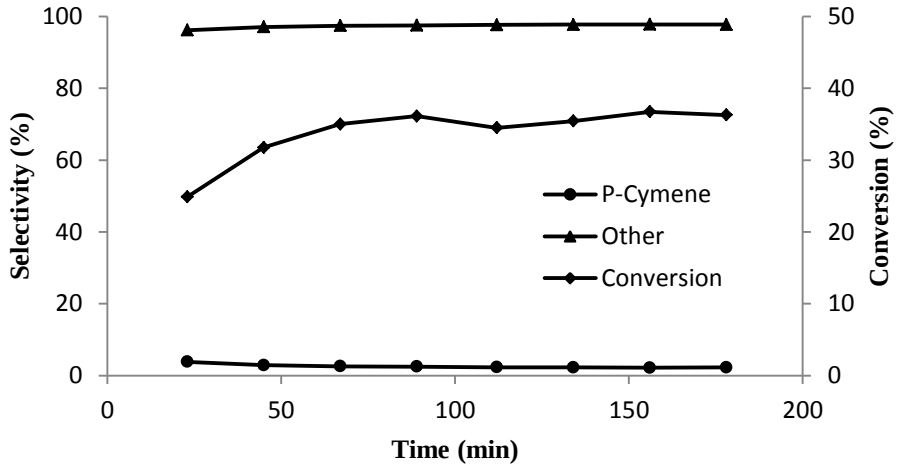

Figure 6.27. Time course for toluene alkylation by propane over 2%Pd/HZSM-5 (0.2 g catalyst, 350 ^{o}C, 1 bar pressure, inlet molar ratio toluene/C_3H_8 = 1:9, 10 mL min^{-1} flow rate, *W/F* = 80 g h mol^{-1}; in-situ catalyst pre-treatment at 350 ^{o}C/1 h in H_2 flow).

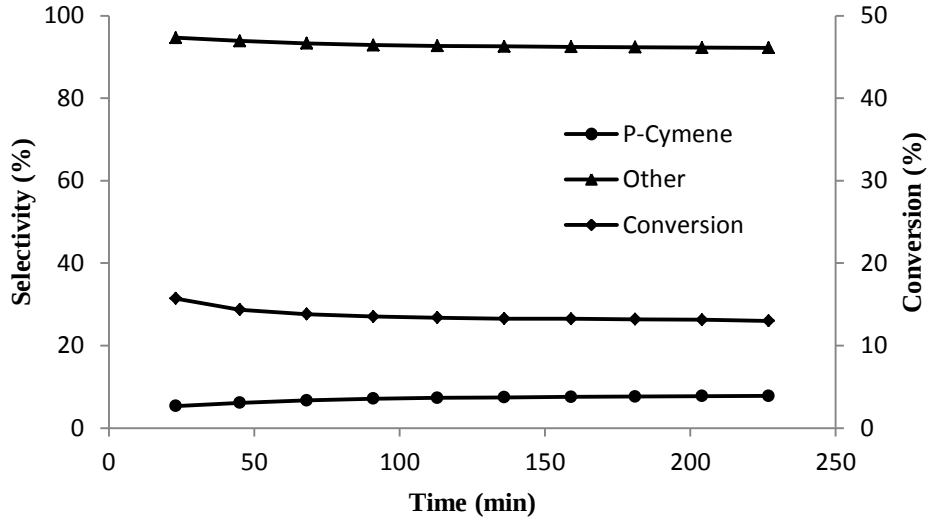

Figure 6.29. Time course for toluene alkylation by propane over 2%Pd/HZSM-5 (0.2 g catalyst, 300 ^{o}C, 1 bar pressure, inlet molar ratio toluene/C_3H_8 = 1:9, 10 mL min^{-1} flow rate, *W/F* = 80 g h mol^{-1}; in-situ catalyst pre-treatment at 300 ^{o}C/1 h in H_2 flow).

6.3.4.2. Alkylation of toluene with propane over mixed and supported Pd-HPA/SiO_2

As expected, the Pd-HSiW/SiO_2 catalysts were much more selective to p-cymene than Pd-HZSM-5, similar to Pt-HSiW/SiO_2 catalysts (section 6.3.3.5). Table 6.15 shows the results for toluene alkylation with propane over both mixed Pd/C + 25%HSiW/SiO_2 and supported Pd/25%HSiW/SiO_2 catalysts with the Pd loading varied from 0.5 to 3%. Figures 6.29-6.31 show the corresponding time courses for the reaction with different Pd loadings. As seen from Table 6.15, p-cymene selectivity generally increases with increasing the Pd loading. Supported Pd/25%HSiW/SiO_2 give the best p-cymene selectivity, up to 70.6% for 3%Pd/25%HSiW/SiO_2.

Table 6.15. Alkylation of toluene with propane over Pd-HPA/SiO_2.[a]

Catalyst	Conv.[b]	Aromatic selectivity[c] (%)				
	(%)	C_6H_6	C_8[d]	C_9[e]	p-Cymene	Other[f]
Pd/C+25%HSiW/SiO_2 (0.5%Pd)[g]	0.6	22.3	20.1	5.5	30.1	22.0
Pd/C+25%HSiW/SiO_2 (1.0%Pd)[g]	1.5	9.2	10.0	3.8	41.8	35.2
Pd/C+25%HSiW/SiO_2 (1.5%Pd)[g]	2.4	7.0	7.8	4.2	44.1	36.9
Pd/C+25%HSiW/SiO_2 (2.0%Pd)[g]	3.0	9.6	10.0	4.1	54.5	21.8
Pd/C+25%HSiW/SiO_2 (2.5%Pd)[g]	3.4	8.5	9.2	2.6	64.6	15.1
2%Pd/25% HSiW/SiO_2	1.7	0	2.5	1.5	68.3	27.7
3%Pd/25% HSiW/SiO_2	2.4	0	2.2	1.9	70.6	25.3

[a]Reaction conditions: 300 ^oC, 1 bar pressure, 0.20 g catalyst, inlet molar ratio toluene/C_3H_8 = 1:9, 10 mL min^{-1} flow rate, *W/F* = 80 g h mol^{-1}; in situ catalyst pre-treatment at 300 ^oC/1 h in H_2 flow, 10 mL min^{-1}. [b]Toluene conversion at 3 h time on stream. [c]Selectivity to aromatic products. [d]A mixture of xylenes and ethylbenzene. [e]A mixture of trimethyl-, methylethyl- and

propylbenzenes. [f]Other products include ortho- and meta-cymene and unidentified alkylbenzenes. [g]Uniform physical mixture 5.0%Pt/C with 25%HSiWSiO_2.

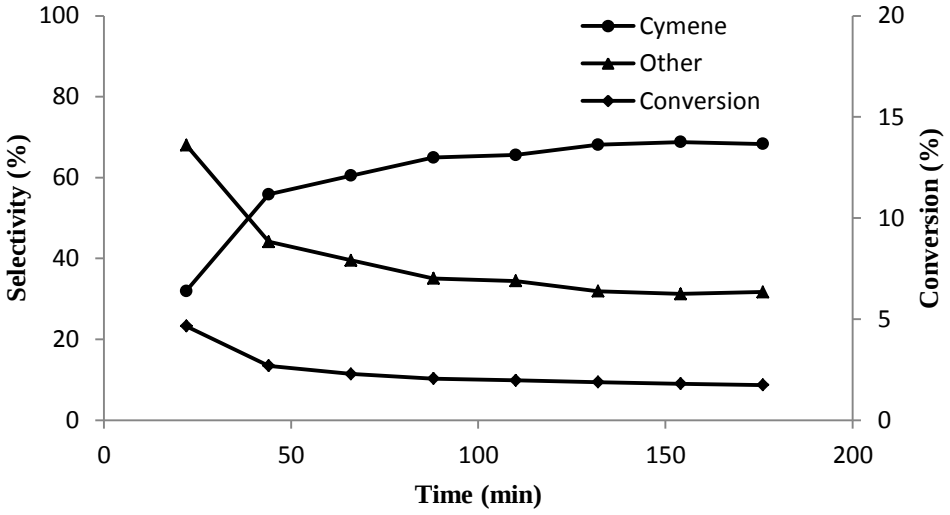

Figure 6.29. Time course for toluene alkylation by propane over 2%Pd/25%HSiW/SiO_2 (0.2 g catalyst, 300 ^oC, 1 bar pressure, inlet molar ratio toluene/C_3H_8 = 1:9, 10 mL min^{-1} flow rate, *W/F* = 80 g h mol^{-1}; in-situ catalyst pre-treatment at 300 ^oC/1 h in H_2 flow).

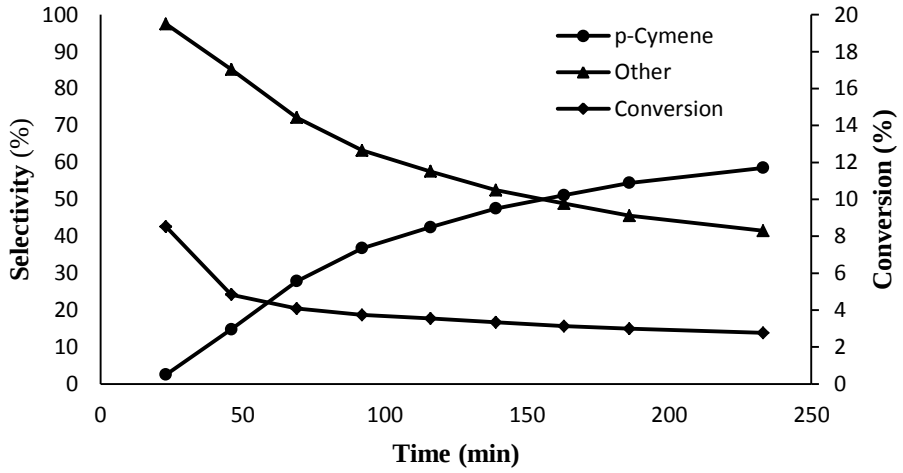

Figure 6.30. Time course for toluene alkylation by propane over 5.0%Pd/C + 25%HSiW/SiO_2 (0.2 g catalyst, 2.0%Pd loading, 300 ^oC, 1 bar pressure, inlet molar ratio

toluene/C_3H_8 = 1:9, 10 mL min^{-1} flow rate, *W/F* = 80 g h mol^{-1}; in-situ catalyst pre-treatment at 300 ^oC/1 h in H_2 flow).

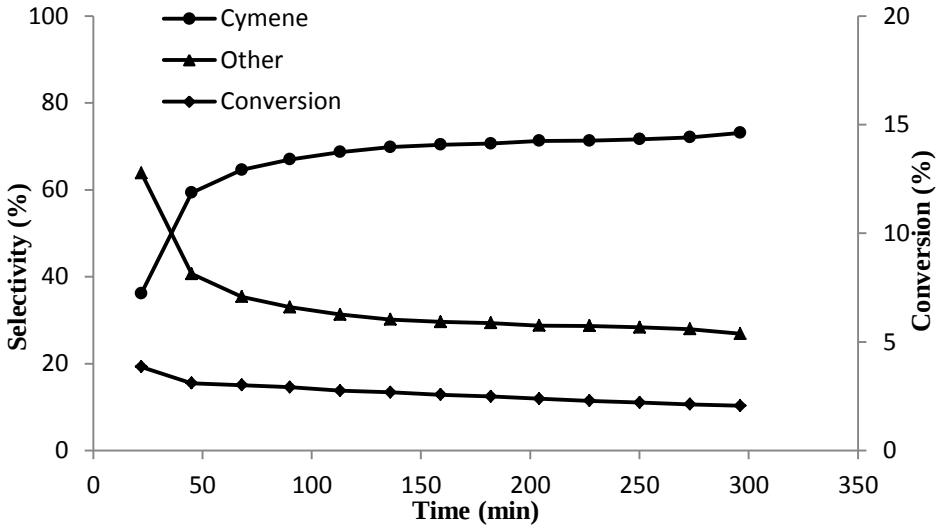

Figure 6.31. Time course for toluene alkylation by propane over 3%Pd/25%HSiW/SiO_2 (0.2 g catalyst, 300 ^oC, 1 bar pressure, inlet molar ratio toluene/C_3H_8 = 1:9, 10 mL min^{-1} flow rate, *W/F* = 80 g h mol^{-1}; in-situ catalyst pre-treatment at 300 ^oC/1 h in H_2 flow).

6.3.4.3. Comparison of Pt and Pd in alkylation of toluene with propane

As illustrated in Table 6.16, for alkylation of toluene with propane the Pd-HSiW and Pd-HZSM-5 catalysts perform similarly to Pt-HSiW and Pt-HZSM-5, albeit the Pd catalysts have generally a lower activity and p-cymene selectivity per metal loading in comparison to the Pt ones.

Figures 6.32 and 6.33 present the time courses for the reaction with mixed Pd and Pt catalysts 5.0%Pd/C + 25%HSiW/SiO_2 (1.5%Pd loading) and 5.0%Pt/C + 25%HSiW/SiO_2 (1.5%Pt loading). It can be seen that the Pt catalysts shows more stable performance (less deactivation) compared to the Pd one.

Table 6.16. Comparison of Pt and Pd in alkylation of toluene with propane.[a]

Catalyst	Temp. (˚C)	Conv.[b] (%)	Aromatic selectivity[c] (%)				
			C_6H_6	C_8[d]	C_9[e]	p-Cymene	Other[f]
Pt/C + HZSM-5 (0.5%Pt)[g]	350	14.1	33.6	31.9	20.9	3.5	10.2
Pd/C + HZSM-5 (0.5%Pd)[g]	350	6.2	32.8	35.4	24.3	5.3	2.2
Pt/C + 25%HSiW/SiO_2 (0.5%Pt)[g]	300	2.4	4.5	5.3	2.9	58.5	28.8
Pd/C + 25%HSiW/SiO_2 (0.5%Pd)[g]	300	0.6	22.3	20.1	5.5	30.1	22.0
Pt/C + 25%HSiW/SiO_2 (1.0%Pt)[g]	300	3.5	1.8	1.9	2.4	69.4	24.5
Pd/C + 25%HSiW/SiO_2 (1.0%Pd)[g]	300	1.5	9.2	10.0	3.8	41.8	35.2
Pt/C + 25%HSiW/SiO_2 (1.5%Pt)[g]	300	3.5	1.3	1.5	2.3	68.3	26.6
Pd/C + 25%HSiW/SiO_2 (1.5%Pd)[g]	300	2.4	7.0	7.8	4.2	44.1	24.7

[a]Reaction conditions: 1 bar pressure, 0.20 g catalyst, inlet molar ratio toluene/C_3H_8 = 1:9, 10 mL min^{-1} flow rate, *W/F* = 80 g h mol^{-1}; in situ catalyst pre-treatment at reaction temperature/1 h in H_2 flow, 10 mL min^{-1}. [b]Toluene conversion at 3 h time on stream. [c]Selectivity to aromatic products. [d]A mixture of xylenes and ethylbenzene. [e]A mixture of trimethyl-, methylethyl- and propylbenzenes. [f]Other products include ortho- and meta-cymene and unidentified alkylbenzenes. [g]Uniform physical mixture 5.0%Pt/C with HPA/SiO_2 or ZSM-5 (Si/Al = 10).

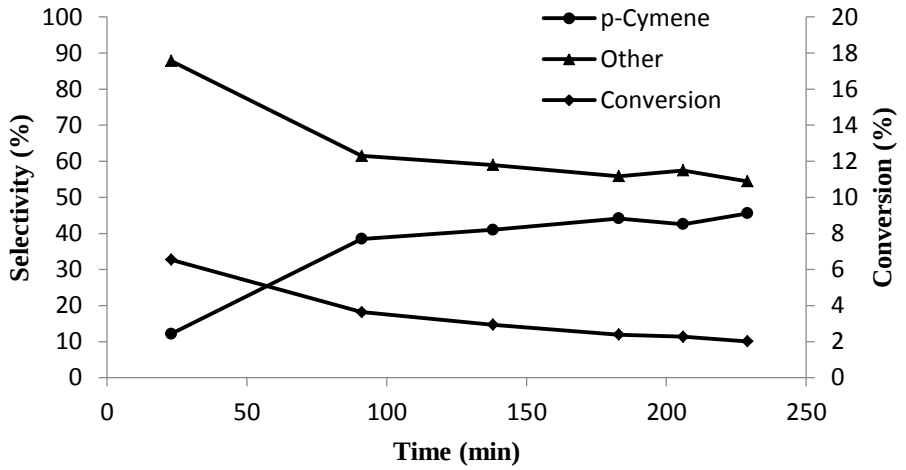

Figure 6.32. Time course for toluene alkylation by propane over 5.0%Pd/C + 25%HSiW/SiO_2 (0.2 g catalyst, 1.5%Pd loading, 300 ^{o}C, 1 bar pressure, inlet molar ratio toluene/C_3H_8 = 1:9, 10 mL min^{-1} flow rate, *W/F* = 80 g h mol^{-1}; in-situ catalyst pre-treatment at 300 ^{o}C/1 h in H_2 flow).

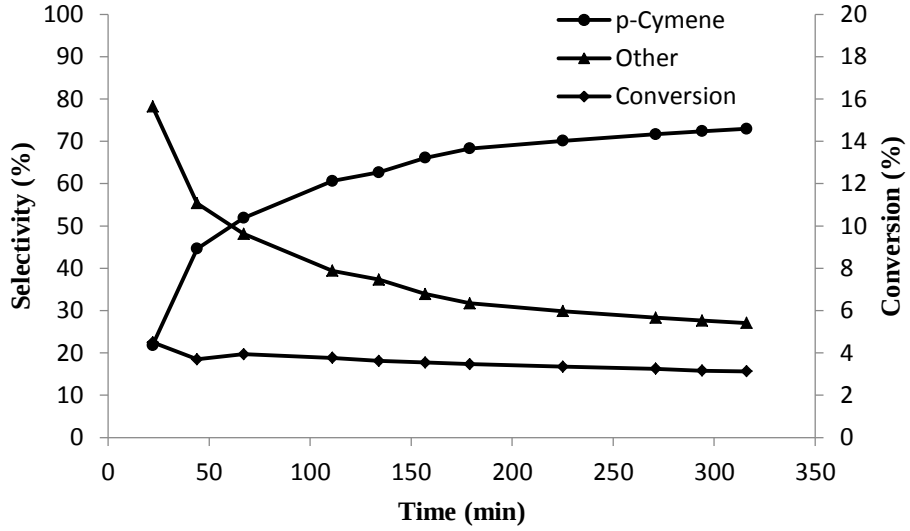

Figure 6.33. Time course for toluene alkylation by propane over 5.0%Pt/C + 25%HSiW/SiO_2 (0.2 g catalyst, 1.5%Pt loading, 300 ^{o}C, 1 bar pressure, inlet molar ratio toluene/C_3H_8 = 1:9, 10 mL min^{-1} flow rate, *W/F* = 80 g h mol^{-1}; in-situ catalyst pre-treatment at 300 ^{o}C/1 h in H_2 flow).

6.4. Conclusions

The alkylation of toluene by propane to yield p-cymene was studied using bifunctional metal-acid catalysts in a fixed bed reactor at 200-350°C and 1 bar pressure. Pt, Pd and Au were used as the metal components and Keggin-type heteropoly acids (HPA), such as $H_3PW_{12}O_{40}$ (HPW) and $H_4SiW_{12}O_{40}$ (HSiW), and zeolite HZSM-5 as the acid components in these catalysts. Most efficiently the reaction occurred over silica-supported Pt/HPA/SiO_2 catalysts giving p-cymene with up to 75% selectivity at 300 ^oC. Pt/HZSM-5 catalysts were much less selective ($\leq$ 5.5% p-cymene selectivity), which may be explained by product shape selectivity control imposed by HZSM-5 microporous environment. The Pd-based bifunctional catalysts performed similarly to Pt catalysts, albeit with a lower activity per metal loading. Gold catalysts, Au/HPA/SiO_2 and Au/HZSM-5, were less active that the corresponding Pt and Pd catalysts. Addition of gold to Pt and Pd in these catalysts had little effect on their activity and p-cymene selectivity in toluene alkylation with propane.

References

1. Cejka, J.; Krejci, A.; Zilkova, N.; Dedecek, J.; Hanika, *J. Micropor. Mesopor. Mater.* **2001,** *44-45*, 499.
2. Cejka, J.; Krejci, A.; Zilkova, N.; Kotrla, J.; Ernst, S.; Weber, A. *Micropor. Mesopor. Mater.* **2002,** *53*, 121.
3. Prokesova, P.; Zilkova, N.; Mintova, S.; Bein, T.; Cejka, J. *Appl. Catal. A* **2005,** *281*, 85.
4. Rigoreau, J.; Laforge, S.; Gnep, N.S.; Guisnet, M. *J. Catal.* **2005,** *236*, 45.
5. Ya, C. C.; Tan, C. S. *Ind. Eng. Chem. Res.* **2007,** *46*, 4421.
6. Bohstrom, Z.; Harelind, H.; Gevert, B.; Andersson, S. I.; Holmberg, K. *RSC Advances*, **2014,** *4*, 28786.
7. Cejka, J.; Wichterlova, B.; Bednarova, S. *Appl. Catal. A* **1991,** *79*, 215.
8. Engelhardt, J.; Lonyi, F. React. Kinet. *Catal. Lett.* **1987,** *34*, 355.
9. Perego, C.; Ingallina, P. *Catal. Today* **2002,** *73*, 3.
10. Parikh, P. A.; Subrahmanyam, N.; Bhat, Y. S.; Halgeri, A. B. *Appl. Catal. A* **1992,** *90*, 1.
11. Sealy, S.; Traa, Y. *Appl. Catal. A* **2005,** *294*, 273.
12. Bressel, A.; Donauer, T.; Sealy, S.; Traa, Y. *Micropor. Mesopor. Mater.* **2008,** *109*, 278.
13. Singer, D.; Alireza, S.; Rezai, S.; Sealy, S.; Traa, Y. *Ind. Eng. Chem. Res.* **2007,** *46*, 395.
14. Alireza, S.; Rezai, S.; Traa, Y. *Catal. Lett.* **2008,** *122*, 91.
15. Alotaibi, A.; Hodgkiss, S.; Kozhevnikova E. F.; Kozhevnikov, I. V. *Catalysts*, **2017,** *7*, 233.
16. Alotaibi, A.; Bayahia, H.; Kozhevnikova E. F.; Kozhevnikov, I. V. *ACS Catalysis*, **2015,** *5*, 5512.
17. Alsalme, A. M.; Wiper, P. V.; Khimyak, Y. Z.; Kozhevnikova, E. F.; Kozhevnikov, I. V. *J. Catal.* **2010,** *276*, 181.

18. Alharbi, W.; Brown, E.; Kozhevnikova, E. F.; Kozhevnikov, I. V. *J. Catal.* **2014,** *319*, 174.
19. Alotaibi, M. A.; Kozhevnikova, E. F.; Kozhevnikov, I. V. *Appl. Catal. A* **2012,** *447-448*, 32.
20. Benson, J. E.; Hwang, H. S.; Boudart, M. *J. Catal.* **1973,** *30*, 146.

Chapter 7: Conclusions

Alkylation of aromatic compounds (benzene and toluene) with alkenes over acid catalysts is an established commercial process for the manufacturing of a wide range of alkylbenzenes and alkyltoluenes. Using alkanes instead of alkenes as the alkylating agents in the aromatic alkylation reactions is a great challenge relevant to the effective functionalization of light alkanes [1-3]. Alkylation of benzene and toluene with propane is a promising pathway to cumene and p-cymene, respectively, which are the key intermediates in the manufacturing of phenol and p-cresol. Previous work has disclosed that bifunctional metal-acid catalysts, in particular those comprising platinum and zeolite HZSM-5, are active in the alkylation of benzene and toluene with ethane in the gas phase [2, 3 and references therein]. However, the achieved selectivity of the Pt/HZSM-5 catalyst to the desired cumene and p-cymene has been very low, which is likely due to the shape selectivity reaction control within zeolite microporous environment leading to product isomerisation and cracking [4, 5]. Therefore, our starting idea was to use in these reactions bifunctional metal-acid catalysts possessing larger pores on a meso/macroporous scale and stronger acidity in order to improve the reaction selectivity. Keggin-type heteropoly acids (HPAs) possessing very strong Brønsted acidity and allowing for broad variation of catalyst texture through supporting them onto appropriate supports were deemed to be a promising option to replace zeolite HZSM-5 in the alkylation catalysts.

Specifically, in our work, heteropoly acids, such as tungstophosphoric acid $H_3PW_{12}O_{40}$ (HPW) and tungstosilicic acid, $H_4SiW_{12}O_{40}$ (HSiW) were used as the acid component and platinum and palladium as the metal component in the bifunctional catalysts for the alkylation of benzene and toluene with propane. Bulk HSiW and HPW possess strong Brønsted acid sites with the initial enthalpy of ammonia adsorption of -171 and -197 kJ mol^{-1}, respectively, which are stronger than those in HZSM-5 zeolite (-130 to -150 kJ mol^{-1}) [6]. Supporting these HPAs on neutral porous supports such as silica can afford solid acid

catalysts with the porosity dominated by mesopores and macropores with no restriction for molecular movement within the catalyst porous structure, hence no confinement effect on the alkylation selectivity.

The main aims of this thesis were:

1) To study the selectivity of benzene alkylation with propane in the gas phase over bifunctional metal-HPA silica-supported catalysts (metal = Pt and Pd, HPA = HSiW and HPW).

2) To study the alkylation of toluene with propane in the gas phase over the same HPA-based catalysts in comparison with the corresponding catalysts based on zeolite HZSM-5.

3) To investigate the effect of gold addition on the performance of the above bifunctional metal-acid catalysts regarding their activity and stability in the alkylation of benzene and toluene with propane.

The bifunctional catalysts used in this study were by and large prepared according to the procedures described previously in the literature or using a modification thereof. These catalysts (fresh and spent) were characterised using several appropriate techniques including the BET texture analysis, XRD, TGA, FTIR, H_2-TPR, metal dispersion measurement by H_2/O_2 titration and CO adsorption, ICP-AES and combustion chemical analysis. The meso/macroporosity of these catalysts was confirmed by the BET analysis. Information about Brønsted and Lewis acid sites in the catalysts was provided by the FTIR spectroscopy of adsorbed pyridine, while the metal loading and the dispersion of supported metal particles were characterised using the ICP-AES analysis and gas chemisorption (H_2 and CO), respectively.

The catalysts were tested for the gas-phase alkylation of benzene and toluene by propane using the continuous flow fixed-bed quartz microreactor (9 mm internal diameter) with on-line GC analysis of reaction products described in Chapter 2. The reactions were

carried out at 250-350 ^{o}C (typically at 300 ^{o}C), ambient pressure and a molar arene/propane ratio of 1:9; the amount of catalysts charged was usually 0.2 g. Three types of catalyst bed configuration were investigated, namely, (i) supported catalysts with the metal and acid components supported together on silica, (ii) catalysts comprising a uniform physical mixture of the two components and (iii) two-bed catalysts with the metal and acid components present in separate beds (the metal component on top and the acid component in the bottom bed). Catalyst testing involved monitoring the conversion of aromatic compounds, product selectivity and stability of catalyst performance (catalyst deactivation) as a function of the time on stream. The mean absolute percentage error in product selectivity and conversion was <10% and the carbon balance was maintained within 95%.

The alkylation of benzene and toluene with propane occurs through the bifunctional reaction pathway (Scheme 7.1) including dehydrogenation of propane to propene on metal sites (step 1) followed by benzene alkylation with propene on acid sites (step 2) [2, 3]. Step (1) is thermodynamically unfavourable, whereas step (2) is feasible. Thermodynamic data for these two steps are given in chapter 4. It is step (2) that imposes restriction on the maximum achievable yield of the alkylated product. We found that reaction rate increased with increasing the metal loading, reaching a plateau as step (1) approached equilibrium. In benzene alkylation with propane over Pt-HSiW catalyst, step (1) was equilibrated at a Pt loading $\geq$ 0.5%, and the alkylation step (2) became the rate-limiting step. In such conditions, the reaction turnover rate (per surface proton site) correlated with the strength of HPA acid sites (the enthalpy of ammonia adsorption). These results, therefore, are in full agreement with the reaction mechanism represented by Scheme 7.1.

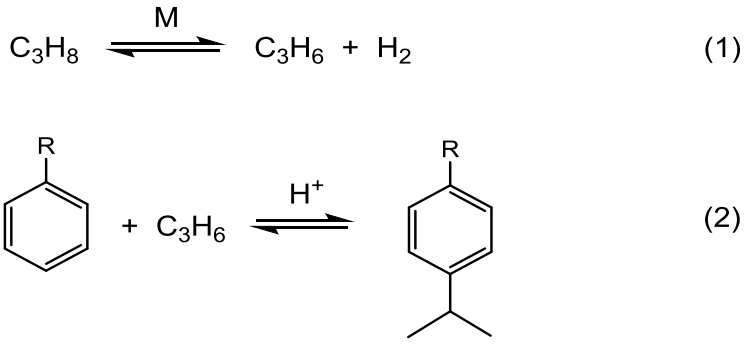

Scheme 7.1. Alkylation of benzene and toluene with propane over bifunctional catalysed pathway (M = Pt and Pd; R = H and CH_3).

The alkylation of benzene with propane over bifunctional metal-acid catalysts, comprising Pt and Keggin HPAs was found to proceed with high selectivity to cumene (isopropylbenzene, iPrPh). With Pt/HSiW/SiO_2 catalyst, cumene was obtained with 90-93% selectivity at 6-8% benzene conversion (6.5% yield) at 300 ^oC and an inlet C_6H_6/C_3H_8 molar ratio of 1:9, which is close to the equilibrium conversion (8.2%) (Chapter 4). Similarly, this catalyst was the most efficient in the alkylation of toluene with propane to give 75% p-cymene selectivity at 300 ^oC. These results significantly exceed the efficiency of the previously reported Pt/HZSM-5 catalyst in these reactions [3].

It was also demonstrated that bifunctional Pd-acid catalysts (Pd-heteropoly acid and Pd-zeolite) are active in the alkylation of benzene and toluene by propane to selectively yield cumene and p-cymene. The mesoporous catalyst Pd/HSiW/SiO_2 was much more selective to cumene (up to 88%) than the microporous catalyst Pd/HZSM-5, which gave only 11-18% cumene selectivity. Overall, the Pd and Pt bifunctional catalysts performed similar in these reactions, albeit the Pd ones were predictably less active than the Pt counterparts based on unit metal loading. This is compensated for by the lower price of Pd compared to Pt. In the case of Pd catalysts, propane dehydrogenation step (1) reached quasi-equilibrium at 1.5 – 2%

Pd loading (cf. ~0.5% Pt loading in the case of Pt catalysts), which can be explained by the lower activity of the Pd catalysts.

Interestingly, the physically mixed and two-bed Pd/C + 25% $HSiW/SiO_2$ catalysts showed high activity, which indicates no reaction limitation by the migration of alkene intermediates between metal and acid sites within these mesoporous catalysts. A similar performance was observed for their Pt counterparts. This, however, is different from the microporous Pd-HZSM-5 catalysts, for which the supported catalysts showed better activity than the physically mixed and two-bed ones.

It has been well documented that bimetallic PtAu and PdAu catalysts frequently have an enhanced performance in comparison to monometallic Pt and Pd catalysts ([7-18] and references therein), for example in hydrogenation [18], hydrodeoxygenation [8,10], hydrodesulphurisation [16,17], oxidation [11-13] and other reactions (for review, see [9,14,15]). The enhancement of catalyst performance by addition of gold can be attributed to geometric (ensemble) and electronic (ligand) effects of the constituent elements in PtAu and PdAu bimetallic species [14,15]. In this work, we looked at the effect of Au additives on the activity and stability of the bifunctional Pt and Pd catalysts in the aromatic alkylation with propane. Addition of gold to Pd-HSiW was found to slightly enhance the activity of Pd catalysts in the alkylation of benzene, although the gold alone was not active. On the other hand, gold had little effect on catalyst activity and p-cymene selectivity in toluene alkylation with propane over the Pt and Pd catalysts. The small effect of Au in our system can be attributed to the propane dehydrogenation step being close to equilibrium. Therefore, any enhancement of the dehydrogenation activity would not cause significant increase in benzene or toluene conversion.

Monitoring catalysts stability in the aromatic alkylation with propane revealed that Pt- and Pd-HPA bifunctional catalysts suffered from deactivation on stream, which may be

explained by catalyst coking. Indeed, coke deposition was found in spent catalysts after alkylation reaction. It was found that catalyst stability depended on the type of catalyst bed. The catalysts comprising the metal and acid components supported together on silica suffered the most from deactivation. In contrast, the mixed and especially two-bed Pt/C + 25%HSiW/SiO_2 catalysts were more stable on stream, which may be explained by their better resistance to coking due to a larger distance between the metal and acid active sites.

Future work on the alkylation of aromatic compounds with alkanes could address issues such as (i) overcoming thermodynamic limitations and (ii) improving catalyst stability to deactivation (coking). The first issue is related to the thermodynamically unfavourable step (1) of alkane dehydrogenation to form the corresponding alkene and hydrogen (Scheme 7.1). With Pt- and Pd-HPA catalysts, this step is equilibrated at a metal loading >0.5% for Pt and >1.5% for Pd [4, 5]. Removing the hydrogen from the reaction system will shift equilibrium in step (1), hence increase the yield of the alkylated product. Previously, this has been achieved using stoichiometric hydrogen scavengers (e.g., Zr_2Fe) [3], however the scavenging effect decreases with time on stream due to saturation of acceptor capacity. In this regard, it would be interesting to investigate palladium membrane catalysts, which could act as the alkane dehydrogenation catalysts and at the same time allow for the separation of hydrogen formed. The use of palladium alloy membranes for separation and purification of hydrogen is well known [8].

The second issue concerns with catalyst coking causing catalyst deactivation. As mentioned above, this can be improved by using appropriate configurations of catalyst bed. Thus, physically mixed bifunctional catalysts and two-bed metal and acid catalysts show better stability to deactivation. Future studies in this direction could further improve catalyst stability in aromatic alkylation with alkanes.

The main results of this work have been published in two papers [4, 5] and also disseminated through presentations on several international scientific conferences (see Abstract).

References

1. Shilov, A. E. *Activation of Saturated Hydrocarbons by Transition Metal Complexes*; Reidel: Dordrecht, **1984**.
2. Caeiro, G.; Carvalho, R. H.; Wang, X.; Lemos, M. A. N. D. A.; Lemos, F.; Guisnet, M.; Ramoa Ribeiro, F. J. *Mol. Catal. A* **2006,** *255*, 131.
3. Smirnov, A. V.; Mazin, E. V.; Yuschenko, V. V.; Knyazeva, E. E.; Nesterenko, S. N.; Ivanova, I. I.; Galperin, L.; Jensen, R.; Bradley, S. *J. Catal.* **2000,** *194*, 266.
4. Alotaibi, A.; Bayahia, H.; Kozhevnikova, E. F.; Kozhevnikov, I. V. *ACS Catalysis*, **2015,** *5*, 5512.
5. Alotaibi, A.; Hodgkiss, S.; Kozhevnikova, E. F.; Kozhevnikov, I. V. *Catalysis*, **2017,** *7*, 233.
6. Alharbi, W.; Kozhevnikova, E. F.; Kozhevnikov, I. V. *ACS Catal.* **2015**, *5*, 7186.
7. Hamilton, H. *Platinum Metal Rev.* **2012,** *56*, 117.
8. Poole, O; Alharbi, K.; Belic, D.; Kozhevnikova, E. F.; Kozhevnikov, I. V. *Appl. Catal. B* **2017,** *202*, 446.
9. Hutchings, G. J. *Chem. Commun*. **2008,** 1148.
10. Sun, K.; Wilson, A. R.; Thompson, S. T.; Lamb, H. H. *ACS Catal*. **2015,** *5*, 1939.
11. Han, Y. F.; Wang, J. H.; Kumar, D.; Yan, Z.; Goodman, D. W. *J. Catal*. **2005,** *232*, 467.
12. Hanrieder, E. K.; Jentys, A.; Lercher, J. A. *J. Catal*. **2016,** *333*, 71.
13. Xu, J.; White, T.; Li, P.; He, C.; Yu, J.; Yuan, W.; Han, Y. F. *J. Am. Chem. Soc*. **2010,** *132*, 10398.
14. Coq, B.; Figueras, F. *J. Mol. Catal. A* **2001,** *173*, 117.
15. Gao, F.; Goodman, D. W. *Chem. Soc. Rev*. **2012,** *41*, 8009.
16. Venezia, A. M.; La Parola, V.; Nicoli, V.; Deganello, G. *J. Catal.* **2002,** *212*, 56.
17. Venezia, A. M.; La Parola, V.; Deganello, G.; Pawelec, B.; Fierro, J. L. G. *J. Catal.* **2003,** *215*, 317.

18. Schwartz, T. J.; Lyman, S. D.; Motagamwala, A. H.; Mellmer, M. A.; Dumesic, J. A. *ACS Catal.* **2016,** *6,* 2047.